The Collaboration for Australian Weather and Climate Research

Australian Government

Bureau of Meteorology

CSIRO

Coupled Modelling and Prediction: from weather to climate - abstracts of the ninth CAWCR Workshop 19 October - 22 October 2015, Melbourne, Australia
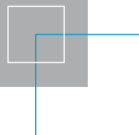
CAWCR Technical Report No. 080

Imtiaz Dharssi, Dave Bi, Gary Brassington, Debra Hudson, Ruth Lorenz, Ying-Ping Wang and Keith Day (editor)

October 2015

www.cawcr.gov.au

Coupled Modelling and Prediction: from weather to climate - abstracts of the ninth CAWCR Workshop 19 October - 22 October 2015, Melbourne, Australia

Imtiaz Dharssi, Dave Bi, Gary Brassington, Debbie Hudson, Ruth Lorenz, Ying-Ping Wang and Keith A. Day (editor)

The Collaboration for Australian Weather and Climate Research,
GPO Box 1289, Melbourne, VIC 3001, Australia

Enquiries should be addressed to:

Imtiaz Dharssi
The Collaboration for Australian Weather and Climate Research:
GPO Box 1289, Melbourne VIC 3001, Australia

i.dharssi @bom.gov.au

Conference sponsors

We would like to acknowledge and thank the following sponsors for their participation in this conference

Copyright and disclaimer

Contents

FOREWORD

The Collaboration for Australian Weather and Climate Research (CAWCR) is a partnership between Australia's leading atmosphere and ocean research agencies: the Bureau of Meteorology and the Commonwealth Scientific and Industrial Research Organisation (CSIRO). CAWCR was established by CSIRO and the Bureau of Meteorology in 2007 to ensure that Australia remains a world leader in climate, weather and oceans research so that it can meet the severe weather and climatic challenges that continue to confront the nation. This research delivers direct benefits to Australian communities, including through the development and implementation of the Australian Community Climate and Earth-System Simulator (ACCESS), which is used for both operational weather forecasting and climate prediction.

The CAWCR Workshop is an annual event that brings together national and international experts to highlight the latest developments in research relevant to CAWCR and its stakeholders. It provides an opportunity to identify gaps, opportunities, build relationships and enhance the quality, breadth and depth of our research efforts. This year's workshop will focus on coupled modelling and prediction across weather and climate timescales, encompassing the key components of earth system modelling: the atmosphere, land, ocean, ice and chemistry. It will address the status and prospects for improving our understanding, simulation and prediction of coupled processes, particularly as related to advancing our capability to predict high impact weather and climate.

The workshop is organised around seven topics:

- Short to medium range coupled modelling
- Land-atmosphere interactions
- Ocean-atmosphere coupled processes
- High impact weather
- Coupled data assimilation and reanalysis
- Scientific computing futures and challenges
- Current status and future opportunities

We are pleased to welcome the prominent scientists and experts from overseas, Australian research agencies and universities who have been invited to give presentations. Keynote speakers include:

- Dale Barker - UK Met Office
- Craig Bishop - US Naval Research Laboratory
- Wenju Cai - CSIRO
- Beth Ebert – Bureau of Meteorology
- Matthew England – University of New South Wales
- Tim Johns - UK Met Office
- L. Ruby Leung - Pacific Northwest National Laboratory
- Adrian Lock - UK Met Office
- Andy Pitman - University of New South Wales
- Kamal Puri - Bureau of Meteorology
- Lesley Seebeck - Bureau of Meteorology
- Hendrik Tolman - NOAA
- Tongwen Wu - Beijing Climate Center

The workshop is hosted by the Bureau of Meteorology and CSIRO and is sponsored by CRAY, Intel, ARC Centre of Excellence for Climate System Science and the National Computational Infrastructure. I would like to thank these sponsors for their generous support of the workshop.

Finally, on behalf of workshop attendees, I sincerely thank the members of the organising committee: Imtiaz Dharssi (chair), David Bi, Gary Brassington, Debra Hudson, Val Jemmeson, Ruth Lorenz, Tim Pugh, Ying Ping Wang, and acknowledge the excellent support provided by Anu Arora, Angela Artiaga, Tony Baldwin, Keith Day, Julie Sortino and Meryl Wiseman.

Dr Peter Craig
Director
Collaboration for Australian Weather and Climate Research

MODELLING ACROSS SCALES: TOWARDS SEAMLESS PREDICTION AND PROJECTION

Kamal Puri

Bureau of Meteorology
k.puri@bom.gov.au

Abstract

Climate variability and change have a major influence on the social and natural environments, and major climate research programmes have been aimed at determining the extent to which climate can be predicted, and to determine the extent of the human influence on climate. A further aim of the programmes is to achieve a deeper and more quantitative understanding of the role of human perturbations to biogeochemical cycles in altering the coupled climate system, and vice versa.

The past decade has seen major improvements in our ability to provide accurate weather forecasts over the 1- to 10-day timescales. These improvements are a result of a number of factors such as major increase in the observation network that provides high resolution (in time and space) information on key atmospheric variables, development of analysis and assimilation methods that allow effective use of these data, improvements in all components of numerical models and development of comprehensive methods to verify and diagnose model output. Despite the notable increase in forecast skill, there are still deficiencies in our ability to accurately predict high-impact weather systems that can have significant impact on society, the economy and the environment; examples of these systems include heavy precipitation, flooding, tropical cyclone landfall, destructive surface winds etc. Improving the skill of high impact weather forecasts is a major scientific and societal challenge. As noted in the \The World Climate Research Programme Strategic Framework 2005-2015" (WCRP-123 WMO.TD-No.1291)1, developments in atmospheric science and technology provide the opportunity to address the predictability of the total climate system for the benefit of society and to address the seamless prediction of the climate system from weekly weather to seasonal, decadal and centennial climate variations and anthropogenic climate change.

Earth system models (ESMs) are essential tools required to address the so-called seamless climate prediction problem. A key aspect in the continuing development of ESMs is the increasing resolution and complexity of the model that now includes the atmosphere, land surface, ocean and sea-ice, aerosols, carbon cycle and atmospheric chemistry. Numerical weather prediction (NWP) models have until recently only included the atmosphere and land surface; however in the past few years ocean and sea-ice have been added for seasonal prediction and tropical cyclone prediction. An important aspect of NWP and seasonal prediction systems is the inclusion of complex data analysis and assimilation methods that provide the capability of assimilating data from a wide range of observation systems, and particularly from satellites. Furthermore there is now a growing interest in environmental prediction. Accordingly, some operational centres have already made a move in this direction by implementing an atmospheric chemistry module in the forecast model and extending their data assimilation system to enable assimilation of chemical species (such a system is already being run at the European Centre for Medium Range Weather Forecast (ECMWF) under the European project Monitoring Atmospheric Composition and Climate, MACC to provide daily analyses and forecasts). Ocean data assimilation is now used routinely and operationally for seasonal prediction. Although coupled data assimilation is currently at a very early stage, it is an area that will see major activity in the future.

As can be seen from the above discussion, the scope of the advanced science and technology that underpins leading practice in Earth system modelling is such that it requires significant resources in research and development, in the infrastructure enabling the strategic and tactical application of the science, and in enabling availability of increasing supercomputing power and data storage. Major coordination and focused team research is now necessary to address the breadth and complexity of the scientific and technical issues. This is the clear message from the centres delivering the most successful outcomes. Accordingly substantial efforts have been expended at the major centres running ESMs in developing the complex infrastructure needed to (i) assemble Earth system coupled models using a coupler, (ii) launch/monitor complex simulations including ensembles, (iii) access, analyse and share results across a wide community, (iv) develop and promote technical and scientific standards for Earth system modelling, and (v) enable efficient running of the models on new computing architectures which comprise clusters with tens of thousands of cores (several hundred thousand in the future).

The presentation will discuss some of the key developments that are ongoing at modelling Centres in order to address the challenges faced by future modelling systems.

SHORT TO MEDIUM RANGE COUPLED MODELING AT THE US NATIONAL WEATHER SERVICE; MOVING TOWARD UNIFIED MODELING APPROACHES

Hendrik Tolman

NOAA / NWS / NCEP / Environmental Modeling Center

hendrik.tolman@noaa.gov

Abstract

Coupled modeling is slowly but surely moving into many operational model applications at the US National Weather Service (NWS).

Historically, the focus has been on particular applications, such as Hurricane Forecasting and Seasonal Forecasting. In the context of moving to a simplified and unified operational model suite, the NWS is tentatively moving to a unified coupled global modeling system, as part of a newly funded Research to Operations (R2O) effort. The presentation will focus on the
development of the Next Generation Global Prediction System (NGGPS) effort at the NWS, with a focus on the position of coupled modeling and data assimilation in this effort.

THE EFFECT OF EAST AUSTRALIAN CURRENT EDDIES ON WEATHER IN EAST COAST LOWS

Chris Chambers[12], Gary Brassington[2], Ian Simmonds[1], Kevin Walsh[1]

[1]*School of Earth Sciences, University of Melbourne, Parkville, Australia*
[2]*Centre for Australian Weather and Climate Research, Bureau of Meteorology, Sydney*

c.chambers@bom.gov.au

Abstract

The relationships between sea surface temperature (SST) distribution and thunderstorms, heavy rainfall, sea level pressure, and surface wind speeds, during four east coast lows are examined using both lightning observations and numerical simulation results. Atmospheric changes caused by the introduction of complex eddy and frontal structures present in Bluelink ocean datasets are investigated using the Weather Research and Forecast model. Maximum convective available potential energy (MCAPE) differences between Bluelink SST simulations and coarse SST simulations indicate that areas of greater MCAPE in the Bluelink simulations are related to regions of warmer waters with horizontal advection often displacing increased MCAPE downwind (Chambers et al., 2015a) . At short timescales of 3 to 6 hours, the differences in MCAPE become larger and more localized and show a compelling correlation with observed lightning. For the damaging Pasha Bulker case, a plume of thunderstorms associated with the coastal damage occurs downwind of a region of enhanced MCAPE, increased rainfall (Chambers et al., 2014) and lower sea level pressure (Chambers et al., 2015b), along the southern flank of a warm eddy. Based on these results it is concluded that the particular features of the warm eddy enhanced the thunderstorm potential over the coastal region and helped in localising the area of greatest impact. Analysis of the impact of changing the SST on surface wind speeds reveals periods of increased and decreased surface wind speeds over warmer waters. The areas and periods of decreased wind speeds are less widespread and run counter to prior research results. Results are presented that suggest that SST induced deep vertical mixing in convection can mix momentum down from the middle troposphere where the vector wind may oppose the surface wind leading to a reduction in surface wind speeds.

References

Chambers C. R. S., Brassington G. B., Simmonds I., and K. Walsh, 2014a: Precipitation changes due to the introduction of eddy-resolved sea surface temperatures into simulations of the "Pasha Bulker" Australian east coast low of June 2007. *Meteorol Atmos Phys* **125:**1-15 doi: 10.1007/s00703-014-0318-4

Chambers, C. R. S., Brassington, G. B., Simmonds, I., and K. Walsh, 2015a: Sensitivity of the distribution of thunderstorms to sea surface temperatures in four Australian east coast lows. *Meteorol. Atmos. Phys.* DOI: 10.1007/s00703-015-0382-4

Chambers, C. R. S., Brassington, G. B., Simmonds, I., K. Walsh, and J. Sheng, 2015b: Sea level pressure response to the specification of eddy-resolving sea surface temperature in simulations of Australian east coast lows. J. Sat. Ocean Met. (accepted July 2015)

GLOBAL COUPLED NWP: RECENT RESEARCH PROGRESS AT THE MET OFFICE

Tim Johns[1], Ann Shelly[2], Dan Copsey[1], Jose Rodriguez[1], Livia Thorpe[1], Sean Milton[1]

[1] *Met Office, Exeter, UK*
[2] *Cumulus, City Financial Investment Company Limited, London, UK*

tim.johns@metoffice.gov.uk

Abstract

Physical interactions between the ocean, atmosphere and sea ice at their interfaces play an important role in the oceanic and atmospheric circulation and modes of variability in the climate system on timescales from diurnal through seasonal, interannual to decadal and beyond. While seasonal and climate models have long recognised the importance of air-sea interaction by using coupled formulations, global numerical weather prediction (NWP) models conventionally prescribe the sea surface temperature (SST) and sea ice as given boundary conditions through the forecast period, either fixed or slowly-varying but not prognostic. Although this has been a useful practical approximation in the NWP context up until now, even on short to medium range NWP timescales it can be regarded as an undesirable simplification as models improve in their resolution and ability to represent coupled interactions more faithfully. It also runs counter to the Met Office's long term seamless model science strategy. Coupled NWP has potential to deliver forecasting benefits relative to uncoupled NWP particularly for phenomena involving strong air-sea interaction on timescales of hours to days, such as diurnal SST variations, diurnal ocean warm layers, land-sea breezes, the Madden-Julian Oscillation, and tropical cyclones. Coupling at high latitudes should enable improved ice-ocean analysis in sea ice marginal zones (Smith et al. 2012) and thereby benefit regional performance in short range NWP.

Research has been undertaken at the Met Office over recent years to examine the potential for globally coupled NWP to supersede uncoupled atmospheric NWP and ocean forecast systems. Given the Met Office's existing requirements to serve NWP as well as marine sector customers, economies of scale could result from moving to coupled NWP systems for both output streams. The research work described here has run alongside an integrated project for global model development (described by D. Walters at this meeting), which is increasingly centred round global coupled models at a range of resolutions and has delivered improvements to model physics/dynamics. It also links closely to research work into coupled data assimilation (coupled DA) more suited for consistent initialisation of the components of coupled NWP models (Lea et al. 2015; described by D. Walters at this workshop). Within the existing model development process, full NWP trials of model science upgrades including DA have mostly been conducted in an atmosphere-only framework so far, but in future coupled NWP trialling is likely to be an increasingly integral part of the model development and assessment process.

The research results outlined in this contribution reinforce our expectation that coupled NWP will ultimately deliver improved operational forecast skill, but a further motivation is that running coupled NWP in research mode provides a useful framework in which to investigate the origins of coupled systematic errors and to help link error characteristics between NWP and longer (seasonal/climate) timescales. We focus here on experiments initialised using analyses taken from separate (uncoupled) atmosphere/land and ocean/ice DA systems rather than initial conditions from coupled DA.

Coupled NWP research phases and experimental designs

Phases in the research so far (Table 1) have used coupled Unified Model/NEMO configurations run at N216-ORCA025 resolution, most recently using the GC2 science configuration. Phase 1 was a pilot study – essentially a technical proof of principle with a rather small sample of cases run – which showed promise but with a scope that limited the ability to derive robust statistical conclusions. In the first two phases of experiments, due to technical limitations, it was necessary to integrate either the ocean/ice or atmosphere/land forward in time by 12 hours from the initial states (model analyses) to achieve a time match-up at the nominal start times. Along with science differences between the configurations used in the coupled NWP hindcasts themselves and those used in the data assimilation that generated the initial analyses, the experiments contain various potential sources of initialisation shock that likely impact the systematic error growth (measured relative to analyses). Some but not all of this deficiency is alleviated in GC2 experiments via a cleaner initialisation but further improvement in this regard is desirable and should be achievable by employing coupled DA for initialisation.

Table 1: Coupled NWP (CNWP) research phases at the Met Office

Phase / model version	Experimental design	References/comments
Phase 1 –an early configuration of HadGEM3	6 winter and 6 summer start dates thro' 2007-08, each run to 30 days. 3-hourly coupling. Includes parallel atmosphere-only and ocean-only controls.	Shelly et al. 2011 (tech report)
Phase 2 – GA3/GO1	Over 100 start dates thro' 2008-10, each run to 15 days. 3-hourly coupling. Includes parallel forced atmosphere-only and ocean-only controls.	Johns et al. 2012 (tech report); Shelly et al. 2014; Johns et al. (in preparation)
GC2	Annual cycle of daily start dates Aug 2011-Sept 2012, run to 15 days, including parallel forced atmosphere-only controls. Feb 2010 daily start dates, run to 6 days. Hourly coupling as standard.	Analysis currently in progress; also used as a basis for CNWP sensitivity tests and science development

Results

Phase 2 hindcasts have been statistically verified for several standard atmosphere variables over large-scale regions against independent ECMWF analyses. Counts were made for 117 start dates where coupled (C) or atmosphere (A) hindcasts are more skilful (lower RMS error relative to EC analysis), and the significance of C vs. A differences was then assessed at 90/95/99% significance levels using a cumulative binomial probability statistic for trials (taking equal probability for C and A in each outcome as the null hypothesis). In the N. Hemisphere and S. Hemisphere extra-tropics we find little significant C/A difference. The tropical region (30N-30S) shows significant improvements in scores/counts for C relative to A however, most notably for 500hPa height and tropical 850hPa winds. Breaking the tropical domain down into Indian Ocean, W. Pacific, E. Pacific and Atlantic sectors reveals that the most significant improvements [99% confidence] originate in the Indian Ocean, C beating A at lead times of 2 to 10 days for 500hPa height, MSLP and 850hPa meridional winds.
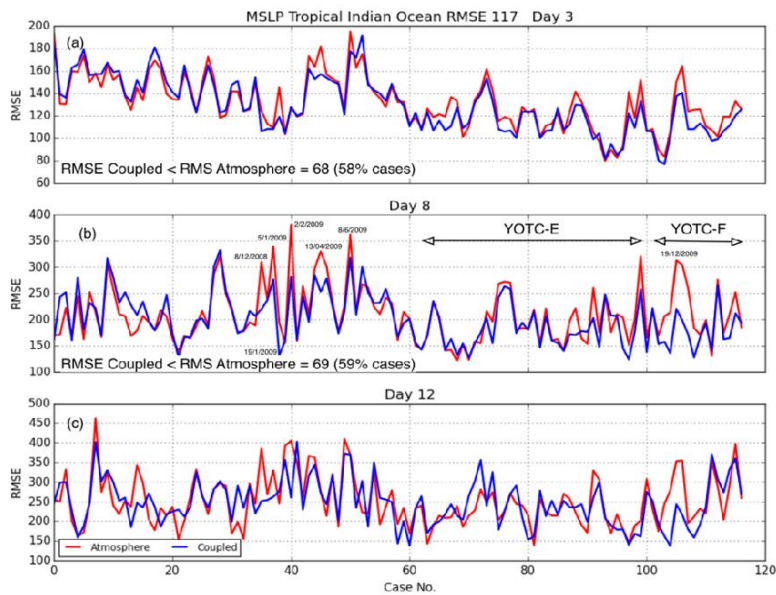
Figure 1: MSLP RMSE for 117 cases over the tropical Indian Ocean sub-domain for Phase 2 coupled (C - blue) and atmosphere-only (A - red) forecasts at days 3, 8 and 12. YOTC-E and YOTC-F MJO periods are marked in the centre panel along with start dates of some case studies where C is a marked improvement over A at day 8.

Figure 1 shows a case-by-case pseudo-time series comparison of C vs. A hindcasts of RMSE for Tropical Indian Ocean MSLP at day 3, 8 and 12 lead times. At days 3 and 8, C outperforms A significantly on average over the 117 cases [95% significance]. At day 8 for example, notably around forecasts initialised between Dec 2008 to Jun 2009, and during the YOTC period around 19 Dec 2009, the RMSE for C drops well below A. Further analysis suggests that the periods of improvement in C relative to A tend to correspond with large MJO amplitudes. The improvement in Indian Ocean scores is consistent with Shelly et al. (2014) who show coupling between the ocean and atmosphere to be beneficial to anomaly correlation scores during Madden Julian Oscillation (MJO) episodes in the YOTC-E and YOTC-F periods in Phase 2 run. Shelly et al. (2014) also show, consistent with earlier studies, that the coupled model maintains the observed lead-lag correlation between outgoing long-wave radiation/precipitation and SST much better than the atmosphere-only model, the latter tending towards inaccurate in-phase anomalies only a few days into the forecast.

Using GC2 coupled NWP experiments initialized in Feb 2010, and focusing on evaluation over the TWP+ region against MTSAT data, we are exploring the potential to introduce a coupled prognostic skin SST scheme to replace the standard atmosphere-ocean coupling, which uses upper ocean layer temperature as the effective SST. The simplest approach tested takes a constant effective thermal conductivity K_e for the upper ocean layer (of thickness h), implicitly solving for the surface energy balance (F_{surf}, net surface heat flux) and skin SST (T_{skin}) in JULES given $T_{toplayer}$ (the temperature of the ocean top layer) via the equation $F_{surf} = 2K_e/h(T_{skin} - T_{toplayer})$. This scheme generates a better diurnal cycle range (Figure 2) and also improves the timing of the diurnal minimum relative to the control, as assessed for Feb 2010. However, the lack of any wind or upper ocean state dependence in K_e means that a more complex parametrization of the diurnal warm layer and cool skin effects, currently under development, is considered to be necessary to enable implementation at a GC release.
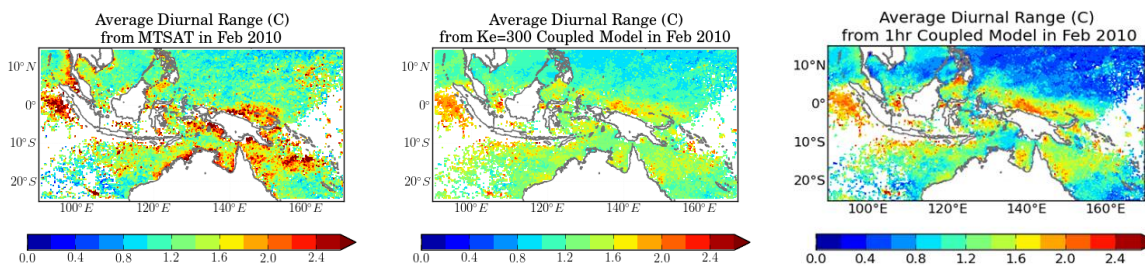
Figure 2: Average diurnal range (dSST) over the TWP+ region through Feb 2010 for MTSAT data representative of skin temperature (left), for T_{skin} in GC2 sensitivity experiments with the simple skin SST scheme using $K_e = 300$ $Wm^{-1}K^{-1}$ (centre), and for the ocean upper layer temperature $T_{toplayer}$ (at 0.5 m) in the GC2 control (right).

For the GC2 annual cycle experiment, Arctic sea ice performance has been evaluated relative to FOAM-v13-NEMOVAR ocean-ice analyses covering the same period. The ocean/ice analyses used to initialise GC2 hindcasts originate from a FOAM-v13-NEMOVAR model reanalysis, run at the identical ORCA025 ocean/ice resolution with near-identical science to the GC2 experiment. Note that FOAM-v13-NEMOVAR includes assimilation of sea ice concentration but not sea ice volume. GC2 runs track the analysed Arctic sea ice volume quite closely out to 15-day lead times (Figure 3, left), but slightly undershoot the September minima. Further analysis shows that a large initialisation shock occurs in the constituent terms of the sea ice energy budget over the first few days of the GC2 hindcasts, visible as large differences at day 1 compared to corresponding terms diagnosed from the analyses converging to much smaller differences compared to analyses at longer lead times (Figure 3, centre and right panels). Although the science used in FOAM-v13 is very similar to that in the GC2 experiment, it actually uses a salinity-dependent freezing temperature for sea water to aid data assimilation, whereas GC2 uses a salinity-independent freezing temperature. In effect, GC2 hindcasts therefore use somewhat "non-native" analyses in this respect. Sensitivity experiments in which salinity-dependent freezing is added to GC2 indicate that the initialisation shock observed in the sea ice budget terms is largely explained by this discrepancy. The cleaner setup with reduced initial shock is likely to be better suited to understanding the development of sea ice and polar ocean systematic errors at short-to-medium range. This finding also has implications for using native rather than non-native ocean/ice analyses for initialisation of coupled NWP experiments in a manner analogous to Transpose-AMIP (Williams et al. 2013).
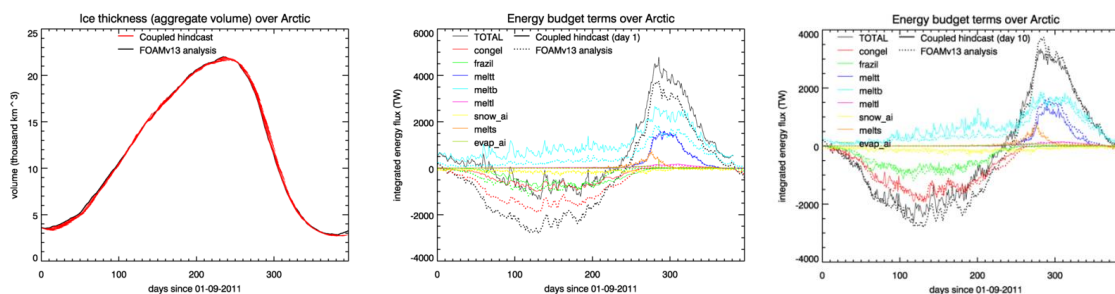
Figure 3: Daily mean time series of total Arctic sea ice volume from FOAM-v13–NEMOVAR reanalysis (black solid line) and 15-day GC2 coupled NWP hindcasts (thin red lines) for start dates from 1 Sept 2011 to mid Sept 2012 (left). Average terms in the sea ice energy budget (including total) at day 1 (centre) and day 10 (right) in the hindcasts (solid lines) compared with corresponding terms in the FOAM analyses (dotted). Note the large model-analysis differences at day 1 and marked adjustment of most terms towards a closer match by day 10.

References

Johns, T.C., Shelly, A., Rodriguez, J.M., Copsey, D., Guiavarc'h, C., and Sykes, P., 2012: Report on extensive coupled ocean-atmosphere trials on NWP (1-15 day) timescales. Met Office Tech. Report

Johns, T. C., Shelly, A., Copsey, D., Rodriguez, J. M., Guiavarc'h, C., Ryan, A., and Milton, S. F., (in preparation): Impacts of Two-Way Air-Sea Coupling in Global Medium-Range Hindcast Case Studies.

Lea, D, J., Mirouze, I., Martin, M. J., King, R. R., Hines, A., Walters, D., and Thurlow, M., 2015: Assessing a new coupled data assimilation system based on the Met Office coupled atmosphere, land, ocean, sea ice model. Monthly Weather Review (accepted)

Shelly, A., Johns, T.C., Copsey, D., and Guiavarc'h, C., 2011: Preliminary case-study experiments with a global ocean-atmosphere coupled model configuration on 1-15 day timescale. Met Office Tech. Report

Shelly, A., Xavier, P. K., Copsey, D., Johns, T. C., Rodriguez, J. M., Milton, S. F., and Klingaman, N. P., 2014: Coupled versus uncoupled hindcast simulations of the Madden-Julian Oscillation in the Year of Tropical Convection. Geophysical Research Letters, 41, 5670-5677, doi:10.1002/2013GL059062

Smith, G. C., Roy, F., and Brasnett, B., 2013: Evaluation of an operational ice–ocean analysis and forecasting system for the Gulf of St Lawrence. Q. J. R. Meteorol. Soc., 139(671), 419-433

Williams, K. D., Bodas-Salcedo, A., Déqué, M., Fermepin, S., Medeiros, B., Watanabe, M., Jakob, C., Klein, S. A., Senior, C., A., and Williamson, D. L., 2013: The Transpose-AMIP II Experiment and Its Application to the Understanding of Southern Ocean Cloud Biases in Climate Models. J. Climate, 26, 3258–3274, doi: 10.1175/JCLI-D-12-00429.1

MODELLING THE COMPOSITE MESOSCALE SIGNATURE OF THE MJO OVER THE MARITIME CONTINENT

Claire L. Vincent[1] and Todd P. Lane[1]

[1]*School of Earth Sciences and ARC Centre of Excellence for Climate System Science, The University of Melbourne*

claire.vincent@unimelb.edu.au

Introduction

Convection in the Maritime Continent is significant for global heat and moisture budgets, and is therefore important for large scale climate modelling. However, the interaction of mesoscale phenomena such as land/sea breezes, flow over steep topography and gravity waves with the large scale variation in cloudiness and precipitation induced by the Madden Julian Oscillation (MJO) makes this a particularly challenging region to resolve in a coarse resolution model.

In the tropics, precipitation is often observed to peak during the afternoon or evening over the land, and in the early hours of the morning over the water. This offshore propagating precipitation has been attributed to the land-breeze (eg. Qian (2008)) and gravity wave propagation (eg. Mapes (2013)). These processes are poorly represented in climate models and NWP models where convection is parametrised.

In this work, we use a mesoscale model with a horizontal resolution of 4 km to examine the changes in the land/sea breezes and far offshore precipitation associated with gravity waves during an MJO event over the Maritime Continent in January 2010. The land-valley breeze and gravity waves are shown to both play important roles in the diurnal cycle of precipitation offshore.

We show that the diurnal cycle in precipitation is slightly enhanced over the land in the lead-up to the MJO period compared with the active and follow-on periods, and show that this is consistent with the modelled profiles of wind, moisture and cloudiness.

Methods

Simulations were conducted using the Weather Research and Forecasting (WRF) model for the 31 day period of January 2010, during which time the MJO passed through the Maritime Continent. Further details of the model set-up are found in table 1 and in Vincent and Lane (2015). Initial and boundary conditions were provided by the ERA-Interim Reanalysis. An inner domain with horizontal resolution 4 km was nested within an outer domain with horizontal resolution 12 km (Fig. 1). Results from the WRF model were compared with the satellite precipitation estimates TRMM 3B42 and CMORPH.
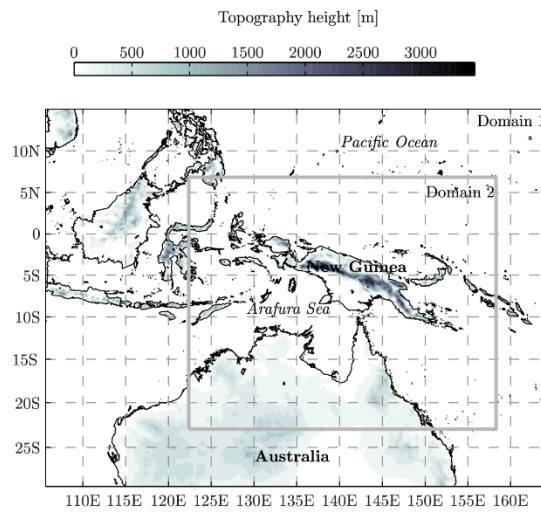
Figure 1. Simulation domains. Domain 1: dx = 12 km. Domain 2: dx = 4 km.

Table 1. Model specifications.

	Domain 1	**Domain 2**
Horizontal resolution	12 km	4 km
Gridpoints (west-east by north-south)	540 x 420	990 x 840
Cumulus parametrisation	Kain-Fritsch	None
Nudging	Wavelengths > 1000 km	None
Vertical levels	79	79
Vertical grid spacing	50—70 m below 1 km, increasing to 650m at 16km	50—70 m below 1 km, increasing to 650m at 16km
Model top	50 hPa	50 hPa

Selected Results and outlook

The WRF model was successfully used to reproduce several aspects of the interaction between the complex topography of the Maritime Continent and the large scale variability in moisture, wind and cloudiness associated with the MJO. Comparison of modelled rain-rate with satellite precipitation estimates suggested that the precipitation was too heavy over the land in the WRF model, and that the peak in the diurnal precipitation cycle was several hours too early. Despite these limitations, the variation in precipitation and extent of offshore propagation with the passage of the MJO appeared consistent between the model and the satellite precipitation estimates.

An important result suggested by the WRF model simulations was that a diurnally oscillating potential temperature anomaly propagates outwards and upwards from the coast in response to the variations in heating over the land, analogous to the tropical seabreeze described by Rotunno (1983). The depth of this anomaly is indicative of a contribution from diabatic effects associated with the deep convection as well as

the radiative heating at the surface, consistent with results of Hassim et al. (2015) who conducted a similar study in an MJO suppressed period.

In Fig. 2, the average potential temperature anomaly at 4pm on a cross section through the steep topography of New Guinea is shown for the 10 days leading up to the active MJO active period and the 10 days directly after the MJO active period. Despite similar heating near the surface, the potential temperature anomaly has greater vertical extent and extends further from the coast in the period directly prior to the MJO active period than directly afterwards. The change in the depth of this anomaly is related to the reduced diabatic heating effects in the relatively drier period after the MJO active period.
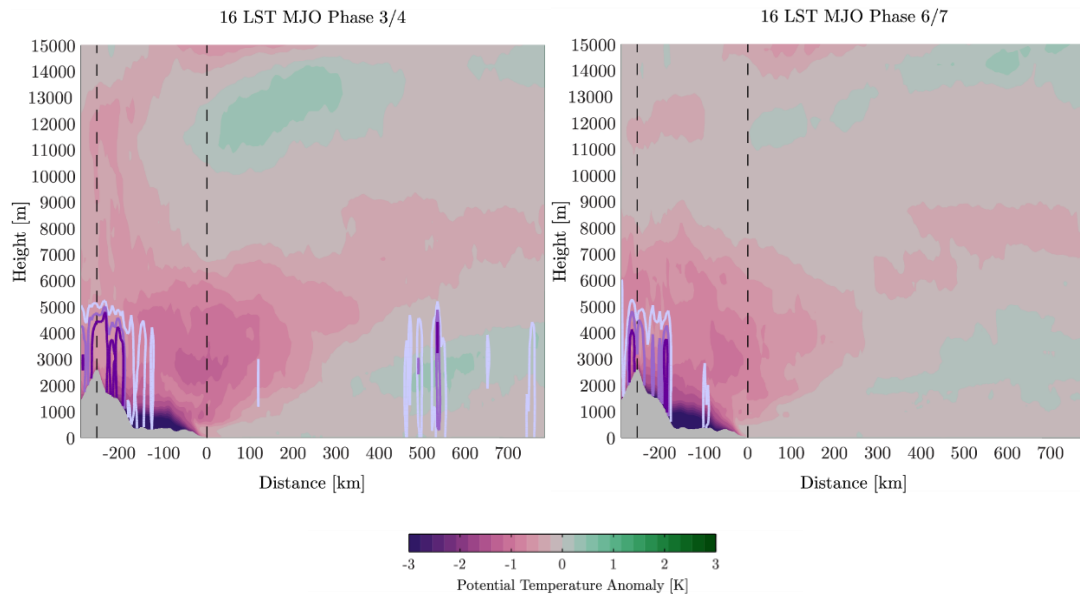
Figure 2: Average potential temperature anomaly at 1600 LST (4pm) on a cross section through New Guinea for the MJO lead-up period (left) and the MJO follow-on period (right). Shading: potential temperature anomaly. Lines: Liquid water mixing ratio. Light purple: 4×10^{-5} kg kg^{-1} Purple: 8×10^{-5} kg kg^{-1} Dark Purple: 12×10^{-5} kg kg^{-1}. Grey shading: silhouette of topography.

We show that in the lead-up to the MJO active period over the Maritime continent, ample moisture, relatively clear skies and light winds are favourable for heavy afternoon precipitation and large diurnal precipitation cycle over the land, consistent with the results of Peatman et al. [2014]. Within 100-200 km of the coast, squall lines propagate offshore with the land and valley breezes during the night, while diurnally varying precipitation as far as 800 km offshore appears to be associated with gravity waves generated by the deep, diurnally oscillating heat source over the land.

Similar effects are present during the MJO active period itself, but increased cloudiness associated with the main MJO envelope and the burst of westerly winds are less favourable for the development of these diurnally oscillating effects. After the MJO active period, supressed precipitation over the land associated with drier air leads to a diminished contribution to the diurnally oscillating heat source from moist convective processes.

This study focussed a single MJO event in January 2010. Efforts to expand the results to a multi-season study that examines the relationship between the MJO and the diurnally varying precipitation patterns across the spatial extent of the Maritime Continent are currently underway.

References

Hassim, M. E. E., T. P. Lane, and W. Grabowski, 2015: The diurnal cycle of rainfall over New Guinea in large-domain, convection-permitting WRF simulations. Atmospheric Chemistry and Physics.

Mapes, B. E., T.T. Warner, and M. Xu, 2003: Diurnal Patterns of Rainfall in Northwestern South America. Part III: Diurnal Gravity Waves and Nocturnal Convection Offshore. Monthly Weather Review, 131, 830–844.

Peatman, S. C., A. J. Matthews, and D. P. Stevens, 2014: Propagation of the Madden-Julian Oscillation through the Maritime Continent and scale interaction with the diurnal cycle of precipitation. Quarterly Journal of the Royal Meteorological Society, 140 (680), 814–825.

Qian, J.-H., 2008: Why Precipitation Is Mostly Concentrated over Islands in the Maritime Continent. Journal of the Atmospheric Sciences, 65 (4), 1428–1441.

Rotunno, R., 1983: On the linear theory of the land and sea breeze. Journal of the Atmospheric Sciences, 40, 1999–2009.

Vincent, C. L. and T. P. Lane, 2015: Evolution of the diurnal precipitation cycle with the passage of a Madden-Julian Oscillation event through the Maritime Continent. Manuscript under preparation.

WAVE-COUPLED PROCESSES IN AIR-SEA MODELLING: FROM TURBULENCE TO CLIMATE

Alexander V. Babanin

Centre for Ocean Engineering, Science and Technology, Swinburne University, Melbourne, Australia

Abstract

It is rapidly becoming clear that many large-scale geophysical processes are essentially coupled with the surface waves, and those include weather, tropical cyclones, climate and other phenomena in the atmosphere and ocean, at air/sea and sea/land interface, and many issues of the upper-ocean mixing below the surface. Besides, the wind-wave climate itself experiences large-scale trends and fluctuations, and can serve as an indicator for changes in the weather climate. In the paper, we will discuss wave influences at scales from oceanic turbulence to climate (see also Babanin et al., 2012, for a review).

On the ocean interface, surface waves are generated by the airflow in the atmospheric boundary layer. These waves define roughness of the surface. Such roughness is dynamic, it moves and grows, and thus changes the very winds which produce the waves. Air-sea fluxes of momentum and energy change as the waves evolve, both in magnitude and direction (if the waves develop mature enough or the airflow weakens).

Below the surface, the waves pass the energy and momentum to the upper ocean by producing turbulence and currents and, depending on the depth of the mixed layer, facilitate or moderate upper ocean mixing. Through the mixing and upwelling/downwelling, sea surface temperature can be changed and thus large-scale air-sea processes can be initiated or changed (see e.g. Chalikov and Belevich (1993) for a detailed schematic of such multiple wave-related dynamics). In finite-depth areas, wave-induced motion and turbulence is the primary forcing for sediment suspension and transport (e.g. Pleskachevsky et al., 2011).

Turbulence

Wave-induced turbulence in the upper ocean can be due to variety of different processes, such as wave-breaking, Stokes drift, Langmuir circulation or wave orbital motion. The latter can either produce turbulence directly or enhance pre-existing oceanic turbulence through instability mechanisms. It should be noted that while the wave-breaking influence is concentrated near the surface (at the scale of wave height which is ~1 m), the others act at the scale of wavelength (~100 m) and therefore are more efficient in mixing through the thermocline. We refer to Babanin (2011), Belcher et al. (2012), Ghantous and Babanin (2014) for recent reviews of the wave-mixing problem.

Wave-induced turbulence on the atmospheric side is responsible for the fluxes in the lower boundary layer (see Chalikov and Rainchik (2011) for accurate description and subdivision of such fluxes). Very close to the wavy surface, nature of the constant-flux layer is essentially altered, by comparison with the wall law, due to wave-coherent pressure/velocity oscillations (Babanin and McConochie, 2013) and due to wave breaking (Iafrati et al., 2013). The latter study showed that a significant proportion of the wave energy lost due to breaking is spent on producing the turbulence in the air rather than in the water.

Swells

The energy spent on turbulence production is a sink of energy for the ocean waves. While wave-breaking is the dominant dissipation mechanism for wind-generated waves, wave-turbulence interactions become major dissipation process for swells (Babanin, 2006, Babanin and Chalikov, 2012). On the atmospheric side, swells can generate winds and such wave-driven wind regimes have been found prevalent in the tropics (Hanley et al., 2010).

Swell is present is some 80% of oceanic waves fields, and therefore swell-turbulence interaction is important for wave forecast, upper-ocean dynamics and tropical meteorology. What is most essential, swell observations, particularly those by satellites, serve as an efficient remote-sensing means for estimating the turbulence production rates (Ardhuin et al., 2009, Young et al., 2013).

Weather and climate

Oceanic conditions of large waves and shallow thermocline can bring about rapid change of air-sea fluxes, and those include heat, moisture and gas exchanges. This can be particularly essential in case of tropical cyclones which are always accompanied by large waves and whose intensity forecast has stagnated for decades. Toffoli et al. (2012), for example, demonstrated a rapid response of the mixed layer depth during a tropical cyclone on the North-Western Shelf of Australia, correlated with increase of the wave height and wave-produced turbulence. Such deepening of the mixed layer should involve colder waters, cool the surface temperature and thus provide negative feedback on the hurricane intensity. On the atmospheric side, the wind stress is also coupled with the tropical cyclone waves (e.g. Reichl et al., 2014).

Significant implications can expected due to wave-coupled influences in the climate modelling context too. Babanin et al. (2009) implemented a wave-mixing scheme in a climate model of intermediate complexity (CLIMBER-2). It was shown that as a result the seasonal temperature modulations and extremes are significantly enhanced, and this effect combines with changes in the global pressure patterns and leads to large localised alterations of precipitation. Qiao et al. (2010) demonstrated significant improvements in modelling the mixed layer depth and sea surface temperature globally, once the wave-induced mixing was introduced in General Circulation Models.

Wave climate

While influencing large-scale air-sea processes, waves as a small-scale phenomenon are subject to changes at the climate scale themselves. By means of the satellite altimetry, Young et al. (2011) demonstrated trends of the mean and extreme wave heights, as well as of the ocean winds, over the period of more than 20 years. Globally, the trends are positive. Zieger et al. (2014) further used the SSM/I satellite data to study regional and seasonal trends for the surface winds, and identified the months and regions which contribute most to the global growth. Southern Ocean is one of such regions, it shows consistent growth over large area and during a significant part of the year.

Changes to the ocean wind/wave climate further contribute to the complicated pattern of climate variability. If the wind/wave growth is due to the global temperature rise, then, like in the case of the tropical cyclones, it can potentially provide a negative feedback by mixing the ocean deeper, cooling its surface and the atmosphere.

References

Ardhuin, F., B. Chapron, and F. Collard, 2009: Observation of swell dissipation across oceans. *Geophysical Research Letters*, 36, L06607, doi:10.1029/2008GL037030

Babanin, A.V., 2006: On a wave-induced turbulence and a wave-mixed upper ocean layer. *Geophysical Research Letters,* 33, L20605, doi:10.1029/2006GL027308, 6p

Babanin, A.V., 2011: *Breaking and Dissipation of Ocean Surface Waves*. Cambridge University Press, 480p

Babanin, A.V., and D. Chalikov, 2012: Numerical investigation of turbulence generation in non-breaking potential waves. *Journal of Geophysical Research*, 117, C00J17, doi:10.1029/2012JC007929, 14p

Babanin, A.V., and J. McConochie, 2013: Wind measurements near the surface of waves. *Proceedings of the ASME 2013 32ⁿᵈ International Conference on Ocean, Offshore and Arctic Engineering OMAE2013, June 9-14, 2013, Nantes, France*, 6p

Babanin, A.V., A. Ganopolski, and W.R.C. Phillips, 2009: Wave-induced upper-ocean mixing in a climate modelling of intermediate complexity. *Ocean Modelling,* 29, 189-197

Babanin, A.V., M. Onorato, and F. Qiao, 2012: Surface waves and wave-coupled effects in lower atmosphere and upper ocean. *Journal of Geophysical Research*, 117, doi:10.1029/2012JC007932, 10p

Belcher, S.E., A.L. M. Grant, K.E. Hanley, B. Fox-Kemper, L.V. Roekel, P.P. Sullivan, W.G. Large, A. Brown, A. Hines, D. Calvert, A. Rutgersson, H. Pettersson, J.-R. Bidlot, P.A.E.M. Janssen, and J.A. Polton, 2012: A global perspective on Langmuir turbulence in the ocean surface boundary layer. *Geophysical Research Letters*, 39, L18605, doi:10.1029/2012GL052932, 9p

Chalikov, D., and M. Belevich, 1993: one-dimensional theory of the wave boundary layer. *Boundary-Layer Meteorology,* 63, 65-96

Chalikov, D., and S. Rainchik, 2011: Coupled numerical modelling of wind and waves and the theory of wave boundary layer. *Boundary-Layer Meteorology*, 138, 1-41

Ghantous, M., and A.V. Babanin, 2014: Ocean mixing by wave orbital motion. *Acta Physica Slovaca*, 64, 1-56

Hanley, K.E., S.E. Belcher, and P.P. Sallivan, 2010: A global climatology of wind-wave interaction. *Journal of Physical Oceanography*, 40, 1263-1282

Iafrati, A., A.V. Babanin, and M. Onorato, 2013: Modulational instability, wave breaking and formation of large scale dipoles. *Physical Review Letters*, 110184504, 5p

Pleskachevsky, A., M. Dobrynin, A.V. Babanin, H. Gunther, and E. Stanev, 2011: Turbulent diffusion due to ocean surface waves indicated by suspended particulate matter. Implementation of satellite data into numerical modelling. *Journal of Physical Oceanography*, 41, 708-724

Qiao, F., Y. Yuan, T. Ezer, C. Xia, Y. Yang, X. Lu, and Z. Song, 2010: A three-dimensional surface wave-ocean circulation coupled model and its initial testing. *Ocean Dynamics*, 60, 1339–1355

Reichl, B.C., T. Hara, I. Ginis, 2014: Sea state dependence of wind stress over the ocean under hurricane winds. *Journal of Geophysical Research*, 119, 30-51

Toffoli, A., J. McConochie, M. Ghantous, L. Loffredo, and A.V. Babanin, 2012: The effect of turbulence induced by non-breaking waves on the ocean mixed layer: Field observations on the Australian North-West Shelf. *Journal of Geophysical Research*, 117, C00J24, doi:10.1029/2011JC007780, 8p

Young, I.R., S. Zieger, and A.V. Babanin, 2011: Global trends in wind speed and wave height. *Science*, 332, 451-455

Young, I.R., A.V. Babanin, and S. Zieger, 2013: The decay rate of ocean swell observed by altimeter. *Journal of Physical Oceanography*, 43, 2322-2333

Zieger, S., A.V. Babanin, and I.R. Young, 2014: Changes in ocean surface winds with a focus on trends of regional and monthly mean values. *Deep Sea Research Part 1*, 86, doi:10.1016/j.dsr.2014.01.004, 56-67

TOWARDS NWP AT CONVECTION-PERMITTING RESOLUTION AT THE BOM

Gary Dietachmayer, Wenming Lu, Susan Rennie, Peter Steinle, Ilia Bermous, Imtiaz Dharssi, Yimin Ma, Greg Roff , Yi Xiao, Hongyan Zhu, Robin Bowen, Jim Fraser[1], Lawrie Rikus and Michael Naughton

Environment and Research Division, Bureau of Meteorology, Melbourne
[1]Bureau National Operations Centre, Bureau of Meteorology, Melbourne

g.dietachmayer@bom.gov.au

Introduction

In 2009 operational NWP at the BoM saw transformational change through the first introduction of a BoM operational NWP system based around the UKMO "Unified Model" and four-dimensional Variational Data-Assimilation system ("VAR"). This first system was "ACCESS-G" (the *Australian Community Climate and Earth-System Simulator* Global-NWP system). Other component systems for regional, tropical-cyclone, and "city" modelling followed thereafter, making up the initial "APS0" Australian Parallel Suite. The follow-up APS1 suite (Fig. 1) began operational deployment in 2012, and elements of the APS2 suite are planned to become operational by the end of 2015.

APS2 is an important step for operational high-resolution NWP at the BoM, as it marks the first significant improvement in resolution in the city-based systems (from 4-5 km previously, to 1.5 km) since APS0 (and the previous "MesoLAPS" systems).

System Design

APS2 ACCESS-C (hereafter: "C2") is based heavily on the NWP system developed for the SREP FDP (Strategic Radar Enhancement Project / Forecast Demonstration Project), which is similar in design to the UKMO "UKV" 1.5km system. However, unlike SREP and UKV, C2 has no Data-Assimilation component, and instead runs as a purely downscaling system from its nesting parent, ACCESS-R. Data-Assimilation for all ACCESS-C domains (not just the Sydney domain in the SREP FDP) is planned for APS3.

Results and Discussion

The move to 1.5 km resolution in C2, even without DA, is important, as it allows the model to run in "convection permitting" mode in which convection is treated explicitly rather than parameterised, and this mode tends to produce more accurate simulations, particularly for precipitation associated with localised convective events (e.g., Weusthoff et al. 2010). Results for all of the C2 domains will be provided in the workshop presentation, here we focus on the Darwin domain because tropical convection is particularly challenging for parameterised models.

Objective verification of high-resolution NWP precipitation poses its own difficulties – the fine-scale structure of the field leads to "double-counting" of errors in traditional error metrics. To avoid this, we adopt the Fractions Skill Score metric (FSS, e.g., Roberts, 2008) in which errors are calculated as a function of spatial *scale*, and improved model accuracy can be measured as a reduction in the scale at which some particular level of error is achieved. Figure Two shows standard box-and-whisker plots of FSS as a function of horizontal scale for six hour forecasts over the Darwin domain. It demonstrates both the

challenge of numerically predicting rain in these environments on these scales (the C2 forecast achieves a reasonable level of accuracy only on scales of 65 km (light rain) to 175 km (heavy)), *and* the very significant improvement of C2 over a C1 research-prototype system, particularly for heavy rain where C1 performed quite poorly.

This improved statistical performance of C2 over C1 can be readily understood through examination of individual cases, such as that depicted in Figure Three. The C2 forecast has its limitations (which will be addressed to some extent in APS3 with the introduction of city-scale ensembles to capture uncertainty and Data-Assimilation to improve initiation), but does a good job of capturing realistic rainfall intensity, and the spatial scale/structure on which rain occurs. In contrast, the heavily parameterised C1forecast produces mainly light rain as smooth fields over very wide areas, together with "coastal locking" of this early-time rain.

Results for other domains, together with analysis of surface wind and 2m temperature forecasts against BoM surface-observations will be provided in the workshop presentation, along with a brief discussion of some of the limitations of the convection-permitting approach, such as "spin-up" of explicit convection near model boundaries.

References

Nigel Roberts, 2008: Assessing the spatial and temporal variation in the skill of precipitation forecasts from an NWP model. Meteorol. Appl. 15, 163–169.

Tanja Weusthoff, Felix Ament, Marco Arpagaus, and Mathias W. Rotach, 2010: Assessing the Benefits of Convection-Permitting Models by Neighborhood Verification: Examples from MAP D-PHASE. Mon. Wea. Rev., 138, 3418–3433.

Figures
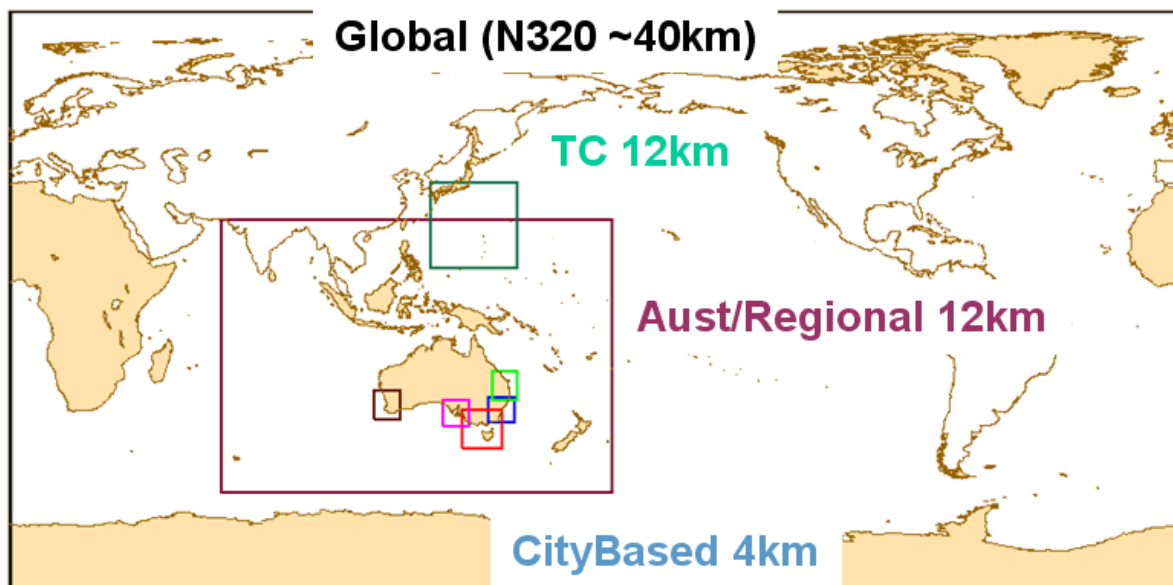
Figure 1: Global ("ACCESS-G"), Regional ("ACCESS-R"), Tropical-Cyclone ("ACCESS-TC"), and "City" ("ACCESS-C") operational NWP system domains and resolutions in APS1.
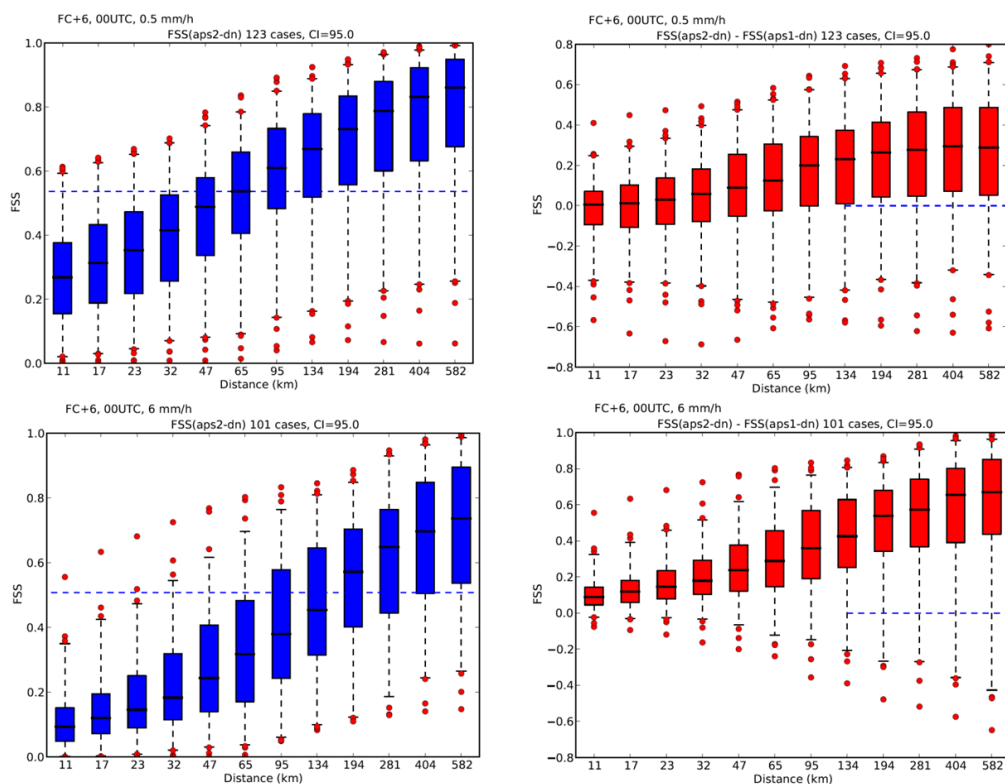
Figure 2: Box-whisker plots of Fractions Skill Score as a function of horizontal length scale. Model data is six-hour forecasts from 00UTC for the Darwin domain. Left column (blue) is for APS2 ACCESS-C (1.5 km), right column is the *difference* between APS2 ACCESS-C and the APS1 research-only ACCESS-C system (4 km) – positive values indicate C2 is more accurate than C1. Top row is light rain (0.5 mm/h), bottom is "heavy" rain (6mm/h).
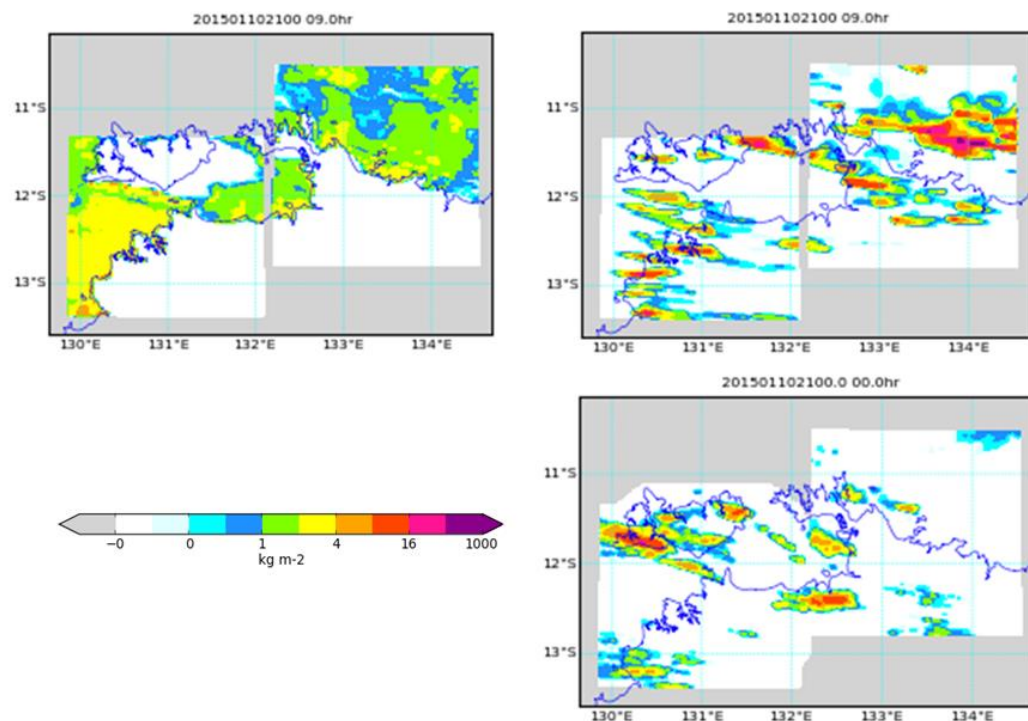
Figure 3: Hourly rainfall-rate over the Darwin radar domain, Jan-10 2015, 2100UTC. Clockwise, from top-left: nine-hour forecast from the APS1 research-only ACCESS-C system (4 km), nine-hour forecast from APS2 ACCESS-C (1.5 km), and radar/rain-gauge blended observations.

ACCESS ENSEMBLE NWP STATUS AND PLANS

Michael Naughton, David Smith and Asri Sulaiman

Environment and Research Division, Bureau of Meteorology, Melbourne

m.naughton@bom.gov.au

Abstract

Ensemble NWP systems have been in use operationally in weather centres internationally since 1993 (Toth and Kalnay, 1993; Molteni et al., 1996). In the Bureau they have been developed and run since the late 1990's, in the GASP and LAPS systems, although they never became fully operational. Then, with the switch to ACCESS, the "AGREPS" version of the UKMO UM MOGREPS system (Bowler et al., 2009) has been developed since 2007, running regularly since 2009. The current system, now called ACCESS-GE, for global ensemble, to distinguish it from the deterministic assimilation-forecast ACCESS-G system, is a 24-member ensemble at 60 km (N216) horizontal resolution, with 70 vertical levels, producing 10-day forecasts twice daily. Initial condition perturbations are calculated using the Ensemble Transform Kalman Filter method with model perturbations using SKEB2 stochastic backscatter and a random physics parameter scheme. The system model uses as inputs analyses and observations from the APS2 pre-operational ACCESS-G 25 km (N512) system, scheduled to become operational in October. The APS2 ACCESS-GE system has been running in research and development modes since 2013, although up until recently it has been using APS1 ACCESS-G N320 inputs. APS2 ACCESS-GE is scheduled to become operational by the end of 2015.

One of the often-used products from NWP ensembles is the ensemble mean, i.e. the forecast formed by taking the mean of all ensemble members. Figure 1 shows the forecast skill of the 1-10 day 850 hPa temperature ensemble mean forecasts, averaged for the month of January 2015, over the 20-90S Southern Hemisphere domain, measured in terms of the root mean square (RMS) error relative to the ACCESS-G analyses. Also plotted are the operational APS1 ACCESS-G deterministic forecast skill, and the RMS spread of the ensemble members relative to the ensemble mean. This shows that after the first 24 hours the ensemble mean is as or more skilful forecast than the deterministic forecast it is based on, and that the spread of the ensemble is in the mean approximately commensurate with the difference between the ensemble mean forecast and the verifying analysis. Figure 2 shows the same skill-spread comparison, for mean sea level pressure, compared with the operational EPS systems from the European (ECMWF), Japanese (JMA) and USA (NCEP) centres.

ACCESS-GE produces a typical range of ensemble products: individual member forecast charts, threshold exceedance probabilities for a rainfall, temperature and winds, and EPSgram time traces of forecasts at specific locations. Operationally, the forecasts will be provided to Bureau operational forecast offices through the VisWeather chart viewing system.

A number of high impact weather displays and applications have been developed, or are planned to be, making use of ACCESS-GE forecasts. These include tropical cyclone strike probability plots, volcanic ash transport modelling, severe thunderstorm forecast guidance, very high resolution bushfire modelling, East Coast low severe rainfall downscaled forecasts, and statistical rainfall forecasting.

Future plans for the ACCESS ensemble are to remain aligned with the UKMO NWP ensemble direction. For APS3 (2017–2018), the plan is to increase the ACCESS-GE ensemble to 4 times daily N400 (33 km), or possibly N512 (25 km), resolution, and to remove the "Limited" tag by enhancing the products and

applications to make more comprehensive use of the ensemble forecasts. It is also planned to introduce an operational ACCESS-CE 2.2 or 1.5 km high resolution ensemble version of ACCESS-C. As with the phased introduction of the global ensemble, in APS3 this is initially tagged as a "Limited" system, then progressing to a full system in APS4 (2019). General plans beyond this are to continue these systems, with the details dependent on current UKMO research in ensemble data assimilation.

Acknowledgements
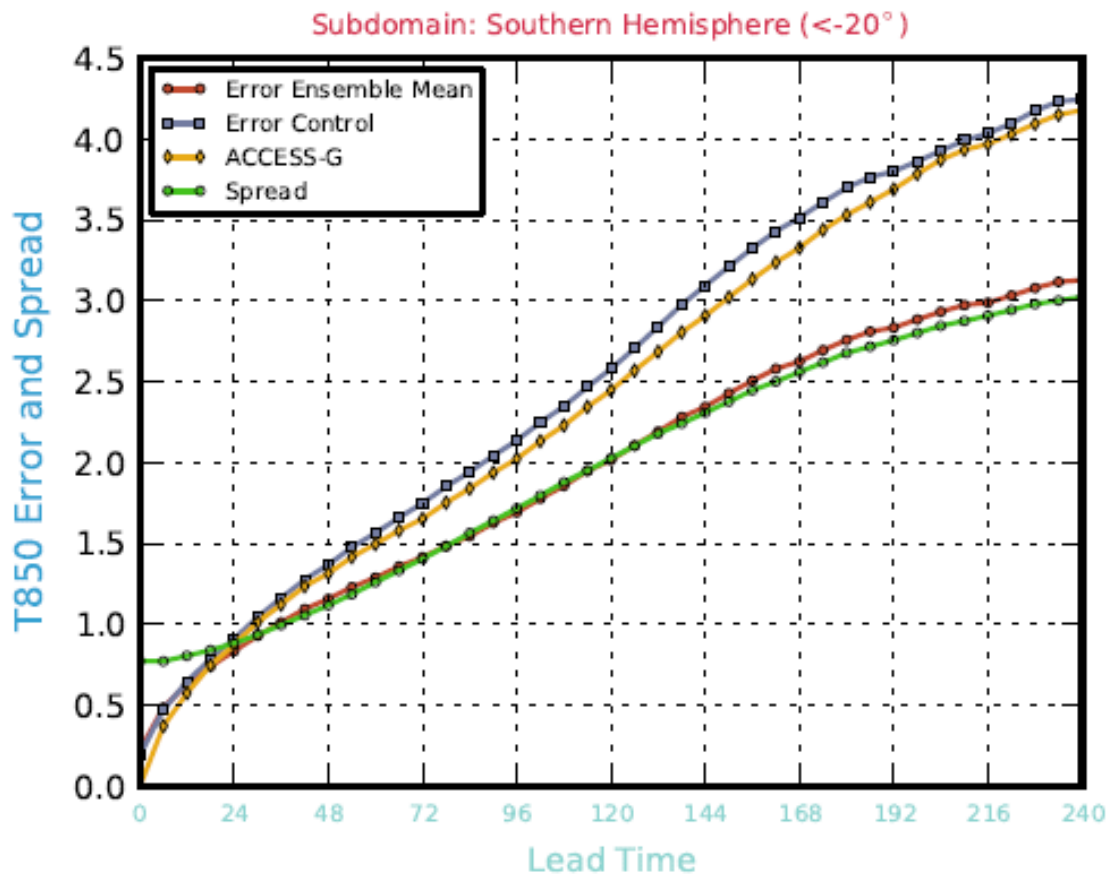
Figure 1: 850 hPa temperature root mean square (RMS) verification against analyses for the Southern Hemisphere region from 20-90S, averaged for the month of January 2015, for ACCESS-GE ensemble mean forecast (red), compared with deterministic ACCESS-G forecast (gold), ACCESS-GE control forecast (blue) and the RMS ensemble spread relative to the ensemble mean (green).
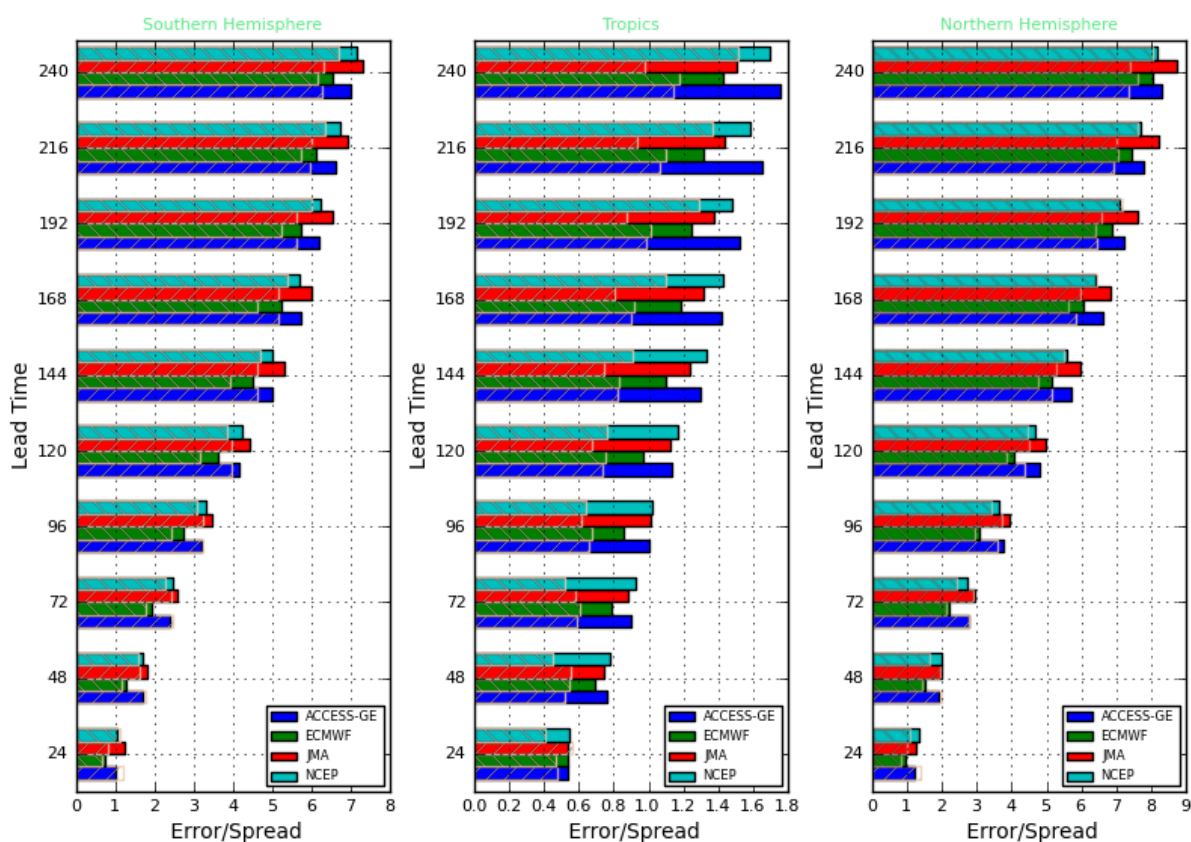
Figure 2: Comparison of ACCESS-GE mean sea level pressure (MSLP) forecast errors and spread with ECMWF, JMA and NCEP EPS systems for January 2015, for Southern Hemisphere (20-90S), Tropics (20S-20N) and Northern Hemisphere (20-90N) domains. Error is indicated by the main horizontal bars, within which spread is shown as diagonal hatching.

References

Bowler, N.E., A. Arribas, S.E. Beare, K.R. Mylne, and G.J. Shutts, 2009: The local ETKF and SKEB: upgrades to the MOGREPS short-range ensemble prediction system. Quart. J.R. Meteor. Soc., **135**, 767 - 776.

Molteni, F., R. Buizza, T.N. Palmer and T. Petroliagas, 1996: The ECMWF Ensemble Prediction System: Methodology and validation. Quart. J.R. Meteor. Soc., **122**, 73-119.

Toth, Z. and E. Kalnay, 1993: Ensemble Forecasting at the NMC: The generation of perturbations. Bull. Amer. Meteor. Soc., **74**, 2317-2330.

Wang, X. and C.H. Bishop, 2003: A comparison of breeding and ensemble transform Kalman filter ensemble forecast schemes. J. Atmos. Sci., **60**, 1140-1158.

FROM DIURNAL VARIABILITY TO LAND-ATMOSPHERE INTERACTIONS: IMPLICATIONS FOR HIGH RESOLUTION MODELING

L. Ruby Leung

Pacific Northwest National Laboratory

Ruby.Leung@pnnl.gov

Abstract

This presentation explores the prospects for high resolution to improve modeling of land processes and land-atmosphere interactions. As land surface heterogeneities associated with topography, soil, and vegetation have important influence on surface hydrology, increasing model resolution has been shown to generally improve land surface model fidelity. Comparing simulations performed using the Community Land Model (CLM) on regular latitude/longitude grids versus unstructured grids following the boundaries of watersheds at a range of resolution between $1/8^o$ and 1°, we showed statistically significant improvement in model scalability using the latter approach of simulating soil hydrology. These suggest that increasing model resolution and using unstructured "watershed" grids may improve land surface model skill in simulating soil moisture, which has important control on the partitioning between surface sensible and latent heat fluxes, and hence land-atmosphere interactions. However, interactions between soil moisture and the boundary layer depend on the relative controls of surface and atmospheric conditions on the development of clouds and convection. Hence the sensitivity of atmosphere models to resolution also plays an important role in modeling land-atmosphere interactions.

The sensitivity of atmosphere and land-atmosphere interactions to model resolution is explored over the central U.S. where organized convection is a ubiquitous mechanism for generating precipitation in the warm season. The U.S. Great Plains is frequented by Mesoscale Convective Systems (MCSs) that develop due to upscale growth of convective disturbances that form near and propagate away from the Rocky Mountains. The MCSs consist of a spectrum of cloud types, ranging from squall lines with trailing stratiform precipitation to more random patterns of convection combined with extensive stratiform rain area. In general, the diurnal cycle of convection depends on the scale of the convective phenomenon. Small convection is short-lived and corresponds directly to the solar heating cycle, whereas larger systems have lifetimes ~tens of hours and have diurnal cycles that are frequently out of phase with the solar cycle. Using the Weather Research and Forecasting (WRF) model at 12 km and 4 km resolution with parameterized and explicitly simulated convection over the U.S., we investigate the impacts of non-hydrostatic dynamics, topography, and representations of convection on simulations of diurnal precipitation. Separating summer days into wet and dry regimes based on soil moisture state in the Great Plains, we evaluate the impacts of model resolution on land-atmosphere interactions due to differences in diurnal precipitation variability captured by the model.

INTERACTIONS BETWEEN LAND CARBON, CLIMATE, AND AEROSOLS IN ACCESS-ESM1 HISTORICAL SIMULATIONS

Rachel M. Law[1], Tilo Ziehn[1] and Peter F. Vohralik[2]

[1]*CSIRO Oceans and Atmosphere, Aspendale, Victoria.*
[2]*CSIRO Manufacturing, Lindfield, New South Wales*

rachel.law@csiro.au

Introduction

Earth system model (ESM) simulations, such as those submitted to the Coupled Model Intercomparison Project (CMIP5), show a positive feedback between climate change and the carbon cycle. Typically, while the oceans continue to take up carbon as atmospheric CO_2 increases into the future, land vegetation transitions from a carbon sink to a carbon source, as respiration increases with increasing temperature. However the magnitude of the carbon-climate feedback is very variable across ESMs (Friedlingstein et al., 2014), primarily driven by variability in the land to atmosphere carbon exchange.

The Australian Community Climate and Earth System Simulator (ACCESS) participated in CMIP5 but did not have the capability for simulating carbon fluxes. This capability has now been added, giving a model version named ACCESS-ESM1 (Law et al., 2015). Land carbon is simulated using the Community Atmosphere Biosphere Land Exchange (CABLE) model including the CASA-CNP biogeochemical module. Ocean carbon is simulated using the World Ocean Model of Biogeochemistry And Trophic-dynamics (WOMBAT). A selection of key CMIP5 simulations have been performed with ACCESS-ESM1, some use prescribed atmospheric CO_2 while others used prescribed anthropogenic carbon emissions and simulate the atmospheric CO_2. Here the focus will be on the historical period using prescribed atmospheric CO_2 and on the land carbon simulation.

Model simulations

ACCESS-ESM1 has been run in two land configurations. In the first, the leaf area index (LAI) is prescribed, while in the second, the LAI is prognostic, determined from the size of the simulated leaf carbon pool, which in turn depends on carbon gained through photosynthesis and lost through respiration. In both cases, nutrient (nitrogen and phosphorus) cycles are simulated, allowing for these nutrients to limit land carbon uptake. Pre-industrial simulations have been run for 1000 years, which is mostly sufficient for the land carbon pools to spin-up. The prognostic LAI case results in a slightly warmer atmosphere (~0.4°C) than in the prescribed LAI case, due to the influence of LAI on the exchange of momentum, energy and water between the land and the atmosphere.

An ensemble of three historical simulations (1850-2005) has been performed with the prognostic LAI case, starting from years 801, 811 and 821 of the pre-industrial simulation. Through this period, the prescribed atmospheric CO_2 increases from 285 to 379 ppm, and anthropogenic aerosols also increase. Volcanic eruptions are prescribed by perturbing the stratospheric aerosol optical depth in four equal area latitude bands. An additional historical simulation, starting from year 801, is run without anthropogenic aerosols.

Results and discussion

The ACCESS-ESM1 surface climate, represented by screen level air temperature and precipitation, evolves through the historical period much as previously published results for ACCESS1.3 (Lewis et al.,

2014). The land temperature anomaly (relative to 1901-1930) reaches around 0.8°C by 2005, with temperature anomalies somewhat lower than observed from 1965-2000. As noted by Lewis et al. (2014), this is attributed to strong aerosol cooling and supported by Rotstayn et al. (2015) who found ACCESS1.3 had a more negative aerosol effective radiative forcing than most CMIP5 models. Land precipitation anomalies also deviate from observations post 1960, being drier in the model simulations than observed. In addition to cooling from anthopogenic aerosols, major volcanic eruptions during the historical period tend to result in cooler and drier conditions for 1-2 years following the eruption.

The response of the land carbon cycle is shown in Figure 1. Gross primary production (GPP), the total land carbon uptake due to photosynthesis, grows by ~19% over the historical period largely driven by increasing atmospheric CO_2 (the so-called CO_2 fertilisation effect). Total respiration (not shown) also grows, both due to the increasing carbon biomass and due to increasing temperature. Thus the net land flux to the atmosphere is relatively small, mostly negative (i.e. a carbon sink) and variable. The sink appears to reach maximum uptake around 1960-1995 and then weakens.

Major volcanic events are generally associated with a positive GPP anomaly resulting in periods of larger net land carbon uptake. Cooling tends to increase photosynthesis in the tropics and reduce respiration globally. The resulting increase in the leaf carbon pool increases leaf area index, further increasing GPP and net land carbon uptake. The feedback through LAI is important; an historical simulation with prescribed LAI gives much smaller land carbon anomalies following the volcanoes.
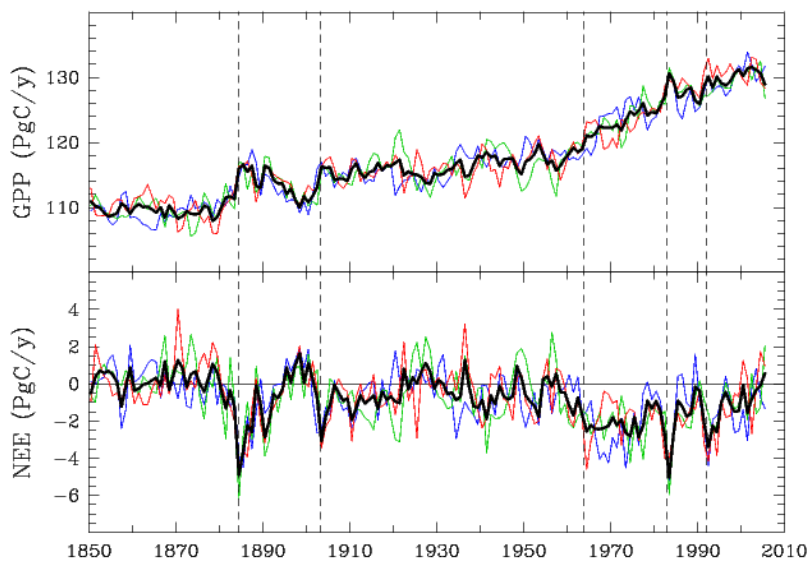
Figure 1: Annual gross primary production (GPP) (upper) and net ecosystem exchange (NEE) (lower) for each ensemble member (coloured lines) and the ensemble mean (bold, black). The units are PgCy^{-1}. Vertical lines mark the times of peak stratospheric aerosol loading for the (left-right) Krakatoa, Santa Maria, Agung, El Chichón and Pinatubo volcanoes.

Land carbon fluxes also respond to natural climate variability, such as that associated with the El Niño-Southern Oscillation (ENSO). We have estimated the sensitivity of the simulated land carbon fluxes to interannual temperature and precipitation anomalies by performing a multiple linear regression of 1915-1960 (avoiding volcanoes) detrended NEE with detrended land temperature and land precipitation. The three ensemble members show relatively similar sensitivity of NEE interannual variability (IAV) to temperature IAV at 4.3-5.1 PgCy^{-1}°C^{-1} (standard error of ~0.8 PgCy^{-1}°C^{-1}) but more variable sensitivity to precipitation IAV at -0.05 to -0.01 PgCy^{-1}mm^{-1} (0.01 PgCy^{-1}mm^{-1} standard error).

Simulated land carbon uptake can be compared to Global Carbon Project (GCP) estimates of the residual land sink (Le Quéré et al., 2015) from 1959 onwards. Mean uptake is comparable, but the temporal

evolution likely differs with reduced uptake in the model simulations from 2000 but increasing uptake in the GCP estimates. We will investigate whether increasing anthropogenic aerosols influence the land carbon simulation particularly from the 1960s.

Conclusions and future work

Land carbon uptake simulated by ACCESS-ESM1 clearly responds to climate variability, whether generated internally or forced through stratospheric aerosol perturbations from volcanic eruptions. The impact of longer-term cooling due to tropospheric aerosols remains to be quantified, and as yet, the model does not account for other effects of aerosols on land carbon fluxes, for example through aerosol deposition onto vegetation.

ACCESS-ESM1 simulations have also been run to 2100 under RCP4.5 and RCP8.5 scenarios and prescribed atmospheric CO_2 and for 1850-2100 using historical and RCP8.5-equivalent CO_2 emissions and simulated atmospheric CO_2. Detailed analyses of these simulations will be the focus of future work.

References

Friedlingstein, P., M. Meinshausen, V. K. Arora, C. D. Jones, A. Anav, S. K. Liddicoat, and R. Knuitti, Uncertainties in CMIP5 Climate Projections due to Carbon Cycle Feedbacks, J. Climate, 27, 511–526, 2014.

Law, R. M., T. Ziehn, R. J. Matear, A. Lenton, M. A. Chamberlain, L. E. Stevens, Y.-P. Wang, J. Srbinovsky, D. Bi, H. Yan and P. F. Vohralik, The carbon cycle in the Australian Community Climate and Earth System Simulator (ACCESS-ESM1). 1. Model description and pre-industrial simulation, Geosci. Model Dev. Disc., 8, 8063-8116, doi:10.5194/gmdd-8-8063-2015,2015.

Le Quéré, C., R. Moriarty, R. M. Andrew, G. P. Peters, P. Ciais, P. Friedlingstein, S. D. Jones, S. Sitch, P. Tans, A. Arneth, T. A. Boden, L. Bopp, Y. Bozec, J. G. Canadell, L. P. Chini, F. Chevallier, C. E. Cosca, I. Harris, M. Hoppema, R. A. Houghton, J. I. House, A. K. Jain, T. Johannessen, E. Kato, R. F. Keeling, V. Kitidis, K. Klein Goldewijk, C. Koven, C. S. Landa, P. Landschützer, A. Lenton, I. D. Lima, G. Marland, J. T. Mathis, N. Metzl, Y. Nojiri, A. Olsen, T. Ono, S. Peng, W. Peters, B. Pfeil, B. Poulter, M. R. Raupach, P. Regnier, C. Rödenbeck, S. Saito, J. E. Salisbury, U. Schuster, J. Schwinger, R. Séférian, J. Segschneider, T. Steinhoff, B. D. Stocker, A. J. Sutton, T. Takahashi, B. Tilbrook, G. R. van der Werf, N. Viovy, Y.-P. Wang, R. Wanninkhof, A. Wiltshire, and N. Zeng: Global carbon budget 2014, Earth System Sci. Data, 7, 47–85, doi:10.5194/essd-7-47-2015,2015.

Lewis, S. C. and D. J. Karoly, Assessment of forced responses of the Australian Community Climate and Earth System Simulator (ACCESS) 1.3 in CMIP5 historical detection and attribution experiments, Aust. Meteor. Oceanogr. J., 64, 87-101, 2014.

Rotstayn, L. D, M. A. Collier and J.-J. Luo, Effects of declining aerosols on projections of zonally averaged tropical precipitation, Environ. Res. Letts., 10, 044018, 2015.

INVESTIGATING SEA SURFACE TEMPERATURE DIURNAL VARIATION OVER THE TROPICAL WARM POOL USING MTSAT-1R DATA

Haifeng Zhang[1,3], Helen Beggs[2], Leon Majewski[2], Xiao Hua Wang[1], Andrew Kiss[1,3]

[1]*The Sino-Australian Research Centre for Coastal Management, School of Physical, Environmental and Mathematical Sciences, UNSW Canberra @ ADFA, ACT 2610, Australia,*
[2]*Bureau of Meteorology, Docklands, VIC 3008, Australia*
[3]*ARC Centre of Excellence for Climate System Science*

haifeng.zhang@student.adfa.edu.au

Introduction

Diurnal variation (DV) of sea surface temperature (SST) plays an important role in air-sea interaction. The parameterization of DV events is potentially useful in air-sea coupled models for weather, seasonal and climate scales. The Tropical Warm Pool (TWP) in the Eastern Indian and Western Pacific Oceans experiences particularly high diurnal warming of the sea surface temperature, exceeding 5°C under low wind speed and high solar insolation conditions. It is therefore considered to be an ideal region for a coordinated study of DV using observations and models.

Data

The dataset used in this study is the four months (January – April 2010) Australian Bureau of Meteorology (Bureau) reprocessed version 3 (v3) Multi-functional Transport Satellite-1R (MTSAT-1R) data with 4 km resolution (Beggs et al., 2013). This data set is a contribution to the "TWP+ data set", a comprehensive dataset (1 January to 30 April 2010) used to quantify DV events and test DV models as part of the Group for High Resolution SST (GHRSST) Tropical Warm Pool Diurnal Variability (TWP+) Project. Further information can be found at https://www.ghrsst.org/ghrsst/tags-and-wgs/dv-wg/twp/.

Before the v3 MTSAT-1R data are used for characterization of the DV events, the validation, including both in-situ validation and cross-validation, is first conducted. For in-situ validation, drifting buoy data within the same period, also obtained from the TWP+ data set, are used. For the cross-validation, the Advanced Along-Track Scanning Radiometer (AATSR) data are utilised. The exact version used in this study is the ARC (ATSR Reprocessing for Climate) v1.1 (Embury et al., 2012).

Other data sets, including the wind speed data and the solar shortwave insolation (SSI) data, are obtained from the Bureau's ACCESS-R (Australian Community Climate and Earth System Simulator-Regional) model.

Validation

In general, validation results show that this v3 MTSAT-1R data set is of fine quality and suitable for SST DV investigations. In the in-situ validation, a 0.003ºC bias and a 0.727ºC standard deviation (STD) are found (Table 1). Minimal day-night biases are revealed by the constant biases (within ±0.25ºC) over the local 24-hour time period. In the meanwhile, in both validation works, an overestimation at low SST conditions (in-situ SST < 27ºC) and underestimation at high SST conditions (in-situ SST > 31ºC) are discovered.

Table 1. Parameters of both in-situ validation and cross-validation. Num represents the number of collocations, STD the standard deviation of the bias, SI the scatter index, R the correlation coefficient and MAD the Median Absolute Difference. In the in-situ validation, daytime is defined from 7:00 to 19:00 Local Solar time (LST) and night-time from 19:00 to 7:00 LST, while in the cross-validation day/night times refer to 10:00/22:00 LST, i.e. local equator crossing times of the AATSR sensor.

		Num	Bias (ºC)	STD (ºC)	SI	R	MAD (ºC)
INSITU	Day	1138	-0.064	0.712	0.026	0.845	0.410
	Night	988	0.080	0.737	0.026	0.902	0.410
	All	2126	0.003	0.727	0.026	0.883	0.410
AATSR	Day	292489	-0.045	0.48	0.017	0.944	0.287
	Night	236639	0.063	0.48	0.017	0.934	0.300
	All	529128	0.003	0.483	0.017	0.940	0.293

Characterization of SST DV events

Using the validated four months v3 MTSAT-1R data, the SST DV events (i.e. the SST rise and fall within a local 24-hour period) over the TWP region are studied. Several concepts should be illustrated first:

(1) SSTfnd: a concept defined by the Group for High Resolution SST (GHRSST) which refers to the temperature free of diurnal temperature variability. In this study, it is calculated as the average value of the values from 0:30 to 5:30 LST.

(2) dSST: the daily SST variation at a given time within a solar day, calculated as the difference between that SST value and the SSTfnd.

(3) dSSTmax: the maximum dSST at one grid point within one solar day.

The monthly mean dSSTmax, the occurrence of dSSTmax larger than 1ºC, monthly mean wind speed, and monthly mean SSI are seen in Figure 1. It is shown that generally, large DV events occur where the wind speed is low and SSI is high.
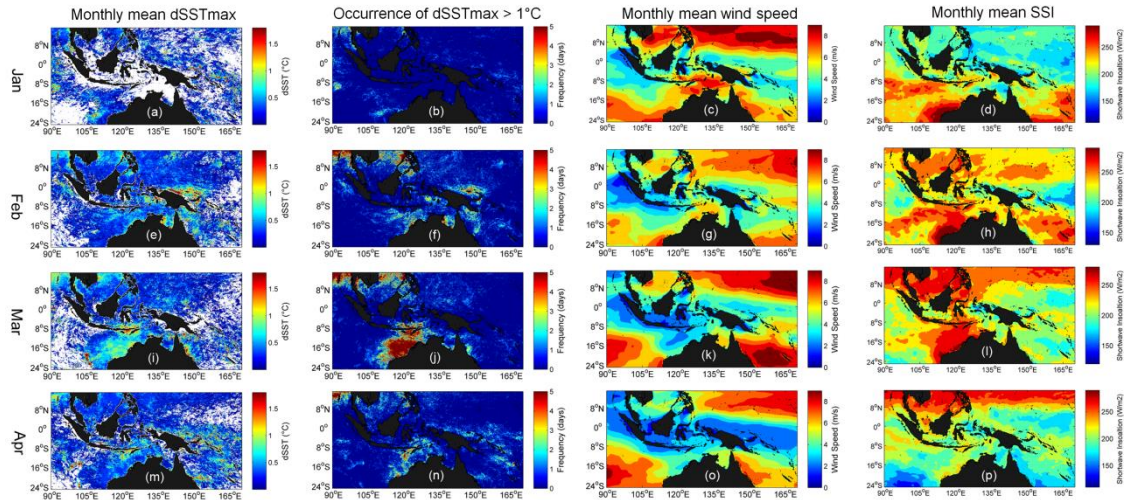
Figure 1. Spatial distribution of all four months in 2010: (a) monthly mean dSST$_{max}$ for January; (b) frequency (days in a month) of dSST$_{max}$ > 1ºC for January; (c) monthly mean daytime (7:00-19:00 LST) wind speed for January; (d) monthly mean daytime (7:00-19:00 LST) SSI for January. The second, third, and fourth rows are the same as the first but for February, March, and April respectively.

The SST DV amplitudes under different wind speed conditions are shown in Figure 2. For wind speeds smaller than 3 ms^{-1}, the monthly mean DV amplitudes are between 1ºC – 1.2ºC. The values reduce to 0.4 ºC – 0.6 ºC when the wind speed is higher than 3 ms^{-1} but smaller than 6 ms^{-1}. If the wind speed is even higher (larger than 6 ms^{-1}), the diurnal cycles are no longer evident.
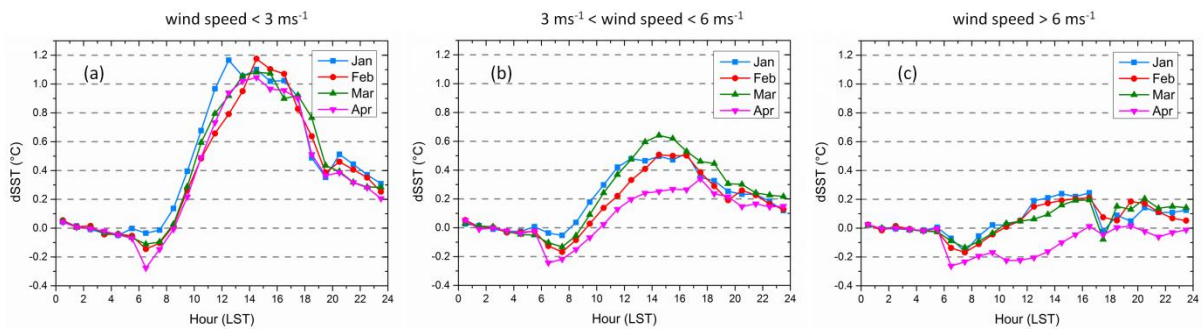
Figure 2. Monthly shape of the diurnal cycles under different wind speed conditions: (a) wind speed < 3 ms^{-1}; (b) 3ms^{-1} < wind speed < 6 ms^{-1}; (c) wind speed > 6 ms^{-1}. Wind speeds are the mean daytime (7:00-19:00 LST) values. The dSSTs at each hour is the average of all measurements calculated.

The relationship between the DV amplitudes and wind speed/SSI values is also investigated. Results show that DV amplitudes are the largest when the wind speed is low and SSI is high (Figure 3). The dominant

role of wind speed is revealed by its larger correlation coefficient with dSSTmax (a negative 0.7) than the correlation coefficient between SSI and dSSTmax (a positive 0.4).
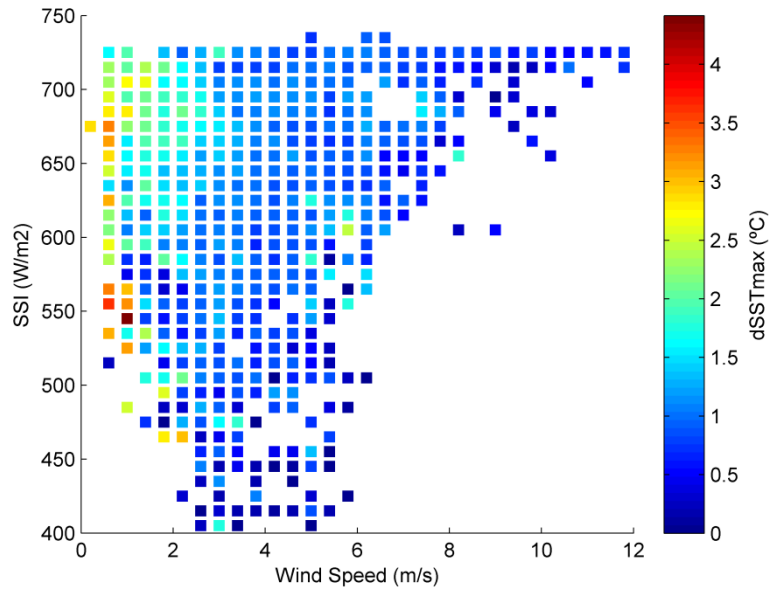
Figure 3. Relationship between dSSTmax and the daily mean SSI and wind speed is investigated by pixels in the selected region and time period (four days from 5-8th March). Shown in the figure are the average dSSTmax values over each 10 Wm^{-2}×0.4 ms^{-1} bin. Note that the SSI starts at 400 Wm^{-2} as there are few pixels falling below this value which are therefore cancelled. Also the daily mean wind speed and SSI are the average values of 7:00 to 19:00 LST.

Conclusions

The validation results indicate that the v3 MTSAT-1R data set is suitable for SST DV investigations and validation of DV models. Plausible relationships are found between DV events and low wind and high SSI conditions, respectively. The dominant role of wind speed in SST DV events over the SSI is also revealed.

References:

Beggs, H., L. Majewski, C. Griffin, R. Verein, P. Sakov, X. Huang, L. Garde, and C. Tingwell, 2013: Report to GHRSST14 from Australia - Bluelink and IMOS, In: Proceedings of the GHRSST XIV Science Team Meeting, Woods Hole, USA, 17 - 21 June 2013, 104-121.
https://www.ghrsst.org/documents/q/category/ghrsst-science-team-meetings/ghrsst-xiv-woods-hole-ma-usa/

Embury, O., C. J. Merchant, and G. K. Corlett, 2012: A reprocessing for climate of sea surface temperature from the along-track scanning radiometers: initial validation, accounting for skin and diurnal variability effects. *Remote Sens. Environ.*, 116, 62–78, doi:10.1016/j.rse.2011.02.028.

EVALUATION OF LAND SURFACE MODELS AGAINST FLUXNET OBSERVATIONS

Gab Abramowitz

Climate Change Research Centre, UNSW and ARC Centre of Excellence for Climate System Science

gabriel@unsw.edu.au

Abstract

Land surface models (LSMs) are designed to run on global and regional grids, coupled to a boundary layer and atmospheric model. In this coupled mode, a range of observationally-based gridded products exist that can provide information about LSM performance in the historical period. These might cover components of the surface radiation budget, water and carbon cycles, as well as surface temperature and precipitation.

Evaluation data uncertainty: Evaluating the key prediction variables of LSMs in the context - for example sensible and latent heat fluxes - is not straightforward. Uncertainties in gridded evaluation data, typically derived from satellite radiance measurements, are also considerable, especially when variability amongst competing products of the same surface variable is included. In this light, 'diagnostic evaluation' - evaluating a model with enough precision and accuracy to be able to pinpoint causes of poor performance - is not normally possible.

Diagnosis in a coupled environment: Even in the improbable case that uncertainty in a gridded product were infinitesimally small, diagnostic evaluation using such a product would still be very difficult. In the coupled environment, the behaviour of a modelling system is a function of the quirks of not only the individual component models making up the coupled system, but the peculiar way in which these components interact. A certain sensitivity of a LSM may only be evident in the presence of a particular group of atmospheric models, for example. In this case, how should we apportion the blame for any identified mismatch between a modelled and 'observed' variable? The variable values are an emergent property of the feedbacks and sensitivities of the entire modelling system, and may well reflect something other then the LSM being evaluated. This is essentially the problem of "confirmation holism" outlined by Lenhard and Winsberg (2010).

Diagnosis in an offline environment: A similar problem applies to LSMs driven offline with prescribed forcing. Meaningful evaluation is contingent upon the fidelity of the gridded forcing data. With several instances of one product's precipitation averages being below another's latent heat flux averages for some regions, the potential for misdiagnosis is clear.

Compensating processes: In the even less likely case of an offline forced experiment with both forcing and evaluation data being error free, we still face considerable hurdles. Attempts at alternative representations of process (or additional process representations), for example, may well result in improvements in common metrics, but we have little ability to categorically state that this improvement is for the right reasons, rather than the result of compensating biases. This issue is compounded by gridded evaluation data products typically being at monthly timescales. The potential for inappropriately compensating processes to arrive at the right aggregated mean flux is very real.

Parameter identifiability: Prescribing LSM parameter values for gridded simulations also presents a range of challenges. Very few of the 30-50 parameters that most modern LSMs require are identifiable at either global or regional scales. In this context, aggregating assumptions about process dependence are made, usually in the form of a small number of vegetation and soil 'types'. This typically reduces the complexity of required spatially varying information to two or three dimensions. The cost of this simplification – using parameter values that are markedly more homogenous and less likely to be precisely appropriate – is relatively unknown. What is clear though, is that is it makes the goal of diagnostic evaluation notably more difficult.

It is in this light that I wish to argue in defence of flux tower data and its unique capacity to fulfil a diagnostic evaluation role. While flux tower data is admittedly at a spatial scale at the very high-resolution extreme of potential LSM applications, it nevertheless has a number of important features that lend it to this diagnostic role:

1. Coincident measurement of (a) a complete set of driving meteorological forcing variables and (b) key prediction fluxes (e.g. latent and sensible heat fluxes), and (c) enough detail of vegetation and soil properties to tightly constrain LSM parameter values;
2. Very high temporal resolution measurements, giving reasonably representative values when averaged up to a typical time step size of a LSM (e.g. half an hour);
3. Broad coverage across vegetation, soil and climate types internationally - more than 500 sites;
4. Established national and international networks between individual data collectors that generally promote data sharing;
5. A maturing collection of data processing and gap-filling methodologies.

Of particular interest is the recent demonstration of consistent empirical relationships between meteorology and latent and sensible heat flux across flux tower sites with different vegetation types and climate regimes (Best et al, 2015; Haughton et al, in review). This work showed that LSMs were not utilising the information available in meteorological forcing about surface fluxes, and that significant gains in LSM performance are clearly attainable.

This talk will try to provide examples of flux tower based evaluation that illustrate these differences, and discuss how known issues with flux tower data, such as energy conservation problems, might affect results.

I'll try to argue that while gridded products provide data to evaluate LSMs at more appropriate spatial scales, we should consider whether flux tower data may indeed provide a much richer source of information for diagnostic LSM evaluation.

The topic for the abstract and talk, while open-ended and at least potentially nebulous, was suggested by the workshop organisers. I thank them for doing this – by interpreting it broadly I hope it will make for an interesting discussion.

References

Best, M.J., G. Abramowitz, H.R. Johnson, A.J. Pitman, G. Balsamo, A. Boone, M. Cuntz, B. Decharme, P.A. Dirmeyer, J. Dong, M. Ek, Z. Guo, V. Haverd, B.J.J van den Hurk, G.S. Nearing, B. Pak, C. Peters-Lidard, J.A. Santanello Jr, L. Stevens, N. Vuichard (2015) The plumbing of land surface models: benchmarking model performance, *Journal of Hydrometeorology*, 16, 1425-1442.

Haughton, N., G. Abramowitz, A.J. Pitman, D. Or, M.J. Best, H.R. Johnson, G. Balsamo, A. Boone, M. Cuntz, B. Decharme, P.A. Dirmeyer, J. Dong, M. Ek, Z. Guo, V. Haverd, B.J.J. van den Hurk, G. S.

Nearing, B. Pak, J.A. Santanello Jr., L.E. Stevens, N Vuichard The plumbing of land surface models: why are models performing so poorly? *Journal of Hydrometeorology*, in review.

Lenhard, J. and E. Winsberg (2010), Holism, entrenchment, and the future of climate model pluralism, *Studies in History and Philosophy of Modern Physics*, 41, 253–262.

EXPLORING AND ATTRIBUTING AUSTRALIAN CARBON CYCLE RESPONSES TO WATER AVAILABILITY

Vanessa Haverd

CSIRO, Oceans and Atmosphere, Yarralumla, Australia

vanessa.haverd@csiro.au

Abstract

There is compelling new evidence that semi-arid ecosystems are playing a pivotal role in the inter-annual variability and greening trend of the global carbon cycle (Ahlström et al. 2015). The situation is exemplified by the vast inland region of Australia, the driest inhabited continent. Using a global model, Poulter et al. (2014) inferred that Australian ecosystems contributed 57% of a record global carbon uptake anomaly in 2011, and have entered a regime of enhanced sensitivity to rainfall since the mid-1990s. Here we present new observation-based evidence confirming the significant role of Australian ecosystems in the 2011 carbon sink anomaly. Our results do not, however, support a shift in sensitivity of vegetation activity to rainfall. Carbon stocks in semi-arid systems are robust to native, year-to-year fluctuations of rainfall. Our evidence suggests that large episodes of carbon cycle variability, like the 2011 anomaly, are driven by pulse-response behaviour of the drought-adapted biota in response to inter- or multi-annual variations in rainfall amount.

Our results are based on a model-data-fusion approach, in which the CABLE land surface model, applied to Australia at 0.05 degree spatial resolution, is constrained by multiple observation types. We will demonstrate the model performance against data from the OzFlux network of flux sties. Further we show that improved representations of coupled soil-canopy processes, developed in the Australian context, afford large improvements to CABLE predictions at globally distributed Fluxnet sites.

References

Ahlström, A. et al., 2015: The dominant role of semi-arid ecosystems in the trend and variability of the land CO2 sink, Science 348, 895-899, doi:10.1126/science.aaa1668

Poulter, B. et al., 2014: Contribution of semi-arid ecosystems to interannual variability of the global carbon cycle, Nature 509, 600-603, doi:10.1038/nature13376

GLOBAL TERRESTRIAL ECOSYSTEM CARBON STORAGE DYNAMICS PROJECTED BY CABLE ARE TRACEABLE BY A TRACEABILITY FRAMEWORK

Xingjie Lu[1], Yiqi Luo[2] and Zheng Shi[2], Lifen Jiang[2], Junyi Liang[2], Will Wider[3] and Ying-Ping Wang[1]

[1]CSIRO Ocean and Atmosphere, Aspendale, Victoria
[2]Department of Microbiology and Plant Biology, University of Oklahoma, Oklahoma, USA
[3]Climate and Global Dynamics Division, National Center for Atmospheric Research, Boulder, Colorado 80307, USA

Chris.lu@csiro.au

Abstract

Modelled changes of terrestrial carbon storage are highly uncertain (Todd-Brown et al., 2014; Tian et al., 2015; Wieder et al., 2015). The uncertainty could be further propagated into projected further climate change. It is very urgent to quantify the contribution of model structure differences to the uncertainty. In this purpose, a framework was recently introduced (Luo et al., in preparation) (Figure 1). The framework decomposes the transient dynamics of terrestrial carbon storage into several traceable components. We apply this framework on Community Atmosphere Biosphere Land Exchange (CABLE) model (Wang et al., 2010). To quantify the contribution of model structures in response to elevating CO_2 and climate change, we designed three global change scenarios for two versions of CABLE: carbon-only (C-only) and coupled carbon-nitrogen (CN). Three scenarios include climate change and elevating CO_2 scenario (SCEC for C-only; SCECN for CN), climate change only scenario (SCC for C-only; SCCN for CN), and elevating CO_2 only scenario (SEC for C-only; SECN for CN). The changes of global terrestrial carbon storage from different scenarios are clearly segregated by three traceable components (Figure 2): global Net Primary Productivity (NPP), global ecosystem residence time, and global carbon storage potential. Effects of elevating CO2, climate change and soil nitrogen limitation on change of terrestrial carbon storage can be shown through the changes of traceable components: a) Increase of NPP in SEC, SECN, SCEC and SCECN explain most increase of terrestrial carbon storage. It indicates elevating atmosphere CO_2 concentration plays a major role in increasing terrestrial carbon storage due to CO_2 fertilisation; b) climate change reduces ecosystem residence time within each plant functional type due to warming. However, to aggregate on global scale, ecosystem residence time increases in SCC. As warming increase NPP in boreal region but decrease NPP in tropical region, redistribution of NPP towards the boreal region where ecosystem residence time is higher may account for the increase; c) soil nitrogen availability slows down the change of terrestrial carbon storage in two ways. On one hand, fast terrestrial carbon storage growth is constrained by nitrogen availability of vegetation carbon uptake. On the other hand, rapid loss of terrestrial carbon storage is also limited by soil nitrogen availability of litter carbon turnover. Transient traceability analysis framework explains most differences among scenarios with several traceable components. The successful application of this framework on CABLE also provides a way for individual model and model intercomparison projects to do model benchmarking and synthesis, thus improve current state of art in carbon cycle projection.
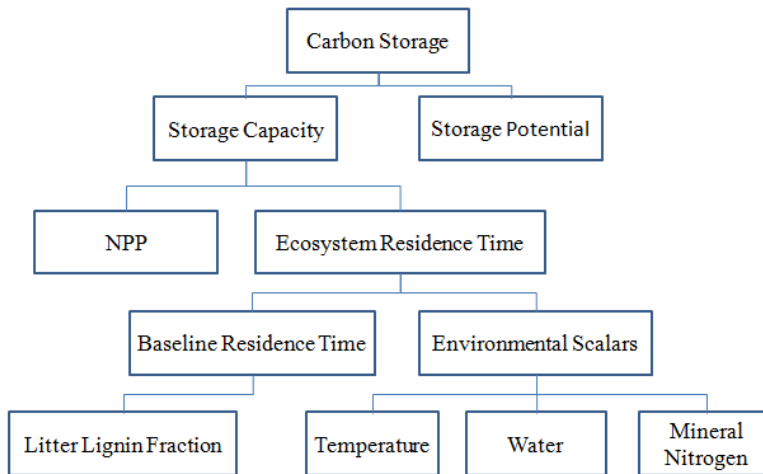
Figure 1: Schematic diagram of the framework of transient traceability analysis.
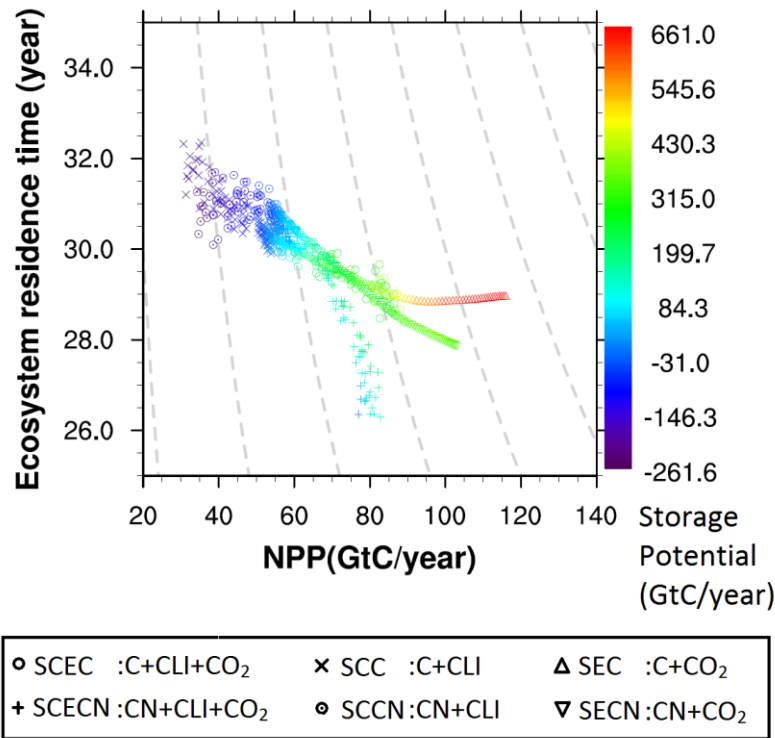
Figure 2. Determining the instantaneous solution of global ecosystem carbon storage change from Community Atmosphere Biosphere Land Exchange (CABLE) model 1901-2100 simulations by carbon influx (ie. annual NPP in x-axis), total ecosystem resident time (τ_E in y-axis) and dynamical disequilibrium solution (δ in color). The redder colour indicates a greater positive dynamical disequilibrium solution (in gigaton C), that is, how much the equilibrium solution is over instantaneous solution. The gray contour lines represent equilibrium solution of total ecosystem carbon storage in gigaton C determined only by NPP and total ecosystem resident time. Each marker shows annual average of three traceable components from 6 different scenarios: S1) C cycle mode, climate and CO2 both change (circle); S2) C cycle mode, climate change only with CO2 fixed (cross); S3) C cycle mode, CO2 change with climate fixed (regular triangle); S4) C and N cycle mode, climate and CO2 both change (plus); S5) C and N cycle mode, climate change only with CO2 fixed (circle-dot); S6) C and N cycle mode, CO2 change with climate fixed (upside down triangle)

References

Luo, Y., Z. Shi, J. Xia, Y. Wang, M. MC, F. Agusto, A. Ahlström, B. Chen, O. Hararuk, A. Hastings, F. Hoffman, J. Jiang, L. Jiang, J. Liang, X. Lu, B. Medlyn, S. Niu, M. Rasmussen, M. Smith, K. Todd-Brown, Y. Wang, Terrestrial carbon storage dynamics: Chasing a moving target. *In preparation*

Tian, H., C. Lu, J. Yang, K. Banger, D. N. Huntzinger, C. R. Schwalm, A. M. Michalak, R. Cook, P. Ciais, D. Hayes, M. Huang, A. Ito, A. K. Jain, H. Lei, J. Mao, S. Pan, W. M. Post, S. Peng, B. Poulter, W. Ren, D. Ricciuto, K. Schaefer, X. Shi, B. Tao,W. Wang, Y. Wei, Q. Yang, B. Zhang, N. Zeng, 2015: Global patterns and controls of soil organic carbon dynamics as simulated by multiple terrestrial biosphere models: Current status and future directions, *Global Biogeochem. Cycles*, 29, 775–792.

Todd-Brown, K. E. O., J. T. Randerson, Hopkins F., V. Arora, T. Hajima, C. Jones, E. Shevliakova, J. Tjiputra, E. Volodin, T. Wu, Q. Zhang, and S. D. Allison, 2014: Changes in soil organic carbon storage predicted by Earth system models during the 21st century. *Biogeosc.*, 11, 2341-2356.

Wang, Ying-Ping, P., R. M. Law, B. Pak, 2010: A global model of carbon, nitrogen and phosphorus cycles for the terrestrial biosphere, *Biogeosc.*, 7, 2261-2282, doi:10.5194/bg-7-2261-2010

Wieder, W. R., C. C. Cleveland, W. K. Smith, K. Todd-Brown, 2015: Future productivity and carbon storage limited by terrestrial nutrient availability, *Nature Geosci*, 8, 441-444.

INFLUENCE OF LAND-ATMOSPHERE FEEDBACKS ON TEMPERATURE EXTREMES IN THE GLACE-CMIP5 ENSEMBLE

Ruth Lorenz[1], Daniel Argüeso[1], Markus G. Donat[1], Andrew J. Pitman[1], Bart van den Hurk[2], Alexis Berg[3], David M. Lawrence[4], Frédérique Chéruy[5], Agnès Ducharne[6], Stefan Hagemann[7], Arndt Meier[8], P. C. D. Milly[9] and Sonia I. Seneviratne[10]

[1]*ARC Centre of Excellence for Climate System Science and Climate Change Research Centre, UNSW Australia, Sydney*
[2]*Royal Netherlands Meteorological Institute, De Bilt, The Netherlands*
[3]*International Research Institute for Climate and Society, Earth Institute at Columbia University, 61 Rt 9W, Palisades, NY 10964, USA.*
[4]*National Center for Atmospheric Research, Boulder, Colorado, USA*
[5]*LMD/IPSL, 4 Place Jussieu, 75252 Paris Cedex, France.*
[6]*Sorbonne Universités, UPMC, CNRS, EPHE, UMR 7619 Metis, 4 place Jussieu, Paris, France.*
[7]*Max Planck Institute for Meteorology, Hamburg, Germany.*
[8]*Centre for Environmental and Climate Research (CEC), Lund University, Sweden.*
[9]*U. S. Geological Survey, Princeton, New Jersey, USA.*
[10]*Institute for Atmospheric and Climate Science, ETH Zurich, Zurich, Switzerland.*

r.lorenz@unsw.edu.au

Abstract

Extreme climate and weather events present major risks for ecosystems and society. Observations show that characteristics of many extreme events, such as heat waves, occurrence of warm nights, and heavy rainfall events, are already changing and many extremes are expected to change in the future under higher atmospheric CO_2 concentrations (e.g. Alexander et al., 2006; Seneviratne et al., 2012, Sillmann et al., 2013). Land surface processes influence the boundary layer and the atmosphere, and can affect extreme events.

We examine how soil moisture variability and trends affect the simulation of temperature and precipitation extremes in six global climate models using the experimental protocol of the Global Land-Atmosphere Coupling Experiment of the Coupled Model Intercomparison Project, Phase 5 (GLACE-CMIP5, Seneviratne et al, 2013). This protocol enables separate examinations of the influences of soil moisture variability and trends on the intensity, frequency and duration of climate extremes through to the end of the 21st century under a business-as-usual (RCP8.5) emission scenario (see Table 1 for experiment set-up).

Table 1: GLACE-CMIP5 experimet set-up, participating global climate models are ACCESS, CESM, EC-EARTH, ECHAM6, GFDL and IPSL

Model Run	Soil Moisture	Time period
CTL	interactive	Either CMIP5 historical run plus RCP8.5 or AMIP run 1950-2100 using CMIP5 sea surface temperature and sea ice.
SMclim	Prescribed to 1971-2000 climatology from CTL	1950-2100
SMtrend	Prescribed to transient seasonal CTL climatology (30 year running means)	1950-2100

We use extreme indices recommended by the Expert Team on Climate Change Detection and Indices (ETCCDI) plus an additional heat wave index. The intensity of hot extremes is represented by the warmest daily maximum temperature each year (hottest day, TXx), while the frequency is expressed by the percentage of days per year when the daily maximum temperature exceeds the 90th percentile calculated for the 1961–1990 base period (warm days, TX90p). The duration of extreme temperature conditions is measured with the Heat Wave Duration (HWD) index based on e.g. Perkins and Alexander (2013).

Removing soil moisture variability significantly reduces temperature extremes over most continental surfaces (Figure 1 a,c,e). Projected trends in soil moisture lead to increases in intensity, frequency, and duration of temperature extremes by the end of the 21st century (Figure 1 b,d,f). However, the ensemble results mask considerable differences in the soil moisture trends simulated by the six climate models. We find that the high inter-model differences in soil moisture trends, which are related to an unknown combination of differences in atmospheric forcing (precipitation, net radiation), flux partitioning at the land surface, and how soil moisture is parameterized, imply considerable uncertainty in future changes in climate extremes.
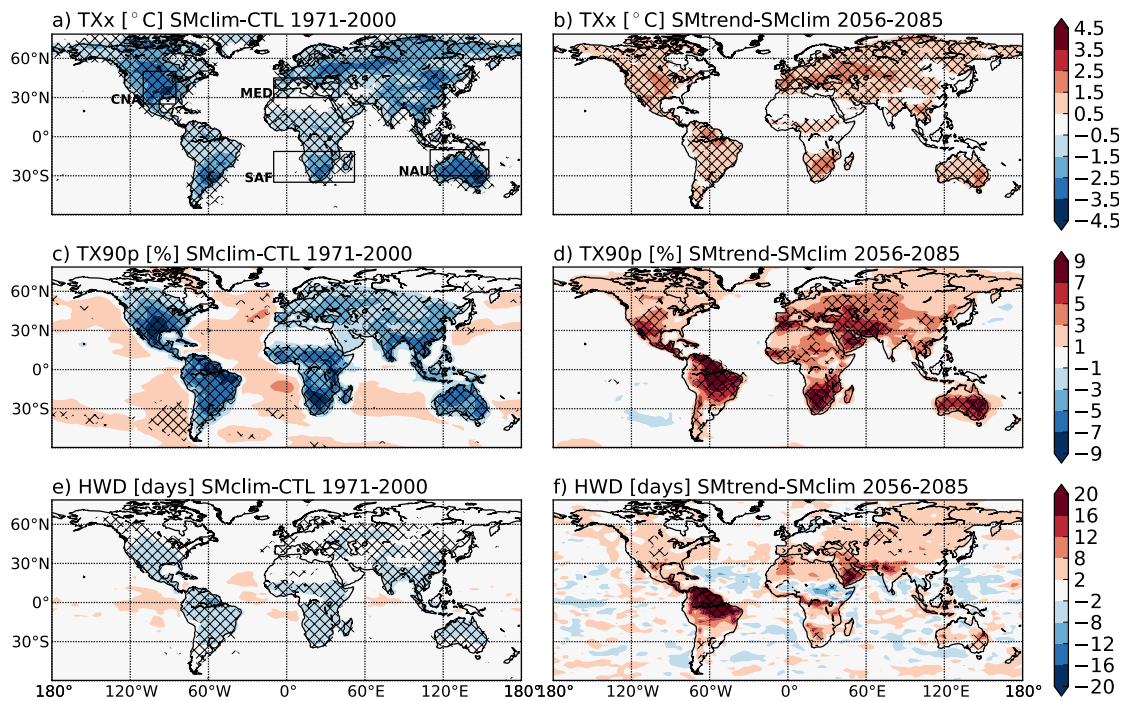
Figure 1: Warmest daily maximum temperature (intensity), warm days (frequency), heat wave duration. Multi-model mean, hatching where statistically significant (KS-test, p-value<0.05). Left column for SMclim-CTL in 1971-2000, right column for SMtrend-SMclim in 2056-2085.

References

Alexander, L. V., X. Zhang, T. C. Peterson, J. Caesar, B. Gleason, A. M. G. Klein Tank, M. Haylock, D. Collins, B. Trewin, F. Rahimzadeh, A. Tagipour, K. Rupa Kumar, J. Revadekar, G. Griffiths, L. Vincent, D. B. Stephenson, J. Burn, E. Aguilar, M. Brunet, M. Taylor, M. New, P. Zhai, M. Rusticucci, and J. L. Vazquez-Aguirre, 2006: Global observed changes in daily climate extremes of temperature and precipitation, J. Geophys. Res., 111 (D5), D05,109, doi:10.1029/2005JD006290.

Seneviratne, S. I., N. Nicholls, D. R. Easterling, C. M. Goodess, S. Kanae, J. Kossin, Y. Luo, J. Marengo,

K. McInnes, M. Rahimi, M. Reichstein, A. Sorteberg, C. Vera, and X. Zhang, 2012: Changes in Climate Extremes and their Impacts on the Natural Physical Environment, in Manag. Risks Extrem. Events Disasters to Adv. Clim. Chang. Adapt. [Field, C.B., V. Barros, T.F. Stock. D. Qin, D.J. Dokken, K.L. Ebi, M.D. Mastrandrea, K.J. Mach, G.-K. Plattner, S.K. Allen, M. Tignor, P. M. Midgley (eds.)]. A, pp. 109–230, Cambridge University Press, Cambridge, UK, and New York, NY, USA.

Seneviratne, S. I., M. Wilhelm, T. Stanelle, B. van den Hurk, S. Hagemann, A. Berg, F. Cheruy, M. E. Higgins, A. Meier, V. Brovkin, M. Claussen, A. Ducharne, J.-L.
Dufresne, K. L. Findell, J. Ghattas, D. M. Lawrence, S. Malyshev, M. Rummukainen, and B. Smith, 2013: Impact of soil moisture-climate feedbacks on CMIP5 projections: First results from the GLACE-CMIP5 experiment. *Geophys. Res. Lett.*, 40 (19), 5212–5217, doi:10.1002/grl.50956.

Sillmann, J., V. V. Kharin, F. W. Zwiers, X. Zhang, and D. Bronaugh, 2013: Climate extremes indices in the CMIP5 multimodel ensemble: Part 2. Future climate projections, J. Geophys. Res. Atmos., 118 (6), 2473–2493, doi:10.1002/jgrd

PACIFIC WIND-DRIVEN CIRCULATION VARIABILITY AND ITS ROLE IN HIATUS / ACCELERATED WARMING DECADES

Matthew England

Climate Change Research Centre, ARC Centre of Excellence for Climate System Science, University of New South Wales, Sydney

m.england@unsw.edu.au

Abstract

Despite ongoing increases in atmospheric greenhouse gases, the Earth's global average surface air temperature remained more or less steady between 2001-2013. Mechanisms proposed to account for this slowdown in surface warming include increased ocean heat uptake, the prolonged solar minimum and changes in atmospheric water vapour and aerosols. While cool sea surface temperature in the east Pacific has been identified as a key component of the global hiatus, it is unclear how the ocean has remained relatively cool there in spite of ongoing increases in radiative forcing. Here we show that a pronounced strengthening in Pacific trade winds over the past two decades – unprecedented in observations/reanalysis data and not captured by climate models – is sufficient to account for the cooling of the tropical Pacific and a substantial slowdown in surface warming via increased subsurface ocean heat uptake (England et al., 2014). The extra uptake has come about via increased subduction in the Pacific shallow overturning cells, enhancing heat convergence in the equatorial thermocline (Figure 1). Some of this heat leaks westward into the Indian Ocean via the Indonesian Throughflow. At the same time, the accelerated trade winds increased equatorial upwelling in the central and eastern Pacific, lowering SST there, which drives further cooling in other regions. Alongside Pacific Ocean SST forcing, the accelerated trade winds appear to have been influenced by recent tropical Atlantic warming (Figure 2; McGregor et al., 2014). The net effect of these anomalous winds is a cooling in the 2013 global average surface air temperature of $0.1 - 0.2°C$, which can account for much of the hiatus in surface warming observed since 2001. Simulations using coupled climate models suggest that a rebound of rapid warming is expected to resume once the anomalous wind trends abate.
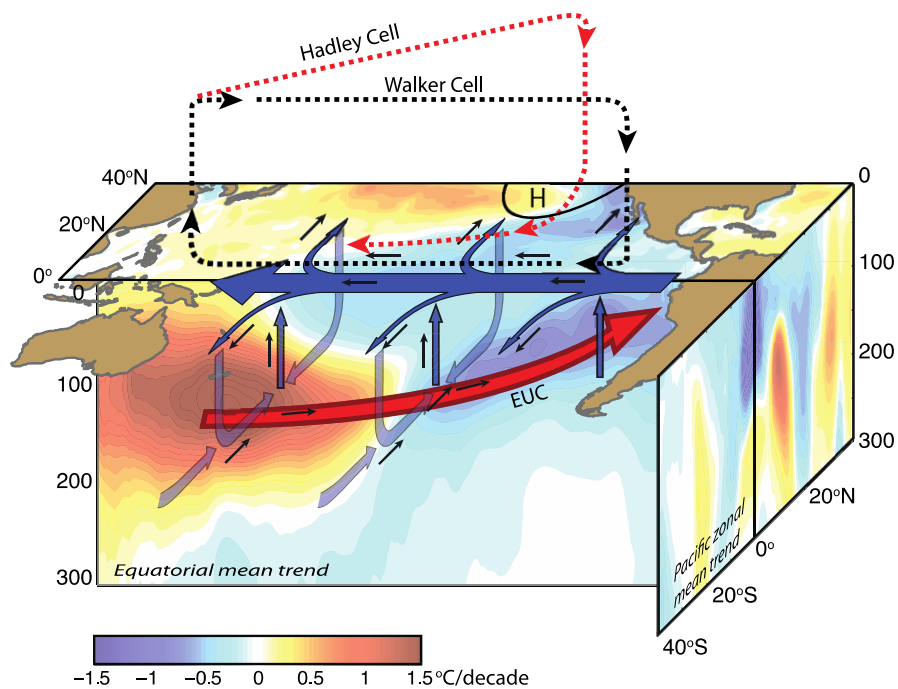
Figure 1. Schematic of the trends in temperature and ocean-atmosphere circulation in the Pacific over the past two decades. Colour shading shows observed temperature trends (°C/decade) during 1992-2011 (i) at the sea surface (Northern Hemisphere only), (ii) zonally-averaged in the latitude-depth sense (as per Fig. S6), and (iii) along the equatorial Pacific in the longitude-depth plane (averaged between 5°N-5°S). Peak warming in the western Pacific thermocline is 2.0°C/decade in the reanalysis data and 2.2°C/decade in the model. The mean and anomalous circulation in the Pacific Ocean is shown by bold and thin arrows, respectively, indicating an overall acceleration of the Pacific Ocean shallow overturning cells, the equatorial surface currents, and the Equatorial Undercurrent. The accelerated atmospheric circulation in the Pacific is indicated by the dashed lines; including the Walker Cell (black dashed) and the Hadley Cell (red dashed; Northern Hemisphere only). An equivalent accelerated Hadley Cell in the Southern Hemisphere is omitted for clarity.
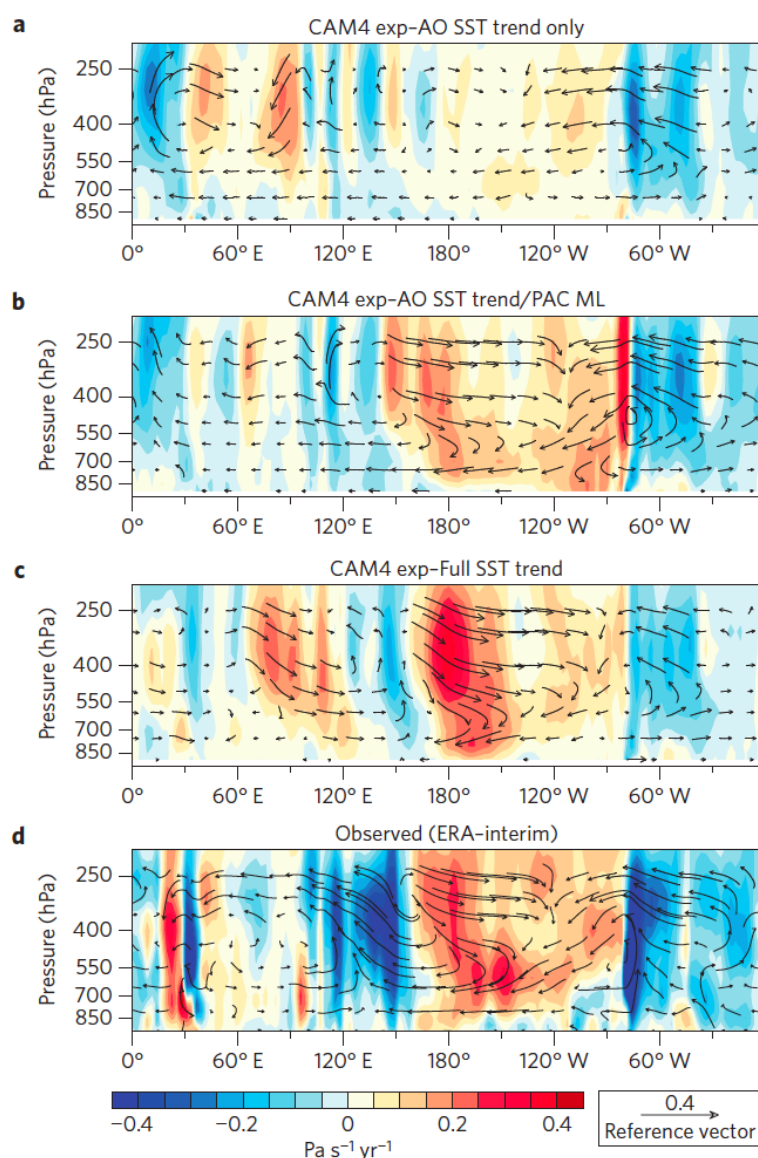
Figure 2. Changes of global Walker circulation. a, Vertical equatorial atmospheric velocity trends (colour scale) over the 1992–2011 period from the CAM4 experiment forced with the Atlantic SST trend, where SSTs are set to climatology in the Pacific and Indian Oceans. Overlying vectors represent the zonal wind trend (m s^{-1} yr^{-1}) and the vertical velocity scaled by a factor of 300. b, As in a, but for the CAM4 experiment forced with the observed Atlantic Ocean SST trend and a Pacific mixed layer. c, As in a, but for the for CAM4 experiment forced with the global observed SST trend and a Pacific mixed layer. d, As in a, but for the ERA-Interim reanalysis.

References

England, M. H., S. McGregor, P. Spence, G. A. Meehl, A. Timmermann, W. Cai, A. Sen Gupta, M. J. McPhaden, A. Purich and A. Santoso, 2014: Recent intensification of wind-driven circulation in the Pacific and the ongoing warming hiatus, *Nature Climate Change*, **4**, 222-227, doi: 10.1038/nclimate2106.

McGregor, S., A. Timmermann, M. F. Stuecker, M. H. England, M. Merrifield, F.-F. Jin and Y. Chikamoto, 2014: Recent Walker circulation strengthening and Pacific cooling amplified by Atlantic warming, *Nature Climate Change*, doi: 10.1038/nclimate2330.

DECADAL VARIABILITY IN GLOBAL TEMPERATURES AND ANTARCTIC SEA

Julie Arblaster[1,2], Jerry Meehl[1], Christine Chung[2] and Cecilia Bitz[3]

[1]*National Center for Atmospheric Research, Boulder, CO, USA*
[2]*Bureau of Meteorology, Melbourne*
[3]*University of Washington, Seattle, WA, USA*

j.arblaster@bom.gov.au

Abstract

A recent slowdown in global temperature rise has prompted many studies on decadal variability in the climate system. After rising rapidly through the 1980s and 1990s, global temperatures showed weaker warming, a slowdown, since around 2000. Around the same time a transition was seen in the major mode of decadal variability in the tropical Pacific – the Interdecadal Pacific Oscillation (IPO) – to its negative phase, with cooler sea surface temperatures in the equatorial Pacific and associated negative rainfall and convective heating anomalies there. This transition of the IPO coincided with an intensification of the Amundson Sea low near Antarctica and an acceleration of the increasing trend in average Antarctic sea ice extent. Temperatures over the southeast U.S. also showed a disappearance of the so-called 'warming hole' at this time, with a switch to warming over that region since 2000.

Understanding these observations hinges on answering the compelling question of how naturally occurring decadal variability combines with the response to increasing greenhouse gases to produce the time evolution of the climate system. Here we use global coupled climate models to investigate this interplay between internally generated decadal variability and scenarios of anthropogenic climate change. We show that the atmospheric teleconnections from the negative phase of the IPO in these models is characterised by anomalies similar to the observed recent sea level pressure and surface wind changes near Antarctica that are conducive to expanding average Antarctic sea ice extent, particularly in the Ross Sea region in winter. These atmospheric circulation changes are linked to precipitation and convective heating anomalies in the tropical Pacific originating from internally-generated decadal variations of the IPO. Thus the recent accelerated increase in Antarctic sea ice extent has a significant contribution from tropical Pacific decadal climate variability. Based on these results and others, predictions of future changes in global temperatures and Antarctic sea-ice extent are made.
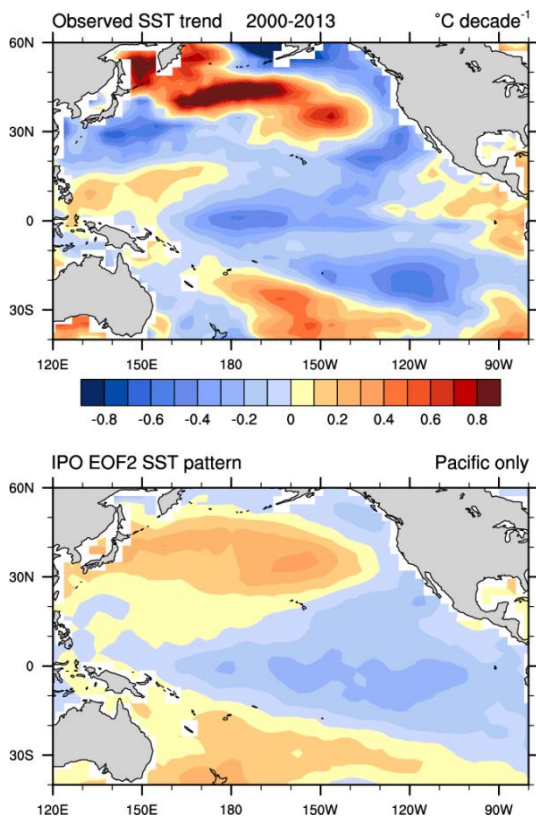
Figure 2: Observed 2000-2013 trends in sea surface temperatures (˚C per decade; top) and the pattern of the Interdecadal Pacific Oscillation (bottom)

References

Meehl, G.A., H. Teng, and J.M. Arblaster, 2014: Climate model simulations of the observed early-2000s hiatus of global warming, *Nature Climate Change*, doi:10.1038/nclimate2357

Meehl, G. A., J. M. Arblaster, and C. T. Y. Chung, 2015: Disappearance of the southeast U.S. "warming hole" with the late 1990s transition of the Interdecadal Pacific Oscillation, *Geophys. Res. Lett.*, 42, 5564–5570, doi:10.1002/2015GL064586.

Meehl G.A., J.M. Arblaster, C. Bitz, C.T.Y. Chung, 2015: Recent Antarctic sea ice expansion driven by tropical Pacific decadal climate variability, submitted

MODELLING THE EARTH SYSTEM WITH ACCESS TO ASSESS THE POTENTIAL CARBON CLIMATE FEEDBACKS ON CLIMATE CHANGE

R. Matear[1], R. Law[2], A. Lenton[1], T. Ziehne[2], and M. Chamberlain[1]

[1] *CSIRO Oceans and Atmosphere, Hobart, Tasmania*
[2] *CSIRO Oceans and Atmosphere, Aspendale, Victoria*

Richard.Matear@csiro.au

Abstract

Earth System Models (ESMs) that incorporate carbon-climate feedbacks represent the present state of the art in climate modelling. Here, we describe the Australian Community Climate and Earth System Simulator (ACCESS)-ESM1 that combines existing ocean and land carbon models into the physical climate model to simulate exchanges of carbon between the land, atmosphere and ocean. The land carbon model can optionally include both nitrogen and phosphorous limitation on the land carbon uptake. The ocean carbon model simulates the evolution of nitrate, oxygen, dissolved inorganic carbon, alkalinity and iron with one class of phytoplankton and zooplankton. From two future projections (RCP4.5 an RCP8.5) we discuss changes in the climate and the impact this has on land and ocean carbon cycles.

LONG-TERM POLEWARD TREND OF THE PACIFIC SOUTH EQUATORIAL CURRENT BIFURCATION FROM HIGH-RESOLUTION OCEAN HINDCAST USING OFAM3

Chaojiao Sun[1], Craig Steinberg[2], Xuebin Zhang[3], and Andreas Schiller[4]

[1]*Oceans and Atmosphere, CSIRO, Perth, Western Australia*
[2]*Australian Institute of Marine Science, Townsville, Queensland*
[3,4]*Oceans and Atmosphere, CSIRO, Hobart, Tasmania*

Chaojiao.Sun@csiro.au

The trend of the Pacific South Equatorial Current (SEC) bifurcation latitude is investigated from a high-resolution ocean hindcast for the past 36 years (1979-2014) and compared with data from two IMOS moorings in the Coral Sea (from 1987 to the present). The much higher spatial resolution of OFAM3 model (0.1 degree resolution) and the mooring data provide us with new insight into the dynamics of the SEC bifurcation and its impact on the western boundary current transports in the South Pacific, as ocean reanalysis products (climate models) typically have the order of 0.5 (1) degree horizontal resolution.

Introduction

The ocean circulation patterns in the Southwest Pacific are complex (Fig. 1a; Ganachaud et al 2014, Steinberg 2007). The SEC impinging on the Australian coast and bifurcates into two branches, one is the equatorward Gulf of Papua Current (GPC), the other the poleward East Australia Current (EAC). The GPC then feeds the New Guinea Coastal Current (NGCC) that feeds the West Pacific warm pool and is a source for the Equatorial Undercurrent (EUC) (e.g., Sen Gupta et al., 2012). The bifurcation point determines the partition of warm water into the tropics and subtropics. The bifurcation latitude is approximately determined by the zero wind stress curl (e.g., Chen and Wu, 2014).

The long-term poleward trend of the SEC bifurcation latitude over the last 60 years has been investigated by Zhai et al. (2014) using SODA version 2.2.4 (Carton and Giese, 2008), which has a horizontal resolution of 0.5 degrees. Recently, Chen and Wu (2015) studied the seasonality of SEC bifurcation using the World Ocean Atlas (2009) and satellite altimetry and the ECMWF Ocean Reanalysis product ORA-S4. Here we study the SEC bifurcation using the OFAM3 hindcast forced with JRA-55 Reanalysis with a much higher resolution (0.1 degree) and the observations from two IMOS moorings in the Coral Sea.
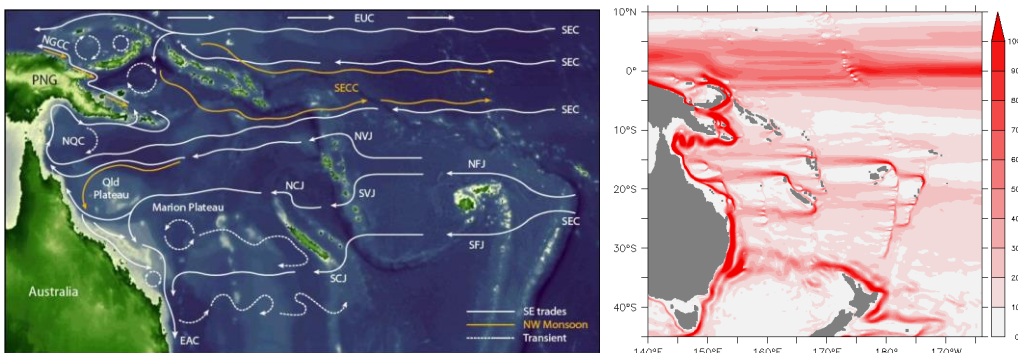
Figure 3: (left) South Equatorial Current (SEC) pathways to the Coral Sea: North Fiji Jet (NFJ), South Fiji Jet (SFJ), North Vanuatu Jet (NVJ), South Vanuatu Jet (SVJ), North Caledonia Jet (NCJ), South Caledonia Jet (SCJ). Once the streams approach the GBR the flow bifurcates to form the East Australian Current (EAC) and a northern arm, called the Gulf of Papua Current (GPC), which is also called the Hiri Current or North Queensland Current (NQC). This branch then feeds the New Guinea Coastal Current (NGCC) that feeds the West Pacific warm pool and is a source for the Equatorial Undercurrent (EUC). The currents in orange indicate major seasonal changes during the NW Monsoon. The NGCC reverses and the Southern Equatorial Counter Current (SECC) reverses the SEC nearest the equator. (right) Main currents (integrated 0-1000m) simulated by OFAM3 hindcast (averaged over 1979-2014) forced with JRA-55 atmospheric reanalysis.

IMOS moorings in the Coral Sea

Since the late 1980s, almost three decades of time series current and temperature data has been collected by AIMS (since 1987) and in partnership with IMOS (since 2007). The currents in the Coral Sea adjacent to the Great Barrier Reef were derived from a pair of current meter moorings along the continental shelf slope (Fig. 2). The array was deployed to provide estimates of geostrophic current anomalies and direct measurements of flow on the continental shelf and slope. The two locations are located near Jewell Reef at 14 20.6' S 145 20.6' E in 360m and near Myrmidon Reef at 18 13.1' S 147 20.5' E in 200m water depth (Table 1). Initially Aanderaa Rotary Current Meters were used but were replaced by ADCPs from the late 1990s so the observations have evolved from a few points in the water column to current profiles.

Work is currently underway to compare observed current data from the Q-IMOS moorings near the bifurcation point with modelling results to gain detailed insight into the seasonality and depth structure.

Table 1: TEACS Current Meter Mooring Positions

STATION	CODE	POSITION	DEPTH	Positions	Period
Myrmidon Reef	MY	18° 13!1 S 147° 20!5 E	200	25,50,75,150	1987 – present
Jewell Reef	JW	14° 20!6 S 145° 20!6 E	352	32,75	2/10/86 – 4/2000

Results

The OFAM3 hindcast is able to reproduce the major currents in the Southwest Pacific region realistically (Fig. 1b). The SEC bifurcation latitude calculated from the long-term-mean of the hindcast is at 15S (Fig. 3a). The bifurcation is defined as where the meridional velocity averaged within a 2° zonal band off the Australian coast is zero, following Qu and Lindstrom (2002). The bifurcation point moves further south with depth (Fig. 3b). Note that the results are not sensitive to the width of the zonal band.

There is a large seasonal variability in the bifurcation (Fig. 4a). Chen and Wu (2015) demonstrated that the seasonal variability of the SEC bifurcation latitude is dependent on the Rossby wave and Kelvin wave dynamics in the South Pacific.

The SEC bifurcation trend over the last 36 years is slightly equatorward (Fig. 4b). This is not inconsistent with the findings by Zhai et al. (2014) that even though over the last 60 years there is a poleward trend, the trend from the 1970s to the present is equatorward. This is in response to the trend of the zero wind stress curl.
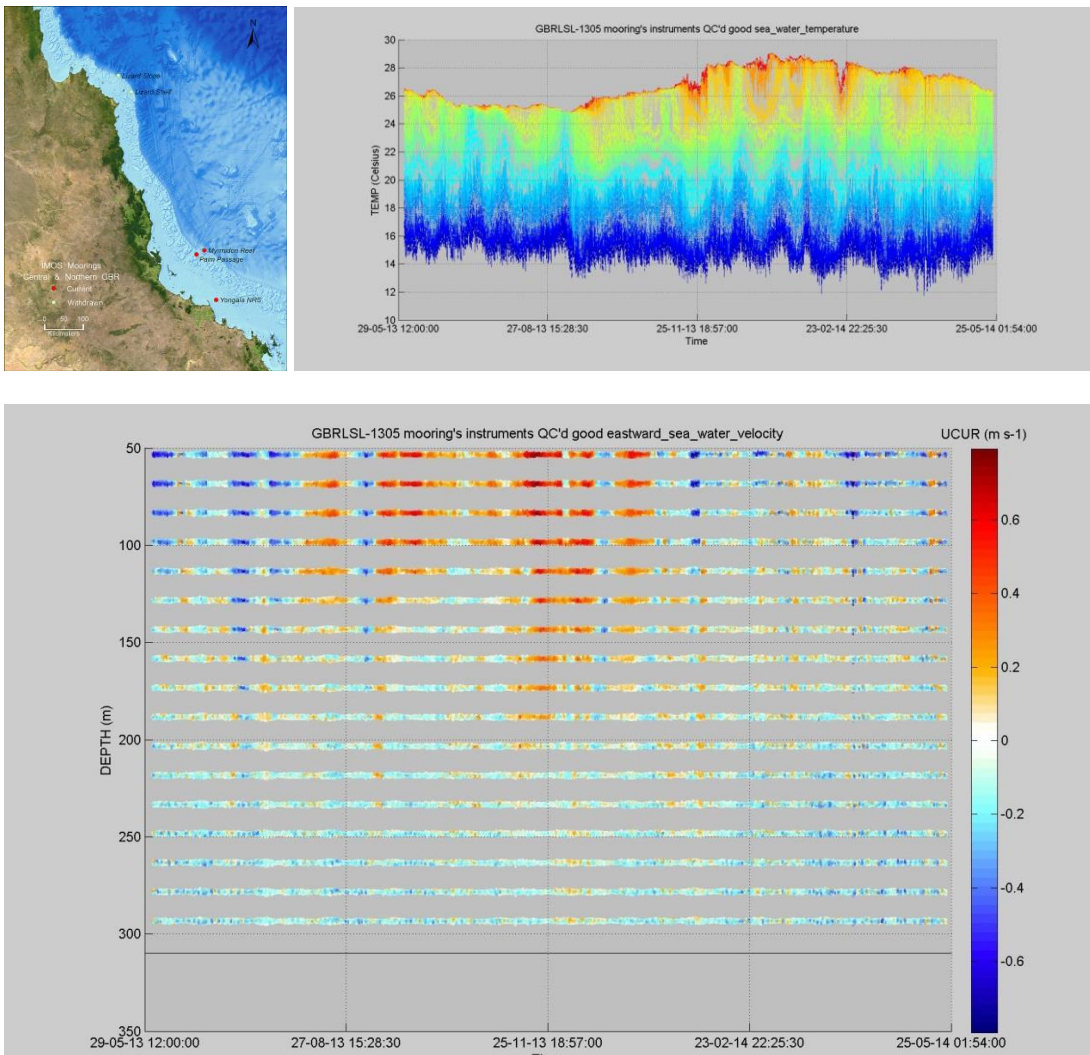
Figure 2: Locations of the Northern Q-IMOS mooring array (upper left). Lizard Slope and Myrmidon extended earlier continental slope boundary current moorings. One-year time series of in-line temperature loggers on Lizard Slope Mooring (upper right). Time series of zonal current observations from the ADCP near Jewel Reef (bottom). Binned current magnitude data is presented throughout the top 300m of the water column.
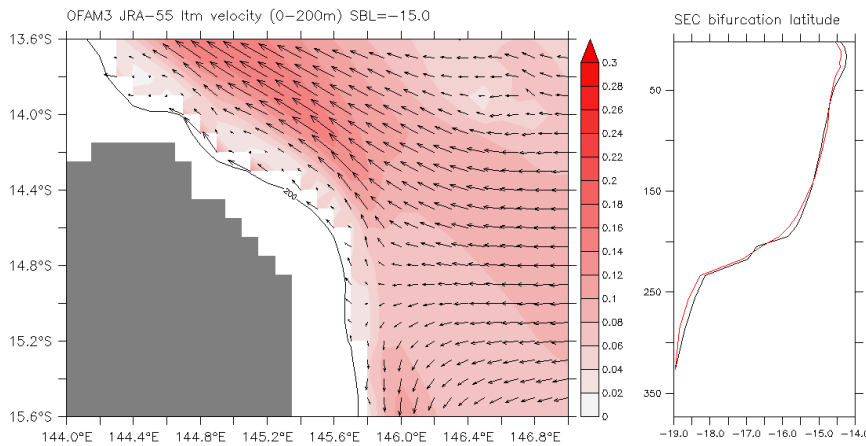
Figure 3: (left) Velocity field averaged over the upper 200m simulated by OFAM3 hindcast (averaged over 1979-2014) forced with JRA-55 atmospheric reanalysis. (right) SEC bifurcation latitude distribution with depth, which is calculated from zero meridional velocity averaged over 2-degree (black) or 1-degree (red) zonal band from the 200m isobath at the Australian coast.
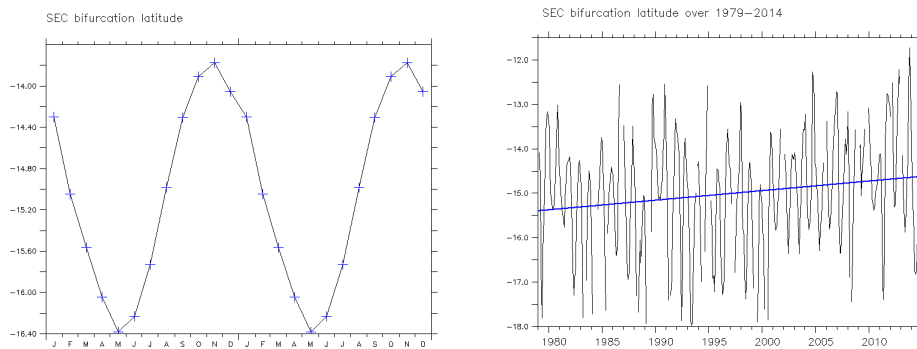
Figure 4: Seasonal climatology SEC bifurcation latitude calculated from 3-month running mean of monthly model output (left). Time series of SEC bifurcation latitude and its linear trend (right).

Discussion and Conclusions

The novelty of this study is the use of a high-resolution (1/10 degree horizontal resolution) ocean hindcast and comparison with long-term mooring data in the Coral Sea near the Pacific bifurcation point. The equatorward trend of the bifurcation over 1979-2014 is a reflection of the large-scale wind stress curl trend in this time period. Progress is on the way to produce future projection in the SEC bifurcation trend using CMIP5 climate ensemble forcing.

References

J.A. Carton and B.S. Giese, 2008: A reanalysis of ocean climate using Simple Ocean Data Assimilation (SODA), Monthly Weather Review, 136, 2999-3017.

Chen Z., and L. Wu, 2015: Seasonal Variation of the Pacific South Equatorial Current Bifurcation. J. Phys. Oceanogr., 45, 1757–1770.

Chen, Z., and L. Wu, 2012: Long-term change of the Pacific North Equatorial Current bifurcation in SODA, J. Geophys. Res., 117, C06016, doi:10.1029/2011JC007814.

Ganachaud, A. S. et al., 2014: The Southwest Pacific Ocean circulation and climate experiment (SPICE). J. Geophys. Res. Oceans, DOI: 10.1002/2013JC009678.

Sen Gupta, A., Ganachaud, A., McGregor, S., Brown, J. N. and Muir, L., 2012: Drivers of the projected changes to the Pacific Ocean equatorial circulation. Geophys. Res. Lett. 39, L09605.

Steinberg, C., 2007: Impacts of climate change on the physical oceanography of the Great Barrier Reef, pp 51-74. In Johnson JE and Marshall PA [eds.], Climate Change and the Great Barrier Reef. Great Barrier Reef Marine Park Authority.

Webb, D.J., 2000: Evidence for shallow zonal jets in the South Equatorial Current region of the Southwest Pacific. Journal of Physical Oceanography, 30 (4), 706-720.

INITIATION AND AMPLIFICATION OF THE NINGALOO NIÑO

Andrew G. Marshall[1], Harry H. Hendon[2], Ming Feng[3] and Andreas Schiller[4]

[1]*Research and Development, Bureau of Meteorology, Hobart*
[2]*Research and Development, Bureau of Meteorology, Melbourne*
[3]*Oceans and Atmosphere, CSIRO, Floreat*
[4]*Oceans and Atmosphere, CSIRO, Hobart*

andrew.marshall@csiro.au

Introduction

Ocean temperatures along the west coast of Australia reached the highest ever recorded in February 2011. Dubbed the 'Ningaloo Niño' (Feng et al. 2013), this unprecedented marine heat wave was associated with an unusual intensification of the Leeuwin Current and culminated in the first ever recorded heat wave bleaching event in the pristine World Heritage Ningaloo Reef. The occurrence of Ningaloo Niños is intimately tied to the variability and dynamics of the Leeuwin Current, the poleward-flowing eastern boundary current that transports warm and fresh water southward along the Western Australian (WA) coast from Northwest Cape to Cape Leeuwin. Although some of the increase in the strength of the Leeuwin Current during Ningaloo Niños appears to be a remote impact of La Niña (e.g. Hendon and Wang 2009), Kataoka et al. (2014) show that local air sea interaction along the west coast also acts to locally enhance the heat waves. Understanding the causes of the heat waves and especially the potential predictability of events and possible links with decadal and longer period fluctuations in the background climate is important for fisheries and other marine ecosystems that are sensitive to the variations in mixing, temperature and transport by the Leeuwin current.

Data

Initiation and amplification mechanisms for Ningaloo Niño events are explored in this work using ocean and atmosphere reanalyses for the period 1960-2011. The primary data are the upper ocean re-analyses provided by the POAMA (Predictive Ocean Atmosphere Model for Australia) Ensemble Ocean Data Assimilation System (PEODAS; Yin et al. 2011), which is used to produce ocean initial conditions for POAMA coupled model seasonal climate forecasts. We further explore variations in upper ocean currents and heat transfer along the Western Australian coast using the high resolution Bluelink reanalysis (BRAN) version 3.5, variations of Australian rainfall and maximum temperatures using the Australian Water Availability Project (AWAP) analyses (Jones et al. 2009), and variations of the Leeuwin Current on the southern portion of the west coast of Australia using GLOSS/CLIVAR monthly sea level observations at Fremantle (115.73°E, 32.05°S), obtained from the University of Hawaii Sea Level Center. We define the Ningaloo Niño index as the average SST anomaly over the box region 110-116°E and 22-32°S, which captures high variability in the marine environment between Ningaloo and Fremantle. A Ningaloo Niño event occurs when the December to February averaged index is greater than one standard deviation above the mean. With this threshold, we identify 11 marine heat wave years: 1960-61, 1961-62, 1966-67, 1979-80, 1982-83, 1983-84, 1988-89, 1994-95, 1996-97, 1999-2000, and 2010-11.
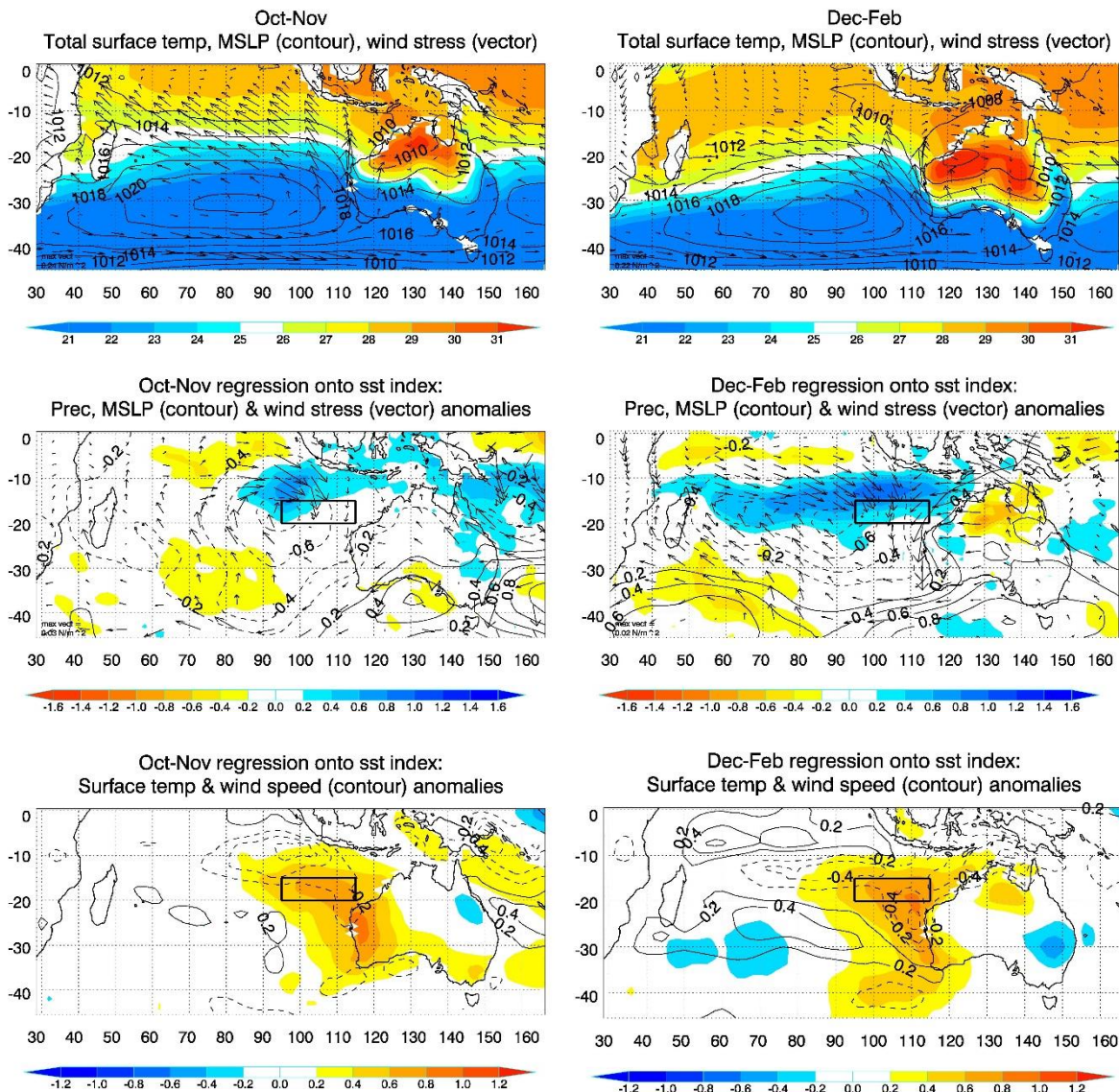
Figure 1: Illustration of the wind-evaporation-SST feedback process during development of the Ningaloo Niño in October-November (left column), and for the peak of the Ningaloo Niño in December-February (right column), by regression onto south-eastern tropical Indian Ocean SST. Upper panels show regression patterns (scaled for a one standard deviation anomaly of the time-varying SST index) for total surface temperature (shaded), MSLP (contoured) and surface wind stress (vector); contour interval is 2 hPa and shading interval is 1°C. Middle panels show regression patterns for anomalous rainfall (shaded), MSLP (contoured) and surface wind stress (vector); contour interval is 0.2 hPa, and shading interval is 0.2 with blue shading representing positive values. (Rainfall anomalies are normalised by their respective standard deviations at each grid point.) Lower panels show regression patterns for anomalous surface temperature (shaded) and wind speed (contoured); contour interval is 0.2 m/s, and shading interval is 0.2°C with blue shading representing negative values. The magnitude of the strongest wind stress vector is printed in the lower left corner of the upper and middle panels. The south-eastern tropical Indian Ocean SST index box region (95-115°E, 15-20°S) is indicated on the top right and lower left panels.

Wind-evaporation-SST feedback

We explore the anomalous atmospheric circulation, precipitation and SST patterns associated with variations of SST in the south-eastern tropical Indian Ocean during the development (October – November) and peak (December – February) stages of the Ningaloo Niño events. The climatological surface circulation to the west of Australia is dominated by a subtropical high, which is commonly referred

to as the Mascarene High. Anticyclonic flow around the high results in trade easterlies on its equatorward flank over the relatively warm tropical Indian Ocean and southerlies along the west coast of Australia, which act against the Leeuwin Current (Figure 1, upper panels). We define a time-varying SST index by spatially averaging the SST anomaly in the box bounded by 95-115°E, 15-20°S, which sits on the north-eastern flank of the Mascarene High and is where the SST anomaly associated with Ningaloo Niño events is strong during its development. We demonstrate how precipitation, mean sea level pressure (MSLP), surface wind stress and surface wind speed are associated with the SST anomaly by performing a linear regression fit between the SST index and each anomaly field at each grid point (Figure 1, middle and lower panels). The development stage of Ningaloo Niño events is promoted by wind-evaporation-SST (WES) feedback that operates to the northwest of the coast on the north-eastern flank of the Mascarene subtropical high: cyclonic anomalies act to reduce the surface wind speed and warm the ocean surface, thereby driving increased rainfall and stronger cyclonic anomalies. The growth and southward expansion of positive SST anomalies along the Australian west coast during the peak of the events is further supplemented by anomalous poleward advection of heat by the Leeuwin Current, which is coupled with the cyclonic anomalies off the coast. The distinctive wedged shaped pattern of the SST anomaly during Ningaloo Niño events thus is seen to reflect the seasonal evolution of the WES feedback operating on the north-east flank of the Mascarene High.

Relationship with Pacific Ocean SST

The strongest Ningaloo Niño events, such as the record strong 2011 event, occur in conjunction with La Niña conditions in the Pacific, which drives westerly wind anomalies to the northwest of Australia that can promote the WES feedback and accelerate the Leeuwin Current via transmission of thermocline anomalies from the western Pacific onto the west Australian coast. However, many Ningaloo Niño events occur independent of La Niña and some Ningaloo Niño events even occur during certain El Niños. We explain this general independence from ENSO because the triggering of Ningaloo Niño events from the Pacific is most sensitive to antecedent SST anomalies in the far western Pacific, rather than in the central Pacific where ENSO typically has greatest magnitude (Figure 2, upper left). To better understand this fuzzy relationship of Ningaloo Niño events with La Niña/El Niño, we calculate the lag correlation of the SST anomaly in September – November (SON) with the Ningaloo Niño index in December – February (DJF) (Figure 2, upper right). The overall pattern is reminiscent of La Niña conditions, but the peak negative correlation in the western Pacific (~-0.6) occurs well west of the Niño-3 box region (defined by 90-150°W, 5°S-5°N) where La Niña events typically have strongest SST cooling. This is reflected by the correlation of the Ningaloo Niño index in DJF with the Niño indices in SON: the correlation with the Niño-4 box region (-0.44; defined by 160°E-150°W, 5°S-5°N) is stronger than with Niño-3 (-0.23), and the peak correlation is even stronger if only the western half of the Niño-4 box is used (-0.54). The premise here is that the initiation of Ningaloo Niño events via the WES feedback is promoted most favourably by a westward shift of the cold anomalies in the Pacific Ocean (compared to a typical La Niña event): The induced cyclonic westerly anomalies over the tropical Indian Ocean are also shifted westward via the atmospheric bridge. This is confirmed by computing the correlation between the negative Niño-3 index and MSLP anomalies (Figure 2, lower left), and between the negative index for the western half of the Niño-4 region and MSLP anomalies (Figure 2, lower right), in SON: A typical La Niña event with maximum negative SST anomaly in the Niño-3 region results in a cyclonic circulation more centred over Australian longitudes (i.e. the pole of the Southern Oscillation is over Darwin), whereas cold anomalies in the west Pacific result in a cyclonic circulation shifted some 20-30 degrees of longitude to the west over the Indian Ocean and resulting anomalous cyclonic northerly flow along the west coast. Thus, a typical La Niña event is less favourable to the generation of anomalous northerlies along the west coast.
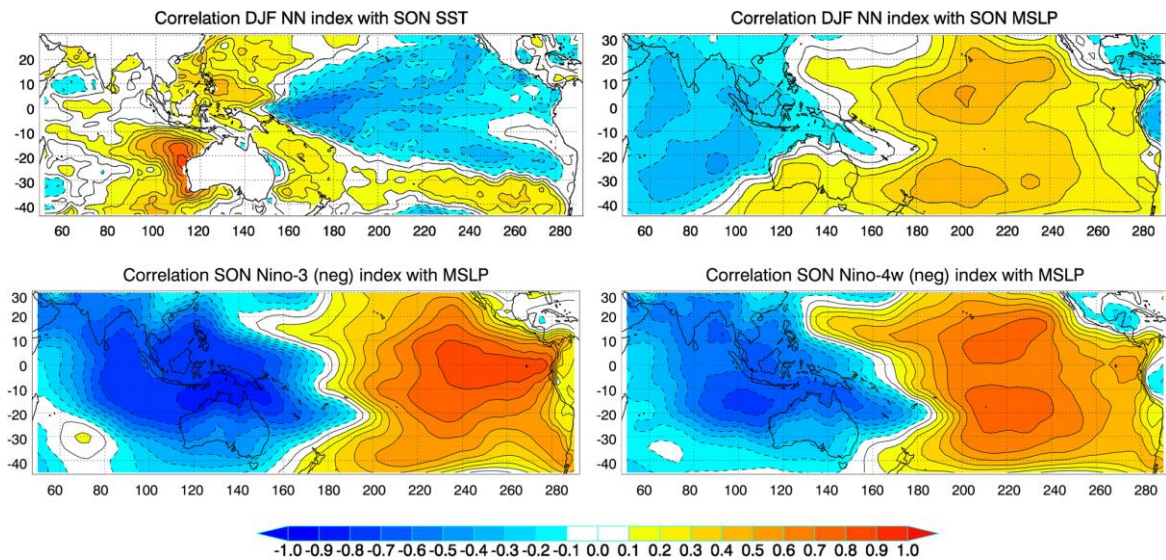
Figure 2: Correlation of the Ningaloo Niño index in DJF with anomalous SST (top left panel) and MSLP (top right panel) in SON, and correlation of the negative Niño-3 (bottom left panel) and negative Niño-4w (bottom right panel) indices with anomalous MSLP in SON.

Concluding remarks

The motivation for this work was to better understand what gave rise to the record large Ningaloo Niño event during early 2011. The results of this study suggest that a combination of remote forcing from La Niña and local amplification along the coast coincided to produce the large 2011 event. We have recently extended this work to explore the role for decadal variations in the background state that act to precondition development of extreme Ningaloo Niño events (Feng et al. 2014).

References

Feng M., M.J. McPhaden, S. Xie, and J. Hafner, 2013: La Niña forces unprecedented Leeuwin Current warming in 2011, Sci. Rep., **3**, 1277. doi:10.1038/srep01277

Feng M., H.H. Hendon, S.-P. Xie, A.G. Marshall, A. Schiller, Y. Kosaka, N. Caputi, and A. Pearce, 2014: Decadal increase in Ningaloo Niño since the late 1990s, Geophys. Res. Lett., doi: 10.1002/2014GL062509

Hendon H.H., and G. Wang, 2009: Seasonal prediction of the Leeuwin Current using the POAMA dynamical seasonal forecast model, Clim. Dyn., **34**, 1129-1137

Jones D.A., W. Wang, and R. Fawcett, 2009: High-quality spatial climate data-sets for Australia, Aust. Meteorol. Oceanogr. J., **58**, 233-248

Kataoka T., T. Tozuka, S. Behera, and T. Yamagata, 2014: On the Ningaloo Niño/Niña, Clim. Dyn., **43**, 1463-1482

Yin Y., O. Alves, and P.R. Oke, 2011: An ensemble ocean data assimilation system for seasonal prediction, Mon. Wea. Rev., **139**, 786-808

A CROSS-TIME SCALE COUPLING AND IMPACT ON FREQUENCY OF EXTREME EL NIÑO EVENTS.

Wenju Cai[1], Guojian Wang[1], Xiao-Tong Zheng[2], Wenxiu Zhong[2], Agus Santoso[3], Arnold Sullivan[1], and Hailin Yan[1]

[1]*CSIRO Oceans & Atmosphere, Aspendale, Vic, Australia*
[2]*Physical Oceanography Laboratory, Qingdao Collaborative Innovation Center of Marine Science and Technology, Ocean University of China, Qingdao, China*
[3]*The University of New South Wales, Sydney 2052, Australia*

wenju.cai@csiro.au

Abstract

Why some El Niños grow into extreme intensity while others don't is a long-standing scientific issue. Here, we show that the mean state associated with a positive phase of the Pacific Decadal Oscillation (PDO) promotes development of strong El Niño events. This association of a positive PDO with more frequent strong El Niño is produced by the majority of 17 climate models participating in Coupled Model Intercomparison Project Phase 5 (CMIP5) with a strong intermodel consensus (Fig. 1).   Because a positive PDO phase is in part a response to El Niño, a positive feedback across time scales operates, substantially influencing the frequency of strong El Niño from one decade to another. This decadal influence must be taken into account in projection of El Niño changes under greenhouse warming.
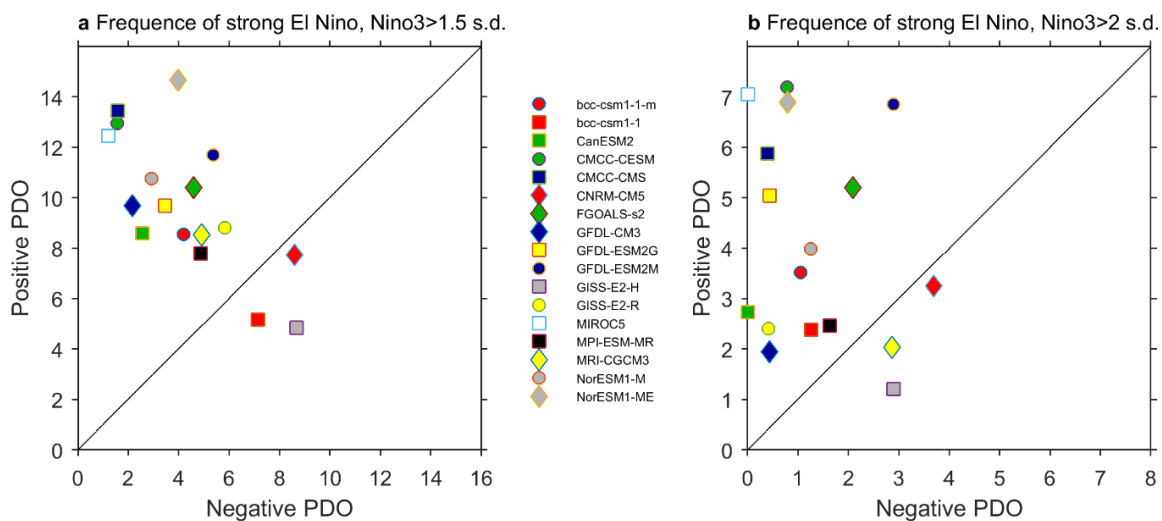
Figure 4 | Frequency (events per 100 years) of strong El Niño (events per 100 years) during the positive and negative phase of the PDO in climate models. The results are obtained from a pre-industrial multi-century-long control experiment with 17 CMIP5 models.   a, The frequency in positive PDO (PDO>0) (y-axis) vs. frequency in negative PDO (PDO<0). A strong El Niño is defined as when the December-January-February average of Niño3>1.5 s.d. b, The same as a but for strong El Niño defined as when the December-January-February average of Niño3>2 s.d.

ENSO VARIABILITY AND CHANGE IN THE ACCESS COUPLED MODELS

Harun A. Rashid

CAWCR, CSIRO Oceans and Atmosphere Flagship, Melbourne, Victoria 3195

Harun.Rashid@csiro.au

Introduction

El Niño–Southern Oscillation (ENSO) is the dominant mode of interannual climate variability, which modulates global weather and climate through atmospheric teleconnections. It owes its existence to the unstable ocean–atmosphere interactions in the tropical Pacific and/or to the excitation by higher-frequency noise of an otherwise stable coupled system (Bjerknes 1969; Battisti and Hirst 1989; Penland and Sardeshmukh 1995). As well as the present-day climate variability, ENSO may also play an important role in determining the future climate change due to human activity. The coupled global climate models (CGCMs) are widely used for understanding and predicting the climate variability and change on various time scales. To be useful in these roles the CGCMs must realistically simulate ENSO and its teleconnection patterns over the historical period, which will then also increase our confidence in the future climate projections provided by these CGCMs. In this paper, we investigate the mechanism of ENSO variability in the historical simulations by the Australian Community Climate and Earth System Simulator (ACCESS) (Bi et al. 2013). We also examine the response of simulated ENSO variability to an enhanced radiative forcing resulting from the quadrupled CO_2 concentration (from its pre-industrial value) using the ACCESS models.

ENSO in ACCESS simulations

ENSO mechanism in the ACCESS historical simulations

The mechanism of the simulated ENSO events is examined in the historical simulations of the ACCESS1.0 and ACCESS1.3 models. This may be elucidated by the lead-lag composites of the zonal wind stress (ZWS), thermocline depth (D20) and SST anomalies presented in Fig. 1. The ZWS anomalies were averaged over the central equatorial Pacific ($160^{o}E$–$150^{o}W$ and $1.3^{o}S$–$1.3^{o}N$) and the D20 and SST anomalies over the eastern equatorial Pacific ($150^{o}W$–$90^{o}W$ and $1.3^{o}S$–$1.3^{o}N$). The composites (El Niño minus La Niña composites divided by 2), made using the Niño3 SST index, are shown for the calendar months over which the typical ENSO events grow and decay.

The composite zonal wind stress anomalies are smaller in the coupled simulations than in observation (Fig. 1a). These anomalies peak in October, September, and December for observation, ACCESS1.0 and ACCESS1.3 coupled simulations, respectively. The SST anomalies, on the other hand, peak in December for observation and ACCESS1.0 simulation, and in March for ACCESS1.3 simulation (Fig. 1c). Thus, the zonal wind stress anomalies peak 2-3 months earlier than when the corresponding SST anomalies peak in observation and the coupled simulations. The composite D20 anomalies (Fig. 1b) peak (i.e., deepen most) one month after the westerly wind stress anomalies (Fig. 1a), but 1-2 months before the corresponding SST anomalies. This coupled evolution of the ZWS, D20 and SST anomalies is a key part of an expanded Bjerknes' positive feedback loop (e.g., van Oldenborgh et al. 2005), which proposes that the central equatorial Pacific westerly anomalies deepen the eastern equatorial Pacific thermocline about a month later through the Kelvin wave propagation. The increased thermocline depth subsequently increases the SST through the thermocline feedback, and the increased SST, in turn, reinforces the westerly anomalies,

thereby completing the positive feedback loop. Thus, the composites in Fig. 1 indicate that the developing phase of ENSO is consistent with this Bjerknes feedback loop in both the ACCESS models, as it is in observation.

The occurrence of the maximum SST anomalies in March in the ACCESS1.3 simulation shows a bias in the seasonal ENSO locking in this model, the mechanism of which has been studied in detail in Rashid et al. (2015).
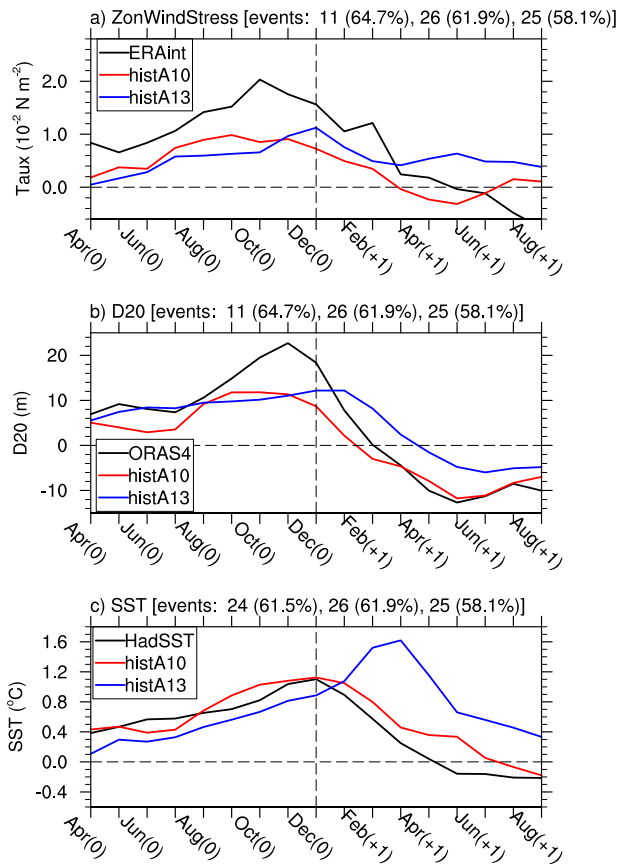
Fig. 1. Lead–lag ENSO composites of the a) ZWS, b) D20 and c) SST anomalies from observations and historical simulations. Only those ENSO events are included in the composites that peak during November, December and January for observation and ACCESS1.0 and during February, March and April for ACCESS1.3. The numbers (and percentages) of ENSO events satisfying this criterion are shown, from left to right, on top of the figures for observation, ACCESS1.0 and ACCESS1.3.

Changes in ENSO variability due to enhanced radiative forcing

The changes in ENSO variability due to an enhanced radiative forcing is studied by comparing ENSO variability simulated in the pre-industrial control and abrupt4xCO2 simulations by the ACCESS models. The strengths of ENSO variability in these simulations are shown by the wavelet spectra of the Niño3 index (Fig. 2). The time-mean spectra are also attached to the right-hand side of the respective panels. It is clear that the ENSO variability is stronger in the abrupt4xCO2 simulations (bottom panels) than in the corresponding pre-industrial control simulations (top panels). Also, the period at which the peak variance occurs has become shorter in the abrupt4xCO2 simulations. The strengthening of ENSO amplitude is larger in ACCESS1.3 than in ACCESS1.0.
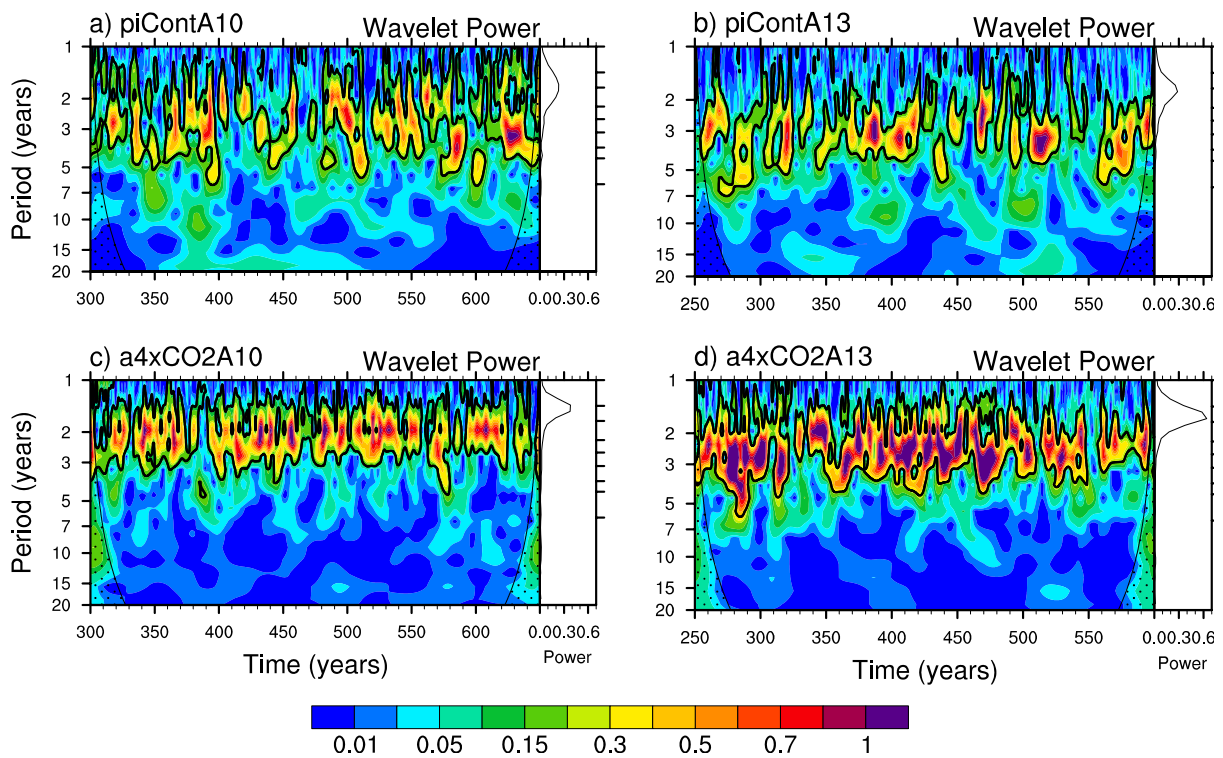
Fig. 2. Wavelet spectra of the Niño3 indices from the: a) ACCESS1.0 pre-industrial control simulation, b) ACCESS1.3 pre-industrial control simulation, c) ACCESS1.0 abrupt4xCO2 simulation, and d) ACCESS1.3 abrupt4xCO2 simulation. The time-mean spectra are attached to the panels on the right-hand side.
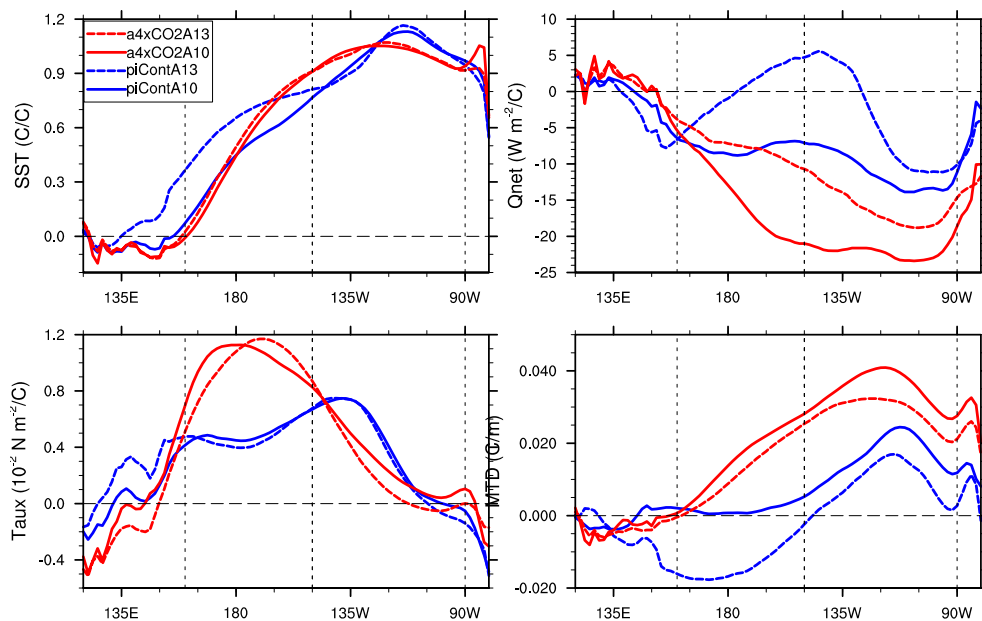
Fig. 3. Longitude profiles of regression coefficients onto the Niño3 index of SST (top left), ZWS (bottom left), and net heat flux (top right) anomalies. The bottom right plot shows the regressions of SST anomalies onto the Niño3 averaged D20 anomalies. The vertical lines indicate the zonal sectors associated with the Niño4 and Niño3 regions.

We now examine the changes in various ENSO feedbacks to understand the causes of strengthening ENSO variability in the abrupt4xCO2 simulation. The main ENSO feedbacks in the equatorial Pacific are shown

in Fig. 3 as the regression coefficients of SST, ZWS, net heat flux anomalies onto the Niño3 index and also the regression coefficient of SST anomalies onto the Niño3 averaged D20 anomalies. There is an increased SST sensitivity to ENSO in the central-eastern Pacific in the abrupt4xCO2 simulation (top left figure; red curves), consistent with the strengthening of ENSO in this simulation. Marked increases in the ZWS feedback (bottom left figures) and the net heat flux feedback (top right figure) are also found. The ACCESS1.3 model shows a positive net heat flux feedback in the central-eastern Pacific in its pre-industrial control simulation. This is a bias in this model resulting from the excessive low-level clouds simulated by this model, which has been extensively discussed in Rashid et al. (2015). The SST sensitivity to the D20 anomalies (the "thermocline" feedback) is also increased significantly in the abrupt4xCO2 simulation (bottom left figure). Therefore, all the main ENSO feedbacks, both positive and negative, become stronger in the ACCESS simulations under the enhanced radiative forcing due to an abrupt4xCO2 concentration, the net effect of which is to strengthen the ENSO variability.

Conclusions

In this paper, we have investigated the mechanism of ENSO variability in the two ACCESS models under the historical condition and the change of ENSO variability due to an enhanced radiative forcing. This is done using the historical, pre-industrial control and abrupt4xCO2 simulations by the ACCESS1.0 and ACCESS1.3 coupled models. We find that

1) The mechanism of ENSO developments in the historical simulation is consisted with the expanded Bjerknes' positive feedback loop: the Kelvin waves excited by the central equatorial Pacific westerly anomalies propagate to the eastern equatorial Pacific and deepen the thermocline there about a month later. The increased thermocline depth then increases the SST through the thermocline feedback, and the increased SST, in turn, reinforces the westerly anomalies, thereby completing the positive feedback loop.

2) The ENSO variability becomes stronger under an enhanced radiative forcing in the two ACCESS models. This strengthening is a result of the net effect of stronger ENSO feedbacks, both positive and negative, in the abrupt4xCO2 simulation than in the corresponding pre-industrial control simulation.

References

Battisti D. S. and Hirst, A. C. 1989: Interannual Variability in a Tropical Atmosphere–Ocean Model: Influence of the Basic State, Ocean Geometry and Nonlinearity. *J. Atmos. Sci.*, **46**, 1687–1712.

Bi D, Dix M, Marsland SJ, et al. 2013. The ACCESS coupled model : description, control climate and evaluation. *Aust Meteorol Oceanogr* J 63:41–64.
Bjerknes, J. 1969: Atmospheric teleconnections from the equatorial Pacific. *Mon. Wea. Rev.*, **97**, 163–172.

Penland, C. and Sardeshmukh, P. D. 1995: The Optimal Growth of Tropical Sea Surface Temperature Anomalies. *J. Climate*, **8**, 1999–2024.

Rashid, H. A. and Hirst, A.C. 2015: Investigating the mechanisms of seasonal ENSO phase locking bias in the ACCESS coupled model. *Clim. Dyn.* DOI 10.1007/s00382-015-2633-y

van Oldenborgh G., Phillip S., Collins M. 2005. El Nino in a changing climate : a multi-model study El Nino. Ocean Sci 1:81–95.

THE SEASONALLY CHANGING CLOUD FEEDBACKS CONTRIBUTION TO THE ENSO SEASONAL PHASE LOCKING

Dietmar Dommenget

School of Earth, Atmosphere and Environment, Monash University, Melbourne

dietmar.dommenget@monash.edu

Abstract

ENSO variability has a seasonal phase-locking, with SST anomalies on average decreasing during the beginning of the year and SST anomalies increasing during the second half of the year. As a result of this, the ENSO SST variability is smallest in April and the so call 'spring barrier' exists in the predictability of ENSO. In this study we analysis how the seasonal phase-locking of surface short wave radiation associated with cloud cover feedbacks contribute to this phenomenon. We base our analysis on observations and simplified climate model simulations. At the beginning of the year, the warmer mean SST in the eastern equatorial Pacific leads to deeper clouds whose anomalous variability are positively correlated with the underlying SST anomalies. These observations highlight a strong negative surface short wave radiation feedback at the beginning of the year in the eastern Pacific (NINO3 region). This supports the observed seasonal phase-locking of ENSO SST variability. This relation also exists in model simulations of the linear recharge oscillator and in the slab ocean model coupled to a fully complex atmospheric GCM. In summary this study has shown that the seasonal phase-locking, as observed and simulated, is linked to seasonally changing cloud feedbacks.

UNDERSTANDING AND PREDICTING THE CONTRAST OF AUSTRALIAN SPRINGTIME RAINFALL OF 1997 AND 2002

E.-P. Lim[1] and H. H. Hendon[1]

[1]*Environment and Research Division, Bureau of Meteorology, Melbourne*

e.lim@bom.gov.au

Abstract

El Niño is known to be one of the most important drivers to the rainfall deficit over Australia. However, Australia received near-normal springtime rainfall during the record strong El Niño in 1997, while it suffered from severe drought, especially in the east, during the weak El Niño of 2002. This study explores the causes and predictability of these different springtime rainfall responses over Australia to El Niño in 1997 and 2002.

Statistical reconstruction of the rainfall anomalies and forecasts produced from the Australian Bureau of Meteorology's dynamical sub-seasonal to seasonal forecast system, Predictive Ocean and Atmosphere Model for Australia (POAMA), suggested that the eastward and westward shifts of the maximum SST warming of El Niño contributed to the near-normal and dry responses of Australian spring rainfall in 1997 and 2002, respectively. Hence, the contrasting rainfall responses were largely predictable. However, the dry conditions in 2002 were significantly enhanced by the occurrence of the record strength negative phase of the southern annular mode (SAM). This extraordinary negative SAM was induced by a sudden stratospheric warming, and therefore, it could only be predicted with the use of realistic atmospheric initial conditions. Furthermore, this negative SAM was only predicted in the atmosphere–ocean coupled configuration of POAMA, suggesting the importance of the atmosphere-ocean coupling in the skillful prediction of the SAM. Consequently, predictability of the severity of the 2002 drought over Australia was strongly constrained by the predictability of the SAM, despite the high predictability of the drier than normal condition of 2002 spring that stems from the anomalous central Pacific warming of 2002 El Niño. Full details of this study can be found in Lim and Hendon (2015).

References

Lim, E.-P. and H. H. Hendon 2015: Understanding the contrast of Australian springtime rainfall of 1997 and 2002 in the frame of two flavors of El Niño. J. Climate, 28, 2804–2822.

COUPLED OCEAN-ATMOSPHERE PROCESSES IN TROPICAL CYCLONES ON SHORT AND LONG TIMESCALES

Kevin J. E. Walsh[1], Alex Babanin[2] and Lachlan Stoney[1]

[1]*School of Earth Sciences, University of Melbourne, Parkville*
[2]*Swinburne University, Hawthorn, Victoria*

kevin.walsh@unimelb.edu.au

Introduction

Considerable work has been performed on the effects of climate on tropical cyclones. Rather less work has been performed on the possible effects of tropical cyclones on climate, in this case ocean climate. Tropical cyclones have substantial effects on ocean conditions on short timescales, as numerous studies have shown. On longer timescales, there is a debate regarding the magnitude of the effect of tropical cyclones on the ocean climate system. Emanuel (2001) proposed that the net ocean heat uptake caused by tropical cyclones must be balanced by a poleward heat transport out of the tropics, thus proposing a significant climate role for tropical cyclone wind forcing. Vincent et al. (2013) used a 0.5 degree resolution global ocean model forced with the CORE-II interannual atmospheric data set, modified to include higher-resolution winds from tropical cyclones. They found that the effect of tropical cyclones on the global poleward heat transport was small due to factors that compensated for the heat input of tropical cyclones, including storage of heat below the thermocline that was then released in subsequent seasons in the tropics instead of being transported poleward. They also found, however, that other more regional effects of tropical cyclone winds were noticeable in their experiments. Bueti et al. (2014) used a higher-resolution ocean model (0.25 degree) to also find noticeable regional ocean climate impacts of tropical cyclone winds.

Another issue affecting the distribution of heat in the ocean is the representation of surface mixing. A number of different mixing schemes are employed in global ocean models. One process that has been largely neglected to date is the possibility that unbroken surface waves might have an effect on ocean mixing processes (Ghantous and Babanin 2014). This effect differs from Langmuir circulations in that it represents a direct impact of the orbital motion of the waves themselves rather than mixing generated by Stokes drift. Here we test the effect of the inclusion of a parameterisation of this wave mixing process, for simulations both with and without tropical cyclone winds.

Methods

The ocean model employed is the Modular Ocean Model (MOM) version 5 (Griffes et al. 2012). The horizontal resolution of the version of the model used is approximately 0.25 degrees. For the ocean mixing, the one-dimensional mixing model GOTM is used (Umlauf et al. 2011) as implemented within the MOM modelling system. The parameterization of wave-induced mixing employed is that of Ghantous and Babanin (2014). The reader is referred to that paper for the details of this parameterization. Here, this parameterization has been implemented in MOM as a modification of the k-epsilon mixing scheme (e.g. Rodi et al 1987). The k-e scheme calculates the competing effects of the turbulent kinetic energy (k) versus the dissipation of that energy, and so calculates an approximate to the turbulent kinetic energy equation. The wave-induced mixing is included as an additional term in the turbulent mixing and is added to the shear production term.

To represent the waves, the wave parameterization of Ganopolski et al. (2001) was employed (see also Babanin et al. 2009). This simple parameterization calculates the wave amplitude a and frequency ω from the anemometer height (10 m) wind speed U, assuming a fully developed sea:

$$a = 0.12 \frac{U^2}{g}$$

$$\omega = 0.82 \frac{g}{U}$$

where g is the gravitational acceleration. Here we assume that the significant wave height $H_s = 2a$ (Babanin et al. 2009).

The model runs are initialized from a MOM5 ocean model run using the CORE-II atmospheric boundary conditions (Large and Yeager 2009; Griffes et al. 2012). The model is run for 32 years (1948-1979) as a spin-up and the model is then run with and without wave-induced mixing after that time, for a period of one year (1980). Tropical cyclone wind fields are incorporated by interpolating the CORE-II atmospheric forcing from 2.5 degrees to 0.25 degree and then artificially inserting tropical cyclones using a wind profile model.

Results

Figure 1 shows results for runs without enhanced tropical cyclone winds, for simulations with and without wave mixing, for average conditions in December 1980, at a depth of 5m. There is a noticeable near-surface effect of the introduction of wave-induced mixing, with temperatures falling by as much as a degree in large parts of the Southern Ocean. In contrast, in the wintertime Northern Hemisphere, the net effect of enhanced mixing is mostly warming. This is explained by noting that in the winter hemisphere, the ocean surface is typically cooling due to air temperatures that are often colder than sea surface temperatures. Thus the introduction of enhanced mixing would tend to make the surface layers more like the deeper regions of the mixed layer, thus causing warming.

Figure 2 shows the specific mixing signature of tropical cyclone-induced mixing, this time including the effect of high-resolution tropical cyclone winds. The introduction of wave-induced mixing causes a reduction in the upwelling in the centre of the track, leading to a corresponding reduction in downwelling on the sides of the track. This reduced downwelling causes the mixed layer to shallow, and this effect appears to be more than compensating for the deepening would occur from increased mixing alone. This typical pattern of response is seen across a number of different intense tropical cyclone cases (not shown).

In conclusion, the introduction of wave-induced mixing appears to have a regional effect on the simulation of ocean climate. The effect is particularly pronounced in tropical cyclones but results analysed to date indicate that the net effect of tropical cyclones on the ocean climate tends to be regional rather than global.
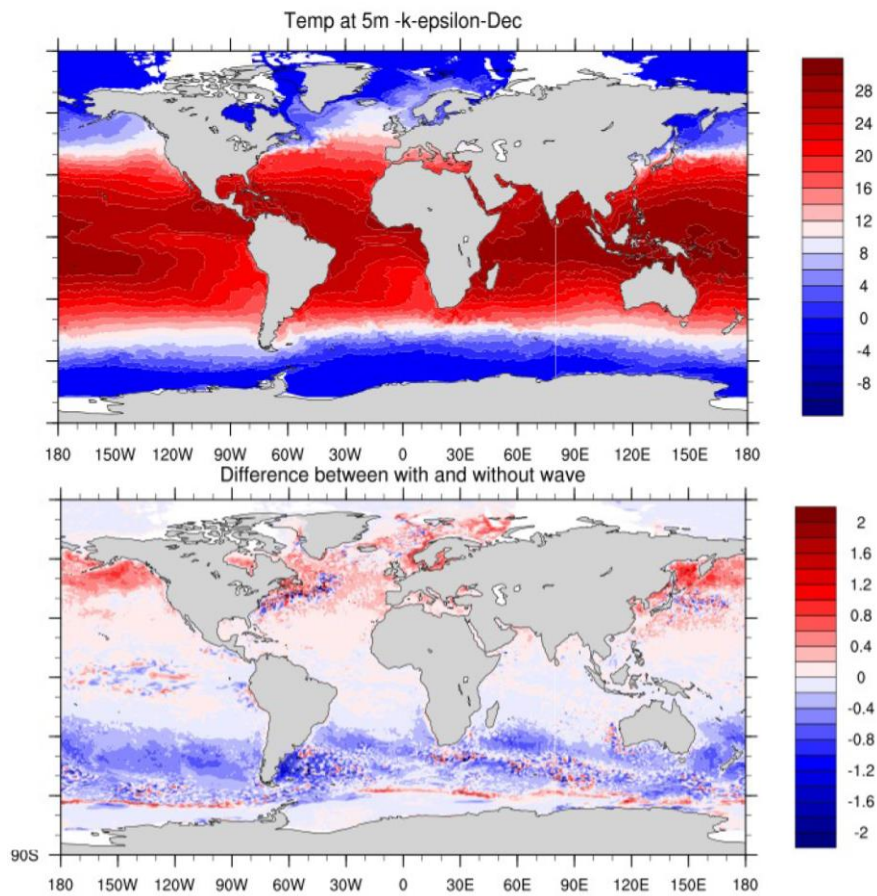
Figure 1. Simulated December 1980 mean temperature at a depth of 5 m (^{o}C), for simulation without wave-induced mixing (top panel) and the difference, wave induced mixing minus without.
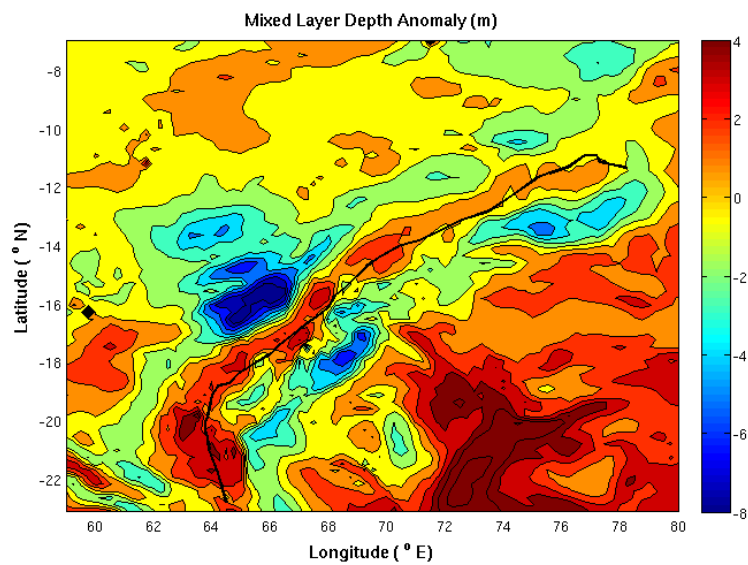
Figure 2. Change in mixed layer depth (m) for Tropical Cyclone Kalunde (2003), wave induced mixing minus without (m), one-month average March 2003. The track of the cyclone centre is indicated by the black line.

References

Babanin, A.V., A. Ganopolski, and W.R.C. Phillips, 2009: Wave-induced upper ocean mixing in a climate modelling of intermediate complexity. *Ocean Modelling,* **29**, 189-197

Bueti, M.R., I. Ginis, and L.M. Rothstein, 2014: Tropical cyclone-induced thermocline warming and its regional and global impacts. *J. Climate*, **27**, 6978-6999.

Emanuel, K.A., 2001: Contribution of tropical cyclones to meridional heat transport by the oceans. *J. Geophys. Res*., **106**, 771-781.

Ganopolski, A., Petoukhov, V., Rahmstorf, S., Brovkin, V., Claussen, M., Elisseev, A., Kubatzki, C., 2001. CLIMBER-2: a climate system model of intermediate complexity. Part II: model sensitivity. *Clim. Dynam*., **17**, 735–751.

Ghantous, M., and A.V. Babanin, A. V., 2014: One-dimensional modelling of upper ocean mixing by turbulence due to wave orbital motion. *Nonlin, Proc. Geophys.,* **21**, 325-338.

Griffies, S. M., M. Winton, B. Samuels, G. Danabasoglu, S. Yeager, S. Marsland, H. Drange, and M. Bentsen, 2012: Datasets and protocol for the CLIVAR WGOMD Coordinated Ocean-sea ice Reference Experiments (COREs), WCRP Report No. 21/2012, pp. 21

Large, W.G. and S.G. Yeager. 2009: The global climatology of an interannually varying air-sea flux data set. *Clim. Dynam.,* **33**, 341-364, doi:10.1007/s00382-008-0441-3.

Rodi, W., 1987: Examples of calculation methods for flow and mixing in stratified fluids. *J.Geophys. Res. Oceans,* **92,** 5305-5328.

Umlauf, L., Bolding, K., and Burchard, H.: GOTM Scientific Documentation.Version 4.2, available at: http://www.gotm.net/pages/documentation/manual/pdf/a4.pdf, last access: 23 March 2011.

Vincent, E.M., G. Madec, M. Lengaigne, J. Vialard, A. Koch-Larrouy, 2013: Influence of tropical cyclones on sea surface temperature seasonal cyclone and ocean heat transport. *Clim. Dynam*., **41**, 2019-2038.

RECENT FOG FORECASTING RESEARCH AT THE MET OFFICE

Adrian Lock and Ian Boutle

Atmospheric Processes and Parametrizations, Met Office, Exeter, UK

adrian.lock@metoffice.gov.uk

Abstract

Fog can have a large impact on society but most customer requirements (in terms of spatial and temporal accuracy) go well beyond what current NWP can achieve. Some progress has been made in recent years in the representation of stable boundary layers, improving near surface nighttime temperature and humidity but with disappointingly little improvement in visibility forecasts. The Met Office has initiated an extensive field campaign, LANFEX, that is giving unprecedented insight into the local and regional variability in near-surface meteorology and fog properties. Some examples are given (with more in the talk) to illustrate the modelling challenges, recent progress and future plans.

Introduction

Fog can certainly be considered extreme weather because of the significant effects it can have on human society. At busy airports with no spare capacity, the required reduced flow rates caused by fog lead to severe delays and cancellation of flights, which has significant cost implications, knock-on effects at other airports around the world, and causes inconvenience to thousands of passengers. But without these safety restrictions the human cost would likely be much higher. Shipping, road and rail traffic are similarly affected by safety considerations, and fog itself can influence the health of vulnerable groups (Tanaka et al. 1998). When all losses are included, severe fog events can easily be as costly as other severe weather events (Gultepe et al. 2007).

Despite this importance, the skill of numerical weather prediction (NWP) in forecasting fog is relatively low. This is due to its complex nature, its existence and development depending almost equally on every physical parametrization within the model, with subtle interactions between them and often a lack of any significant large-scale forcing. Furthermore, in many sites fog occurs only relatively rarely and can often be patchy in nature, making meaningful deterministic site-based forecasts, and verification, extremely hard. Ultimately probabilistic approaches have to be the way forward but these still require sufficient data to be suitably calibrated, and identifying appropriate ways to retune the underlying model is made harder because fog can be generated through several very different mechanisms (radiation fog, advection fog, stratus lowering into fog, etc) which could well have different biases.

Several systems are used at the Met Office to guide forecasting of low visibility. The UKV gives deterministic forecasts over the UK area on a 1.5km grid, with its own analysis, and includes a prognostic aerosol that interacts with the model's microphysics as well as visibility diagnosis. MOGREPS-UK is a 12 member ensemble over the UK on a 2.2km grid which, in its current configuration, down-scales the global ensemble. To give further guidance on the spatial heterogeneity of fog, the "London Model" has been introduced for this winter that runs twice-daily on a 333m grid over the wider London area (down-scaling the UKV). Despite only sampling uncertainty from the global ensemble, MOGREPS-UK has shown significant local variability in fog, thus illustrating the importance of the large scale forcing for fog (timing of fronts, low cloud cover, surface windspeed, etc). This winter MOGREPS-UK is being enhanced to perturb around the UKV analysis and also to introduce stochastic variations to model parameters in order to sample uncertainty in small-scale physics, and so increase the spread in low visibility forecasts. Other

downscaling methods are being explored in postprocessed output, including neighbourhood techniques, as well as statistical and empirical forecasting methods. To help coordinate activities across the Met Office, a Low Visibility working group meets on a 6 monthly basis.

A key component to the Met Office strategy is the mounting of a major field campaign called LANFEX. This is amassing a wealth of data that is being used in its own right and in combination with very high resolution modelling studies to improve our understanding of fog processes and to improve the representation of those processes in the MetUM.

Current biases in stable boundary layers

A particular challenge with fog is to accurately represent stable boundary layers (SBL). This is hard owing to the weak and sometimes intermittent behaviour of turbulence and its interaction with other small-scale processes (especially a coupling to the land surface with strong dependence on its local characteristics, but also with radiative fluxes, drainage flows, gravity waves, low-level jets and a wide zoo of mesoscale atmospheric phenomena). A key and challenging prerequisite is also an accurate forecast of low level cloud cover but that is beyond the scope of this presentation.

In parallel suite 31 (PS31, January 2013) developments were introduced to the representation of the surface and stable boundary layers in the UKV that reduced (by around a third in trials) a large average warm nighttime screen temperature bias. This error was worst under light winds and clear skies when turbulence might be expected to be weak and intermittent. A significant nocturnal clear sky warm bias persists, however, and is associated with a cold daytime bias. Detailed comparisons with observations from the Met Office Observation Based Research unit at Cardington have found that this suppressed diurnal range of surface air temperature is associated with an excessively large diurnal range of near-surface soil temperature. This suggests the coupling between atmosphere and soil is too strong and recent tests with more realistic local surface and vegetation properties, combined with further reductions to SBL turbulent mixing, have shown some significant improvement in the remaining nighttime warm bias. Further investigation into the representation of the vegetation canopy is on-going but it is clear that improving the dataset of vegetation properties (over the UK but also globally) is a high priority.

A further challenge arising from the model's systematically suppressed diurnal range in surface temperature is for data assimilation to distribute the resulting increments correctly in the vertical, both above the surface and also down into the soil. Currently the screen temperature increment is simply copied into the top soil level (in order to improve the persistence of the increment into the forecast). Given the 10cm thickness of this level, however, this has the potential to have an excessive impact on the surface energy budget in the opposite phase of the diurnal cycle. Similarly, the strong diurnal variation of boundary layer depth also implies that the screen-level increments should be correlated over a much smaller depth at night than during the day, a variability that is not yet possible with the climatological statistics currently used. For example, excessive propagation vertically of the cooling increment necessary to correct a nocturnal warm bias at screen level (which is typically associated with a cold bias 100-200m above the surface), could exacerbate the tendency for a cold daytime bias.

High resolution fog observations and modelling

Comparisons with detailed observations at Cardington over the last few years have investigated the ability of a variety of models to simulate fog. Porson et al (2011) found the Met Office large-eddy and single-column models did well with many aspects but failed to deepen the fog layer sufficiently, suggesting an influence from local heterogeneity that was not represented. They also noted the role of aerosols or haze within, and above, the fog layer in controlling the radiative balance. Price et al (2014) showed the benefit of using ensemble simulations as a research tool, finding a systematic tendency in the MOGREPS-UK ensemble to lift fog into low stratus.

Expanding on these successes, and given the strong requirement to improve fog forecasts, the Met Office has mounted a major field campaign, known as LANFEX, deploying local observing networks in two separate regions (illustrated in Fig.1) to sample the local heterogeneity of the flow as well as fog. One region, around Cardington, offers the opportunity to study fog processes in a relatively homogeneous environment where any heterogeneity and development of the fog is more likely to occur due to internal processes rather than being constrained by the local topography. The other, in Shropshire, has small scale complex terrain with fog often being very different between adjacent valleys, or even different parts of the same valley. It is likely that this is due to external factors, i.e. the role of drainage flows and surface heterogeneity in this more complex environment, and so these observations contrast with those made at Cardington. A crucial part of LANFEX is to combine these observations with high resolution MetUM simulations. These are being used as a tool to understand the important processes in fog formation and development, and also to validate and help improve the model parametrizations.
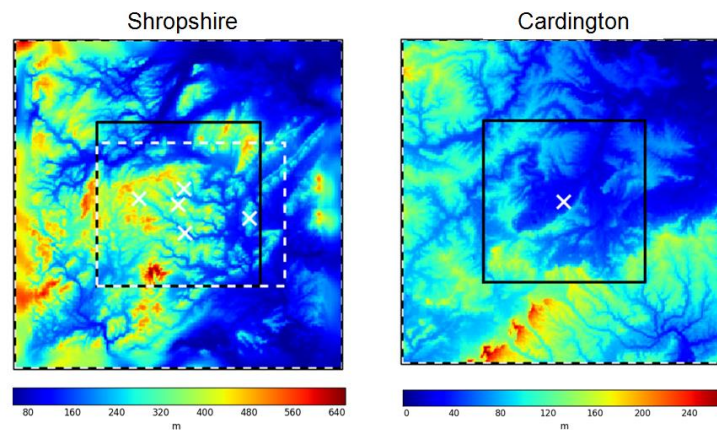
Figure 1: orographic height for the 80km square area surrounding the two LANFEX regions (note the different colour scales)

Stable boundary layers, fog and the influence of orography

Boutle et al (2015) have evaluated the performance of the LM (at 333m) for forecasting low visibility events compared to the UKV (at 1.5km). Much of the signal was dominated by a significant impact from the default settings in the model cloud parametrization that led to systematically less cloud (motivating on-going research to enhance its flexibility and realism). Benefits were found, however, from the higher resolution orography generating additional turbulent mixing in the SBL that gave thinner and patchier fog (see Fig.2). Enhanced turbulence driven by subgrid drainage flows has already been introduced in the UKV but has little impact with these scales of orography and so further work will investigate alternative approaches.
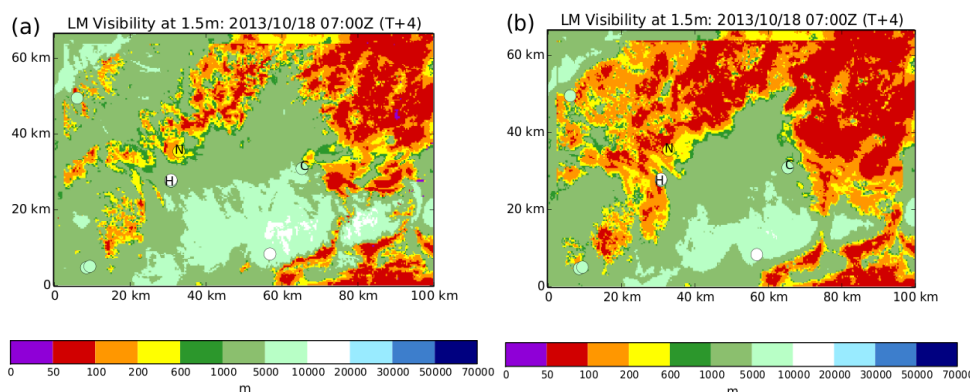
Figure 2: Visibility forecasts for 07 UTC on 18 October 2013 from (a) the LM and (b) the LM with UKV orography. Filled circles show the available observations.

Microphysics of fog

A significant benefit of the PS31 UKV upgrade to the parametrization of SBLs was to greatly improve the skill of the model at forecasting high relative humidity at the screen level, increasing the frequency to be much closer to that observed, especially in winter (see verification of RH>96% in Fig 3a). It might be thought that such an improvement to the model's moisture distribution ought to deliver significant benefit to the forecasting of low visibility but, disappointingly, Fig.3b shows that there has been no appreciable improvement.

The importance of aerosol on visibility was highlighted by Wilkinson et al (2013) who introduced a reduction in near-surface cloud droplet concentration to mimic the suppression of droplet activation in stable fog layers. More recent MetUM comparisons with a LANFEX case study at Cardington found the fog became optically thick far more rapidly than was observed, resulting in excessive downwelling longwave radiative fluxes and surface warming, combined with fog-top radiative cooling, that caused the fog to transition into a thick well-mixed mature fog far too early in the evening. Experiments where the specified cloud droplet number profile was reduced to better match the observed succeeded both in maintaining an optically thin fog and also increasing the rate of fog deposition to the surface to better match those observations too. As real fogs mature and become more turbulent so their droplet numbers are found to increase. In order to realistically represent this evolution, greater complexity in the microphysical scheme may be required and such tests will be conducted over the coming year.

The diagnosis of visibility has also come under scrutiny. Developed many years ago, this calculates the scattering from appropriately hydrating the model's prognostic aerosol mass but, for simplicity, assumes single values for the aerosol properties. This has the effect of making the diagnosed visibility very sensitive to small changes in relative humidity. Alternative methods are currently being investigated to increase the robustness of this diagnosis, such as assuming a distribution of aerosol. Longer term, the extent to which the aerosol chemistry needs to be interactive will also be investigated.
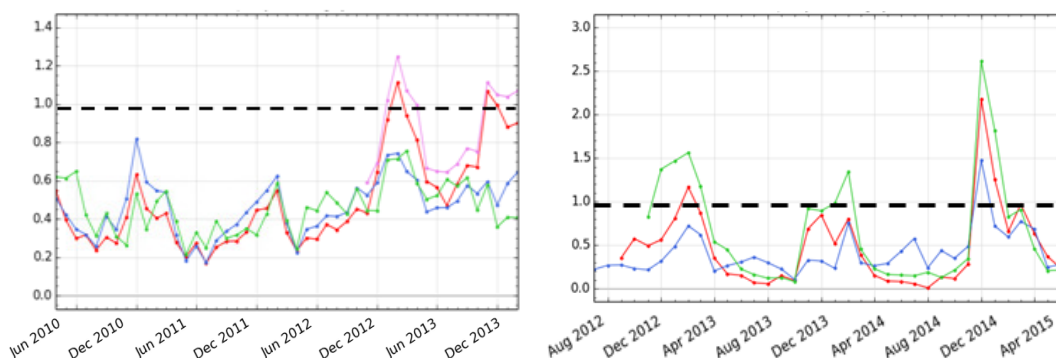
Figure 3: 3 year monthly average time series, compared to SYNOP sites over the UK, at T+24 of (a) frequency bias for RH>96%, for UKV, NAE (old 12km LAM over Europe), Euro4 (newer 4km LAM over Europe) and GM; (b) frequency bias for visibility less than 1km, for UKV, Euro4 and GM. Note that the visibility bias in Dec 2014, and to a lesser extent Jan 2015, was exceptionally high but these months had very little observed fog making the results statistically rather unreliable. A package of changes to improve the representation of stable boundary layers was introduced in Jan 2013.

References

Boutle, IA, Finnenkoetter, A, Lock AP and Wells H (2015) The London Model: forecasting fog at 333 m resolution. *Q. J. R.Meteorol. Soc,* doi:10.1002/qj.2656.

Gultepe I, Tardif R, Michaelides SC, Cermak J, Bott A, Bendix J, Muller MD, Pagowski M, Hansen B, Ellrod G, Jacobs W, Toth G, Cober SG. (2007) Fog research: A review of past achievements and future perspectives. *Pure Appl. Geophys.* 164: 1121–1159

Porson, A, Price, J, Lock, A, Clark, P (2011) Radiation Fog. Part II: Large-Eddy Simulations in Very Stable Conditions. *Bound. Layer Meteor.,* 139, 193–224.

Price, J, Porson A, Lock A. (2015) An observational case study of persistent fog and comparison with an ensemble forecast model. *Bound. Layer Meteor.* 155: 301–327

Tanaka, H, Honma S, Nishi M, Igarashi T, Teramoto S, Nishio F, S A. (1998) Acid fog and hospital visits for asthma: an epidemiological study. *Eur Respir J* 11: 1301–1306

Wilkinson, JM, Porson ANF, Bornemann FJ, Weeks M, Field PR, Lock AP. (2013) Improved Microphysical Parametrization of Drizzle and Fog for Operational Forecasting using the Met Office Unified Model. *Q. J. R.Meteorol. Soc.* 139: 488–500

PREDICTION HIGH IMPACT WEATHER: THE WEATHER READY NATION APPROACH

Hendrik L. Tolman

NOAA / NWS / NCEP / Environmental Modeling Center.

hendrik.tolman@noaa.gov

Abstract

As of April 1, 2015, the US National Weather Service (NWS) has been formally re-organized. The reorganization went beyond the changing the organizational structure, and is focused around the Weather Ready Nation (WRN) concept. In this concept, weather prediction is considered "end-to-end", going from defining high-impact weather forecast requirements, to modeling, service provisions, and decision support, ultimately focusing on responses of the public to the information provided by the NWS. The presentation will focus on the NWS reorganization, the WRN concept, and its impact on dealing with high-impact weather.

IMPROVING FLOOD FORECASTING SKILL USING REMOTE SENSING DATA

Valentijn R.N. Pauwels, Stefania Grimaldi, Yuan Li, Ashley Wright and Jeffrey P. Walker

Department of Civil Engineering, Monash University, Clayton

Valentijn.Pauwels@monash.edu

Abstract

Floods are among the most devastating natural disasters in Australia. The average annual cost of floods over the last 40 years has been estimated to amount to $377 million, with the 2010-2011 Brisbane and South-East Queensland floods alone leading to $2.38 billion in economic damage, and 35 confirmed deaths.

During the last 5 decades, significant research efforts have been paid towards the monitoring of the global water cycle through satellite remote sensing. The advantage of remote sensing data is the opportunity to provide information at large spatial scales and cover areas that are difficult or impossible to monitor using on-ground techniques. For these reasons there is an increasing interest towards the use of remote sensing data for water management purposes. This presentation will focus on the use of satellite remote sensing data for flood forecasting.

Operational flood forecasting systems typically consist of a hydrologic model, which estimates the amount of water entering a river system, and a hydraulic model, which models the flow of water inside the river system. Therefore, the use of remote sensing data in both types of models will be investigated for the improvement of flood forecasting systems. Remotely sensed soil moisture data will be used to improve the hydrologic model predictions (i.e., the modeled hydrograph into the river network), while remotely sensed water levels and/or flood extent data will be used to improve the hydraulic model predictions (i.e., the modeled water velocities, heights, and floodplain extents).

This presentation will provide an overview of the initial results from the project. Our approach towards to problem will be explained, and the models and test sites that form the basis of the project will be presented.

COUPLED SYSTEMS: FROM PHYSICAL SCIENCE TO COMMUNITY SAFETY

Michael Rumsewicz

Bushfire and Natural Hazards CRC, Melbourne

michael.rumsewicz@bnhcrc.com.au

Abstract

In July 2014, all Australian governments agreed that a new National Fire Danger Rating System is a national priority.

Work has begun on a national statement of functional requirements, the identification of scientific readiness and gaps, a map to manage the system, and indicative costs for a new Australian system. This information will be used to inform future work and investment decisions by all Australian governments.

The intention of a new system would be to incorporate contemporary science that more accurately predicts bushfire risk. This includes factors for fire weather, fuel condition, ignition likelihood, fire behaviour, fire suppression and fire impact.

A national system based on new science that provides more accurate and nuanced predictions of the bushfire risk will better inform decision-makers in their efforts to prevent and respond to bushfires. It will help to:

• protect the community through more targeted preparation and response activities
• deliver interventions to reduce the number, size and cost of fires
• reduce unnecessary disruption to business, government and communities caused by over-warning
• improve fire planning through better distributing resources where they are most needed, and
• enhance community resilience by improving the public's awareness of their immediate exposure to risk.

What is the fire danger rating system?

The Fire Danger Rating System is used by Australian fire and emergency service organisations to calculate the risk of a bushfire occurring and the potential for impact or damage. The system supports a range of critical decisions that are made in response to the threat of a bushfire. This may include readiness activities, such as pre-positioning firefighting resources, issuing public safety warnings and information, or limiting the potential for ignitions through the use of total fire bans or the closure of national parks and schools.

Why the need for change?

The science behind the current system remains largely unchanged since its development in the 1960s. It is limited in the number of factors it can consider to determine fire danger. The system does not, for example, consider new weather inputs developed by the Bureau of Meteorology or potential impacts of a fire. This inhibits the preparedness and response capabilities of emergency services, especially in complex and time-critical operations.

This presentation will discuss how the Fire Danger Ratings System is in itself a complex coupled system, incorporating modelling of meteorological and fire processes, the environment, human behaviour, and communication with the ultimate goal of protecting the community.

DEVELOPING AND IMPROVING THE FLOOD FORECASTING SERVICE

Justin Robinson, Chris Leahy and Johan Veldema.

Bureau of Meteorology

Abstract

HyFS is the Bureau's next generation hydrological forecasting system. The key business driver of the implementation of the system was to provide the Bureau with a national hydrological forecasting system that would be effective, robust and sustainable, allow future expansion, and meet operational best practice. This year HyFS will be fully transitioned to operations across Australia.

HyFS connects the Bureau's hydrological forecasting models with weather and ocean models and real time observations. HyFS is underpinned by a national rainfall and river data collection system that provides real-time data for more than 8000 rainfall and river sensors. It integrates forecast rainfall guidance from NexGenFWS, ACCESS and ECMWF as well as tidal and coastal sea level forecasts from OceanMAPS, and radar-rainfall observations from Rainfields.

HyFS supports the Bureau's existing hydrological models, empirical forecasting techniques and the new SWIFT set of forecasting tools developed by CSIRO through the WIRADA alliance. It allows flood forecasters to use historical flood information through peak heights and the ability to overlay historical floods in real time over the current observations and forecasts.

Forecaster training and development is supported by HyFS-Water Coach, the flight-simulator of hydrological forecasting. It enables forecasters to relive their favourite flood events, demonstrate their competency by forecasting historic events or to test new forecasting approaches in a mode similar to operations.

HyFS is a true enterprise system that is specifically designed to evolve to support new services and to bring the latest forecasting techniques to the operational forecaster's desk.

This paper looks at future plans for HyFS – HyFS 2020. These build on the foundation provided by HyFS to harmonise bespoke manual flood warning services that are currently provided by the Bureau. As part of the recommendations of the ANZEMC Standardisation Taskforce for Hazards Services, the flood warning service needs to automate and harmonise; (i) the alerting service, (ii) the Victorian flood scenario product and (iii) the NSW riverine flash flood service. The automation of these services will bring exciting scientific, technical, operational and service challenges.

The automated alerting service will replace the manual river levels alert system in Tasmania and a variety of other river and rainfall alerting services provided by the Bureau. Initially the focus will be on observed levels with the aim to extend the alerts to include forecast rainfall and river levels.

The automated flood scenario product will replace an existing manual product developed by the Victorian Regional Office, which provides the Emergency Services with an indication of possible flooding over a

range of forecast rainfall amounts. This service is ideally suited to make use of the new ensemble rainfall forecasts now becoming available.

The automated flash flood guidance service focuses on riverine flash flooding (for catchments with a response time less than 6 hours). It will replace the current service provided in NSW. This service is likely to utilise continuous modelling, an approach that is ideally suited to leverage off the short-term ensemble rainfall forecasts and high resolution numerical modelling that will be delivered as part of the Bureau's super computer project.

The paper will provide an overview of HyFS and the scientific, technical, operational and service challenges in releasing these automated services. It will examine the potential for improved flood warning services that can leverage off the government's investment in the Bureau's new super-computer.

MORE ACCURATE FIRE DANGER WARNINGS THROUGH THE USE OF NWP SYSTEMS

Vinodkumar[1,2] and Imtiaz Dharssi[1]

[1]*Bureau of Meteorology, Australia*

[2]*Bushfire and Natural Hazards Cooperative Research Centre, Australia*

v.kumar2@bom.gov.au

Abstract

The McArthur Forest Fire Danger Index (FFDI) used in Australia has a component representing fuel availability called the Drought Factor, which in turn is partly based on soil moisture deficit, commonly calculated as either the Keetch–Byram Drought Index (KBDI) or Mount's Soil Dryness Index (SDI). The KBDI and SDI are essentially simplified water balance models to estimate soil moisture depletion in the upper soil levels, and are driven by precipitation and maximum temperature analyses. In this study, we compare these two old empirical models against an emerging new approach in soil moisture estimation in the form of land surface modelling. Validation of these models are carried against *in situ* observations of soil moisture from OzNet and CosmOz networks in Australia. The results indicate that soil moisture from land surface model employed within Bureau of Meteorology's operational numerical weather prediction (NWP) model produce a better skill than KBDI and SDI. The average correlations obtained over all sites are 0.76, 0.64 and 0.74 for NWP, KBDI and SDI respectively.

Introduction

The ignition, spread and temporal variations in fire danger depend heavily on fuel availability (FMC; Chandler *et al.*, 1983). Because fuel availability measures are not always readily available, fire danger rating systems include sub-models to estimate this quantity from weather observations. The McArthur Forest Fire Danger Index (FFDI; McArthur 1967) used in Australia for instance, has a component representing fuel availability called the Drought Factor, which in turn is partly based on soil moisture deficit which is commonly calculated in Australia as either the Keetch–Byram Drought Index (KBDI; Keetch and Byram, 1968) or Mount's Soil Dryness Index (SDI; Mount 1972). These two empirical water balance models are, however, over-simplified and may lead to large uncertainties in the estimated soil moisture deficit. With the advancement in the science of soil moisture estimation and prediction in the form of physically based land surface models, more comprehensive and systematic measures of soil moisture is now available. Research is already started to deliver a better provision of soil dryness products with greater accuracy at a much higher spatial and temporal resolution for use in fire danger ratings. This study intends to be of a preliminary nature to this research and describes the comparison between soil moisture from old empirical models (KBDI and SDI), a land surface model and *in situ* observations.

Data and Methodology

For the present study, KBDI and SDI are generated for the whole of Australia at 0.05^{o} x 0.05^{o} resolution using the Australian Water Availability Project (AWAP) daily rainfall and daily maximum temperature data (Jones *et al.*, 2007) for a period of 40 years, from 1974 – 2014. The two sources of *in situ* data used for this study are from the OzNet and Australian Cosmic Ray Sensor Network (CosmOz) soil moisture monitoring networks. OzNet data used in this study consists only observations from the Murrumbidgee

Soil Moisture Monitoring Network (Smith *et al.*, 2012). CosmOz is the first national network of cosmic ray soil moisture probes and comprise of 13 sites situated at different locations over different climate zones in Australia (Hawdon *et al.*, 2014). The numerical weather prediction (NWP) soil moisture dataset used in this study are analyses from the old (called Australian Parallel Suite – 0; APS0) and current (Australian Parallel Suite – 1; APS1) versions of the Australian Community Climate and Earth Simulator (ACCESS) global modelling system employed operationally by the Bureau of Meteorology. APS0 had a horizontal resolution of about 80 km and APS1 that of about 40 km.

Since the different soil moisture datasets mentioned above are represented in different forms and units, to enable a fair product comparison, all are scaled between [0, 1] using their own maximum and minimum values from the respective lengthy time series. In order to match the daily time steps of the KBDI and SDI fields, the NWP model and *in situ* data are averaged over each day. A spatially collocated sub-set using the nearest neighbour technique with respect to the *in situ* observation locations are then made from these daily averaged gridded model (NWP, KBDI and SDI) fields. For all stations, correlations, bias, and root mean square difference are calculated for the whole period in which the comparing data overlaps.

Results and discussions

Comparison with OzNet

In order to assess the accuracy of the soil moisture estimates from APS1, KBDI and SDI, an evaluation is made against the soil moisture observations from OzNet hydrological network. The verifications are made with datasets which span for a period of 21 months, i.e. from September 2009 to May 2011. OzNet provides soil moisture observation for the top 30 cm layer (0 – 30 cm deep) which is used in this study for comparisons.

The correlation, bias and RMSD calculated for APS0, KBDI and SDI with respect to the OzNet sites are given in Table 1. The values represent an average taken over 30 stations. The results show that, in general, the APS0 correlations are higher than that from both KBDI and SDI. The average correlation values across all OzNet sites for APS1, KBDI and SDI are 0.72, 0.64 and 0.71 respectively. The APS0 soil moisture usually correlates very well with the observations, where 90% of sites showing a correlation of 0.6 or more. Biases are in average of 0.02, -0.26 and -0.02 for APS0, KBDI and SDI respectively. KBDI in general display a large wet bias, which suggest that the evapotranspiration estimates in KBDI are rather under-estimated. Though SDI presents on an average a wet bias, it doesn't systematically exhibit any wet bias at all stations. Averaged RMSD for APS0, KBDI and SDI are 0.19, 0.36 and 0.23 respectively. The higher RMSD in KBDI signify that the errors in soil moisture are larger in KBDI compared to APS0 and SDI.

Table 1. Comparison of normalized soil moisture between OzNet *in situ* observations located at Murrumbidgee catchment area and ACCESS NWP model (APS0), KBDI and SDI. The values represent an average over 30 sites.

Correlation [-]			Bias [-]			RMSD [-]		
APS0	**KBDI**	**SDI**	**APS0**	**KBDI**	**SDI**	**APS0**	**KBDI**	**SDI**
0.72	0.64	0.71	0.02	-0.26	-0.02	0.19	0.36	0.23

Comparison with CosmOz

The three modelled root-zone soil moisture estimates from APS1, KBDI and SDI are evaluated against daily average measurements from CosmOz cosmic ray probe sites across Australia. Since APS1 dataset had the shortest span among the four data types, a subset of CosmOz, KBDI and SDI data set were produced based on APS1 time period for sensible verification. This period spans about 31 months, from

May 2012 to Dec 2014. The statistical scores of this verification is presented in Table 2. The verifications results using CosmOz data displays a similar pattern to that from the OzNet, where the NWP soil moisture product exhibit a good skill over the KBDI and SDI products. The mean correlations obtained for APS1, KBDI and SDI in this case are 0.8, 0.63 and 0.76 respectively. The average bias obtained for APS1, KBDI and SDI are 0.01, -0.22 and -0.07 respectively. KBDI again shows a rather large wet bias over all stations. Since the CosmOz observations are scattered all over Australia, this implies that KBDI under-predict the soil moisture deficit substantially, regardless of the climate zone. SDI doesn't exhibit any consistent wet or dry pattern spatially, similar to APS1. RMSD are in average of 0.15, 0.32 and 0.20 respectively for APS1, KBDI and SDI.

Table2. Comparison of normalized soil moisture between CosmOz observations and APS1, KBDI and SDI. The values represent an average over 13 sites.

Correlation [-]			Bias [-]			RMSD [-]		
APS1	**KBDI**	**SDI**	**APS1**	**KBDI**	**SDI**	**APS1**	**KBDI**	**SDI**
0.80	0.63	0.76	0.01	-0.22	-0.07	0.15	0.32	0.20

Summary

The validation study done in this work use *in situ* observations from OzNet and CosmOz network to assess the reliability of NWP, KBDI and SDI soil moisture products. In general, the NWP soil moisture gives a better performance compared to KBDI and SDI, and as depicted by the correlation, bias and RMSD values. This is despite the fact that NWP soil moisture were calculated at a much coarser resolutions (~ 40 – 80 km) and use its own precipitation estimates - which are generally associated with lot of errors - to drive the soil moisture. As compared to this, KBDI and SDI soil moisture estimations use observation based precipitation analysis and are done at a much higher resolution (~5 km). Over most of the sites on which comparisons were made, KBDI soils are significantly wetter than other three datasets. This wet bias seen in KBDI could have its implication for fire danger ratings, where it is used, as this would potentially downgrade the fire potential. SDI, although displays a much better temporal soil moisture variation than KBDI, usually fail to catch the rapid drying / wetting phases seen in the observations.

It is worth noting that there is still a lot of scope to improve soil moisture products from land surface models used in NWP by using advanced data assimilation techniques (Dharssi *et al.*, 2013). As the next step, research will be performed to calculate soil dryness using satellite remote sensing measurements, land surface model simulations and data assimilation techniques. Consequently, this research is intended to lead to the provision of soil dryness products with greater accuracy at a much higher spatial and temporal resolution.

References

Chandler, C., Cheney, P., Thomas, P., Trabaud, L., & Williams, D., 1983: *Fire in forestry, forest fire behaviour and effects.* New York: John Wiley & Sons.

Dharssi, I., Candy, B., Bovis, K., Steinle, P., & McPherson, B., 2013: Analysis of the linearised observation operator in a land surface data assimilation scheme for numerical weather prediction. *20th International Congress on Modelling and Simulation* (pp. 2862-2868). Adelaide: The Modelling and Simulation Society of Australia and New Zealand.

Hawdon, A., McJannet, D., & Wallace, J., 2014: Calibration and correction procedures for cosmic-ray neutron soil moisture probes located across Australia. *Water Res. Research, 50*(6), 5029-5043.

Jones, D. A., Wang, W., & Fawcett, R., 2009: *Climate data for the Australian Water Availability Project: Final milestone report.* Melbourne: National Climate Centre, Bureau of Meteorology.

Keetch, J. J., & Byram, G. M., 1968: *A drought index for forest fire control.* Asheville: U.S. Department of Agriculture and Forest Service.

Mount, A. B., 1972: *The derivation and testing of a soil dryness index using runoff data.* Hobart: Tasmanian Forestry Commission.

Smith, A. B., Walker, J. P., Western, A. W., Young, R. I., Ellett, K. M., Pipunic, R. C., . . . Ritcher, H., 2012: The Murrumbidgee Soil Moisture Monitoring Network data set. *Water Res. Research, 48*(07).

TROPICAL CYCLONE FORECASTING USING THE HIGH RESOLUTION ACCESS MODEL

Xingbao Wang, Jeff Kepert, Noel Davidson, Yi Xiao

Research and Developmental Branch, Bureau of Meteorology, Melbourne, Australia

Xingbao.Wang@bom.gov.au

Abstract

The offshore oil and gas industry in Australia's northwest operates in a harsh and remote environment, in which tropical cyclones pose a significant risk to safe and efficient operations. Improved forecasts offer a significant opportunity to mitigate this risk, and to this end we are developing a new tropical cyclone NWP system for the northwest. This system builds on our experience with ACCESS-TC, but differs from it in being on a larger and fixed domain instead of relocatable, by running twice-daily instead of only when a cyclone has formed, by having higher resolution (~4 km grid), by forecasting to 5 instead of 3 days, and by including a wave model. The system is called ACCESS-TCX, with the X standing for "extended", and aims to address specific issues around forecast length, tropical cyclogenesis and wave prediction.

We have tested various ACCESS model configurations for this purpose over both northern Australia and the northwest Pacific Ocean, nested in either the global (ACCESS-G N512) or regional (ACCESS-R12) models. The new system improves the TC intensity forecast, however the tracks at present are slightly worse compared with the coarser resolution nesting model. Our most recent experiments include data assimilation and a TC bogus, and further improve the predicted TC intensity, particularly for strong TC. Case study and real time runs have shown that the TC forecast accuracy in terms of track and intensity (measured by sea level centre pressure and maximum 10-m wind around the centre) is quite sensitive to the model resolutions, physics, initial condition (IC) and lateral boundary conditions (LBC). The intensity and track can be significantly changed using different IC and LBC coming from ACCESS-G (N512) or ACCESS-R. The forecasts are also sensitive to the model dynamics, with ENDGAME dynamics usually producing a stronger TC than the older New Dynamics. While we have demonstrated that ACCESS-TCX has the potential to provide good TC track and intensity forecasts, further testing is required to determine the best combination of model dynamics, physics, and data assimilation.

MODELLING THE FIRE WEATHER OF THE BLUE MOUNTAINS FIRES OF 17 OCTOBER 2013

Simon E. Ching[1, 3], Robert J. B. Fawcett[2] and Jeffrey D. Kepert[2, 3]

[1]Bureau of Meteorology, Adelaide, South Australia
[2]Bureau of Meteorology, Docklands, Victoria
[3]Bushfire and Natural Hazards CRC, Melbourne, Victoria

e.ching@bom.gov.au

Introduction

In October 2013, a number of significant fires broke out in New South Wales, including the Blue Mountains region. The most intensive fire activity occurred between 13 and 26 October, when there were 627 incidents and 164 054 hectares burned. The fires on the afternoon of 17 October were the most destructive, with more than 200 houses destroyed across the Blue Mountains region (NSW Rural Fire Service, 2014).

Progression of Fires

The fires in the Blue Mountains Region proper consist of the State Mine Fire and the Mount York Road Fire (Figure 1). The State Mine Fire was ignited on 16 October and spread to the southeast during the night and the morning of 17 October. Later, the fire spread rapidly to the east from about noon, with the estimated area burnt increased from 1 036 ha at 11:56 am to 12 436 ha by 9:46 pm local time (Figure 1). The Mount York Road Fire was ignited on the afternoon of 17 October. While not as extensive when compared with the State Mine Fire, it had an estimated burnt area of 492 ha by 7:46 am on 18 October.

The areal extension of the State Mine Fire on the 17 October was phenomenal – a 10+ fold increase in less than 10 hours. It is of both practical and academic interest to investigate if meteorological conditions had been inducive to the enormous spreading of the fire during that day; if so, what are those meteorological conditions?

Figure 1. Progression of fire perimeters from the afternoon of 16 October 2013 to the morning of 18 October 2013. The legend specifies the day of month and time of the fire perimeters in AEDT. The black triangle marks the approximate position of the Mount Boyce AWS.

Meteorological Conditions

Synoptic Situation and AWS observations at Mount Boyce

A cold front passed through New South Wales on 17 October. The wind change accompanying the cold front was a complex one, manifested in the Blue Mountains area as several small abrupt directional changes, embedded within the general trend of northwesterlies gradually backing to the southwesterlies throughout the day (Figure 2).

Mount Boyce is the closest AWS to the Blue Mountains Fires (Figure 1). The conditions at Mount Boyce on 17 October is characterized by a modest maximum air temperature of 22.5 °C, very dry conditions with dew point temperatures dipping to –7.6 °C around 03 UTC (2 pm AEDT), and windy conditions with one-minute wind speeds reaching 20.6 m s^{-1} (74 km h^{-1}) and gusts reaching 28.3 m s^{-1} (102 km h^{-1}) during the afternoon.

Figure 2. Meteogram of Mount Boyce AWS from 16/10/2013 03 UTC to 18/10/2013 09 UTC. Solid dots with thin black borders in the foreground are numerical model simulation data. Fainter dots in the background are AWS observations. Top panel shows the temperatures (black) and dew point temperatures (red). Middle panel shows the wind direction. Bottom panel shows 1-minute wind speeds (green) and wind gusts (cyan).

Forest Fire Danger Index (FFDI)

In Australia, the McArthur forest fire danger index (FFDI, Noble et al., 1980) is a key tool for assessing forest fire danger (Dowdy et al., 2009). The FFDI is used by fire agencies to estimate fire danger and is defined as

$$FFDI = 2 \exp \left[-0.45 + 0.987 \ln (D) - 0.0345 H + 0.0338 T + 0.0234 V \right]$$

(in the Mark 5 version) where H is the relative humidity (in %), T is the temperature (in °C), V is the 10-m wind speed (in km h^{-1}) and D is a drought factor between 1 and 10 which represents the fuel availability and is a function of the soil-moisture deficit and recent rainfall (Griffiths 1999). FFDI values reaching 50, 75, and 100 are considered "Severe", "Extreme" and "Catastrophic" in terms of fire danger, respectively.

Considering the modest maximum temperature of 22.5 °C, the severity of fire danger of the day is mainly contributed to by the dry and, particularly, windy conditions (Figure 2). With entries representative of the conditions of the day, Table 1 highlights the strong sensitivity of FFDI to depressed dew point temperatures and elevated wind speeds, and illustrates that catastrophic values were reached. The question, then, is what caused the low relative humidity and high winds?

Table 1. FFDI values from various combinations of temperatures, dew point temperatures and wind speeds, representative of the conditions at Mount Boyce during 17 October 2013, assuming a drought factor of 10.

Temperature (°C)	Dew Point (°C)	Wind Speed (m s^{-1})	FFDI
20.0	0.0	12	27.1
22.5	0.0	12	33.6
20.0	−7.6	12	40.2
20.0	0.0	23	68.6
22.5	−7.6	23	118.7

The Simulation

Numerical Model Configuration

In this study, the simulation was performed using the Australian Community Climate and Earth-System Simulator (ACCESS). The model is version 8.5 of the Unified Model developed at the UK Met Office, as implemented at the Bureau of Meteorology. The initial condition was the Bureau's operational global analysis valid at 03 UTC on 16 October 2013, and was run at successively finer nests, beginning with an approximately 40-km mesh on a global domain (STAGE1), 4.0 km (STAGE3), 1.3 km (STAGE4) and 440 m (STAGE5) on progressively smaller domains, all with 70 hybrid vertical levels. The global model had a model top of 80 km, with the nested models having a model top of 40 km.

Mountain Waves

Vertical cross-section from the simulation showed a marked downward extension of the stronger winds aloft in the general vicinity of the fire ground (Figure 3). Examination of the vertical velocity showed a clear mountain wave signature. This pattern persisted for about 6 hours from about 00 UTC to 06 UTC on the 17th, which coincides with the rapid fire spread period. This appears to be the cause of the elevated surface winds and associated gustiness seen in the observational data.
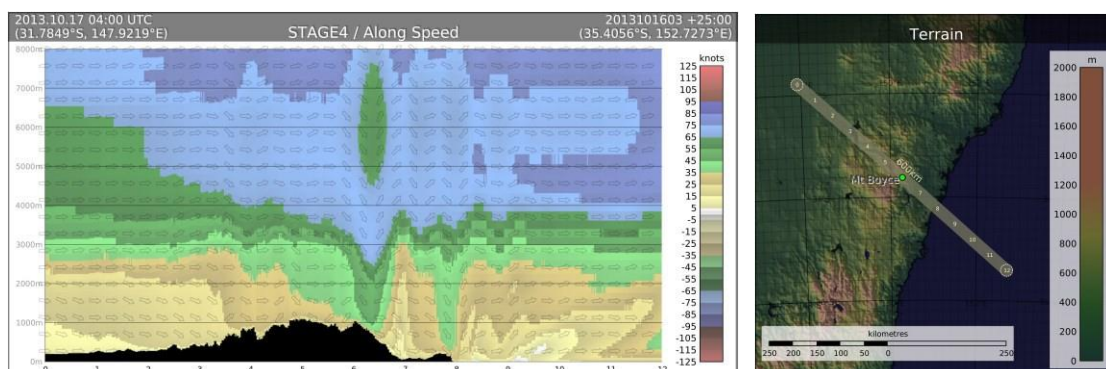
Figure 3. Left: Vertical cross-section of horizontal wind speed along a line through Mount Boyce at 04 UTC on 17 October (1.3 km nest). Positive (negative) values indicate flow from left (right) to right (left). Arrows indicate three-dimensional wind directions projected onto the cross-sectional plane. The figures 0 to 12 along the horizontal axis are position markers 50 km apart. Mount Boyce is located at the position marker 6. Right: Model terrain height and orientation of the cross-section.

The potential for mountain waves to escalate fire behaviour was discussed by Sharples (2009), and they were shown to be responsible for overnight escalations in fires at Margaret River (Kepert and Fawcett 2013) and Aberfeldy (Wells et al., 2014). This case is of particular interest because the phenomenon occurred during the day, rather than at night when the nocturnal inversion provides near-surface conditions very favourable for mountain waves.

Dry Slot

Though not reaching the observed Mount Boyce –7.6 °C dew point, a marked northwest-southeast orientated dry slot was present in the simulation from about 22 UTC 16 October to 07 UTC 17 October. The magnitude of the dryness and arrival timing was arguably well represented. However, a secondary, less marked drying period observed at Mount Boyce AWS around 0630 UTC was not captured by the simulation (Figures 2, 4).
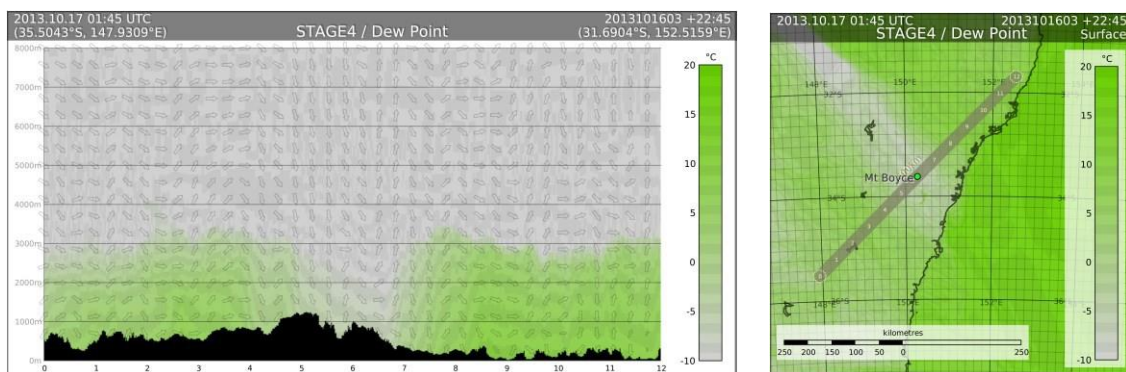
Figure 4. Left: Vertical cross-section of dew point temperature along a line through Mount Boyce at 01:45 UTC on 17 October (1.3-km nest). Arrows and the position markers 0 to 12 as in Figure 3. Right: Surface dew point temperatures of the simulation at the same time. Also shown is the orientation of the vertical cross-section.

Figure 4 (left) shows the vertical cross-section of the dry slot in the simulation. While there was vertical motion in the vicinity of the dry slot, the simulation did not clearly reveal a secondary cross-frontal circulation associated with the dry slot as described by Mills (2005, 2008). Further analysis suggests the dry slot is actually a dry nose of a cooler and otherwise moist airmass spreading from the southwest. Later during the afternoon, the dry slot is dissipated in an interaction with rainfall as it moved over to northeastern New South Wales.

References

Dowdy, A, G. A. Mills, K. Finkele and W. de Groot, 2009: Australian fire weather as represented by the McArthur Forest Danger Index and the Canadian Forest Fire Weather Index, CAWCR Technical Report No. 10

Griffiths, D. 1999: Improved formula for the Drought Factor in McArthur's Forest Fire Danger Meter, Australian Forestry, 62(2), 202-206

Kepert, J. D and R. J. B. Fawcett, 2013: Meteorological aspects of the Margaret River fires of November 2011, In Piantadosi, J., Anderssen, R.S. and Boland J. (eds) MODSIM2013, 20th International Congress on Modelling and Simulation, Modelling and Simulation Society of Australia and New Zealand, December 2013. ISBN: 978-0-9872143-3-1

Mills, G. A, 2005: On the sub-synoptic scale meteorology of two extreme fire weather days during the Eastern Australian fires of January 2003, Aust. Met. Mag., 54, 265-290

Mills, G. A., 2008: Abrupt surface drying and fire weather Part 1: overview and case study of the South Australian fires of 11 January 2005, Aust. Met. Mag., 57, 299-309

Noble, I. R., G. A. A. Bary and A. M. Gill, 1980: McArthur's fire danger meters expressed as equations, Australian Journal Ecology, 5, 201-203

NSW Rural Fire Surface 2014: Bush Fire Bulletin, Volume, 36, No 2/2014

Sharples, J. J., 2009: An overview of mountain meteorological effects relevant to fire behaviour and bushfire risk, International Journal of Wildland Fire, 2009, 18, 737-754

Wells, T., C. S. Yeo and R. J. B. Fawcett, 2014: Meteorological and fire behavioural lessons learned from the Aberfeldy Fire, Victoria, 17 January 2013. Poster, 2014 Conference of the Australian Fire and Emergency Services Council and the Bushfire and Natural Hazards Cooperative Research Centre, Wellington, New Zealand, 2 – 5 September.

EMERGING METHODS FOR HIGH IMPACT WEATHER PREDICTION AND OBSERVATION

Elizabeth E. Ebert

Environment and Research Division, Bureau of Meteorology, Melbourne

e.ebert@bom.gov.au

Abstract

New remotely sensed observations, the growing ability to view and quantitatively use third party data including from social media, improvements in the resolution and skill of numerical weather prediction (NWP) models and techniques for post-processing their output to add further value, are all contributing to more accurate and timely weather knowledge in Australia. Converting high impact weather knowledge into improved prediction of hazards and their impacts will involve modelling across domains, which is a priority of the World Weather Research Program (WWRP) High Impact Weather project.

New observations

Without a doubt the most exciting new source of meteorological observations over Australia is the Himawari-8 geostationary satellite operated by the Japan Meteorological Agency. Operational since July 2015, the 10-minute imagery from Himawari-8 is revolutionising our ability to watch weather unfold. The 2.5-min rapid scan capability for target areas such as over tropical cyclones (TCs) will enable more precise characterisation of cyclone position and intensity. The Advanced Baseline Imager's higher spatial and spectral resolution, with 16 bands in the visible and infrared spectrum (500 m resolution in the red channel, 1 km in blue and green channels, and 2 km in near-infrared and infrared), has been casually described as "a MODIS on a geo". MODIS's suite of multi-spectral satellite products can potentially be adapted for use with Himawari data to provide rapid-update full-disk information for a variety of applications. The 10-minute temporal resolution offers enormous opportunities to develop improved nowcasting applications for thunderstorms, flash floods, fire (hot spot) detection, TC intensification, and other high impact weather. The increased accuracy and timeliness of derived atmospheric motion vectors will enhance the accuracy of NWP.

Australia's radar network will undergo a staged upgrade to dual polarimetric capability, starting with the capital city radars in 2017. Transmitting and receiving both horizontally and vertically polarised pulses provides better measurements of the target (generally hydrometeors), giving information on the most likely precipitation type, more accurate rain rates, and improving quality control to remove artifacts. In terms of high impact weather, dual-polarimetric radar will provide better detections of hail size and concentration and heavy rain rates that could lead to flooding.

Australia's lightning network is also being upgraded to include long-range cloud-to-ground lightning coverage over the Melbourne and Brisbane Flight Information Regions (mainly for aviation) and a high-resolution national lightning service with improved in-cloud detection efficiency. These new data will offer greater flexibility to provide lightning information to the

public, and will enhance our ability to detect and characterise thunderstorms. Prototype lightning tracking algorithms are in development to inform severe weather warnings and provide value-added services to industry.

New types of observations from third party networks, crowd-sourcing, and social media such as Twitter, also offer promise for detecting and characterising high impact weather and verifying hazard impact forecasts. Forecasters currently monitor a variety of channels to get the latest information, and the Bureau's observations are incorporated into situational awareness tools used by emergency managers and other stakeholders. Technologies for mining these new data sources in an automated fashion are rapidly being improved, and their use in data assimilation and weather analysis is a hot area of research. Major challenges include data access and formats and especially quality control.

Improved NWP and derived products

Advances in high performance computing are enabling NWP at higher spatial and vertical resolutions than ever before, providing better predictions of convection and detailed local atmospheric circulations. The 1.5 km APS2[1] version of the ACCESS model uses explicit rather than parameterised convection, resulting in significant improvements in the representation of rainfall as compared to the APS1 version (P. Steinle, personal communication). The Sydney 2014 Forecast Demonstration Project showed that a 1.5 km rapid update cycle (RUC) ACCESS model with radar assimilation more accurately represented the evolution of sea breezes, and that forecasters could confidently use the RUC to predict the mode of convection on high impact weather days (Steinle 2015). Researchers are running the ACCESS model at sub-kilometre resolutions to better understand the processes associated with extreme bushfire and storm events (e.g., Kepert 2015), and within a few years it may be possible to run such a sub-km model operationally to simulate extreme events in real time.

Ensemble predictions support probabilistic forecasting and risk-based decision making at a variety of space and time scales. The Bureau runs, or is developing, ensemble-based applications for a large number of high impact weather types including fire weather, thunderstorms, heat stress, heavy rain, strong winds, flood, waves, volcanic ash, and TCs. For example, Figure 1 shows experimental EPSgrams to support fire weather forecasting, based on output of the 24-member ACCESS-GE global ensemble (Ebert *et al.* 2015). These products have been enthusiastically received by the NSW Rural Fire Service and should become be part of the Bureau's operational service in future.

ACCESS-GE is an important source of ensemble guidance, along with the ECMWF, poor man's (multi-model), time-lagged, and stochastic ensembles. Ensemble-based multi-week predictions are starting to bridge the gap between weather and seasonal climate regimes to predict such phenomena as heat waves, dry/wet spells and likelihood of TC genesis. To assist with short range prediction, a 2.2 km convection allowing ensemble similar to MOGREPS-UK will be implemented in 2018.

This substantial growth in NWP capability calls for new ways to deal with the increasingly large quantity of output. Improved post-processing techniques are being developed and applied to downscale and remove bias, generate alerts for forecasters, and derive new products such as thunderstorm probability. Operational forecast production systems now make direct use of NWP and NWP-based products, supporting a trend toward greater automation of routine forecasts.

---

[1] APS refers to Australian Parallel Suite with each version signifying a major upgrade.

Prediction of hazards and their impacts

Spatial weather information can feed directly into hazard impact prediction. Opportunities are emerging to partner with the emergency management, health, infrastructure, resource, and other sectors to provide new targeted products to help meet their needs. NWP rainfall forecasts are now used as direct input to the Bureau's hydrological models, and a new project on fire predictive services is exploring how best to link spatial predictions of temperature, wind, humidity and precipitation directly to models of fire behaviour. To provide the depth of information needed for decision making,
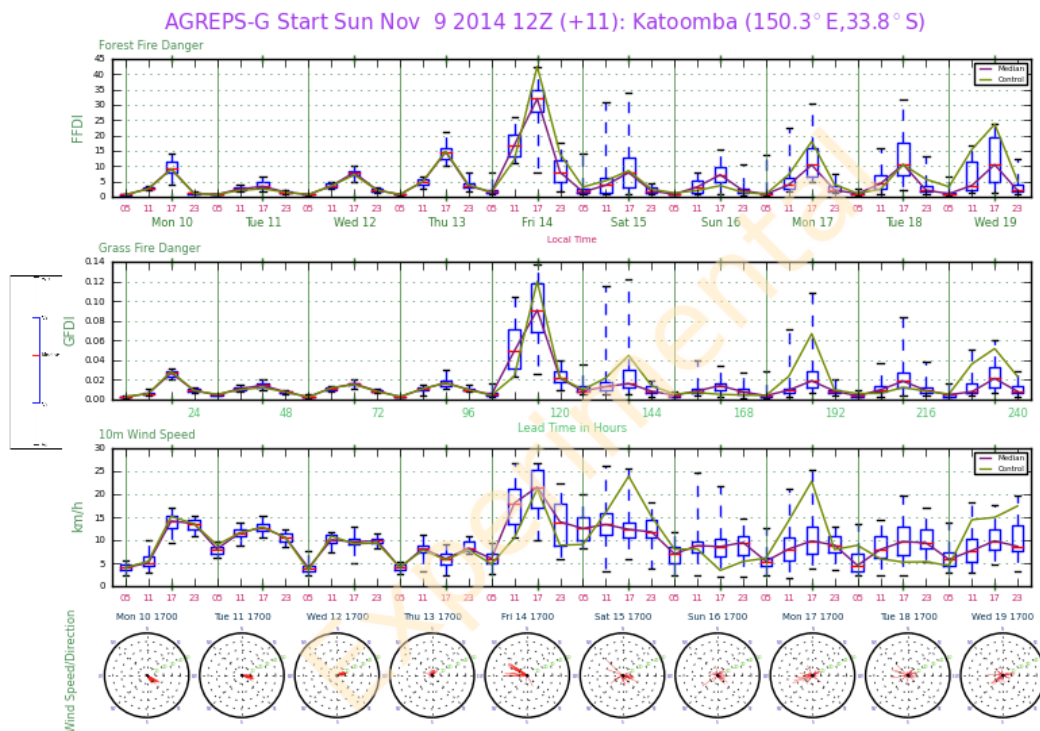
Figure 1: EPSgrams of forest fire danger index (FFDI), grass fire danger index (GFDI), 10m wind speed and wind direction for Katoomba, NSW for a 10-day period in November 2014 during the Sydney FDP. The peak in FFDI on day 5 shows enhanced fire danger, with the large uncertainty in wind direction on that day reflecting differences in the timing of frontal passage in the individual ensemble members.

ensemble predictions are likely to be the preferred source of input to downstream models. For example, Louis and Matthews (2015) used time-lagged high resolution ensemble NWP from the ACCESS RUC model to drive the Phoenix fire spread model, demonstrating the feasibility of generating probabilistic fire spread predictions.

To further seamless modelling across domains, WMO's World Weather Research Programme has initiated a new 10-year High Impact Weather project that aims to improve community resilience through *improving forecasts for timescales of minutes to two weeks and enhancing their communication and utility in social, economic and environmental applications* (Golding and Jones 2015; Figure 2). Through the HIWeather project researchers will work with operational forecast centres and external partners to conduct relevant research and development of systems that will boost proactive risk reduction and effective emergency response to weather-related hazards.

The HIWeather project will address a large number of research questions including: How far in advance can we predict high impact weather and associated hazards? How can new data sources be exploited to observe weather hazards and impacts and initialise models? What are improved

approaches to assessing weather-related vulnerability and risk? Applications will be developed to provide weather, hazard and impact forecasts based on dynamic modelling, decision support tools that link hazards with risk and vulnerability, and tools for communication and evaluation of hazards and impacts. Activities will include forecast and research demonstration projects (FDPs and RDPs), case study evaluation, workshops on specific hazards and applications, development of applications for/with specific users, inter-comparisons of techniques, and reviews of better practice. An important aspect of HIWeather is deep engagement with practitioners in risk, economics, and social science to help translate improvements in science into improved decision making and more effective response.

The HIWeather project will demonstrate applications for five hazards: urban flood, wildfire, localised extreme wind, disruptive winter weather, and urban heat waves and air pollution. With the exception of disruptive winter weather, these hazards all seriously threaten life and property in Australia. The excellent relationship between the Bureau of Meteorology, CSIRO, the Bushfire and Natural Hazards Cooperative Research Centre, and state and national emergency management agencies positions us well to mutually benefit from participation in this international project.
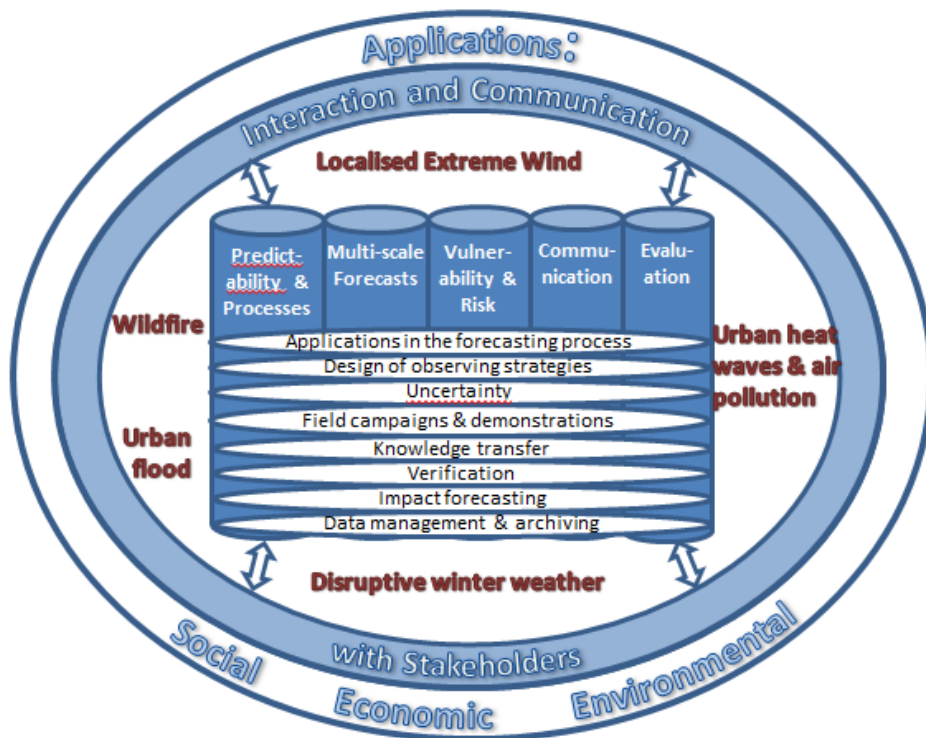
Figure 2: Conceptual diagram of the High Impact Weather project, initiated in 2015. Through the five research themes (pillars) and cross-cutting activities and issues, researchers and operational forecasting centres will work together to address the gaps in capability needed to deliver improved community resilience.

References

Ebert, E., M. Cope, A. Wain, S. Lee, and D. Smith, 2015: The Air Quality Sub-Project of the Sydney Forecast Demonstration Project (FDP). *Final Workshop on the Forecast Demonstration Project, Melbourne, 28 April 2015*.

Golding, B. and S. Jones, 2015: The High Impact Weather Project. In Brunet, G., S. Jones and P.M. Ruti (eds), *Seamless Prediction of the Earth System: from Minutes to Months*, WMO-No. 1156, (ISBN 978-92-63-11156-2), Geneva, 455-460.

Kepert, J., 2015: High-resolution ensemble prediction of an East Coast Low. *CAWCR 9th Annual Workshop, Melbourne, 19-22 October, 2015.*
Louis, S.A. and S. Matthews, 2015: Fire spread prediction using a lagged weather forecast ensemble. *MODSIM 2015.*

Steinle, P., 2015: Performance of convective scale DA during the Sydney Forecast Demonstration Project. *CAWCR 9th Annual Workshop, Melbourne, 19-22 October, 2015.*

HIGH-RESOLUTION ENSEMBLE PREDICTION OF AN EAST COAST LOW

Jeffrey D. Kepert[1,3], Robert J.B. Fawcett[2], Simon Ching[1,3], William Thurston[1,3] and Kevin J. Tory[1,3]

[1]*Bureau of Meteorology Research and Development*
[2]*Bureau of Meteorology Climate Information Services*
[3]*Bushfire and Natural Hazards Cooperative Research Centre*

Abstract

East coast lows are intense low-pressure systems that form close to the east coast of Australia, most commonly along the New South Wales coast. A severe east coast low occurred from 20 – 23 April 2015, with the worst impact on 21 April. It was a major flood event for Dungog and Maitland, and caused at least four deaths. Dozens of houses lost their roofs, over 200,000 houses were without power, and 57 schools closed.

We have prepared a 24-member high-resolution ensemble simulation of the storm, by downscaling the prototype ACCESS-GE global ensemble to 1.3 km grid spacing, along with a similar downscaling of the deterministic operational ACCESS-G to a 440-m grid. The downscaling began with a global simulation, and then nesting within that to successively higher resolution but smaller domain. The final three resolutions had grid spacings of approximately 4 km, 1.3 km and 440 m. The ensemble simulation was initialized at 0000 UTC on 20 April 2015 and ran for 48 hours of model time. The deterministic simulation was initialized at 0300 UTC on 20 April 2015 and ran for 78 hours of model time.

Analysis of the simulations is in its early stages. Figure 1 shows the forecast ensemble-mean rainfall from the event, averaged over the 24 ensemble members, together with the verifying analysis. Clearly, the forecast matches reality very well. None of the individual ensemble members showed such a close match, and one known benefit of ensemble prediction is the improved accuracy of the mean forecast. However, the mean forecast falls short on peak rainfall in the Dungog area, which is about half as strong as observed. Figure 2 shows plots of the forecast probability of rainfall exceeding 100 mm and 400 mm, defined as the proportion of the ensemble that exceeds these thresholds. Note how the ensemble singles out the Dungog area as being of moderate risk of extreme rainfall.

In east coast lows, the strongest winds and heaviest rain often occur immediately to the south of small-scale lows that form right on the coast within the overall envelope of the larger-scale system. The ensemble shows considerable spread in the timing, location and amplitude of these systems, indicating that although the area around Dungog carries the highest risk, a substantial part of the coast is at risk of significant rain and strong winds.

These rainfall forecasts could also be valuable as input into an ensemble of hydrological models, giving a prediction of various levels of flood risk. Figure 4 shows a box-and-whisker plot of the hourly distribution of rain within the ensemble, averaged approximately over the catchment upstream of Dungog, Note that this area is larger than the peak rain in the analysis, and ensemble rain totals averaged over this area were less than 300 mm even though some members had peak rainfall totals above 500 mm. This figure confirms the significant risk of sustained very heavy rain over a prolonged period. However, it also shows that some members were predicting relatively light rain in this region. In these cases, the rain mostly fell elsewhere.

The existence of these simulations opens up several strands for continued research. The existence of the ensemble may offer opportunities to apply ensemble-based analysis methods to study the dynamics of east coast lows, and thereby complement previous research on this topic. We hope to explore also the predictability of mesoscale features within the overall system, noting the considerable spread in the location and timing of these features between the ensemble members. Over the next decade or so, ensemble prediction at these resolutions will progressively become available to operations, perhaps initially as a severe weather run-on-demand system. The need to interpret, use and communicate the resulting data so as to obtain good value from it will require substantial changes to the way forecasters operate, and similar changes to the planning and protocols of end users such as emergency services, government and the general public. We hope that this example of an ensemble prediction of a notable severe weather event will help to illustrate the possibilities and promote debate on the shape of future severe weather services.
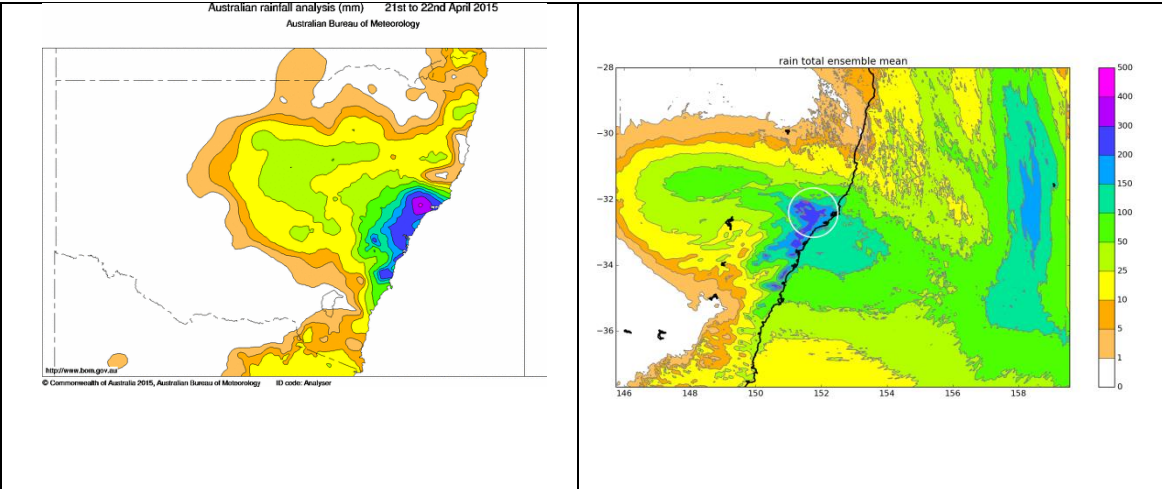
Fig. 1: Operational high-resolution rainfall analysis (left) and ensemble-mean (right) total rainfall over the 48 hours to 9 am and 11 am EDT respectively on 22 April 2015. The white circle indicates the location of Dungog.
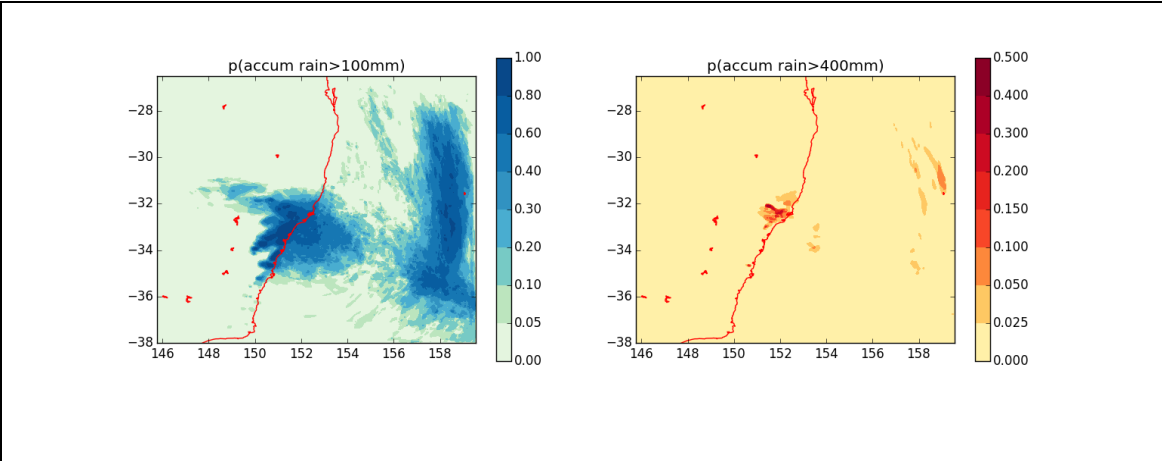
Fig. 2: Probability of rainfall exceeding 100 mm (left) and 400 mm (right) for the 48 hours of the ensemble simulation.
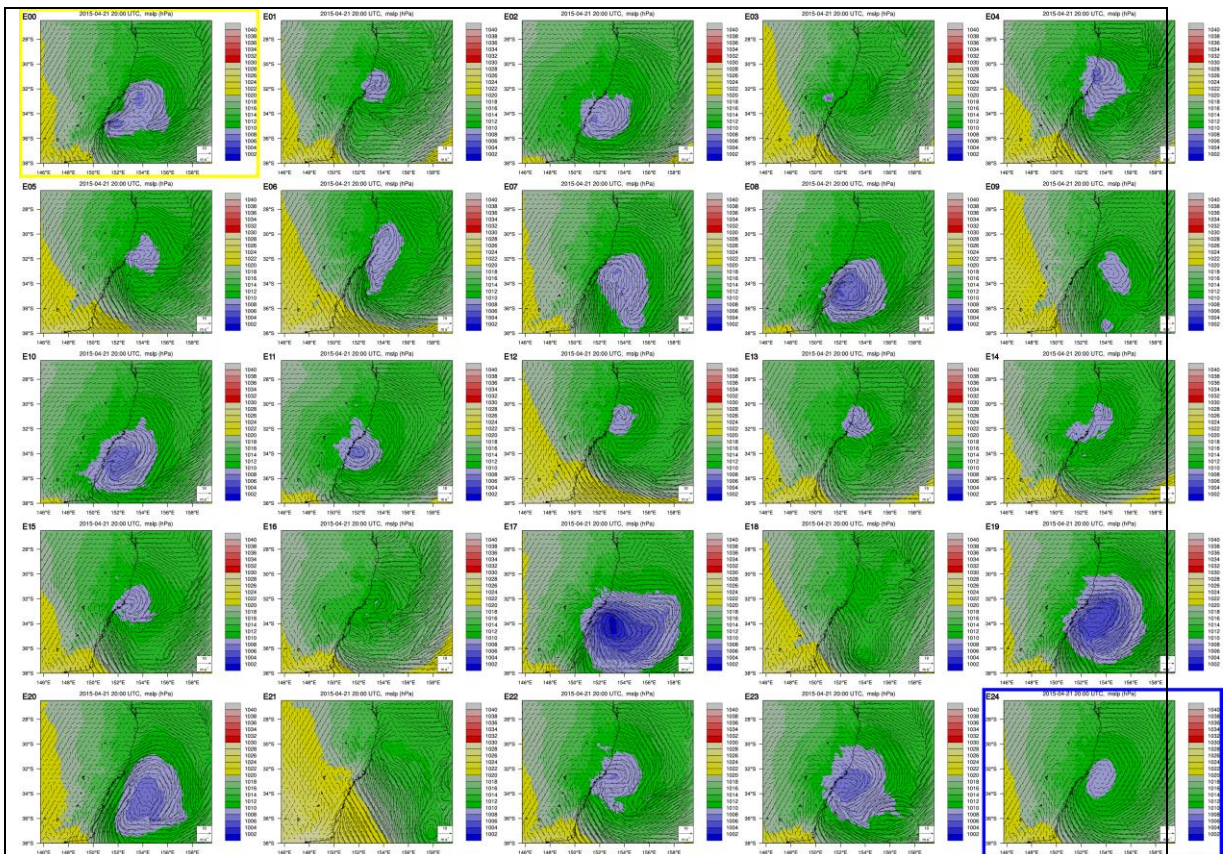
Fig. 3: Mean sea-level pressure from the 1.3-km ensemble simulation of the east coast low valid at 2000 UTC on 21 April 2015. The control member is in the yellow box (top left), and the ensemble mean in the blue box (bottom right). Pressures below 1010 hPa are shown in blue/purple shades, indicating the location of the mesoscale lows.
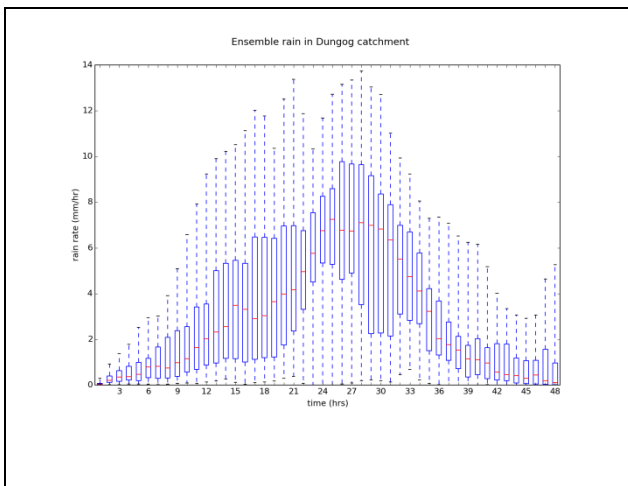
Fig. 4: Box-and-whisker plots of hourly rainfall amount from 11 am 20 April 2015 EDT. The boxes show the upper and lower quartiles, the red line the median, and the whiskers show the range.

HOW WELL DO LAND MODELS HANDLE EXTREMES?

Andy Pitman

ARC Centre of Excellence for Climate System Science

a.pitman@unsw.edu.au

Abstract

Land models have been routinely and thoroughly tested using a range of observational products at point, continental and global scales. With a little calibration, careful choice of sites or periods, the models appear to work well. When tested independently or compared against new data or formally benchmarked, some very worrying characteristics emerge.

I will present two examples. The first is the impact, on ACCESS1.3, of changing the parameterization of stomatal conductance. I will show that once observational data are used to re-parameterize stomatal conductance, the simulation of extreme temperatures by ACCESS1.3 is improved, and the future projections of extreme temperatures and heatwave intensity change quite dramatically. The second example is the simulation by CABLE2.0 of drought. I will show that when CABLE2.0 is evaluated for drought it performs very poorly, but this can be resolved by revising the hydrological parameterization used. I will then demonstrate that problems apparent in CABLE2.0 are replicated in many other land models, including JULES, but not in some other models, including CABLE-SLI.

The common theme here is rigorous, objective and systematic evaluation of models to find not how well they perform, but when they fail. This has to be followed by a rigorous, objective and systematic re-parameterization of processes within a model evaluation system coupled with a strict version control environment.

We can celebrate that the CABLE leadership team has built such an environment and CABLE is now improving rapidly. This forms the basis of a far better foundation to simulate land-related extremes in the future.

TRANSPOSE AMIP EXPERIMENTS FOR TESTING THE POTENTIAL IMPACTS OF LAND-SURFACE MODELS ON ACCESS NWP

Greg Roff and Huqiang Zhang

Earth System Modelling Program, R&D Section, Australian Bureau of Meteorology

h.zhang@bom.gov.au

Introduction

One of the key tasks for making ACCESS (Australian Community Climate and Earth System Simulator) a seamless forecasting system from weather to climate is to share the same or similar physics configurations in its NWP and climate applications. This paper introduces the setup procedure and some preliminary results from Transpose AMIP II experiments with ACCESS GA6 configuration and N96L85 resolution. The experiments are focused on evaluating the potential impacts of different land-surface models (LSMs) on ACCESS NWP applications, with two different land models JULES and CABLE being used. Note these two schemes have been used in the ACCESS coupled climate models for CMIP5 (Bi et al 2013, Kowalczyk et al., 2013) and are currently being implemented for a new version of coupled ACCESS climate model. The Transpose-AMIP II experimental procedure here is designed to run such climate configurations in weather forecast (hindcast) mode, so we can examine the impacts of different LSMs on NWP-like hindcasts in a fast and efficient manner. The diagnosis of these experiments can also be valuable for understanding the model climate simulations.

Experimental Setup

The Transpose-AMIP-II (hereafter named T-AMIP) experimental procedure (http://hadobs.metoffice.com/tamip/) consists of 64 global 5-day hindcasts, consisting of 4 sets of 16 5-day hindcasts at 30 hour intervals starting at 00UTC on the 15th of October 2008, January 2009, April 2009 and July 2009. This staggering of the start times and dates ensures sampling throughout the annual and diurnal cycles and these particular periods have been chosen to tie in with the Year of Tropical Convection (YOTC, http://yotc.ucar.edu/). Note also that the same procedures could be applied to other periods in the ERA-40 and ERA-Interim re-analyses or indeed any analysis/re-analysis data sets.

In this analysis, we compare a set of ACCESS T-AMIP runs based on UM GA6 (Global Atmosphere 6.0), with different options for LSMs. GA6 is the current U.K. Met Office global atmospheric model configuration and is the atmospheric component of the GC2 (Global Coupled configuration 2) climate model (Williams et al., 2015). The configuration here is based on the vn8.5 code with Met Office GA6.0 patches for both the Unified Model (UM) and the Joint UK Land Environment Simulator (JULES). As part of the current ACCESS development, the Australian land surface model. Community Atmosphere Biosphere Land Exchange (CABLE) (Kowalczyk et al., 2006), is being implemented into GA6 through the JULES coupling interface. In the analysis, we also compare GA6 T-AMIP results with an earlier ACCESS version (ACCESS 1.3, also using CABLE) which is described in more detail in Roff (2014) and referred to as A13c below. We run GA6 configured with either CABLE or the

standard JULES model, and refer to these as GA6c and GA6j below. Note the GA6c model is still under development and so its results here are very preliminary.

The setup procedures, datasets, scripts, models and outputs for these experiments are documented in more detail on the web at the NECTAR Climate and Weather Science Laboratory: ACCESS Model Experimental Library
(https://trac.nci.org.au/trac/access/wiki/AccessModelExperimentLibrary)
in the "Transpose-AMIPII configurations" section. The T-AMIP procedure for each of these models required the following steps:

1. Model state variables were initialised from the European Centre for Medium Range Weather Forecasting (ECMWF) YOTC analyses, http://apps.ecmwf.int/datasets/data/yotc-od. The
2. Sea Surface Temperatures and Sea Ice extent also came from the ECMWF YOTC dataset.
3. Atmospheric composition, solar forcing, land use and aerosol concentration initialisation came from the ACCESS 1.3 AR5 RCP4.5 (see http://cmip-pcmdi.llnl.gov/cmip5 for details).
4. Land surface model initialisation came from corresponding model AMIP climatologies.
5. Non-state variable prognostics which spin-up quickly (such as cloud fraction) were initialized to zero.

The GA6j and GA6c N96L85 run jobs operate on 256 processors and take ~4-5 minutes walltime to complete a single 5 day hindcast using a 20 minute timestep, so ~4-5 hours for a full T-AMIP run over all 64 dates. This run time is the same as required for A13c N96L38 using the same timestep but only 64 processors.

Preliminary results

For T-AMIP to be useful we need to show that the fast process biases found in expensive AMIP runs can be seen in the much cheaper T-AMIP runs. Here we compare GA6j T-AMIP outputs against its corresponding AMIP simulation.
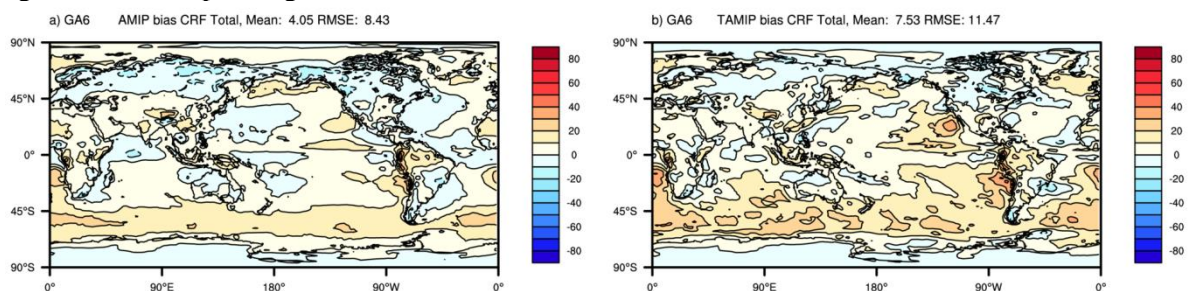
Figure 4 GA6j (a) AMIP and (b) T-AMIP Total Cloud radiative forcing. See text for details.

Figure 1 shows the GA6j AMIP and T-AMIP annual mean Total cloud radiative forcing (CRF) biases, relative to the ISCCP observations 1983–2007 mean. In both AMIP and T-AMIP the Total CRF has a strong positive bias in the Southern Ocean as well as off the south-western coasts of Africa and North and South America. From the corresponding short- and longwave forcing plots (not shown), these are mainly due to the short-wave forcing. Both models indicate that the faster and cheaper T-AMIP experimental procedure is able to simulate the climate biases seen in full AMIP runs. Similar results can be seen for other fields (eg T2m, Total precipitation) and are also seen in A13c outputs (Roff, 2014).

Figures 2 and 3 are an example of NWP testing for ACCESS GA6 with JULES and CABLE for 5-day hindcasts for 16 January 2009. As the model is initialized with "realistic" atmospheric initial condition and with observed SSTs, we can verify the model hindcasts with corresponding observations. Figure 2 shows the daily rainfall (shaded colours) and MSLP (contour lines) forecasts and compared against the observed daily rainfall totals from rainfall observations. For this case, the rainfall hindcasts are similar between the two configurations, but we do see differences developing for temperature forecasts (Figure 3).
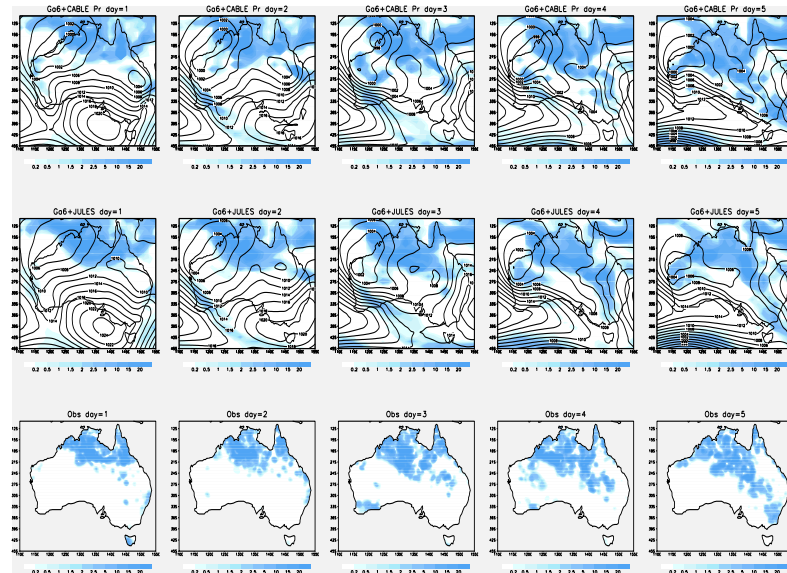
Figure 2: Preliminary daily results from 5-day rainfall hindcasts on 16/01/2009. Left to right is hindcast day while top to bottom show results from GA6c, GA6j and observations.

We know land-surface initial conditions are important for NWP application but the default T-AMIP configurations use model AMIP climatologies in their initialisations. Thus, in this study we have also examined the model hindcasts by superimposing scaled soil moisture and soil temperature anomalies from ERA-interim product into the model initial conditions. Comparison of the modelling results suggests that "realistic" land initialisation can reduce the model hindcasting error, particularly for convective rainfall.
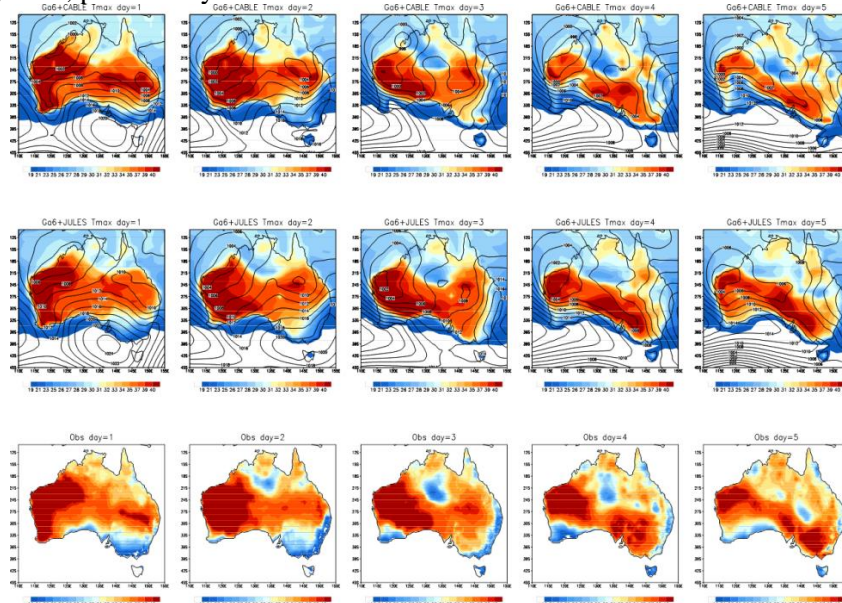
Figure 3: As in Figure 2 but for 5-day Tmin hindcasts on 16/01/2009.

Conclusions

This paper discusses the setup procedure and initial results from Transpose-AMIP simulations using the A13c, GA6j and GA6c models. The biases seen in AMIP simulations can also be seen in the T-AMIP simulations, thus justifying the use of these cheaper model runs to examine some biases seen in the more expensive AMIP runs. Preliminary results also demonstrated the usefulness of T-AMIP in testing the potential impacts of land-surface modelling for ACCESS NWP. Thorough NWP-like comparison between GA6-JULES and GA6-CABLE is being conducted with more case studies and detailed comparisons over regional and global domains. More tests with higher resolutions for selected extreme weather events will also be pursued.

References

Bi et al., 2013: The ACCESS coupled model: description, control climate and evaluation, Australian Meteorological and Oceanographic Journal 63:1March 2013

Kowalczyk, E.A., Y.P. Wang, R.M. Law, H.L. Davies, J.L. McGregor and G. Abramowitz, 2006: The CSIRO Atmosphere Biosphere Land Exchange (CABLE) model for use in climate models and as an offline model, http://www.cmar.csiro.au/eprint/open//kowalczykea_2006a.pdf

Kowalczyk, E., Stevens, L., Law, R.M., Dix, M., Wang, Y.P., Harman, I.N., Haynes, K., Srbinovsky, J., Pak, B. and Ziehn, T. (2013). The land surface model component of ACCESS: description and impact on the simulated surface climatology, *Australian Meteorological and Oceanographic Journal,* 63, 65-82.

Roff, G., 2014: ACCESS Transpose-AMIP: Experimental Procedure and Preliminary Results, CAWCR Res. Let., (accepted October 2014)

Williams, K.D., et al., 2015: The Met Office Global Coupled model 2.0 (GC2) configuration, Geosci. Model Dev., 88, 1509–1524

MULTI-DECADAL TREND IN TERRESTRIAL EVAPOTRANSPIRATION AND ITS IMPLICATION ON GLOBAL CLIMATE MODELS

Yongqiang Zhang[1], Jorge L. Peña-Arancibia[1], Francis H.S. Chiew[1]

[1] CSIRO Land and Water, Canberra, ACT 2601, Australia

yongqiang.zhang@csiro.au

Abstract

Evapotranspiration (ET) is a key component of the energy and water cycle. Over land, ET is a subtle combination of evaporation from the soil (Es), transpiration from plants (Et), and direct evaporation of precipitation intercepted by plants (Ei), an intricate process that has large implications for climate and global change. There are numerous studies focusing on estimating ET and its trends and possible causes. However, no studies have analysed the contribution to these trends of each ET component in detail (Jung *et al.*, 2010, Miralles *et al.*, 2014). This study used gridded global meteorological and satellite data from 1981–2012 at 0.50° spatial resolution as inputs to a simple physical model (PML) to compute global terrestrial ET components. The PML model and ET components were validated using a range of observations from point to global scale including: flux tower data, catchment rainfall and streamflow data, global satellite-derived soil moisture and vegetation optical depth data. Globally, annual variability in ET estimated from PML falls well within the inter-quantile range of annual variability simulated by nine global land surface models (Figure 1). We find a positive trend in the global ET in the past 30 years, which is mainly driven by vegetation greening trends (Figure 1). The global trend in ET is not significant ($p > 0.05$) when trends in leaf area index are removed. When the greening trend was included, Et and Ei showed a significant positive trend, but countered by a strong negative trend in Es. We also find that multi-annual variability of Et and Es estimated by the PML model is larger than those from global earth system models. However, when trends in leaf area index are removed, the PML model simulates a smaller annual variability that often falls within the inter-quartile range of the global earth system models. These results indicate that it is essential to represent vegetation dynamics realistically in global earth models for better accurately predict multi-decadal trends in ET and its components.
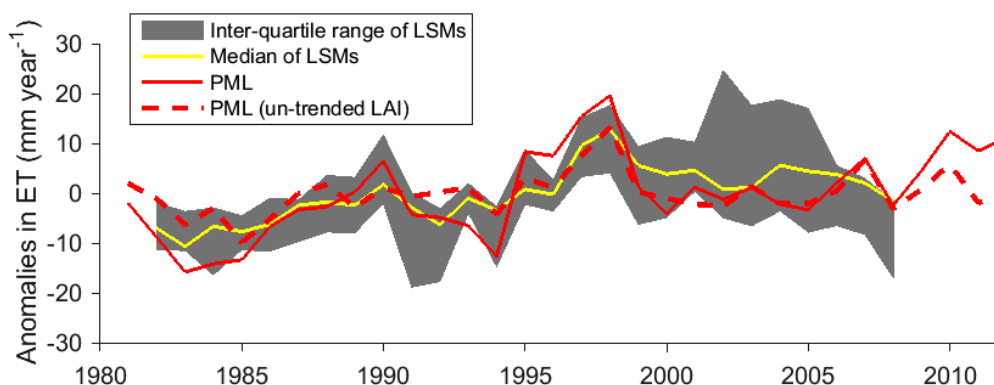
Figure 1. Anomalies of annual ET obtained from the Penman-Monteith-Leuning evapotranspiration model (PML) and nine land surface models (LSMs) for 1982 to 2011

References

Jung M, Reichstein M, Ciais P *et al.,* 2010: Recent decline in the global land evapotranspiration trend due to limited moisture supply. Nature*,* 467, 951-954.

Miralles DG, Den Berg MJ, Gash J *et al.,* 2014: El Niño-La Niña cycle and recent trends in continental evaporation. Nature Climate Change*,* 4, 122-126.

IMPACT OF SUMMER HEATWAVES ON FOREST PRODUCTIVITY IN SOUTHERN AUSTRALIA

E. van Gorsel

CSIRO, Oceans and Atmosphere, Yarralumla, Australia

Eva.Vangorsel@csiro.au

Abstract

Climate extremes and in particular heat waves are becoming hotter, they last longer and occur more often. This is likely to profoundly affect ecosystems, as many ecological processes are more sensitive to climate extremes than to changes in mean states. The impact of climate extremes on terrestrial ecosystems is poorly understood but important for predicting feedbacks to climate and climate change.

Eucalyptus trees, Mulga and Banksia Woodlands are known to be among the most adaptive plant species on Earth, allowing them to thrive under some of the hardiest ecological conditions. During the summer of 2012-2013, Australia experienced the warmest summer on record and a series of particularly intense heat waves.

We have used continuous eddy covariance measurements of ecosystem-scale energy and carbon dioxide fluxes to analyse the ecosystem response to these extreme weather conditions. We will show how the energy balance terms change throughout the heat wave and analyze the short time consequences of evapotranspiration, primary productivity and ecosystem respiration to the record temperatures under increasingly low soil moisture conditions.

PROBABILISTIC STATE ESTIMATION FOR COUPLED MODELS

Craig H. Bishop

Marine Meteorology Division, Naval Research Laboratory, Monterey, USA

bishop@nrlmry.navy.mil

Introduction

Overview

Weakly, moderately and strongly coupled Data Assimilation (DA) is defined; outstanding coupled DA questions are identified and possible solutions identified with the help of an idealized coupled model.

Weak, moderate and strong levels of DA coupling

Coupled ocean-atmosphere-wave-ice-land-aerosol models promise to significantly extend the time horizon to which useful forecasts can be made (Buizza and Leutbecher, 2015). Relatively sophisticated uncoupled DA schemes have been developed for uncoupled sub-models of the coupled system such as the ocean and atmosphere. One can use these uncoupled models and DA schemes to initialize coupled model forecasts but a drawback of this approach is that observational information is propagated forward in time by the uncoupled models rather than the potentially superior coupled model. A more satisfactory variation on this approach is to simply replace the uncoupled model "first guesses" of observations used in the uncoupled DA schemes by a first guess that from the coupled model. This approach is called *weakly coupled DA*. In general, weakly coupled DA does not allow oceanic (atmospheric) observations to affect the analysis of the atmosphere (ocean). However, as shown by Laloyaux et al. (2015), if an outer-loop is employed in such a system, oceanic (atmospheric) observations do affect the atmospheric (oceanic) analysis. Thus, the outer loop turns a weakly coupled DA scheme into a *moderately coupled* DA scheme.

Since physics couples properties of each of the sub-components together, errors in the forecast of one component of the coupled model will covary with errors in other components. A DA scheme that uses a model of the error covariances between one-or more sub-components of the coupled system is called a *strongly coupled* DA scheme and, in theory, the strongly coupled schemes should be more accurate than any of the other schemes. A 4DVAR strongly coupled DA would feature an outer-loop just like that of Laloyaux et al. (2015) but unlike Laloyaux et al., it would also feature non-zero models of the error covariances between model sub-components such as the atmosphere and ocean.

Outstanding Coupled DA Questions

1. The very differing time and space scales of major oceanic and atmospheric features have led some to wonder whether strongly coupled DA has much potential advantage over weakly coupled DA. Are these differing time and space scales a limiting factor for strongly coupled DA?
2. DA windows for pure ocean models have ranged from 1-10 days (Laloyaux et al., 2015) while those for the atmosphere range from 1-12 hrs. The long DA window for the ocean accommodates late arriving observations from Argo floats, Altimeters and Sea Mammals that can take anywhere from 1-5 days to reach forecasting centers. In addition, a long 3-10 day DA window typically contains more observations to tie down

the relatively slowly evolving but small scale oceanic eddies and deep ocean model error dynamics can remain quasi-linear over a 10 day period. In contrast, for the atmosphere, error dynamics can become strongly non-linear in as little as 6 hrs, observations arrive a few hrs after they are taken and there are enough observations in a 6 hr period to tie down most of the key atmospheric features. What then should be the time window(s) for n ocean-atmosphere coupled DA system designed for making timely real-time forecasts?

3. Currently, the leading DA technique in meteorology is 4DVAR which relies on the Tangent Linear (TL) (or gradient) of the non-linear model and its Adjoint. The barrier of building and maintaining TLs and adjoints of the entire coupled system has, so far, proved insurmountable. Might the new approach of ensemble based TLs and adjoints be used to surmount this barrier?

An idealized coupled DA framework

To provide a simple framework to test and evaluate strategies for coupled DA, a new simplified coupled model was created by coupling four realizations of model 1 of Lorenz (2005).
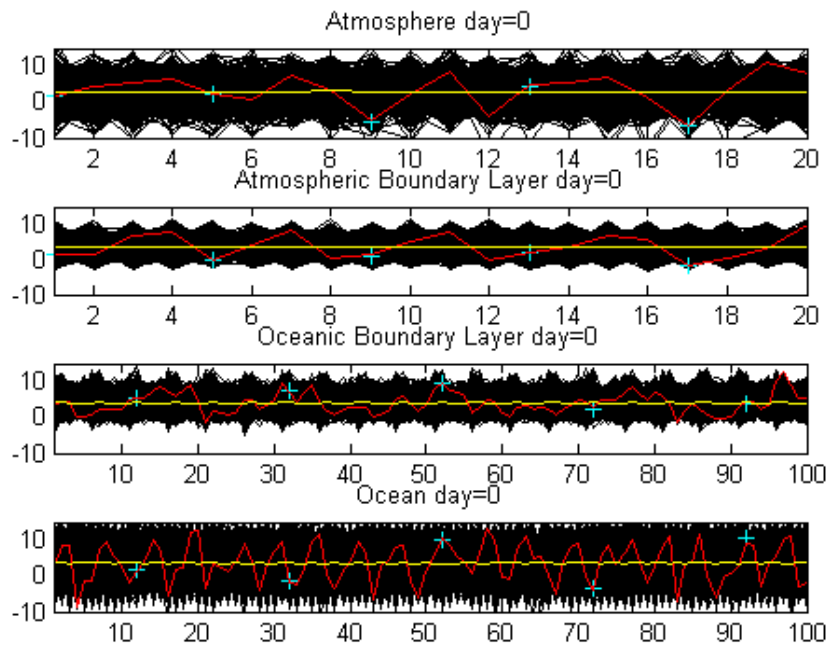
Figure 1: Ordinate axis gives the value of the models "zonal-wind-like" variables at each of the levels. Abscissa axis gives both the horizontal location of the model variable and the horizontal index of the associated grid point. Red line gives the initial true state of the idealized coupled model. Black lines give individual ensemble members obtained by randomly sampling the climatology of the model. The yellow line gives the mean of this ensemble. Cyan crosses give the locations and values of error prone observations. Observation locations move each DA cycle.

The resulting model has two atmospheric levels of 20 variables and two oceanic levels of 100 variables each. The upper most atmospheric layer has only weak coupling to the other layers (see Figure 1). It features relatively large scale chaotic waves with predictability time scales very similar to the atmosphere (~10 days). The lower atmospheric layer has a moderate coupling to the upper ocean layer. It features chaotic waves of a similar scale to the upper atmosphere, but the predictability time scale is longer (~45 days) due to its coupling to the more slowly evolving ocean. The upper most ocean level is moderately coupled to the lower atmosphere and features chaotic waves with wavelengths characteristic of both the large scale

waves of the upper atmosphere and the smaller scale waves of the deeper ocean. Its predictability limit is also about 45 days. The lowest ocean layer has relatively weak coupling to all other layers and features chaotic but slowly evolving waves of a much smaller length scale than those of the atmosphere. The predictability limit of waves in this deepest ocean layer is about 180 days.

An ensemble was initialized with random draws from a very long free run of the coupled model. This climatological ensemble was then used in the Ensemble Kalman Filter (EnKF) (Burgers et al., 1998). In order to avoid having to localize the ensemble covariances, a 480 member ensemble was used. The black lines on Figure 1 depict the initial state of these ensemble members. The cyan crosses identify the error prone observations to be assimilated. The observations were assimilated in two distinct ways:

    (i)   Strongly coupled DA in which a perturbed observations EnKF uses observations from the ocean and atmosphere to update the ensemble at every single model grid point, and

    (ii)   Weakly coupled DA in which only atmospheric (oceanic) observations are used to update the atmosphere (ocean)

After using the observations to initialize the ensemble, a 6 hr ensemble forecast was made and then this was used to assimilate a new set of observations, and so on. In this way, we obtained two parallel 6 hr DA cycles over a 5 day period. The mean square error of the ensemble mean for each of the methods was tracked as the DA cycles proceeded. Repeating the procedure in a statistically independent way allowed us to accurately measure the statistical significance of differences between weakly and strongly coupled DA performance. Twenty eight independent 5 day DA experiments were performed. Each line on Figure 2 shows how the mean square error (mse) of the analysis ensemble mean evolved through time in each of these experiments. The fact that the dashed blue lines give higher mse than the solid black lines in the first 4-5 DA cycles suggests that strongly coupled DA was significantly superior to weakly coupled DA.
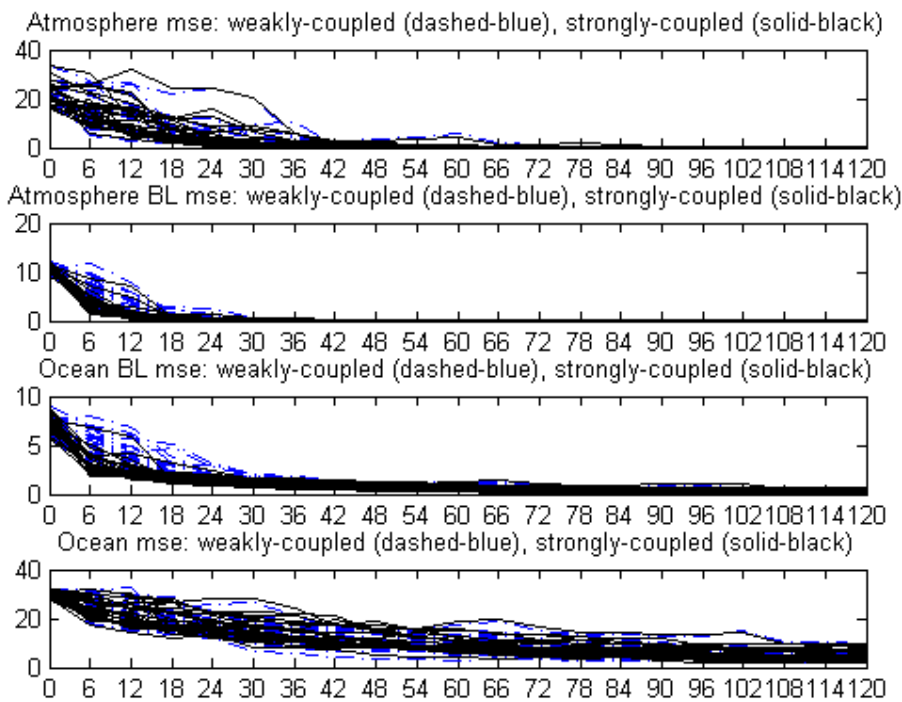
Figure 2: Ordinate-axis is mse, Abscissa-axis is time (in hrs). DA was performed every 6 hrs. Blue lines pertain to weakly-coupled DA, black lines pertain to strongly-coupled DA.

The magnitude and statistical significance of these apparent improvements is given in Figure 3. It shows that the reduction in mse due to strongly coupled DA is statistically significant in the atmospheric and oceanic boundary layers over almost the entire 5 day DA period. The percentage improvement is particularly large in the first DA experiment – when the pure climatological ensemble is employed.
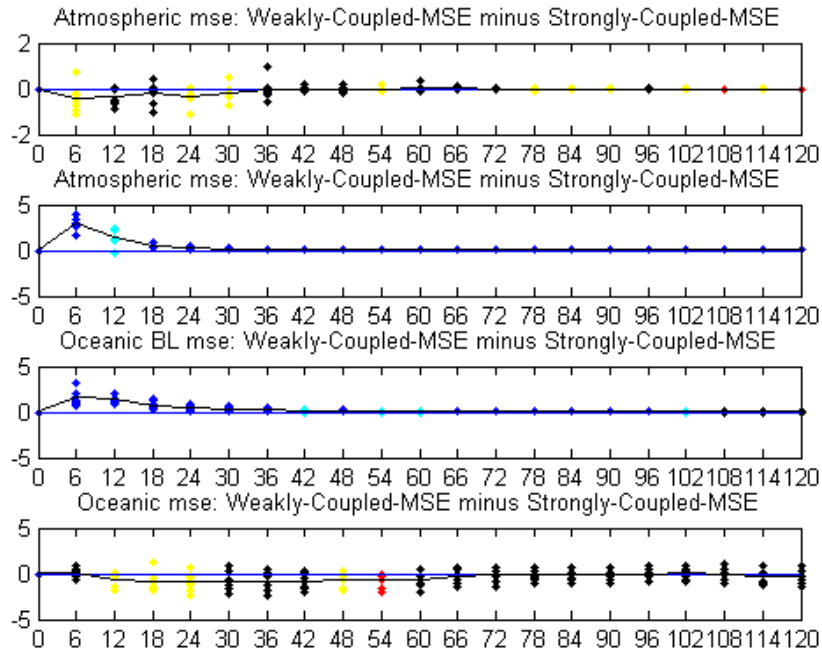
Figure 3: Blue diamonds => 99% statistical confidence in superiority of strongly-coupled over weakly coupled. Cyan diamonds => 95% statistical confidence in superiority of strongly-coupled over weakly coupled. Yellow diamonds => 95% statistical confidence in superiority of weakly-coupled over strongly coupled. Red diamonds => 95% statistical confidence in superiority of weakly-coupled over strongly coupled. Black diamonds => statistical confidence, either way, is less than 95%.

Conclusions

In this simple model, strong differences in the length and time scales of oceanic and atmospheric structures do not prevent strongly coupled DA from outperforming weakly coupled DA. The simple model allows one to vary the strength of inter-fluid coupling and examine its effect on the value of strongly coupled DA and other algorithmic variations. Further uses of the framework for addressing coupled model specific DA questions will be given in the talk.

References

Burgers, Gerrit, Peter Jan van Leeuwen, Geir Evensen, 1998: Analysis Scheme in the Ensemble Kalman Filter. Mon. Wea. Rev., 126, 1719–1724.

Buizza R., and M. Leutbecher, 2015: The forecast skill horizon. . *Q. J. Roy. Met. Soc.,* doi:10.1002/qj.2619

Laloyaux, P., M. Balmaseda, D. Dee, K. Mogensen, and P. Janssen, 2015: A coupled DA system for climate reanalysis. *Q. J. Roy. Met. Soc.,* doi: 10.1002/qj.2629

REANALYSIS BENEFITS FROM HIGHER SPECTRAL SPATIAL AND TEMPORAL RESOLUTION EOS

John Le Marshall[1,3], David Howard[1], Yi Xiao[1], James Jung[2], Jin Lee[1], Paul Lehmann[1], Chris Tingwell[1] , Robert Norman[3] , Jaime Daniels[4] Steve Wanzong[4] and Tim Morrow[5]

[1] *Bureau of Meteorology, Australia,* [2] *Cooperative Institute for Meteorological Satellite Studies, Madison, WI, USA,* [3] *RMIT University, Melbourne, Australia,* [4] *NOAA NESDIS, STAR* [5] *Melbourne University.*

j.lemarshall@bom.gov.au

Abstract

The importance of higher spectral, spatial and temporal resolution satellite observations for analysis and reanalysis is underlined by recent numerical experiments over the southern hemisphere. These show that the life of a high quality numerical forecast is extended by a factor of four by using Earth Observations from Space (EOS) (Le Marshall et al., 2013a). That is a one-day operational forecast not using satellite data is of the same quality as a four-day operational forecast which used satellite data when both are verified against the all data (with satellite) analysis. Considerable benefit has also been documented in the northern hemisphere. The importance of EOS for severe weather prediction such as tropical cyclone and heavy rainfall forecasting has also been shown.

Technology development has enabled higher spectral, spatial and temporal resolution observations from space and this has resulted in more accurate and higher spatial and temporal resolution inferred geophysical parameters in analysis and reanalysis. Here we show the benefit to analysis and reanalysis of higher resolution observations from current and future hyperspectral infrared sounding, microwave sounding, radio occultation limb sounding and high resolution wind estimation from space. In particular, we note the benefits of Himawari-6, 7 and 8 data. We also show the potential to improve current analysis, reanalysis and forecast capability by better use of current observational capacity and by better use of past observation platforms.

The impact of high resolution EOS

In the case of hyperspectral data, improvements in analysis and forecasting derived from an increased use of channel numbers have been demonstrated (Le Marshall et al., 2006), including significant gains in the analysis and forecasting of moisture fields (Le Marshall et al., 2014). The considerable benefit available from the use of cloudy radiances has also been demonstrated (Le Marshall et al., 2008). Finally, the effective use of data over land still remains to be achieved. In this regard, the requirement for accurate estimates of the emissivity remain, with accurate estimation requiring an increased availability of surface viewing channels.

In relation to microwave sounding, radio occultation sounding and high resolution wind estimation again the link between high resolution observations and high quality analysis, reanalysis and forecasts has been established. In particular, in relation to Himawari-6, 7 and 8, the benefits of the generation and assimilation of near continuous high density AMVs are well documented (Le Marshall et al., 2013b). Because of the increase in the spatial and temporal

resolution of observations accompanying the move from Himawari-7 to Himawari-8, higher spatial and temporal

Fig. 1 (a) Himawari-7 AMVs tracked using the IR and VIS channels at 00 UTC on 20 August 2015 from the operational system	Fig. 1 (b) Himawari-8 AMVs tracked using the IR (11 µm) channel at 00 UTC on 20 August 2015 using the next generation operational system
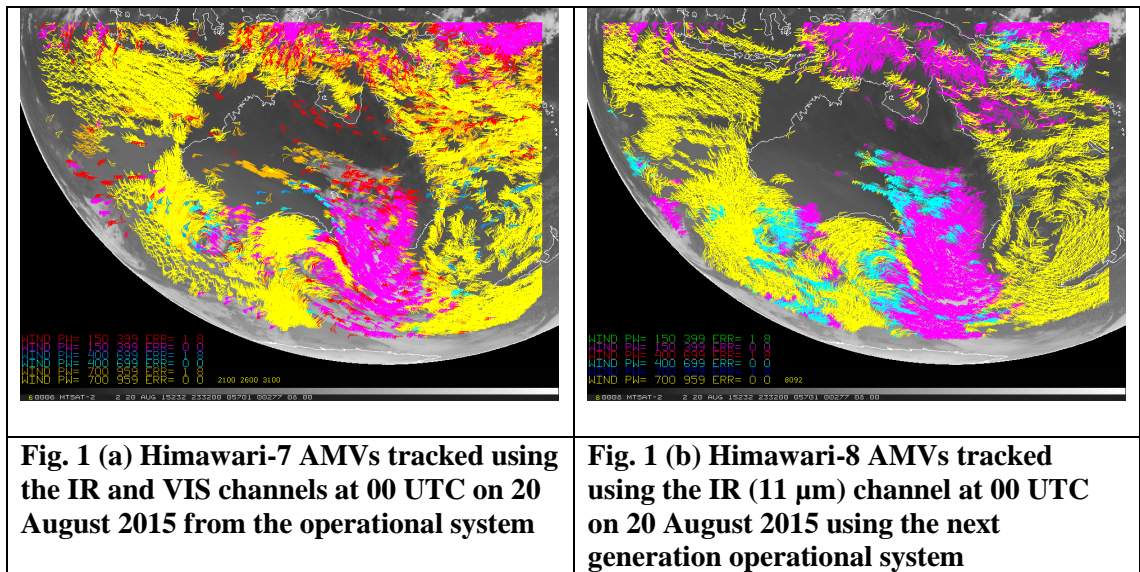
density AMVs are being produced locally in Australia from Himawari-8 observations. An example of local Himawari-7 11µm IR and Visible feature tracked winds at 00 UTC on 20 August 2015 is shown in Figure 1 (a) and an example of local 11 µm IR feature tracked winds for Himawari-8 over the same Himawari-7 image is shown in Figure 1 (b). The dense coverage of Himawari-8 winds over the tropics to the north of Australia is also shown in Figure 2. In these images, low level vectors are coloured yellow, middle level cyan and upper level vectors magenta, with higher accuracy

Fig. 2 Coverage of AMVs from Himawari-8 in the tropics to the north of Australia 06 UTC 6 September 2015	Fig. 3 Himawari-8 level of best fit height assignment statistics for CH.14 AMVs for September 2015 (see text)
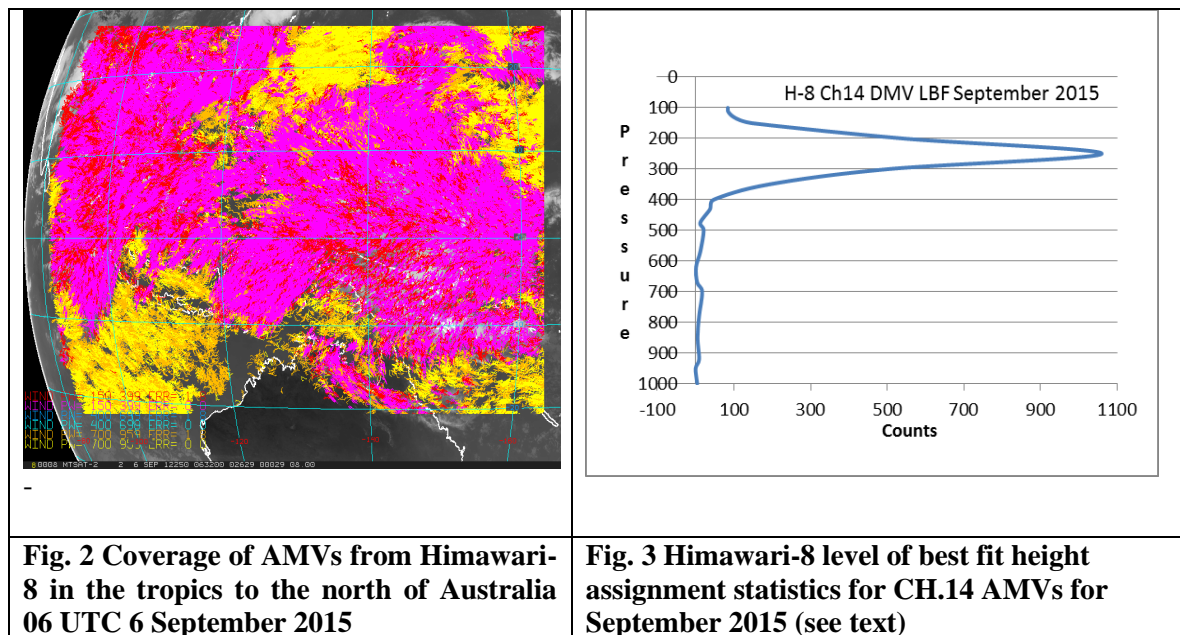
vectors being displayed. An indication of the accuracy of the height assignment in the new local Himawari-8 system AMV system is also shown in Figure 3. Here for Channel 14 Himawari-8 AMVs height assigned between 230hPa and 270hPa, the number of winds (AMVs) are plotted

against the level of best fit (hPa) for September 2015. In general the winds are associated with a height assignment accuracy which renders them suitable for NWP.

Verification statistics are also shown in Table 1 for Himawari-8 before final thinning and selection prior to being passed to the NWP system. In the table MMVD means mean magnitude of vector difference and RMSVD means root mean square vector difference. Although the initial wind error estimates for the Himawari-8 are similar to those from Himawari-7, it needs be noted that, due to the vast increase in wind data in the case of Himawari-8, the Himawari-8 wind observations can be thinned using the Expected Error (Le Marshall et al., 2004) associated with each vector and other error characterisation data, to produce a far denser and more accurate wind field than previously available. This process provides fields suitable for assimilation in NWP, with errors being similar to or less than the errors of the NWP background field at radiosonde sites. It is anticipated that use of these data in operational NWP has the potential to provide improved analysis, reanalysis and prediction and a study examining full use of the data to this end is expanding as further denser data sets become available. Some early work in this area has already been completed using 10 minute Himawari-6 special observations collected in 2014 and additional advanced sounder data in the Bureau of Meteorology's next-generation operational forecast model APS-2.

Table 1 Verification Table for Himawari-8 IR (channel 14) AMVs compared to radiosondes 18 August – 18 September 2015			
AMV Type	Category	m/s	NOBS
Low Sep. <150km	MMVD	3.00	4911
	RMSVD	3.61	
	BIAS	0.71	
Low Sep. <50km	MMVD	2.36	473
	RMSVD	2.75	
	BIAS	0.29	
Middle Sep. <150km	MMVD	3.16	1202
	RMSVD	3.78	
	BIAS	-0.61	
High Sep. <150km	MMVD	4.11	15688
	RMSVD	4.88	
	BIAS	-0.64	

Summary

In summary, EOS form a vital part of current NWP. Benefits to analysis and reanalysis are now being demonstrated as a result of the improved spatial, spectral and temporal resolution observations that are available from current space-based platforms, with the potential for further improvement when fuller use is made of current and past observing capability. These benefits and those soon to be demonstrated from future space-based platforms indicate considerable potential for providing a significant improvement in numerical analysis, reanalysis and prediction and an increase in social and economic benefits to the community.

References

Le Marshall, J. F., A. Rea , L Leslie, R. Seecamp and M. Dunn. 2004. Error characterization of atmospheric motion vectors. Aust. Meteor. Mag. **53**,123-131.

Le Marshall, J., Jung,J., , Zapotocny, T., J., Derber, J., Treadon, R., Lord, S., Goldberg, M. and W. Wolf. 2006. The Application of AIRS Radiances In Numerical Weather Prediction. *Aust. Meteor. Mag*. 55, 213-217.

Le Marshall, J., Jung,J., , Goldberg, M.., Barnet, C., Wolf, W., Derber, J., Treadon, R. and S. Lord. 2008. Using Cloudy AIRS Fields of View in Numerical Weather Prediction. *Aust. Meteor. Mag*.57, 249 – 254.

John Le Marshall, Jin Lee, Jim Jung, Paul Gregory and Belinda Roux, 2013a. The Considerable Impact of Earth Observations from Space on Numerical Weather Prediction, 2013. *Aust. Meteor. and Ocean. Jnl.*, **63**, 497-500.

John Le Marshall , Rolf Seecamp, Yi Xiao, Paul Gregory, Jim Jung, Peter Steinle, Terry Skinner, Chris Tingwell and Tan Le. 2013b. The Operational Generation and Assimilation of Continuous Winds in the Australian region and their Assimilation with 4DVar. 2013. *Wea. Forecasting,* **28,** 504 – 514.

John Le Marshall, James A. Jung, Jin Lee, Chris Barnet and Eric S. Maddy. 2014. Improving Tropospheric and Stratospheric Moisture Analysis with Hyperspectral Infrared Radiances, 2014. *Aust. Meteor. and Ocean. Jnl.*, **64**, 283-288.

TOWARDS A UM-BASED REGIONAL REANALYSIS FOR EUROPE

Dale M. Barker, Richard Renshaw and Peter Jermey

Weather Science, Met Office, Exeter, UK

dale.barker@metoffice.gov.uk

Introduction

Model-based reanalyses attempt to reconstruct past climate and specific historical weather events through an 'optimal' combination of past observations and state-of-the-art weather/climate models via the process of data assimilation (DA). Typically, the reanalysis dataset consists of 3-6hourly snapshots of the Earth System (atmosphere, ocean, land, cryosphere) through time (selected cases to multi-decadal sequences). Unlike observation-only based reanalysis datasets, model-based reanalyses provide complete gridded analyses of many fields simultaneously; both observed variables (e.g. winds, temperatures, precipitation, etc.) as well as unobserved fields (fluxes, 3D cloud, etc.) via the complex, multivariate, dynamically and physically consistent processes represented within modern models and DA systems.

Over the past few decades, there have been an increasing number of global reanalysis efforts. The ECMWF's reanalysis series (ERA15, ERA40, ERA-INTERIM, ERA-CLIM, ERA5) have provided complete, ever-improving multidecadal datasets of a range of global weather/climate indicators for analysis by researchers worldwide. Similar efforts have been undertaken in the US (NCEP-NCAR, NCEP-DoE, CFSRR, MERRA, etc.) and Japan (e.g. the recently completed JRA55 global dataset) with the Chinese Meteorological Administration also now considering a similar activity. Reanalysis efforts do not come cheap, requiring enormous human efforts to recover, quality control, and bias correct imperfect/incomplete observation datasets. In addition, significant HPC resource is required to run DA and weather/climate models over the extensive periods required to extract statistically significant climate signals. For this reason, perhaps the primary beneficiary of 40-50yr reanalyses to date has been the NWP community, via the extensive model evaluation testbed provided in long time reanalysis mode (standard NWP trials are typically only run over a few months at most). This is changing however, with the advent of centurial timescale reanalyses (e.g. NOAA's 20CR V3 will run from 1850 to the present day, see also Compo et al. 2011). The goals for this type of reanalysis are specifically to understand longer-term climate signals/trends, sacrificing resolution and most of the modern observing network in an attempt to separate true climate trends from artifacts of a rapidly changing 20th century observing network.

Regional reanalysis performs an analogous role to regional NWP – utilizing limited-area models at high-resolution to permit local detail and the inclusion of additional physical parameterisations (e.g. microphysics), thus providing a more detailed analysis of particular weather parameters than is achievable in global models (see e.g. Fig. 1). Data assimilation at high-resolution additionally permits the use of more spatially dense observing networks, and better treatment of all observations through an improved short-range background forecast used as input to DA, locally-tuned forecast error covariances, etc. Several regional reanalyses have been attempted (e.g. NOAA's North American Regional Reanalysis – NARR, NCAR's Arctic System Reanalysis – ASR, and India's South Asia Regional Reanalysis – SARR). The NARR in particular has successfully illustrated the ability of regional reanalysis to improve on global

reanalysis precipitation fields when compared to independent rainfall observations (Mesinger et al. 2006).

The Met Office contribution to the field of DA-based regional reanalysis began in 2010 through involvement in the EU-cofunded EURO4M reanalysis project (2010-2014 – http://www.euro4m.eu). The goal of the EURO4M project was to provide 'timely and reliable information about the state and evolution of the European climate, combining observations from satellites, ground-based stations and results from comprehensive model-based regional reanalyses'. The Met Office's major role in EURO4M was to lead WP2 (Model-Based Reanalysis) in collaboration with colleagues at SMHI, Meteo France, Meteo-Suisse, and the University of East Anglia (UEA). The major deliverables of the EURO4M project: the development of a UM-based regional reanalysis capability nested within ECMWF's ERA global reanalysis, and results from an initial pilot 2-year (2008-2009) pilot reanalysis, are described further below.
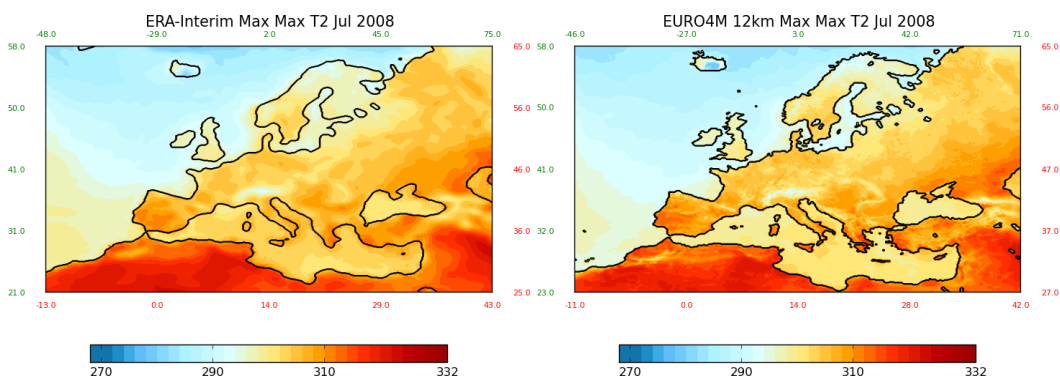
Figure 1: July 2008 maximum day max temperature:12km EURO4M (left) and ~80km ERA-Interim (right)

EURO4M UM Regional Reanalysis Scientific/Technical Configuration

The initial EURO4M UM regional reanalysis configuration was based on the Met Office North Atlantic/European (NAE) regional model (Bush et al, 2006) operational in 2013. The model domain (Fig. 1) is a 12km latitude/longitude grid oriented with respect to a rotated pole. The regional reanalysis makes use of the UM's four-dimensional variational (4DVAR) DA scheme (Rawlins et al. 2007) running on a 6-hour cycle with analyses at synoptic hours: 00Z, 06Z, 12Z, 18Z. Each analysis uses observations throughout the 6-hour interval T-3 to T+3. The analysis increments are calculated on a 24km grid, half the resolution of the full UM. The benefits of using 4DVAR over the cheaper 3DVAR algorithm are clearly seen in Figure 2 for a wide range of parameters. A wide range of observations are assimilated, including surface (screen temperature, humidity, 10m wind, surface pressure, visibility, cloud), upper air (temperature, humidity, wind), satellite AMV (Atmospheric Motion Vectors) winds, satellite (AIRS, ATOVS, IASI, SEVIRI) radiances, scatterometer surface wind, ground-based GPS signal delay (affected by column humidity), and GPS radio occultation bending angle. Further details can be found in Renshaw et al (2013).

The UM regional reanalysis makes maximum use of ECMWF's extensive global reanalysis observation datasets (representing several person-decades of effort in data recovery, correction etc.). In EURO4M, ERA-Interim analyses archived in ECMWF's MARS (Meteorological Archive and Retrieval System) were used as the source of lateral boundary conditions for the

regional reanalysis. To enable this close coupling between Met Office and ECMWF reanalysis efforts, a major technical effort has been undertaken in EURO4M to port the entire UM system to run on ECMWF's HPC. Secondary benefits of this strategy have been a) Faster turnaround for the reanalysis than would have been possible on the Met Office's own HPC, and b) The potential to make use of the UM system at ECMWF for additional, compute-intensive NWP/climate testbed activities in future.
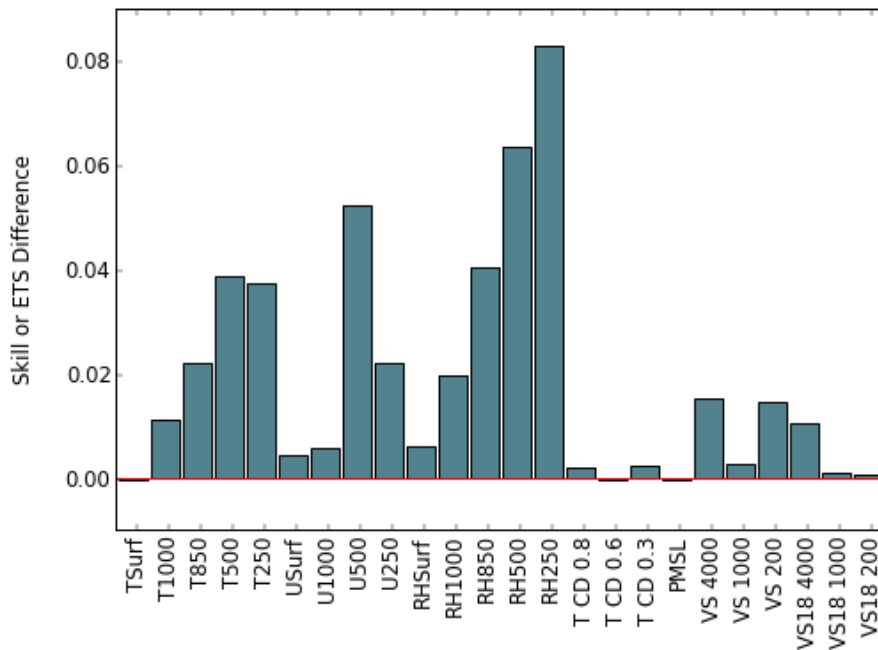
Figure 2: Percentage skill score and ETS differences for 4DVAR vs 3DVAR, Sept 2009 for a variety of meteorological parameters (for reference, average annual improvement in NWP = 1-2%=0.01-2)

EURO4M Reanalysis Evaluation

The quality of a reanalysis is best done via comparison against independent, unassimilated observations. Fig. 3 provides an illustrative example from Renshaw et al. (2013) – the evaluation of 24hour precipitation accumulation for each month during 2008 against (unassimilated) European rain-gauge observations, for a variety of rainfall thresholds. The regional (UM, 4DVar) reanalysis is clearly more skilful at representing observed accumulated rainfall than the global (ERA-INTERIM) reanalysis. The additional skill of the regional reanalysis is particular noticeable for higher rainfall intensities. Comparison with the benchmark UM-based regional climate model (RCM - same model, LBCs but no DA) and downscaler (same model, LBCs but ERA global initial conditions) indicate the importance of both resolution AND high-resolution, advanced assimilation to provide quality reanalysis products.

Current and Future Work

Since 2014, the Met Office has been engaged in the follow-on Uncertainties in Ensembles of Regional ReAnalyses (UERRA) project (2014-2018). In UERRA, the Met Office again leads the data assimilation work package (WP2) and will extend the EURO4M pilot reanalysis to cover the satellite-era (1978-present). The second major enhancement in UERRA is to develop an ensemble-based regional reanalysis, the first of its kind in the world, in order to provide quantitative estimates of uncertainty for use by the European regional reanalysis user community. The developments undertaken in EURO4M and UERRA have been undertaken

with a view to developing a regional-reanalysis component of an operational European climate service, to begin in the next few years as part of the Copernicus programme.
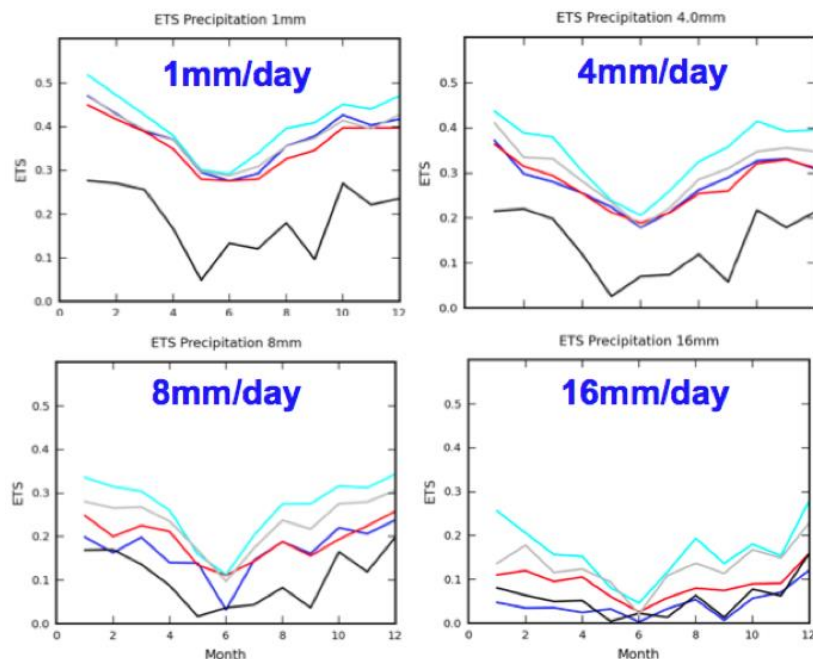
Figure 3: 24hr accumulated precipitation skill (ETS) for the entire EURO4M area through each month of 2008 for ERA-INTERIM global reanalysis (blue), UM 12km 4DVar regional reanalysis (cyan), HIRLAM 22km 3DVar regional reanalysis (red), UM downscaler (grey), and UM RCM (black). Rainfall thresholds of 1mm, 4mm, 8mm, 16mm /day are shown.

References

Bush, M., Bell, S., Christidis, N., Renshaw, R., Macpherson, B., Wilson, C., 2006: "Development of the North Atlantic European Model (NAE), into an operational model." Met Office Forecasting Research Technical Report, No. 470 (http://www.metoffice.gov.uk/archive/forecasting-research-technical-report-470)

Compo, G. P. and Coauthors, 2011:: "The 20th Century Reanalysis Project" Q. J. R. Met. Soc., 137, 1-28.

Mesinger, F., et al., 2006: North American Regional Reanalysis. BAMS, DOI:10.1175/BAMS-87-3-343.

Rawlins, F., Ballard, S.P., Bovis, K.J., Clayton, A.M., Li, D., Inverarity, G.W., Lorenc, A.C., Payne, T.J., 2007: "The Met Office Global 4-Dimensional Data Assimilation System" Q. J. R. Met. Soc., 133, 347-362.

Renshaw, R., Jermey, P., Barker, D., Maycock, A., and Oxley, S., 2013: "EURO4M Regional Reanalysis System" Met Office Forecasting Research Technical Report, No. 584 (http://www.metoffice.gov.uk/archive/forecasting-research-technical-report-584

COUPLED DATA ASSIMILATION FOR SEASONAL PREDICTION

Yonghong Yin, Oscar Alves, Debra Hudson, Robin Wedd, Harry Henden

Environment and Research Division, Bureau of Meteorology, Melbourne

y.yin@bom.gov.au

Abstract

Predictive Ocean Atmosphere Model for Australia (POAMA, http://poama.bom.gov.au/) is a state-of-the-art seasonal forecast system based on a coupled ocean - atmosphere model, a data assimilation system and a strategy for generating forecast ensembles. POAMA-2 is the current operational seasonal prediction system run by Bureau operations. This system forms the basis for the Bureau operational ENSO forecasts and the monthly and seasonal climate outlook, as well as a range of other products. The data assimilation/initialisation systems for POAMA-2 include an ensemble ocean data assimilation system (PEODAS; Yin et al. 2011) and an atmosphere/land initialisation (ALI; Hudson et al. 2011) system. PEODAS is an approximate form of the EnKF which was developed based on the multivariate ensemble optimum interpolation of Oke et al (2005), but uses covariances from a time evolving model ensemble. By using ALI, the atmospheric component is nudged towards pre-existing atmospheric analyses. To initialise the ensemble forecasts for POAMA-2, an ensemble of perturbed ocean and atmosphere states are generated using a coupled-model breeding method (Hudson et al. 2013).

The perturbations generated by the coupled breeding methods display significant state-dependence for both atmosphere and ocean components and can be used for estimation of error covariances in an ensemble data assimilation system. A preliminary version of an ensemble coupled data assimilation system (called PECDAS) has been developed. The first version of the system is weakly coupled, only ocean observations are assimilated into the coupled model and the atmospheric component is nudged towards pre-existing atmospheric analyses. PECDAS generates ensemble perturbations using the same coupled breeding methods as in POAMA-2 but the unperturbed analyses is done by using the background states from the coupled model run and using modified methods of the ALI and the PEODAS for atmosphere and ocean components respectively. The ocean error covariances are estimated from the flow-dependent ensemble perturbations. The performance of PECDAS reanalysis is evaluated through a series of comparisons with assimilated and independent observations/analyses and also with those from PEODAS and experiments without ocean or atmosphere data assimilations.

The Bureau's seasonal prediction system continues to be developed. The next version of the POAMA system will be called ACCESS-S. ACCESS-S will use a new version of the assimilation code (EnKF-C) developed by Pavel Sakov (Sakov 2015), written in C and more efficient on massively parallel systems. The PECDAS approach will be developed based on the code of the EnKF-C developed by Pavel. It is likely that we will use a full ETKF version of this code, rather than the approximate form of the EnKF used in PEODAS.

References

Hudson, D., Alves, O., Hendon, H.H. and Wang, G., 2011: The impact of atmospheric initialisation on seasonal prediction of tropical Pacific SST, Clim. Dyn., 36, 1155-1171

Hudson, D., A. Marshall, Y. Yin, O. Alves, and H. Hendon, 2013: Improving intraseasonal prediction with a new ensemble generation strategy. Mon. Wea. Rev., 141, 4429-4449, DOI: 10.1175/MWR-D-13-00059.1

Oke, P. R., A. Schiller, D. A. Griffin and G. B. Brassington, 2005: Ensemble data assimilation for an eddy-resolving ocean model of the Australian region, Q. J. R. Meteorol. Soc., 131, 3301-3311

Sakov, P., 2015: EnKF-C user guide, arXiv:1410.1233.

Yin, Y., O. Alves, and P. R. Oke, 2011: An ensemble ocean data assimilation system for seasonal prediction, Mon. Wea. Rev., 139, 786-808

IMPACT OF SALINITY ASSIMILATION ON SEASONAL FORECASTS

Mei Zhao, Harry H. Hendon, Oscar Alves and Yonghong Yin

Environment and Research Division, Bureau of Meteorology, Melbourne

m.zhao@bom.gov.au

Abstract

We assess the sensitivity of the simulated mean state and coupled variability to systematic initial state salinity errors and the impact of improved ocean initial conditions for predicting El Niño-Southern Oscillation (ENSO) and Indian Ocean dipole (IOD) in seasonal forecasts using the Australian Bureau of Meteorology Predictive Ocean Atmosphere Model for Australia (POAMA) coupled model. This analysis is based on two sets of hindcasts that were initialized from old and new ocean initial conditions, respectively. The new ocean initial conditions are provided by an ensemble multivariate analysis system that assimilates subsurface temperatures and salinity and is a clear improvement over the previous system, which was based on univariate optimal interpolation, using static error covariances and assimilating only temperature without updating salinity.

Large systematic errors in the salinity field around the thermocline region of the tropical western and central Pacific produced by the old assimilation scheme are shown to have strong impacts on the predicted mean state and variability in the tropical Pacific for the entire 9 months of the forecast. Forecasts initialized from the old scheme undergo a rapid and systematic adjustment of density that causes large persistent changes in temperature both locally in the western and central Pacific thermocline, but also remotely in the eastern Pacific via excitation of equatorial waves. The initial subsurface salinity errors in the western and central Pacific ultimately result in an altered surface climate because of induced temperature changes in the thermocline that trigger a coupled feedback in the eastern Pacific. These results highlight the importance of accurately representing salinity in initial conditions for climate prediction on seasonal and potentially multiyear time scales.

Hindcasts using the new ocean initial conditions have better skill at predicting sea surface temperature (SST) variations associated with ENSO than do the hindcasts initialized with the old ocean analyses. The improvement derives from better prediction of subsurface temperatures and the largest improvements come during ENSO-IOD neutral years. We show that improved prediction of the Niño3.4 SST index derives from improved initial depiction of the thermocline and halocline in the equatorial Pacific but as lead time increases the improved depiction of the initial salinity field in the western Pacific become more important. Improved ocean initial conditions do not translate into improved skill for predicting the IOD but we do see an improvement in the prediction of subsurface temperatures in the Indian Ocean (IO). This result reflects that the coupling between subsurface and surface temperature variations is weaker in the IO than in the Pacific, but coupled model errors may also be limiting predictive skill in the IO.

OCEANIC TELECONNECTIONS AS REVEALED IN MODELS AND REANALYSES WITH APPLICATION TO DECADAL FORECAST INITIALISATION

Terence J. O'Kane

CSIRO Oceans and Atmosphere

terence.okane@csiro.au

Abstract

A key question in decadal prediction is the difficult problem of separating internal low-frequency variability from the forced response in the climate system. Recent work (Monselesan et al 2015) has revealed the spatiotemporal characteristics of internal variability by comparing ensemble averages of in-band fractional variances in Coupled Model Intercomparison Project Phase 5 (CMIP5) preindustrial control simulations to estimates from observations and reanalyses. This study showed, in both models and reanalyses, that for sea surface temperature and sea level height anomalies variability on time scales less than 5 years is predominantly in the tropics and has the spatial signature of El Niño–Southern Oscillation. On progressively longer time scales the variance moves to the extratropics and from middle to higher latitudes while displaying spatially coherent features. These results confirm that whereas seasonal predictability is largely derived by the tropics, decadal variability resides in the subtropical and mid-latitude oceans. Therefore initial conditions for successful decadal to multi-decadal prediction must effectively sample the most dynamically relevant unstable modes of the subtropical and higher latitude oceans and in particular the Southern Ocean (O'Kane et al 2013). A key question is how is this memory communicated from the subtropics to the tropics where strong coupling to the atmosphere occurs? Two possible candidates are large scale nonlinearly modified eddies (baroclinically unstable waves) and density compensated disturbances.

Ocean storm tracks have previously been associated with the midlatitude western boundary currents (WBCs) and the Antarctic Circumpolar Current (ACC), however a recent study (O'Kane et al 2015) has demonstrated pathways for communicating coherent signals from the subtropics and mid-latitudes to the tropics. One such mechanism is via large-scale baroclinically unstable waves occurring within waveguides associated with potential density gradients in the subtropical regions of the Southern Hemisphere (SH) oceans where the trade winds and westerlies meet and at depths associated with mode water formation. In contrast to the Northern Hemisphere subtropics, the SH pathways are more extensive allowing large-scale coherent disturbances to communicate information westward from the midlatitudes to the subtropics (South Pacific Ocean) and from the subtropics to the tropics (Indian Ocean). Using an ocean general circulation model, a simple potential energy transfer diagnostic and focusing on the South Pacific, they identified the relevant nonlinearly modified structures comparing their propagation characteristics to planetary Rossby waves calculated using a shallow water model. Rather than planetary Rossby waves, they showed the modeled wave-like disturbances were inherently nonlinear, multiscale and amplified where topography occurs via resonant interactions. The location of the disturbances were found to coincide with regions of high variability in sea surface height observed in satellite altimetry and their speeds found to closely match the observed large-scale coherent westward propagating structures. This study provides evidence that, in addition to the midlatitude WBCs and the ACC, significant ocean storm tracks

are also manifest in the SH subtropics.

In a further study (Sloyan and O'Kane 2015) optimally interpolated monthly time series Tasman Sea XBT data were compared to a comprehensive set of ocean data assimilation models forced by atmospheric reanalysis in order to investigate the decadal variability and stability of the Tasman Sea thermocline and the transport variability of the East Australian Current (EAC), the Tasman Front, and EAC-extension. They found that anomalously weaker EAC transport at 25S corresponds to an anomalously weaker Tasman Front and anomalously stronger EAC-extension. They further showed that, post about 1980 and relative to the previous 30 years, the anomalously weaker EAC transport at 25S is associated with large-scale changes in the Tasman Sea; specifically stronger stratification above the thermocline, larger thermocline temperature gradients, and enhanced energy conversion. Significant correlations were found between the Maria Island station Sea Surface Temperature (SST) variability and stratification, thermocline temperature gradient, and baroclinic energy conversion suggesting that nonlinear dynamical responses to variability in the basin-scale wind stress curl are important drivers of decadal variability in the Tasman Sea. They further showed that the stability of the EAC is linked, via the South Caledonian Jet, to the stability of the pan-basin subtropical South Pacific Ocean ''storm track''.

South Pacific subtropical density compensated temperature and salinity (spiciness) anomalies are known to be associated with decadal equatorial variability, however, the mechanisms by which such disturbances are generated, advect and the degree to which they modulate the equatorial thermocline remains controversial. During the late 1970's a climate regime transition preceded a period of strong and sustained El Nino events. Using an ocean general circulation model forced by the constituent mechanical and thermodynamic components of the reanalysed atmosphere O'Kane et al 2013 showed that the late 1970's transition coincided with the arrival of a large-scale, subsurface cold and fresh water anomaly in the central tropical Pacific. An ocean reanalysis for the period 1990–2007 that assimilates subsurface Argo, XBT and CTD data, reveals that disturbances occur due to the subduction of negative surface salinity anomalies from near 30◦ S, 100◦ W which are advected along the $\sigma = 25$–26 kgm^{-3} isopycnal surfaces. These anomalies take, on average, seven years to reach the central equatorial Pacific where they may substantially perturb the thermocline before the remnants ultimately ventilate in the region of the western Pacific warm pool. Positive (warm–salty) disturbances, known to occur due to late winter diapycnal mixing and isopycnal outcropping, arise due to both subduction of subtropical mode waters and subsurface injection. On reaching the equatorial band (10◦ S–0◦ S) these disturbances tend to deepen the thermocline reducing the model's ENSO. In contrast the emergence of negative (cold–fresh) disturbances at the equator are associated with a shoaling of the thermocline and El Nino events. Process studies are used to show that the generation and advection of anomalous density compensated thermocline disturbances critically depend on stochastic forcing of the intrinsic ocean by weather. They further show that in the absence of the inter-annual component of the atmosphere forcing Central Pacific El Nino events are manifest.

Recent studies (Maes and O'Kane 2014, Maes et al 2015) have revealed the crucial role of salinity and its stabilizing (e.g. salinity barrier layer) or destabilizing (e.g. density compensation) effects. Maes and O'Kane examined daily vertical profiles of temperature and salinity from an ocean reanalysis over the period 2001–2007. They find significant seasonal variations in the Brunt-Vaisala frequency profiles are limited to the upper 300 m depth. Based on this, they determined the ocean salinity stratification (OSS) to be defined as the stabilizing effect (positive values) due to the haline part of N^2 averaged over the upper 300 m. In many regions of the tropics, the OSS contributes 40–50% to N^2 as compared to the thermal stratification and, in some specific regions, exceeds it for a few months of the seasonal cycle. Away from the tropics, for example, near the centers of action of the subtropical gyres, there are

regions characterized by the permanent absence of OSS. In such regions salinity has a destabilizing effect i.e. OSSU=OSS<0 and the regions of high variance in OSSU map closely onto the coherent features described by O'Kane et al 2014.

The identification of the unstable growing modes of the ocean provide not only mechanisms by which decadal variability is communicated to the tropics from the subtropics but allow the application of modern ensemble prediction methods to characterize predictability and initialize decadal forecasts via the same mathematical framework as underpins numerical weather prediction (O'Kane et al 2011).

Monselesan, D. P., T. J. O'Kane, J. S. Risbey, and J. Church (2015), Internal climate memory in observations and models, Geophys. Res. Lett., 42, doi:10.1002/2014GL062765.

O'Kane, T. J., R. J. Matear, M. A. Chamberlain, J.S. Risbey, B.M. Sloyan and I. Horenko, Decadal variability in an OGCM Southern Ocean: Intrinsic modes, forced modes and metastable states, Ocean Modelling 69 (2013) 1–21

O'Kane, T. J., R. J. Matear, M. A. Chamberlain, E. C. J. Oliver, and N. J. Holbrook (2014), Storm tracks in the Southern Hemisphere subtropical oceans, J. Geophys. Res. Oceans, 119, 6078–6100, doi:10.1002/2014JC009990.

Sloyan, B. M., and T. J. O'Kane (2015), Drivers of decadal variability in the Tasman Sea, J. Geophys. Res. Oceans,120, doi:10.1002/2014JC010550.

O'Kane, T.J., R.J. Matear, M.A. Chamberlain, and P.R. Oke (2014) ENSO regimes and the late 1970's climate shift: The role of synoptic weather and South Pacific ocean spiciness, Journal of Computational Physics 271 19–38

Maes, C.,and T. J. O'Kane (2014), Seasonal variations of the upper ocean salinity stratification in the Tropics, J. Geophys. Res. Oceans, 119, 1706–1722, doi:10.1002/2013JC009366.

O'Kane, T.J., P.R. Oke and P.A. Sandery (2011) Predicting the East Australian Current, Ocean Modelling 38 (2011) 251–266
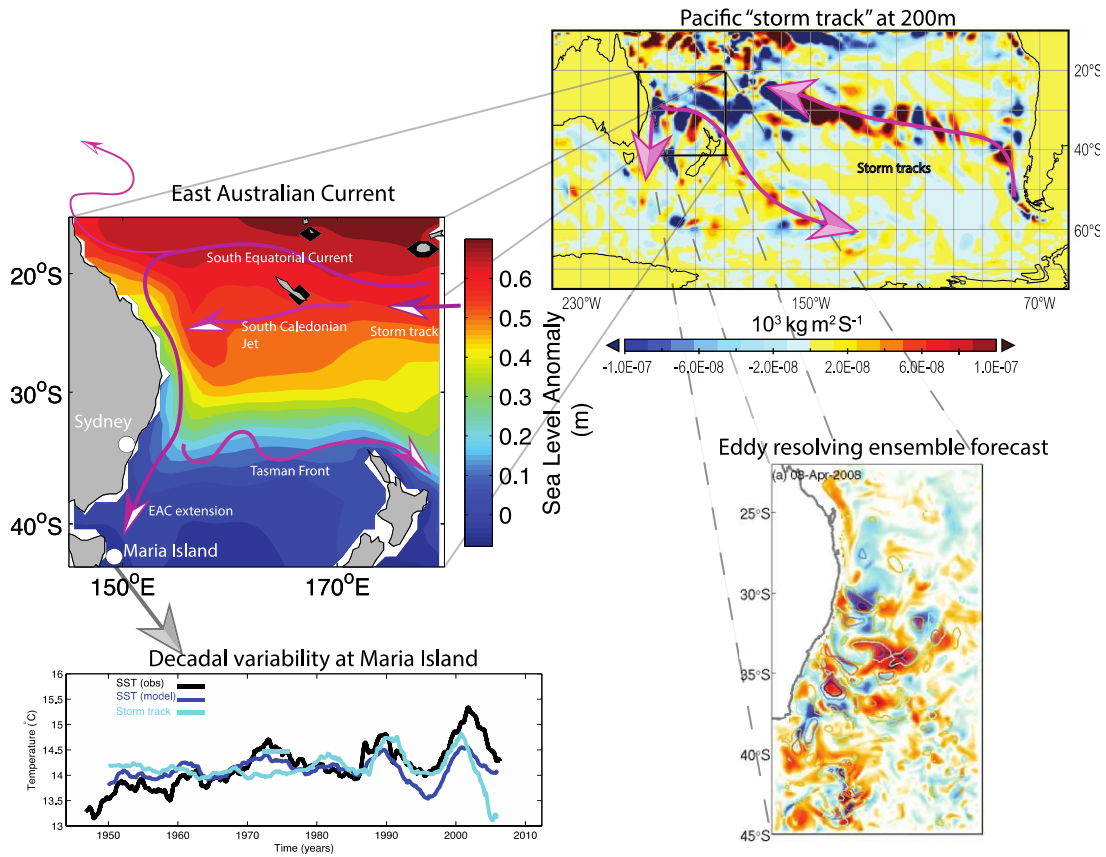
Schematic describing the relationship between the South Pacific Ocean storm track and the variability and predictability of the East Australian Current.

A NEW 'ENERGETIC' APPROACH INTO THE VARIABILITY AND TRENDS OF THE HADLEY CIRCULATION AND ENERGY TRANSPORTS TO THE HIGH SOUTHERN LATITUDES

Ghyslaine Boschat[1] and Ian Simmonds[2]

[1]*ARC Centre of Excellence for Climate System Science and School of Earth Sciences, University of Melbourne, Melbourne.*

[2]*School of Earth Sciences, University of Melbourne, Melbourne.*

ghyslaine.boschat@unimelb.edu.au

Abstract

The Hadley circulation is a major atmospheric overturning and is responsible for most of the energy transport from the low tropics to the extratropics. It consists of ascent of equatorial air associated with high-rainfall regimes, a poleward mass transport in the upper atmosphere and subsidence over extensive subtropical 'dry zones'. Understanding the variations in the strength and extent of this large-scale circulation bears obvious societal importance for Australia and other global climates. However there is, as yet, no clear consensus on the mechanisms controlling the current and future behaviour of the cell.

This work provides new perspectives on the variability and trends of the Hadley circulation, by exploring its structure within an energy (rather than a mass) framework. In this approach, spatial contrasts in the meridional transport of energy and its internal, latent and potential components are determined at different vertical levels, and for both hemispheres. This decomposition is performed using updated 6-hourly reanalysis data, which allows us to calculate seasonal means but also account for the role of stationary and transient eddy activity in the subtropics and midlatitudes. This *interactive* perspective presents the opportunity to integrate the climatology, variability and trends of the Hadley circulation into a broader and perhaps more comprehensive picture. Our analysis also reveals the important interannual signals associated with the meridional heat transports on to the Antarctic continent.

FUTURE OPPORTUNITIES IN ATMOSPHERIC CHEMISTRY-CLIMATE COUPLED MODELLING

Jenny A. Fisher[1], Robyn Schofield[2], and Michael S. Long[3]

[1]*Centre for Atmospheric Chemistry, University of Wollongong, Wollongong NSW*
[2]*School of Earth Sciences, University of Melbourne, Melbourne VIC*
[3]*School of Engineering & Applied Sciences, Harvard University, Massachusetts, USA*

jennyf@uow.edu.au

Abstract

Atmospheric chemistry and climate are closely linked through a number of atmospheric feedbacks. Atmospheric constituents that are formed chemically in the atmosphere— such as methane, tropospheric ozone and aerosols— impact incoming and outgoing radiation (Monks et al., 2009), and aerosols also impact moisture budgets by serving as cloud condensation nuclei (Andreae & Rosenfeld, 2008). The atmospheric chemistry of these and related species is in turn controlled by climate variables including temperature, humidity, precipitation, stagnation, and transport patterns, among others. These interactions are complex and multi-faceted, resulting in impacts of different magnitude and sign from an individual forcing agent. For example, warmer temperatures simultaneously drive ozone increases via increased emissions from wildfires, soils and lightning and ozone decreases via decreased removal by plants (Fiore et al., 2012). Estimating the net impacts of changing climate on atmospheric composition (and vice versa) is therefore challenging and requires coupled models that accurately represent both climate and chemistry processes.

Despite significant recent progress in our understanding of atmospheric chemistry, state-of-the-science chemical schemes used in earth system models remain subject to large uncertainties. For example, a recent comparison of coupled chemistry-climate models using different chemical schemes found that uncertainties in tropospheric ozone lead to radiative forcing uncertainties of up to 30% (Stevenson et al., 2013). For this reason, atmospheric chemistry schemes are often evaluated using multi-model comparisons (e.g., Fisher et al., 2015; Stevenson et al., 2013; Zeng et al., 2015). Such comparisons serve several purposes, including: (1) highlighting knowledge gaps evidenced by disagreements between models, or by disagreements between the model ensemble and observations; (2) prioritising future measurements that will best address these identified knowledge gaps; and (3) prioritising model development efforts. However, it can be difficult to attribute inter-model discrepancies in these comparisons as the models typically differ not only in chemical scheme, but also in horizontal and vertical resolutions, vertical extent, and treatment of radiation and cloud interactions (Lamarque et al., 2013).

We are embarking on a project to capture the benefits of multi-model comparisons for improving coupled chemistry-climate simulations— without the confounding influences caused by inter-model differences beyond the chemical scheme. Our work will build on the newly developed ACCESS-UKCA version of the Australian Community Climate and Earth System Simulator (ACCESS), which incorporates the United Kingdom Chemistry and Aerosols (UKCA) scheme. We plan to couple to ACCESS-UKCA a second atmospheric chemistry scheme, GEOS-Chem, that has recently been re-engineered to function as an atmospheric chemistry module within any Earth system model (Long et al., 2015). By using the two independent schemes in the same modelling framework, we will be able to uniquely attribute

major differences in model runs to differences in the chemical schemes. This will allow identification of the most important uncertainties in ACCESS atmospheric chemistry, and facilitate prioritised future development of ACCESS-UKCA. In this lightning talk, we will briefly introduce the project's rationale and preview the exciting future opportunities for coupled chemistry-climate modelling that it will enable.

References

Andreae, M.O. and D. Rosenfeld, 2008: Aerosol–cloud–precipitation interactions. Part 1. The nature and sources of cloud-active aerosols, Earth-Science Reviews, 89 (1–2), 13-41.

Fiore, A.M., V. Naik, D.V. Spracklen, A. Steiner, N. Unger, M. Prather, D. Bergmann, P.J. Cameron-Smith, I. Cionni, W.J. Collins, S. Dalsøren, V. Eyring, G.A. Folberth, P. Ginoux, L.W. Horowitz, B. Josse, J.-F. Lamarque, I.A. MacKenzie, T. Nagashima, F.M. O'Connor, M. Righi, S.T. Rumbold, D.T. Shindell, R.B. Skeie, K. Sudo, S. Szopa, T. Takemurat, G. Zeng, 2012: Global air quality and climate, Chem Soc Rev, 41, 6663-6683.

Fisher, J.A., S.R. Wilson, G. Zeng, J.E. Williams, L.K. Emmons, R.L. Langenfelds, P.B. Krummel, and L.P. Steele, 2015: Seasonal changes in the tropospheric carbon monoxide profile over the remote Southern Hemisphere evaluated using multi-model simulations and aircraft observations, Atmospheric Chemistry & Physics, 15: 3217-3239.

Lamarque, J.-F., D.T. Shindell, B. Josse, P.J. Young, I. Cionni, V. Eyring, D. Bergmann, P. Cameron-Smith, W.J. Collins, R. Doherty, S. Dalsoren, G. Faluvegi, G. Folberth, S.J. Ghan, L.W. Horowitz, Y.H. Lee, I.A. MacKenzie, T. Nagashima, V. Naik, D. Plummer, M. Righi, S.T. Rumbold, M. Schulz, R.B. Skeie, D.S. Stevenson, S. Strode, K. Sudo, S. Szopa, A. Voulgarakis, G. Zeng, 2013: The Atmospheric Chemistry and Climate Model Intercomparison Project (ACCMIP): overview and description of models, simulations and climate diagnostics, Geoscientific Model Development, 6, 179-206.

Long, M. S., R. Yantosca, J.E. Nielsen, C.A. Keller, A. da Silva, M.P. Sulprizio, S. Pawson, D.J. Jacob, 2015: Development of a grid-independent GEOS-Chem chemical transport model (v9-02) as an atmospheric chemistry module for Earth system models, Geoscientific Model Development, 8, 595-602.

Monks, P.S., C. Granier, S. Fuzzi, A. Stohl, M.L. Williams, H. Akimoto, M. Amann, A. Baklanov, U. Baltensperger, I. Bey, N. Blake, R.S. Blake, K. Carslaw, O.R. Cooper, F. Dentener, D. Fowler, E. Fragkou, G.J. Frost, S. Generoso, P. Ginoux, V. Grewe, A. Guenther, H.C. Hansson, S. Henne, J. Hjorth, A. Hofzumahaus, H. Huntrieser, I.S.A. Isaksen, M.E. Jenkin, J. Kaiser, M. Kanakidou, Z. Klimont, M. Kulmala, P. Laj, M.G. Lawrence, J.D. Lee, C. Liousse, M. Maione, G. McFiggans, A. Metzger, A. Mieville, N. Moussiopoulos, J.J. Orlando, C.D. O'Dowd, P.I. Palmer, D.D. Parrish, A. Petzold, U. Platt, U. Pöschl, A.S.H. Prévôt, C.E. Reeves, S. Reimann, Y. Rudich, K. Sellegri, R. Steinbrecher, D. Simpson, H. ten Brink, J. Theloke, G.R. van der Werf, R. Vautard, V. Vestreng, Ch. Vlachokostas, R. von Glasow, 2009: Atmospheric composition change – global and regional air quality, Atmospheric Environment, 43 (33), 5268-5350.

Stevenson, D. S., P.J. Young, V. Naik, J.-F. Lamarque, D.T. Shindell, A. Voulgarakis, R.B. Skeie, S.B. Dalsoren, G. Myhre, T.K. Berntsen, G.A. Folberth, S.T. Rumbold, W.J. Collins, I.A. MacKenzie, R.M. Doherty, G. Zeng, T.P.C. van Noije, A. Strunk, D. Bergmann, P. Cameron-Smith, D.A. Plummer, S.A. Strode, L. Horowitz, Y.H. Lee, S. Szopa, K. Sudo, T. Nagashima, B. Josse, I. Cionni, M. Righi, V. Eyring, A. Conley, K.W. Bowman, O. Wild, A,

Archibald, 2013: Tropospheric ozone changes, radiative forcing and attribution to emissions in the Atmospheric Chemistry and Climate Model Intercomparison Project (ACCMIP), Atmospheric Chemistry & Physics, 13, 3063-3085.

Zeng, G., J.E. Williams, J.A. Fisher, L.K. Emmons, N.B. Jones, O. Morgenstern, J. Robinson, D. Smale, C. Paton-Walsh, and D.W.T. Griffith, 2015: Multi-model simulation of CO and HCHO in the Southern Hemisphere: Biogenic emissions and model uncertainties. Atmospheric Chemistry & Physics, 15, 7217-7245.

THE NEW MET OFFICE COUPLED ATMOSPHERE/LAND/OCEAN/SEA ICE DATA ASSIMILATION SYSTEM

Daniel J. Lea , Isabelle Mirouze, Matthew J. Martin, Robert R. King, Adrian Hines, David Walters and Michael Thurlow

Met Office, Exeter, United Kingdom

daniel.lea@metoffice.gov.uk

Introduction

The Met Office has developed a weakly-coupled data assimilation (DA) system (described in detail in Lea et al. 2015) using a global coupled model configuration. At present the analyses from separate ocean (Waters et al. 2014) and atmosphere DA (Rawlins et al. 2007) systems are combined to produce coupled forecasts. The aim of coupled DA is produce a more consistent analysis for coupled forecasts which may lead to less initialisation shock and improved forecast performance.

The coupled model combines the atmospheric model MetUM (Met Office Unified Model), global atmosphere 4.0 (Walters et al. 2014) at 60 km horizontal resolution on 85 vertical levels, the ocean model NEMO (Nucleus for European Modelling of the Ocean) at 25 km (at the equator) horizontal resolution on 75 vertical levels, and the sea-ice model CICE at the same resolution as NEMO. The atmosphere and the ocean/sea-ice fields are coupled every 1-hour using the OASIS coupler. The coupled model is corrected using two separate 6-hour window data assimilation systems: a 4D-Var for the atmosphere with associated soil moisture content nudging and snow analysis schemes on the one hand, and a 3D-Var FGAT for the ocean and sea-ice on the other hand. The background information in the DA systems comes from a previous 6-hour forecast of the coupled model. Figure 1 shows how all the components fit together in the coupled DA system.

Experiments

To isolate the impact of the coupled DA, 13-month experiments have been carried out, including 1) a full atmosphere/land/ocean/sea-ice coupled DA run, 2) an atmosphere-only run forced by OSTIA SSTs and sea-ice with atmosphere and land DA, and 3) an ocean-only run forced by atmospheric fields from run 2 with ocean and sea-ice DA. In addition, 5-day and 10-day forecast runs, have been produced from initial conditions generated by either run 1 or a combination of runs 2 and 3. The different results have been compared to each other and, whenever possible, to other references such as the Met Office atmosphere and ocean operational analyses or the OSTIA SST data.
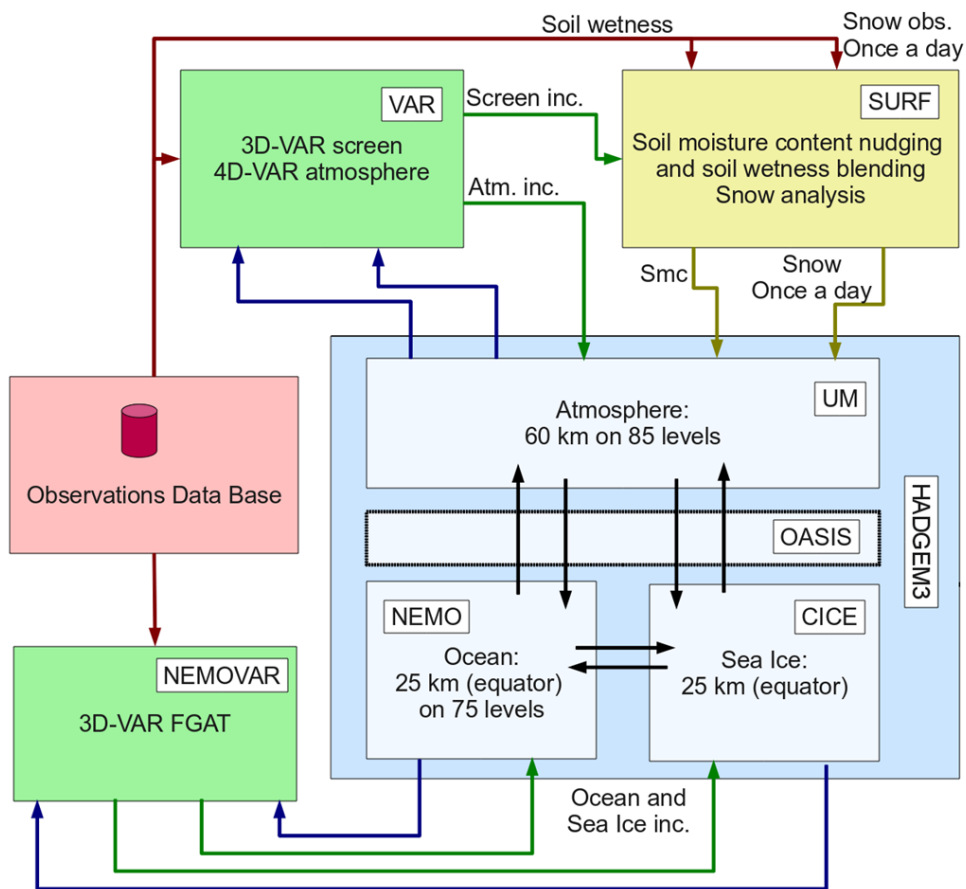
Figure 1: Schematic of the coupled DA system.

Results

The performance of the coupled DA is similar to the existing separate ocean and atmosphere DA systems. The same error covariances are used in the coupled and uncoupled DA runs so tuning these and other aspects may improve the coupled DA results further. In addition, the coupled model also exhibits some biases which do not affect the uncoupled models. An example is precipitation and run off errors affecting the ocean salinity. This of course impacts the performance of the ocean data assimilation. This does, however, highlight a particular benefit of data assimilation in that it can help to identify short term model biases by using the differences between the observations and model background (innovations) and the mean increments. Coupled DA has the distinct advantage that this gives direct information about the coupled model short term biases. By identifying the biases and developing solutions this will improve the short range coupled forecasts, but may also improve the coupled model on climate timescales.

References

Lea, D. J., I. Mirouze, M. J. Martin, R. R. King, A. Hines, D. Walters and M. Thurlow, 2015: Assessing a new coupled data assimilation system based on the Met Office coupled atmosphere, land, ocean, sea ice, *Monthly Weather Review (in press),* doi: http://dx.doi.org/10.1175/MWR-D-15-0174.1

Rawlins, F., S. P. Ballard, K. J. Bovis, A. M. Clayton, D. Li, G. W. Inverarity, A. C. Lorenc, and P. T. J, 2007: The Met Office global four-dimensional variational data assimilation scheme. *Q. J. R. Meteorol. Soc.,* 133, 347–362.

Walters, D. N., and Coauthors, 2014: The Met Office Unified Model Global Atmosphere 4.0 and JULES global land 4.0 configurations. *Geoscientific Model Development,* 7 (1), 361–386, doi:516 10.5194/gmd-7-361-2014, http://www.geosci-model-dev.net/7/361/2014/.

Waters, J., M. J. Martin, D. J. Lea, I. Mirouze, A. T. Weaver, and J. While, 2014: Implementing a variational data assimilation system in an operational 1/4 degree global ocean model. *Q. J. R. Meteorol. Soc.*, doi:10.1002/qj.2388.

PERFORMANCE OF CONVECTIVE SCALE DA DURING THE SYDNEY FORECAST DEMONSTRATION PROJECT

Peter Steinle, Yi Xiao, Susan Rennie, Xingbao Wang, Alan Seed, Aurora Bell[1], Mark Curtis

Environment and Research Division, Bureau of Meteorology, Melbourne
[1]Hazards, Warnings and Forecasts Division, Bureau of Meteorology, Melbourne

p.steinle@bom.gov.au

Introduction

A high resolution Numerical Weather Prediction (NWP) system was trialled during the Sydney Forecast Demonstration Project (FDP) of 2014. This system is based on the 1.5km United Kingdom Variable-grid (UKV) system of the Met Office. Convective scale models such as this are widely considered by operational centres as an effective way of providing high quality, short range, automated forecast guidance.

The system provided a proto-type for future operational NWP systems within the Bureau. The FDP was a critical part of informing both how such systems could be integrated within the Bureau's forecast process and the strengths and weaknesses of the underlying numerical systems.

The two main mechanisms by which the FDP assessed the quality of the NWP systems were via the detailed, subjective assessment of forecasters and extensive, objective verification. The approaches are equally important. The value of statistical, objective verification to NWP is well established; however such scores measure a limited number of aspects of forecast performance. As a result, objective assessments play a dual role, as they measure the impact of the guidance on the forecasters' decision making as well as highlighting any limitations of the objective assessment.

This presentation provides an overview of the operation of the high resolution, rapid update NWP system, followed by objective assessments. Reviewing the assessments leads to recommendations on the future developments required to provide an NWP system that is capable of meeting the Bureau's service requirements.

Numerical Prediction System

The Bureau's operational NWP systems use the standard practice of assimilating observations to update initial conditions every six hours. This choice makes sense for forecasting synoptic scales, however there are many important small scale features that have a predictability limit of less than this period. Increased computing power enables NWP systems with sufficient spatial resolution to model these small scale features over a useful domain, using a more appropriate analysis-forecast cycle.

The NWP components (forecast model, observation processing and variational analysis) of the UKV are consistent with the Bureau's next operational system, ACCESS Parallel Suite 2 (APS2). The Bureau's operational systems, APS1 use older versions of the software. Never the less, the main differences between APS1-City and the FDP NWP system was the resolution, the use of explicit convection and the Rapid Update Cycle (RUC) data assimilation. The differences

in the software versions were more associated with technical capability than major scientific differences. The lateral boundary conditions for the RUC were provided by a pre-operational version of the APS2 global system. This can hamper the RUC, as APS1-R runs with short cut off and so the boundary conditions provided to APS1-SY can be, in effect more recent.

The assimilation system was the 3-dimensional version of the ACCESS variational analysis system. A 4D-Var version, similar to that used in APS1-R was assessed but there was not time to resolve occasional instabilities in time for downstream applications to be finalized before for the FDP.

The assimilation was triggered 55 minutes after the nominal analysis time (i.e. the 1200UTC analysis was initiated at 1255UTC) using observations from T-30minutes to T+30 minutes. The observations used by the RUC included:

- One minute data from automatic weather stations (surface pressure, screen temperature and dew point and 10m winds)
- Aircraft reports (AMDAR)
- Radiosondes & Pilot balloon flights if they arrived in time
- Doppler winds (Rennie et al. 2015)
- Local atmospheric motion vectors from MTSAT
- AMSU-B/MHS channels 3, 4 and 5 from polar orbiting satellites

The RUC also used Latent Heat Nudging based on Rainfields. The strength of the nudging coefficients had to be reduced to prevent excessive latent heating/vertical motion during strongly convective events. The relaxation coefficient was reduced from 0.5 to 0.2, and the latent heat release was capped at 30° per day.
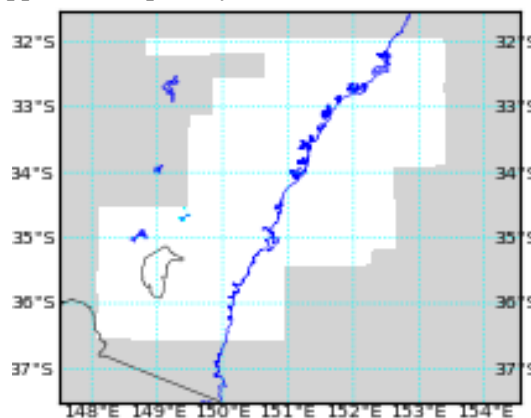
Figure 5 The rainfall verification domain, determined by the coverage of RAINFIELDS data (white areas) from Canberra, Wollongong, Sydney(2) and Newcastle radars. The southern end of Namoi radar is also used.

Objective Verification

The two main forms of verification conducted were verification of rainfall forecasts against radar plus gauge hourly rainfall estimates from Rainfields and observations of 2m temperature, 2m dew point, 10m wind and surface pressure. The surface weather station observations used in the verification were not quality controlled, but all forecasts were corrected for differences between model and station surface elevation. The surface observing network is routinely monitored by the Bureau forecasters and Observation and Infrastructure Division, so systematic

errors and reliability issues are thought to be small. The correction of differences in station and model elevation is important, as expensive high-resolution models should provide more information than a simple downscaling of lower resolution models. The correction for difference in surface elevations is consistent with the corrections applied by the assimilation scheme.

Rainfall

The verification of rainfall amounts used the Fractions Skill Score (FSS). There are limitations in using this over the small areas covered by the radars of eastern NSW, due to boundary effects, none the less it provides a reliable method of comparing different forecasts, and is widely used to verify rainfall forecasts. The domain used for verification is shown in Fig. 1.
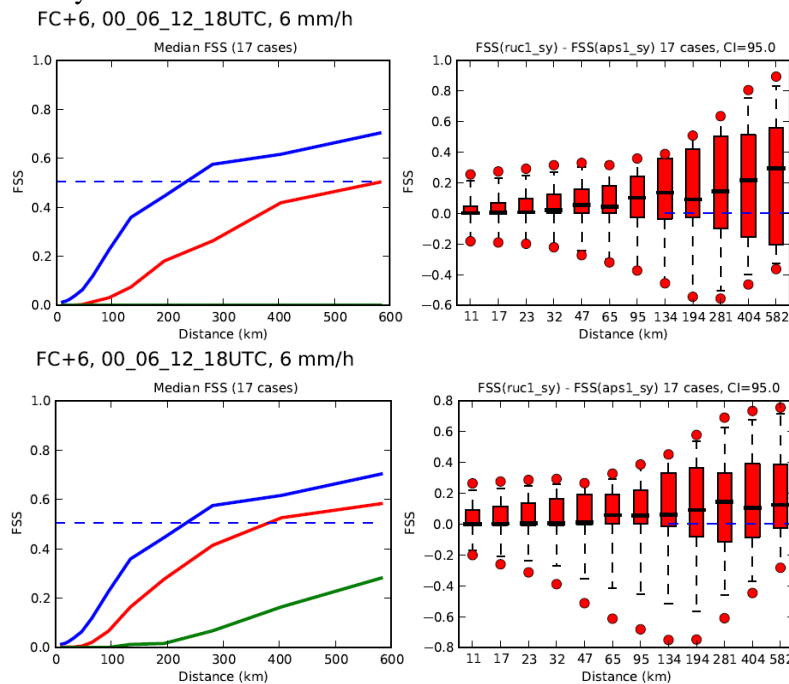

Figure 6 FSS for a six hour forecasts threshold of 6mm hr^{-1} for a six hour difference between the RUC base-time and other models, the bottom row is the same base-time. Left hand column are median values for each distance. Right hand column shows the distribution of differences in FSS between the RUC and APS1-SY, boxes show the inter-quartile range and whiskers give 95% confidence intervals. RUC is in blue, APS-SY is red and APS1-R is in green. Verifying rainfall analyses were at 00, 06, 12 and 18UTC. The theoretical level of skill is given by the blue dashed line. The median is marked by the thick black line in the each box.

Scores are calculated using RUC basetimes that differ from the APS1-R and APS-SY basetimes by both six and zero hours – reflecting the range of differences in forecast lengths. Examples are shown for a threshold of 6 mm hr^{-1} in Fig. 2 (left side). Higher rainfall rain rates suffer from small sample sizes. Lower thresholds show a similar story as the 6mm hr^{-1} threshold. The distribution of the differences between the RUC FSS and APS1-SY FSS for a subset of the length scales is also shown (Fig. 2 right side). The RUC clearly outperforms the APS1 systems. These results are consistent with longer period verifications conducted in pre-FDP trials. The relative performance for 12 hour forecasts is similar to the 6 hour performance.

The effect of the boundary conditions however can be seen when assessing forecasts from 0300, 0900, 1500 and 2100UTC as these are the runs that use the oldest boundary conditions. The comparisons between the RUC and APS1-SY are closer with no clear indication of one system

being better than the other. This indicates that the RUC could be improved by using boundary conditions from the regional system at least for some basetimes.

Near surface variables

The value of the rapid update analysis can be seen by the root mean square (RMS) difference between observations and forecasts generally decreasing as the length of the forecast decreases for all variables. The exception being associated with the well-known evening dew point problems of all ACCESS systems.

Table 2 Improvement of 6 hour RUC forecasts vs APS1-SY and APS1-R for near surface elements around 0600UTC (afternoon).

Element	RUC RMS	% impr. (SY) 0hr offset	% impr. (R) 0hr offset	% impr. (SY) 6hr offset	% impr. (R) 6hr offset
T_2m	2.0	0	11	8	17
Td_2m	3.0	0	2	6	9
10m windspeed	2.4	6	-1	7	3

Table 3 As for Table 1, but for 12 hour forecasts

Element	RUC RMS	% impr. (SY) 0hr offset	% impr. (R) 0hr offset	% impr. (SY) 6hr offset	% impr. (R) 6hr offset
T_2m	2.0	7	15	5	9
Td_2m	3.0	5	7	7	8
10m windspeed	2.4	7	3	9	2

Tables 1 and 2 show the percentage improvement relative to APS1-SY, of the RUC forecasts. At a given point in time the percentage of improvement of the RUC will lie somewhere in between the two offsets. The improvement in wind forecasts can be attributed to both the increased resolution and the time it takes for local topographic circulations to spin up in APS1-SY.

The performance of APS1-R winds at first seems anomalously good. A contributing factor to this is APS1-R having relatively smooth wind fields, and so the RUC scores suffer from double penalties although it was considered to be providing better guidance. The improvement in the forecasts was mainly for coastal stations, indicating that improved wind (sea breeze) forecasts are influencing temperature forecasts as well. Inland stations are almost randomly distributed between RUC or APS1-SY providing better forecasts. This is ascribed to the lack of small scale forcing on observations inland. These areas are also heavily influenced by soil moisture, which is currently based on the global system. This can produce large inconsistencies with higher resolution models.

Subjective verification

Overall the RUC forecasts were well received by the forecasters. There were however a few issues that were repeatedly raised. Firstly there seemed to be a lack of variation between runs, despite new observations being used that indicated that changes were required. The use of 4D-Var rather than 3D-Var would be expected to improve this. Another factor is that the background error covariances were very broad and isotropic. A new method for estimating the horizontal scale of these covariances is expected to greater variability between runs. .

Despite these problems, there were clearly a number of successes for the RUC, and these are documented on the FDP Wiki. While individual examples do not necessarily correspond to sustained performance, they do serve to both indicate what the system is capable of, and

highlight where the objective verification may need to be enhanced. Some of the most obvious areas are validating the initiation of convection and the secondary development of convection

Conclusion and Further Work

Overall the RUC outperformed existing operational NWP systems for short-range forecasts of rainfall, temperature, dew point and wind.

There are number of deficiencies that should be addressed before the Bureau could see the full benefits of such a system. The most promising options, as mentioned above and based on the Met Office experience with a similar system include:

- Use 4D-Var rather than 3D-Var
- The use of ensembles
- Assimilation of more observations such as :
    - cloud information from Himawari-8 in the RUC and the nesting models
    - high resolution atmospheric motion vectors from Himawari-8
- Enhanced spreading of information by the analysis via
    - The use of ensemble information within the data assimilation process (i.e. Hybrid 4D-Var), and
    - Revised static background error covariances that are more localized
- A soil moisture analysis system that is consistent with the model soil types.
- Calibration of cloud processes within the forecast model

ESTIMATION OF ACOUSTIC PROPERTIES OF THE EAST AUSTRALIAN WATERS

Paul S. Hartlipp

The Australian Defence Force Academy, University of New South Wales, Canberra.

p.hartlipp@adfa.edu.au

Abstract

A high resolution ROMS model was used to estimate the acoustic properties of the East Australian Waters. Currently we derive a climactic run from the WOA oceanic temperature and salinity historical profiles on a 4 kilometre grid with 50 sigma layers. In addition we force the model with TPX08 tidal forcing to reproduce both surface and internal tides throughout the water column. The velocity results were compared with available mooring observations to check both tidal ellipse major axis parameters and frequency distribution to insure the model replicates observed internal tidal behaviour, both in frequency and magnitude. We do this throughout the water column for all available, existing observations.

Using these temperature fields, we coupled our model run results with Bellhop, a 2-D acoustic ray tracing program. We ran cases at 25 different latitudes, taking temperatures from 100 different hours and for 6 different source depths for a total of 15,000 cases. We look for sound channels within the water column and the effects of the EAC, latitude, topography, and eddies in ray propagation and transmission loss. In short our work creates a high resolution Australian east coast hydrography and investigates how that hydrography effects local acoustic propagation with a future eye to operations.

TRENDS IN SUPERCOMPUTING & ANALYTICS AND IMPLICATIONS FOR EARTH SYSTEM MODELLING

Phil Brown

Segment Leader, Earth Sciences, Cray, United Kingdom

philipb@cray.com

Abstract

This talk will discuss some of the technology trends which are impacting the scientific computing community, looking at the evolution in achieved performance across a range of CPU generations, the future technology directions and the implications for application developers looking to target current and future systems. I will also touch on some emerging data analysis techniques and how they may drive a convergence of compute and analysis stages within a modelling workflow.

NCI ENABLING EARTH SYSTEMS SCIENCE USING HIGH PERFORMANCE COMPUTING & DATA

Ben Evans

NCI - The Australian National University.

Ben.Evans@anu.edu.au

Abstract

The Earth Systems Science community requires access to highly optimised modern models, access to well-managed national and international datasets, and well-integrated functional and performant computational environments. Over the last 18 months, NCI has taken significant steps forward in each of these areas. NCI has led an activity to update, analyse and improve the performance of the ACCESS models that are used from Australian weather to climate systems, spanning the various priority components of the earth system: atmosphere, ocean, data assimilation, sea ice, and the coupled systems used by seasonal forecasting and climate prediction. Through its National leadership role in Earth Systems Data under the NCRIS Research Data Services program, NCI has assembled over 10 PBytes of priority research data collections spanning a wide range of disciplines, in particular from geosciences, geophysics, environment, climate, weather, and water resources. To facilitate access, maximise reuse and enable integration across the disciplines, data have been built into a platform that NCI has called, the National Environmental Research Data Interoperability Platform (NERDIP). The platform is co-located with the significant HPC and cloud systems at NCI. As well as organising the data, NCI has been improving the data to be more readily available as High Performance Data (HPD) sets that are structured to facilitate uptake in HPC environments. This capability offers new unparalleled opportunities to undertake innovative Data-intensive Science at scales and resolutions never before attempted, as well as enabling participation in new collaborations in interdisciplinary science.

OPTIMISATION OF UNIFIED MODEL RADIATION CALCULATIONS FOR XEON PHI

Luke Mason[1], Rupert Ford[2], Chris Maynard[3]

[1]*Intel Parallel Computing Centre, Hartree Centre, STFC.*
[2]*Application Performance Engineering Group, STFC.*
[3]*The Met Office, Exeter U.K.*

Abstract

The Intel Parallel computing centre at the Hartree Centre has been porting the Unified Model for native execution on the Xeon Phi coprocessor. Our work focuses on the radiation routines and is made challenging by a large number of low trip count loops with a flat profile. The Unified Model is written in Fortran and the radiation calculation is threaded with OpenMP, the threading is performed over segments or tiles of calculation points. There are two main aspects of our optimisation strategy, removal of peel and remainder loops and tuning for cache performance. The removal of remainder loops is performed by limiting tile sizes to multiples of the vector width and so exploits the existing segment data structures. No data alignment is present and so peel loops are common, they are significantly harder to treat than the remainder loops with loops requiring analysis to determine if aligned accesses are possible. Tiling is further exploited to tune the calculation for cache performance and large benefits have been seen from tuning the tile size (Figure 1). The implementations of these optimisations will be described along with an analysis of the benefits of each.
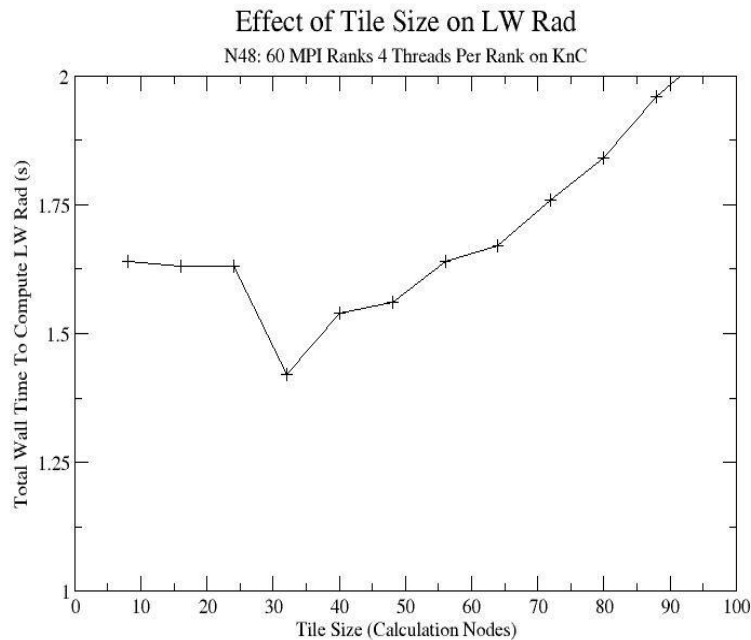
Figure 1 - Effects of tuning tile size

FROM CSIRAC TO CRAY (AGAIN) AND ONWARDS

Rob Bell

CSIRO, Melbourne

robert.bell@csiro.au

Abstract

This talk will review a little of the history of computing support for ocean and atmospheric sciences in Australia, will give details of the Bureau's new Cray systems, and will surmise on future paths.

STATUS/PLANS FOR NWP UPGRADES OVER THE NEXT 5 YEARS AT THE MET OFFICE

Dale M. Barker

Weather Science, Met Office, Exeter, UK

dale.barker@metoffice.gov.uk

Abstract

Met Office's core NWP capabilities are based on global and high-resolution UK model implementations of the Unified Model (Davies et al. 2005). Fig. 1 illustrates the basic configuration details as of mid-2015.
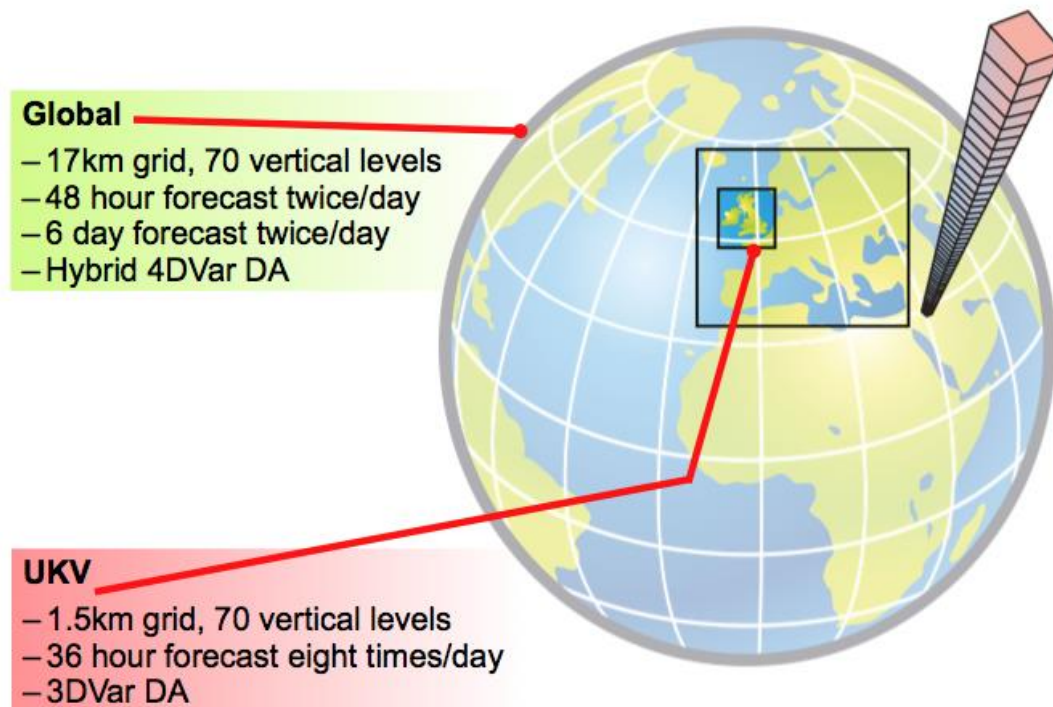
Figure 1: Global and UK deterministic model configuration details as of mid-2015. Note the Met Office Global Regional Ensemble Prediction System (MOGREPS) also runs operationally with 12 members (plus time lagged products) in both global (MOGREPS-G, 33km) and UK (MOGREPS-UK, 2.2km) domains.

The procurement of a new Cray XC40 HPC at a cost of £97 million provides the opportunity for a step-change in Met Office science capabilities and resulting weather and climate services. The hardware will arrive in three tranches during 2015 (phase 1a: x1 current capability), 2016 (1b: x5) and 2017 (1c: x15). Initial porting of all operational systems to the Cray phase 1a was completed successfully in August 2015, allowing the retirement of the previous IBM P7 HPC.

An initial (HPC-neutral) science upgrade (PS37) is currently planned for Spring 2016 on the 1a system, including a range of satellite and data assimilation changes (variational bias correction, SSMI/S, CrIS correlated observation errors, new covariance model. etc). Fig 2. illustrates the

very significant improvement in global NWP skill (against analyses, similar but smaller trend against observations) that the PS37 package has indicated in preliminary (79 day) trials. Note in particular the ~10% reduction in T+24 500hPa height error in the Northern Hemisphere due predominantly to the implementation of a variational bias correction technique for satellite radiances, replacing the Harris and Kelly (2001) scheme used at the Met Office for many years.
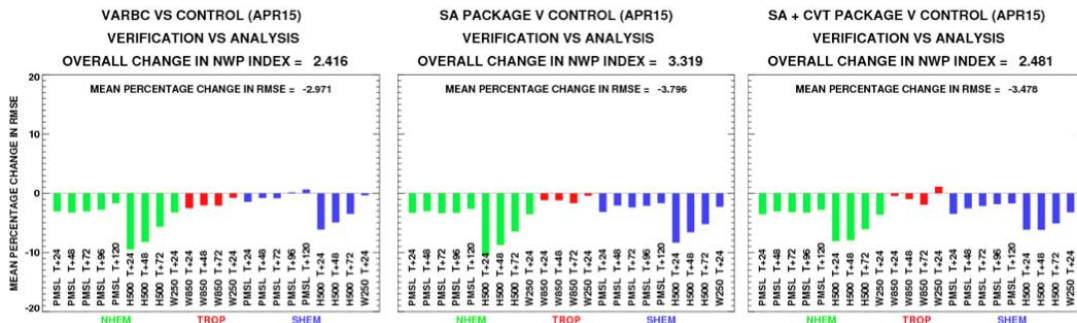

Figure 2: Percentage change in root mean square error for the range of standard variables (PMSL, 500hPa height, 250/850hPa winds) and forecast ranges that make up the Met Office global NWP index: Variational bias correction (VARBC) vs control (left), VARBC+additional satellite data (SA) vs control (centre) and VARBC+SA+CVT (right). Trial period 10th April – 26th June 2015.

The subsequent upgrade to Cray 1b/c systems will boost HPC capacity, opening the door to more computationally intensive upgrades. The following major operational upgrades are proposed during the life of the HPC (qualitatively new, non-incremental capabilities in **bold):**

- Short-range global model/ensemble at 10/20km resolution, including enhanced vertical resolution, improved physics**, coupled ocean- atmosphere and advanced data assimilation e.g. global RUC** (x10 HPC of 2015 system).
- UK model/ensemble with expanded domain, enhanced vertical resolution, ensemble size, and potentially increased (1.5km) resolution (x15).
- **Hourly 4DVar-based UK NWP-Nowcasting system** (x7 cost current UKV).
- Increased atmospheric horizontal/vertical resolution seasonal forecast system (GloSea – x5).
- Significant resolution upgrades to a variety of AQ, dispersion, ocean, wave, and surge models – providing competitive world-class capabilities in these generally computationally-light applications (x10-50).
- **Sub-km (100-300m) configurations e.g. London model implemented in 'fast model setup' for selected real-time test periods.**

The sequence and timescale for implementing the above major upgrades is currently under review, as further details of costs (Cray optimization work ongoing), benefits (further trials, some of which only possible once upgraded HPC in house) and customer requirements emerge. The talk at the CAWCR workshop will provide an up-to-date assessment of the latest implementation plans together with selected results.

SHORT TO MEDIUM-RANGE PREDICTION: SUCCESS AND CHALLENGES

Gary B. Brassington

Environment and Research Division, Bureau of Meteorology, Melbourne

g.brassington@bom.gov.au

Abstract

The Bureau of Meteorology support global operational forecasts for the atmosphere, land-surface, hydrology, ocean and wave conditions. With the exception of sea-ice, they form the basis for a high resolution coupled earth system. We will review the status and performance of each of these prediction systems and review research results on the impact of coupled modelling and prediction in the Australian region. Finally we will highlight the leading gaps and outline the prospects and opportunities for contributing to this international challenge.

SEASONAL PREDICTION: TOWARDS ACCESS-S

Oscar Alves and Debra Hudson

Environment and Research Division, Bureau of Meteorology, Melbourne

o.alves@bom.gov.au

Abstract

In recent years the Bureau of Meteorology seasonal climate outlooks have become more skilful, more useful and more popular. However, the present seasonal prediction system, POAMA-2, is low-resolution (250 km) and somewhat dated relative to systems operated by the leading meteorological centres abroad. In 2015 the decision was taken to replace POAMA-2 with a new seasonal forecasting system referred to as ACCESS-S (the seasonal prediction version of ACCESS – the Australian Community Climate and Earth-System Simulator). This will bring seasonal prediction into the national ACCESS modelling framework, which utilises the latest local and overseas developments. ACCESS-S will operate at a N216L85 atmospheric resolution and a 0.25 degree ocean resolution. Running this high resolution system is facilitated by the advent of the Bureau's new supercomputer in 2016.

One of the key partners in ACCESS is the UK Met Office (UKMO), with whom we have strong collaboration in weather forecasting. The development of ACCESS-S will strengthen our collaboration with the UKMO by extending our partnership to include seasonal prediction and allow us to leverage the latest developments from overseas more rapidly. ACCESS-S will use the latest coupled model available from the UKMO.

The coupled model in ACCESS-S will be the same coupled model that is used for seasonal prediction at the UKMO. However, rather than simply importing the UKMO seasonal prediction system, the aim is to jointly develop the system with the UKMO under the ACCESS framework. In order to satisfy key stakeholders and meet Bureau service needs, both a larger hindcast set and ensemble size (for hindcasts and real-time forecasts) than used at the UKMO will be needed, and the forecasts will need to be extended out to at least 9 months (UKMO forecasts only go out to 6 months). The locally developed data assimilation and ensemble generation scheme will also be implemented into the system. Data assimilation can be at least as complex as the model itself.

One of the most obvious improvements with ACCESS-S will be forecasts with more regional detail. In ACCESS-S the resolution will be 60 km in the Australian region (compared to 250 km in the current system). At this resolution the model will be able to, for example, differentiate between the climates of western and eastern Tasmania and will better represent the Great Dividing Range, which plays a key role in the spatial distribution of rainfall. Increased resolution will also improve the representation of important large-scale climate drivers, like the El Niño Southern Oscillation, potentially leading to better multi-week and seasonal forecast accuracy over Australia.

Going forwards, the Bureau will play a significant role in contributing to the development of the UKMO coupled model, specifically focussing on atmospheric and oceanic processes that are critical to the Australian region.

GLOBAL COUPLED MODEL DEVELOPMENT ACROSS TIMESCALES

David Walters, Ed Blockley, John Edwards, Helene Hewitt, Tim Johns, Sean Milton
and Keith Williams

Met Office, Exeter, United Kingdom

david.walters@metoffice.gov.uk

Global Atmosphere development across timescales

The Met Office's journey towards seamlessly modelling the atmospheric component of the global and regional weather and climate system is described in detail by Brown et al. (2012). Our original motivation for the development and use of the Met Office Unified Model (UM) was to reduce the technical overhead of maintaining a separate code base, dynamical core and collection of parametrizations for global atmospheric climate modelling, global numerical weather prediction (NWP) and regional NWP. Over the following 25 years, the focus gradually shifted towards developing seamless atmospheric model configurations to take advantage of the recognised synergies between climate and NWP modelling (Martin et al., 2010, Senior et al., 2010).

In recognition of this, in 2010 the Met Office reorganised its Global Model Evaluation and Development teams for weather and climate modelling into a single strategic area (GMED) within the newly created deputy directorate of Foundation Science. The team was tasked with leading the development and evaluation of a science configuration of the UM (and a corresponding configuration of the JULES land surface model) that could be used for global model applications across all timescales. The first such configurations were labelled Global Atmosphere 3.0 (GA3.0) and Global Land 3.0 (GA3.0), which are described in detail in Walters et al. (2011).

In practice, the operational implementation of GA3 and GL3 did not remove a small number of long-standing differences between global NWP and global climate configurations of the UM, and the resulting configuration was labelled as the GA3.1/GL3.1 "branch" configuration as opposed to the GA3.0/GL3.0 "trunk". Exposing, documenting and examining these differences, however, helped to understand weaknesses in our parametrization schemes and improve these to perform better across all timescales[2]. As a result, the number of these branches is reducing with

---

[1] An example of this is the convection scheme's "CAPE timescale" which is a fixed timescale over which we allow the convection scheme to remove instability from the column. There have been many attempts to improve either the UM's predictability, variability or mean climate by adjusting this parameter; for this reason, it is one of the parameters that was different between GA3.0 and GA3.1 and is still different between the latest GA6.0 and GA6.1. To attain optimal performance on all of these measures, and hence remove this difference between configurations, has proved impossible with the existing parametrization. Instead, this single number will be replaced in GA7.0 by a spatially-and temporally-varying CAPE timescale that is a function of the large-scale vertical velocity in the grid box. It is expected that as well as allowing the removal of a GA "branch" setting, this will improve the realism of the model in each individual system in a way that may not have happened were each system developed in isolation.

time and we hope that in GA7.0 the only difference between the GA/GL trunk and the operational NWP configuration will be the number of JULES land-surface tiles.

Global coupled model development for seasonal-to-climate timescales and early work on Global Coupled NWP

The global model development process is currently governed by the INTEGRATE project, which started in 2011 and runs through to the end of 2015. In addition to developing and assessing the GA/GL configurations, GMED and the INTEGRATE project are responsible for the delivery of coupled model configurations for use on monthly-to-seasonal, decadal and climate prediction timescales, although the responsibility for developing the component ocean and sea ice configurations lies elsewhere.

The ocean component uses a configuration of the NEMO ocean model developed and governed by the Joint Ocean Modelling Programme (JOMP), which is a joint venture between the Met Office, the National Oceanography Centre and the British Antarctic Survey. During the early stages of the INTEGRATE project, the coupled model was run with slightly different ocean configurations at different ocean model resolutions, whilst the configurations used for operational ocean forecasting and those developed by the JOMP were also subtly different. Over the past 4 years, however, the JOMP have adopted a Global Ocean (GO) development process analogous to that used for the atmosphere, which delivers a single configuration for use in forced ocean and coupled simulations across all timescales.

In a similar manner, the sea ice component currently uses a configuration of the CICE sea ice model developed and governed by the Joint Sea Ice Modelling Programme (JSIMP) with contributions from the Met Office, the Centre for Polar Observation and Modelling, the National Oceanography Centre and the British Antarctic Survey. As with the JOMP, the JSIMP have adopted a Global Sea Ice (GSI) development process to deliver a configuration for use across all timescales.

An important point in the development and assessment of a coupled model is that the coupled configuration is not just a collection of component model configurations, but includes the scientific and technical choices made in coupling these components together. To recognise this and to allow us to document the resulting configurations, we denote the coupled configurations developed under the INTEGRATE project as Global Coupled (GC) configurations. The most recently developed configuration is GC2.0 (Williams et al., 2015), which is illustrated schematically in Figure 1. This is the first set of global model configurations that has been developed for and implemented across all of the Met Office's operational/production global modelling systems. GA6.1/GL6.1 went operational in deterministic global NWP and the MOGREPS short- and medium-range ensemble prediction systems in July 2014. GO5.0/GSI6.0 went operational in the FOAM ocean forecasting system in February 2015, whilst GC2.0 was implemented in the GloSea monthly-to-seasonal and DePreSys decadal prediction systems in February 2015 and December 2014 respectively. Finally, a GC2.0 configuration of the HadGEM3 climate model was used for a series of coupled climate change simulations in 2014/15.

An important deliverable from the INTEGRATE project has been an investigation into the impact of coupled modelling on the global NWP and ocean forecasting systems. Elsewhere in this workshop, Tim Johns will present results from coupled NWP case studies using recent model configurations (including GC2.0) showing examples of promising performance,

particularly in the tropics. Dan Lea has also provided an update on the development and assessment of a weakly coupled data assimilation system, which again looks competitive with the atmosphere- and ocean-only assimilation schemes. Because of this, the Met Office plans to replace its atmosphere-only global NWP and forced ocean forecasting systems with a global coupled NWP model over the next 2-4 years. The challenge for the follow-up to the INTEGRATE project, therefore, is to allow the pace of development of the component configurations to continue whilst developing and delivering a coupled model configuration for use across all timescales.
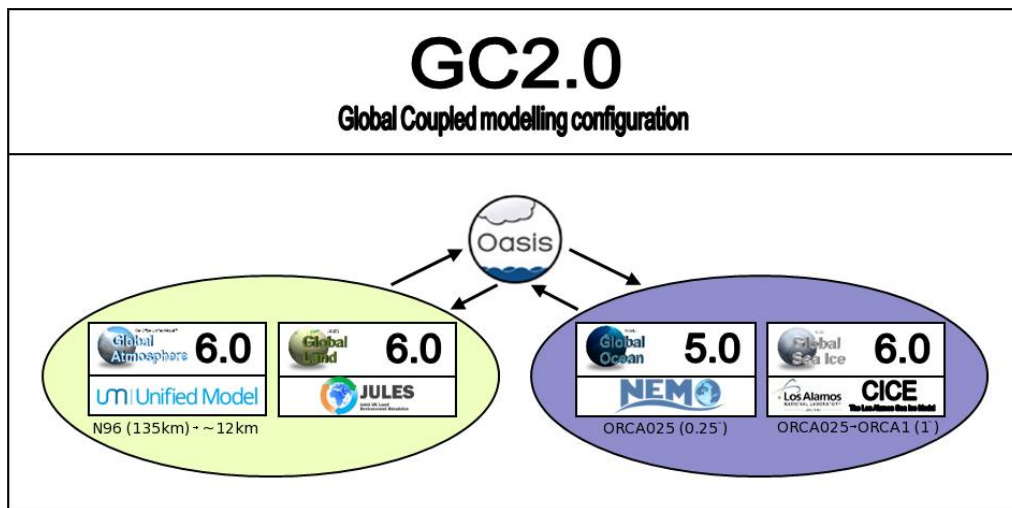

Figure 1: A schematic describing the latest global coupled model configuration built around the UM: Global Coupled 2.0 (GC2.0). The atmosphere and land components use the GA6 and GL6 configurations of the UM and JULES respectively, whilst the ocean and sea ice components use the GO5 and GSI6 configurations of NEMO and CICE. In addition to the component model configurations, the definition of GC2.0 includes the scientific and technical details of the coupling (via OASIS3).

Global Coupled development across timescales

Our proposed approach to developing a coupled model configuration for use across all timescales, which in turn is comprised of the best possible component model configurations, is to follow the INTEGRATE project with a collaborative coupled modelling programme. This will govern the development and evaluation of the Global Coupled configuration and have a strategic overview and input into the development of the individual component models.

The development of the component model configurations will continue as business as usual activities, each with their own governance and responsibilities. The development of the Global Atmosphere configurations may be overseen directly by the UM consortium whilst the Global Land configurations could be developed with more input from and interaction with the JULES Science and Applications Committee. This will allow us to continue to work with and deliver to our UM and JULES partners, whilst involving them further in the development and decision making process. Similarly, the JOMP and JSIMP will continue to develop the GO and GSI configurations to collaborate with and deliver to all of the contributing partners and their requirements. The role of the coupled modelling programme in this framework would therefore be the planning and prioritisation of the release schedule and the assessment of the coupled model and maintaining and delivering the GC configuration for implementation and further development.

The details of this process and its governance have yet to be decided. For example, it is unclear whether an annual cycle (such as the "template" annual cycle used by the GA development process) will be possible for coupled NWP, where much longer trials are required to test the impact of ocean model changes. An important point, however, is that whatever process is adopted, this will be a gradual evolution of the GC development process rather than a radical change from the current approach.

References

Brown, A., S. Milton, M. Cullen, B. Golding, J. Mitchell and A. Shelly, 2012: "Unified modeling and prediction of weather and climate: a 25-year journey", *Bull. Amer. Meteor. Soc.*, **93**, 1865–1877. doi: http://dx.doi.org/10.1175/BAMS-D-12-00018.1

Martin, G.M., S.F. Milton, C.A. Senior, M.E. Brooks, S. Ineson, T. Reichler and J. Kim, 2010, *"Analysis and reduction of systematic errors through a seamless approach to modeling weather and climate"*, J. Climate, **23**, 5933–5957.
doi: http://dx.doi.org/10.1175/2010JCLI3541.1

Senior, C. A., A. Arribas, A.R. Brown, M.J.P. Cullen, T.C. Johns, G.M. Martin, S.F. Milton, D.M. Smith, S. Webster, S. and K.D. Williams, 2010: "Synergies between numerical weather prediction and general circulation climate models", in: "The development of atmospheric general circulation models", editors: Donner, L., Schubert, W. and Somerville, R., Cambridge University Press, Cambridge, UK.

Walters, D.N., M.J. Best, A.C. Bushell, D. Copsey, J.M. Edwards, P.D. Falloon, C.M. Harris, A.P. Lock, J.C. Manners, C.J. Morcrette, M.J. Roberts, R.A. Stratton, S. Webster, J.M. Wilkinson, M.R. Willett, I.A. Boutle, P.D. Earnshaw, P.G. Hill, C. MacLachlan, G.M. Martin, W. Moufouma-Okia, M.D. Palmer, J.C. Petch, G.G. Rooney, A.A. Scaife, and K.D. Williams, 2011, *"The Met Office Unified Model Global Atmosphere 3.0/3.1 and JULES Global Land 3.0/3.1 configurations, Geosci. Model Dev.*, **4**, 919-941.
doi: http://dx.doi.org/10.5194/gmd-4-919-2011

Williams, K.D., C. M. Harris, A. Bodas-Salcedo, J. Camp, R. E. Comer, D. Copsey, D. Fereday, T. Graham, R. Hill, T. Hinton, P. Hyder, S. Ineson, G. Masato, S. F. Milton, M. J. Roberts, D. P. Rowell, C. Sanchez, A. Shelly, B. Sinha, D. N. Walters, A. West, T. Woollings, and P. K. Xavier, 2015, "*The Met Office Global Coupled model 2.0 (GC2) configuration*", *Geosci. Model Dev.*, **8**, 1509—1524.
doi: http://dx.doi.org/10.5194/gmdd-8-521-2015

SYSTEM MODEL (BCC-CSM) DEVELOPMENT AND ITS OPERATIONAL APPLICATIONS FOR SUB-SEASONAL TO SEASONAL PREDICTION

Tongwen Wu

Beijing Climate Center, China Meteorological Administration, Beijing, China

twwu@cma.gov.cn

Abstract

The National Climate Center (NCC), China Meteorological Administration was established in 1995. Since that time, NCC begun to develop climate models for short-term climate predictions and scientific research on climate change. The first-generation atmospheric general circulation model (BCC−AGCM1.0) and an ocean-atmosphere coupled model (BCC−CM1.0) is developed and used for operational seasonal forecast in NCC in 2005. In 2010, the fully-coupled Beijing Climate Center Climate System Model version BCC−CSM1.1 with T42L26 coarse resolution (approximately 2.8125×2.8125 degrees) and BCC-CSM1.1m with T106L26 moderate resolution (approximately 1.125∘×1.125 degrees) were frozen and used to finish CMIP5 experiments. In 2014, the BCC-CSM1.1m is used for operational climate forecasts from one month to one year time-scale to replace the first-generation operational system. The performance is overviewed.

The Sub-seasonal to Seasonal climate prediction (S2S) Project is a joint research project proposed by WWRP/THORPEX-WCRP. The BCC climate model is one of 11 models in the subseasonal to seasonal (S2S) prediction project. The S2S model BCC_CSM1.2 is the updated version in 2014. It is a fully coupled model, in which the atmospheric component is the BCC_AGCM with a T106 horizontal resolution and 40 hybrid sigma/pressure vertical layers, the land component is the BCC Atmosphere and Vegetation Interaction Model, and the ocean and sea ice components are GFDL MOM4 and SIS respectively. Multi-source reanalysis data, including NCEP Reanalysis I, oceanic reanalysis from BCC Global Ocean Data Assimilation System, BCC merged precipitation dataset are used in the initialization of S2S model. A simple lagged average forecasting (LAF) method is adopted to produce 4 ensemble forecasts for a certain forecast experiment. We have finished the S2S re-forecast experiments which start on every day from 1 Jan 1994 to the end of 2014. The reforecast data has been provided to the ECMWF S2S center. A real-time S2S forecast operation in CMA is conducted every day since 2015. Some performance especially in S2S predictability and prediction skill is presented. The some evaluation of CMA S2S prediction data will be shown. The impact of SST initial state on the MJO forecast skill is discussed (Figure 1). The current configuration of S2S operational forecast system is using BCC-CSM1.2 at a T106L26 (approximately 110km) resolution. Future plans include the use of a new model version (BCC-CSM2) with higher resolution (T266L26, approximately 45km).

In CMA, a monthly-scale Dynamical Extended-Range Forecast system version 2 (DERF2) was also built up based on BCC AGCM. In addition, the seasonal-to-interannual climate prediction system using BCC-CSM coupled model was built and operational run since January 2015. In the coming 2 years, all these climate forecast operations will be integrated into an integrated system of subseasonal-seasonal-interannual seamless climate forecast (named as BCC-CPS1) based on BCC coupled climate model.

In recent years, the BCC modelling group has worked towards improving the Beijing Climate Center Climate System Model BCC-CSM) model for the coming CMIP6. There are three versions of BCC models including a low-resolution version of BCC Earth System Model (BCC-ESM1-LR), a medium-resolution version of BCC-CSM2-MR, and a high-resolution version of BCC-CSM2-HR. Their main differences are their atmospheric resolutions i.e. T42L40 in BCC-ESM1-LR, T106L40 in BCC-CSM2-MR, and T266L40 in BCC-CSM2-HR. They have however the same oceanic resolution, that is, 1/3 degree in tropics and 1 degree in high latitudes. Up to now, some model physics are updated. With contract to previous versions, the newly-developed models have better performance of simulation especially in cloud amount, QBO (Figure 2), diurnal variation of precipitation, and etc. All the three versions of BCC models will be frozen before Jan. 2016. Different configurations will be run for separate CMIP-MIPs and BCC plans to contribute simulations to 13 MIPs including AerChemMIP, C4MIP, CFMIP, DAMIP, DCPP, GDDEX, GMMIP, HighResMIP, LS3MIP, LUMIP, OCMIP6, RFMIP, and ScenarioMIP.

References

Huang, A., Y. Zhang, Z. Wang, T. Wu, D. Huang, Y. Zhou, Y. Zhao, Y. Huang, X. Kuang, L. Zhang, Y. Fang, Y. Guo, 2013: Extended range simulations of the extreme snow storms over southern China in early 2008 with the BCC_AGCM2.1 model,J. Geophys. Res. Atmos., 118, 8253–8273

Jie, W., T. Wu, J. Wang, W. Li, X. Liu, 2014: Improvement of 6–15 day precipitation forecasts using a time-lagged ensemble method. Adv. Atmos. Sci., 31(2), 293–304.

Jie, W., T. Wu, J. Wang, W. Li, T. Polivka, 2015: Using a Deterministic Time-Lagged Ensemble Forecast with a Probabilistic Threshold for Improving 6-15 Day Summer Precipitation Prediction in China, Atmospheric Research, 156: 142–159.

Liu, X., T. Wu, S. Yang, W. Jie, S. Nie, Q. Li, Y. Cheng, X. Liang, 2015: Performance of the Seasonal Forecasting of the Asian Summer Monsoon by BCC_CSM1.1(m). Adv. Atmos. Sci., doi: 10.1007/s00376-015-4194-8.

Liu, X., T. Wu, S. Yang, Q. Li, Y. Cheng, X. Liang, Y. Fang, W. Jie, S. Nie. 2014. Relationships between interannual and intraseasonal variations of the Asian - western Pacific summer monsoon hindcasted by the BCC_CSM1.1(m). Adv. Atmos. Sci., 31, 1051–1064.

Wu, T., 2012: A Mass-Flux Cumulus Parameterization Scheme for Large-scale Models: Description and Test with Observations, Clim. Dyn., 38:725–744.

Wu, T., R. Yu, F. Zhang, 2008: A modified dynamic framework for atmospheric spectral model and its application, J. Atmos.Sci., 65, 2235-2253.

Wu, T., R. Yu, F. Zhang, Z. Wang, M. Dong, L. Wang, X.Jin, D. Chen, L. Li, 2010：The Beijing Climate Center atmospheric general circulation model: description and its performance for the present-day climate, Climate Dynamics, 34, 123-147.

Wu, T., L. Song, W. Li, Z. Wang, H. Zhang, X. Xin, Y. Zhang, L. Zhang, J. Li, F. Wu, Y. Liu, F. Zhang, X. Shi, M. Chu, J. Zhang, Y. Fang, F. Wang, Y. Lu, X. Liu, M. Wei, Q. Liu, W. Zhou, M. Dong, Q. Zhao, J. Ji, L. Li, M. Zhou, 2014: An overview of BCC climate system model development and application for climate change studies. J. Meteor. Res., 28(1), 34-56.

Wu, T., W. Li, J. Ji, X. Xin, L. Li, Z. Wang, Y. Zhang, J. Li, F. Zhang, M. Wei, X. Shi, F. Wu, L. Zhang, M. Chu, W. Jie, Y. Liu, F. Wang, X. Liu, Q. Li, M. Dong, X. Liang, Y. Gao, J. Zhang, 2013: Global carbon budgets simulated by the Beijing climate center climate system model for the last century. J Geophys Res Atmos, 118, 4326-4347.
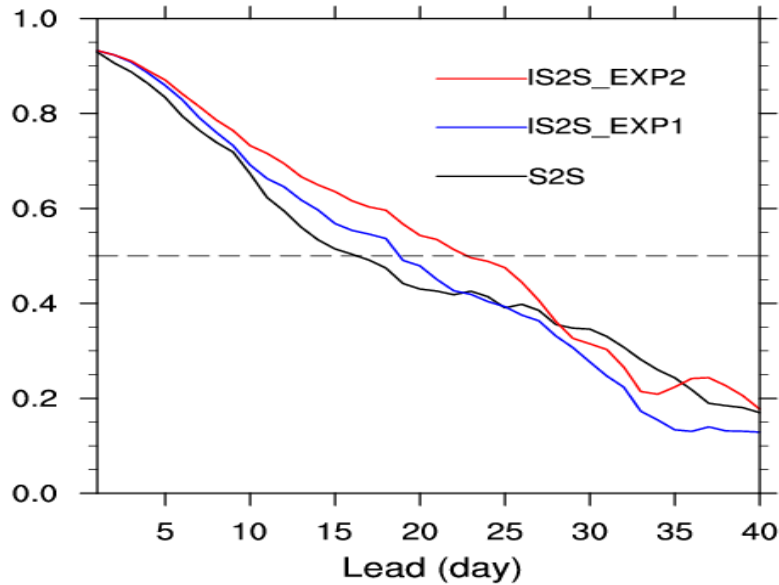
Figure 1. MJO bivariate anomaly correlation for BCC S2S prediction experiments (denoted S2S using atmosphere initials from NCEP R1 and ocean initials from BCC_GODAS), improved S2S experiment 1 (denoted IS2S_EXP1 using atmosphere initials from NCEP FNL and ocean initials from BCC_GODAS), and improved S2S experiment 2 (denoted IS2S_EXP2 using atmosphere initials from NCEP FNL and ocean initials from BCC_GODAS and OISST). The experiments are conducted once per month during 2000-2013, and the dashed line represents the useful skill of 0.5.
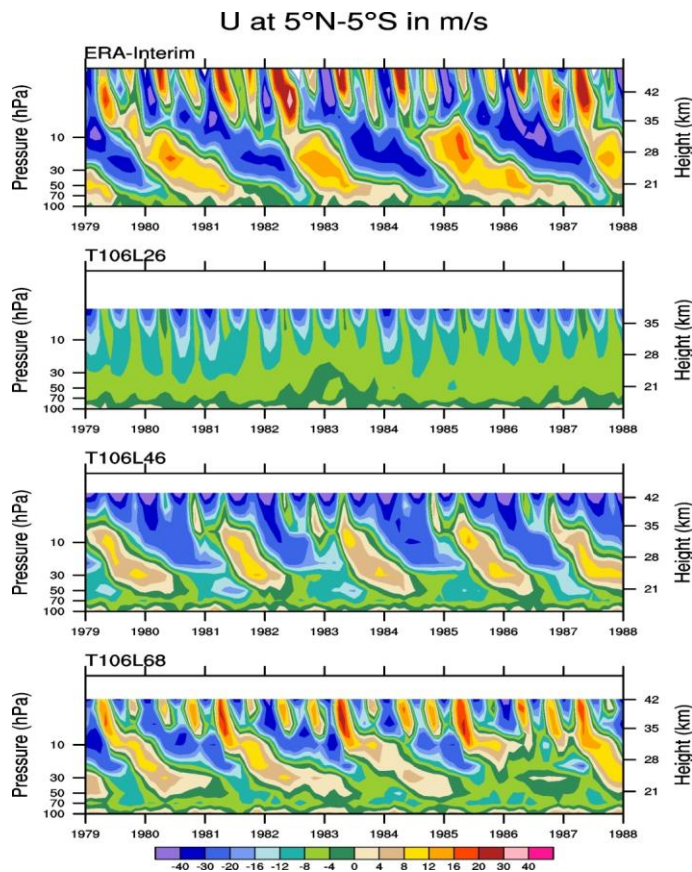

Figure 2. The vertical profiles of 5S-5N zonal wind monthly means from Jan. 1979 to Dec. 1988 from (a) ERA-Interim observation and BCC-AGCM simulation with different vertical resolutions of (b) T106L26, (c) T106L46, and (d) T106L68.

TOWARDS CMIP6 – CSIRO PLANS

Tony Hirst[1], on behalf of the ACCESS Modelling Team

[1]*CSIRO Oceans and Atmosphere, Aspendale, Victoria.*

tony.hirst@csiro.au

The Australian Community Climate and Earth System Simulator (ACCESS) is an initiative aiming for a national approach to weather and climate modelling. Principal partners are the Bureau of Meteorology (BoM) and CSIRO, through the Collaboration for Australian Weather and Climate Research (CAWCR), and participating universities, in particular through the ARC Centre of Excellence for Climate System Science (ARCCSS). The initiative has recently contributed multi-century simulations from two versions of the initial ACCESS coupled climate model to the Coupled Model Intercomparison Project phase 5 (CMIP5), namely ACCESS1.0 and ACCESS1.3. Subsequently, the ACCESS carbon cycle model including the terrestrial (CASA-CNP) and oceanic (WOMBAT) biogeochemical models has been coupled to an upgraded version of ACCESS1.3 to form the initial ACCESS Earth System Model (ACCESS-ESM1).

This talk discusses the development of the next generation of the ACCESS coupled climate model, ACCESS-CM2, the corresponding Earth system model, ACCESS-ESM2, and the plans for contribution to CMIP6. Presently ACCESS-CM2 is running in prototype form, consisting of the Met Office GA6 atmosphere and JULES land surface model, the LANL CICE5 sea ice model, the NOAA/GFDL MOM5 ocean model and the CERFACS OASIS-MCT coupler. The atmospheric model includes the new 'ENDGame' dynamics and an increase in the vertical resolution from the 38 levels of the CMIP5 versions to 85 levels. Immediate plans are to further upgrade the atmospheric model to GA7 and to incorporate the Australian community land surface model CABLEv2. Subsequently, the ACCESS carbon cycle model will be coupled to form ACCESS-ESM2. In the longer term, the ACCESS atmospheric chemistry model (based on UKCA) will also be coupled to form an enhanced version of the ACCESS-ESM2 model, allowing for the study of climate/atmospheric chemistry feedbacks.

The current ACCESS-CM2 suite comprises three versions distinguished by the horizontal resolution, namely (1) 'standard resolution' atmosphere and ocean (notionally 140 km and 1 degree latitude/longitude respectively), as for the CMIP5 versions, (2) standard resolution atmosphere and high resolution ocean (0.25 degree latitude/longitude), and (3) high resolution atmosphere (notionally 60 km) and ocean. The high resolution ocean component is based on that implemented by the ARC Centre of Excellence for Climate System Science (ARCCSS). Century-scale trial simulations have been conducted with the former two versions, and preliminary results will be presented.

The ACCESS partners' planned contribution to CMIP6 will be discussed. ACCESS–CM2/ESM2 is planned to form the basis of this contribution. The initial contribution to CMIP6 is planned to be at standard resolution, given computational and other constraints. Commitment has been made to participate in 8 CMIP6-endorsed MIPs, chosen to address specific stakeholder and scientific interests. The simulations will be done in collaboration involving the CSIRO, ARCCSS and the BoM. Options for potential subsequent contributions at higher-resolution are discussed, with reference to the significant computational resources that would be required.

TOWARDS CMIP6: MET OFFICE MODELLING PLANS AND EXPECTATIONS

Tim Johns[1], Catherine A. Senior[1], Alistair Sellar[1]

[1] Met Office Hadley Centre, Exeter, UK

tim.johns@metoffice.gov.uk

Physical climate and Earth System models under development

Global climate model development at the Met Office is now focussed around the HadGEM3 flagship physical coupled model, which is subject to an ongoing coordinated model development process leading, via science update cycles, to successive "Global Coupled" (GC) model releases (see also D. Walters' contribution in this session). In contrast to the Met Office's Earth System Model (ESM) development practice for previous CMIP exercises and IPCC assessments (e.g. HadGEM2-ES for CMIP5/AR5), a broader UK collaborative process is now in train for the development of a new Earth System Model UKESM1, built on the HadGEM3-GC physical climate model, teaming Met Office staff with colleagues in UK universities/institutes.

The latest GC model release (HadGEM3-GC2; Williams et al. 2015), which includes the ENDGame dynamical core, when run at an atmospheric resolution of N216 with 85 vertical levels and ocean resolution of 0.25 degrees with 75 vertical levels, has recently shown considerable benefits in seasonal forecasting (Scaife et al. 2014) and other systems. Critically, this model simulates credible mid-latitude weather systems. HadGEM3-GC2 and successor GC releases, run at this resolution, will provide our main tool for understanding drivers of regional climate over the coming decades. Development of the new Earth System Model UKESM1 (Figure 1) continues in earnest, major efforts having recently gone into the chemistry and aerosol package, UKCA, and the ocean biogeochemistry, MEDUSA2. A simplified version of the UKCA atmospheric chemistry scheme, using offline oxidants and a full tropospheric sulphur cycle, has recently been developed and coupled to the GLOMAP-mode aerosol scheme. This version of UKCA-GLOMAP will form part of the next physical climate model release, HadGEM3-GC3, which will in turn form the physical core of UKESM1.
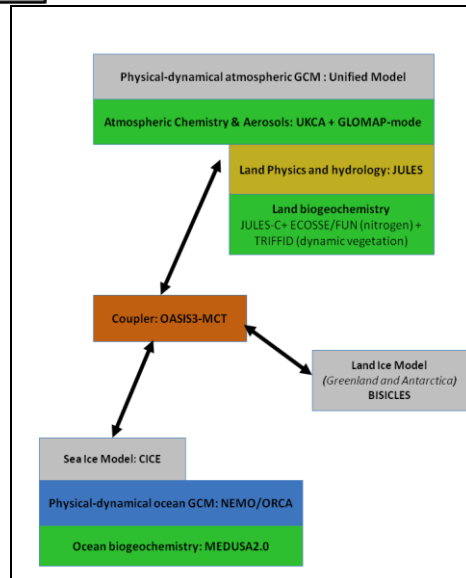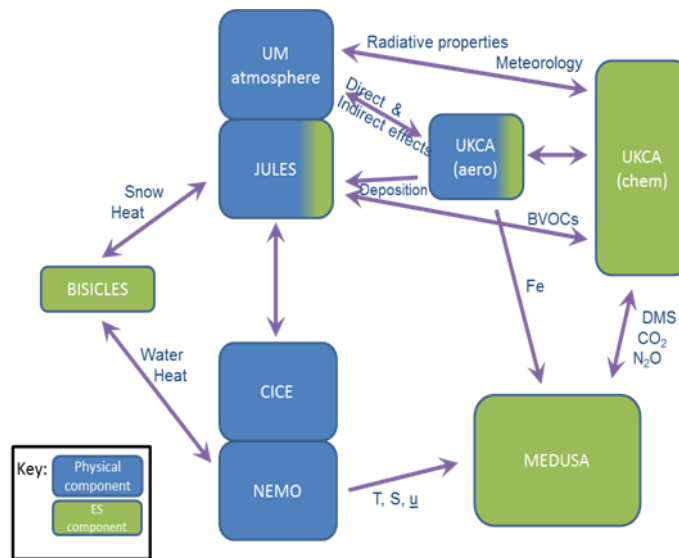
Figure 1: Simplified schematics of UKESM1 model components and couplings (left) and component clusters (right). Model components connected to the OASIS-MCT coupler as a cluster operate as a single executable and are launched as independent executables run on separate processing elements

Engagement in CMIP6

HadGEM3-GC3 and UKESM1 will together comprise the main modelling tools to be used by the Met Office and the wider UK climate science community to engage in CMIP6 experiments (Meehl et al. 2014). Participation in some of the CMIP6 sub-projects outside of the core 'DECK' (Diagnosis, Evaluation and Characterisation of Klima) experiments (Figure 2) will be led directly by the Met Office while the UK academic community (Natural Environment Research Council sponsored) will lead on other sub-projects. Depending on the nature of the sub-projects, either GC3 or UKESM1 at high ('HI': N216 or ~60 km atmosphere) or low ('LO': N96 or ~150 km atmosphere) horizontal resolution will be utilised, judgements being based on suitability for the experiments concerned weighing up projected computational cost. Decisions on the model configurations deployed are also dependent in some cases on ongoing work to develop a mixed HI/LO resolution UKCA coupling within UKESM1, which would reduce the computational cost compared to HI. A coordinated process has been established for the

deployment of UKESM1 and HadGEM3-GC3 on CMIP6 activities, including oversight of science aims, HPC utilisation and data dissemination activity to the Earth System Grid. The technical infrastructure supporting UKESM1 development and CMIP6 science has commonality with that now in place to support other collaborative Met Office model development partnerships.
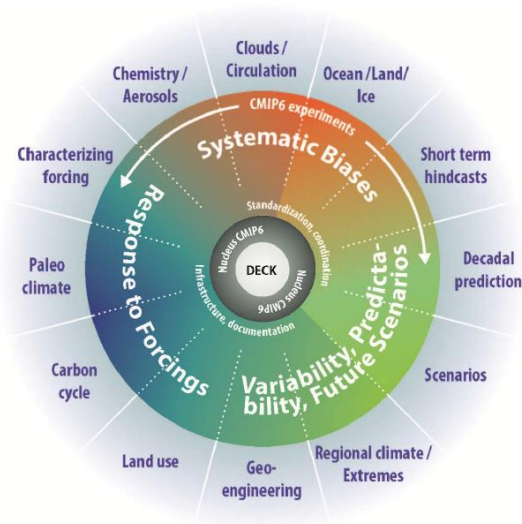

Figure 2: Schematic of the proposed experiment design for phase 6 of the Coupled Model Intercomparison Project (CMIP6) (after Meehl et al. 2014)

Pre-CMIP6 idealized experiments: HadGEM3-GC2 vs. HadGEM2-ES

In anticipation of CMIP6, a series of idealized climate change idealized experiments with HadGEM3-GC2 (analogous to CMIP6 DECK experiments) has been performed and analysed, in part to give early guidance on the optimal choice of resolution for GC3 and UKESM1 configurations for specific CMIP6 sub-projects. Comparisons have been drawn with CMIP5 (and particularly HadGEM2-ES). The results outlined here are documented in more detail in Senior et al. 2015 (in preparation).

Climate Sensitivity and Feedbacks

Analysis shows GC2's global climate sensitivity (TCR[3]: 1.9K/2.1K and ECS[4]: 3.1K/3.2K at N216/N96 resolutions respectively) sits close to the middle of the CMIP5 range, substantially lower than that of HadGEM2-ES (TCR: 2.5K and ECS: 4.6K). GC2 has very different LW and SW cloud feedbacks compared to HadGEM2-ES but shows only small differences between 'HI' and 'LO' resolutions with respect to global mean climate sensitivity and its breakdown into clear sky and cloud feedbacks (Figure 3). Some of the GC2 versus HadGEM2-ES clear sky shortwave feedback difference is thought to be related to the control state sea ice distribution, GC2 having a marked warm bias in the Southern Ocean. GC3 development has targeted this systematic error to some extent, but in general the climate sensitivity of GC3 to CO_2 forcing is expected to be similar to GC2. The full scenario response in GC3 including all anthropogenic forcing factors is more uncertain at this stage since aerosol and land use schemes are undergoing significant development between GC2 and GC3. Similarly the full Earth System

---

[3] Transient Climate Response in 1%-per-annum experiment
[4] Effective Climate Sensitivity to doubled CO_2

feedbacks with UKESM1 need to be evaluated before it will be clear where the new model sits relative to the CMIP5 multi-model regarding its climate carbon-cycle feedback and global mean temperature response.
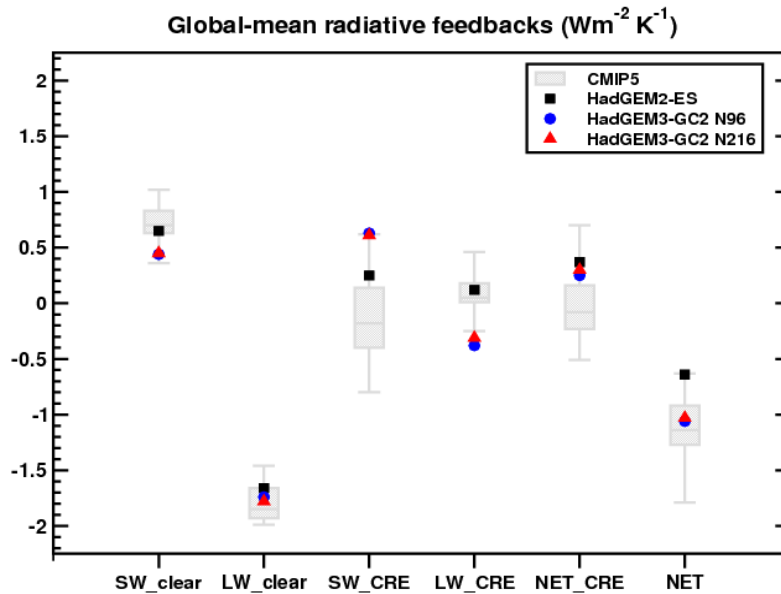

Figure 3: Global mean radiative feedbacks (shortwave and longwave, clear sky and cloud radiative effect, and net) for HadGEM3-GC2 (physical model) at 'LO' and 'HI' resolution compared with HadGEM2-ES (ESM) and the CMIP5 multi-model ensemble

Arctic Sea Ice Sensitivity

Understanding the observed decline over recent decades of Arctic sea ice extent at its September annual minimum and quantifying future projections towards an ice-free summer state in the Arctic are of high scientific and political interest. The climate sensitivity of Arctic sea ice (the gradient of the linear fit of September monthly mean ice area against global temperature change in an idealised 1%-pre-annum CO_2 experiment) has been examined in HadGEM3-GC2 in comparison to HadGEM2-ES (Figure 4). The simulated Arctic ice area is initially larger in HadGEM3-GC2 at N96 than N216, potentially due to a 2K warmer regional temperature in the N216 control simulation. The Arctic sea ice climate sensitivity is larger in magnitude at N216 (-17.2 ± 0.2 %K^{-1}) than at N96 (-14.3 ± 0.2 %K^{-1}), the latter value being a very close match to HadGEM2-ES. Atmospheric model resolution appears to play a larger role in the sea ice sensitivity than do developments to the model physics between HadGEM2-ES and HadGEM3-GC2 or the absolute sea ice area or Arctic regional temperatures in the control simulations. The mechanism for this resolution dependency in HadGEM2-GC2 is being investigated, increased poleward atmospheric heat transport at higher resolution being one potential factor. It should be noted that HadGEM3-GC3 will include upgrades to implement multi-layer thermodynamics in the CICE sea ice component which may have some impact on the sea ice sensitivity for the CMIP6 models.
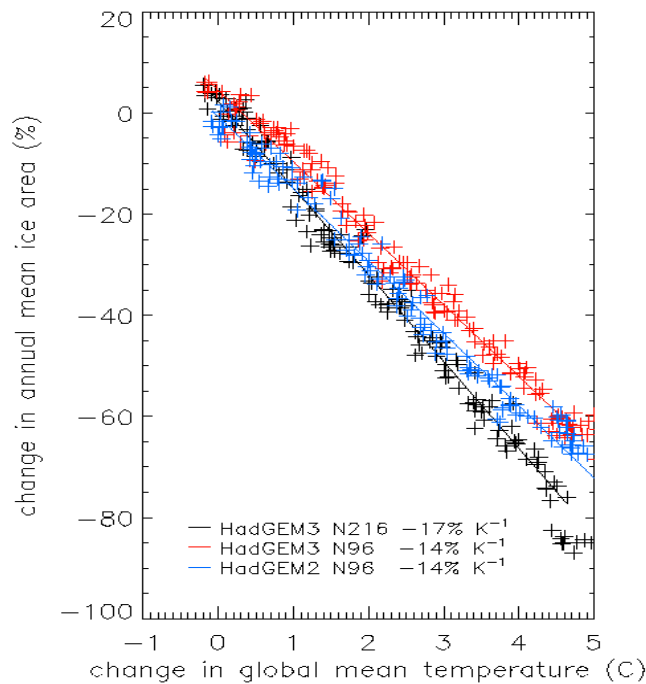
Figure 4: Least squares fit between changes in Arctic sea ice area (%) and global annual surface temperature (^{o}C) under the 1%-per-annum CO_2 idealised scenario, changes being calculated with respect to 150-year means of the control runs (parallel to the 1%-per-annum runs)
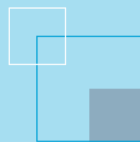
References

Meehl, G. A., Moss, R., Taylor, K. E., Eyring, V., Stouffer, R. J., Bony, S., and Stevens, B., 2014: Climate Model Intercomparisons: Preparing for the Next Phase, Eos Trans. AGU, 95(9), 77-78

Scaife, A. A., Arribas, A., Blockley, E., Brookshaw, A., Clark, R. T., Dunstone, N., Eade, R., Fereday, D., Folland, C. K., Gordon, M., Hermanson, L., Knight, J. R., Lea, D. J., MacLachlan, C., Maidens, A., Martin, M., Peterson, A. K., Smith, D., Vellinga, M., Wallace, E., Waters, J., and Williams, A., 2014: Skillful long-range prediction of European and North American winters. Geophys. Res. Lett. 41, 2014GL059,637, doi:10.1002/2014gl059637

Senior, C. A., Andrews, T., Burton, C., Chadwick, R., Clark, R, Copsey, D., Graham, T., Hyder, P. Jackson, L., McDonald, R., Ridley, J., Ringer, M., and Tsushima, Y., 2015: Idealised Climate Change simulations with a high resolution physical model: HadGEM3-GC2. (manuscript in preparation)

Williams, K. D., Harris, C. M., Bodas-Salcedo, A., Camp, J., Comer, R. E., Copsey, D., Fereday, D., Graham, T., Hill, R., Hinton, T., Hyder, P., Ineson, S., Masato, G., Milton, S. F., Roberts, M. J., Rowell, D. P., Sanchez, C., Shelly, A., Sinha, B., Walters, D. N., West, A., Woollings, T., and Xavier, P. K., 2015: The Met Office Global Coupled model 2.0 (GC2) configuration. Geosci. Model Dev., 8, 1509-1524, doi:10.5194/gmd-8-1509-2015